THE UNIVERSITY
of EDINBURGH

THE ROLE OF 4E-BP2 IN NEURONAL TRANSLATION

THE UNIVERSITY
of EDINBURGH

Stella Kouloulia

Doctor of Philosophy

The University of Edinburgh

2019

Declaration

I declare that this thesis has been composed by me and that the work included is my own unless otherwise clearly stated and acknowledged and that this work has not been submitted for any other degree or professional qualification.

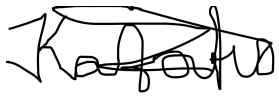

This thesis is dedicated to my inspiration,
στον άνθρωπό μου, Βαγγέλη, for teaching me
to always look for the hidden things in life and science
and get the greatest reward,
discoveries that go far beyond my imagination.

Acknowledgements

As this PhD journey has come to its end, I would like to thank some people that made this experience not only unique but a life's lesson for me. Firstly, I would like to thank my supervisor Christos Gkogkas for all the trust, help and advice during this challenging project. I also want to thank him for all the exciting scientific discussions that we had, making me love this project up to the point that I feel part of it.

I would also like to thank my second supervisor, Paul Skehel, for always being positive and willing to help and support me. Lastly, I would like to thank Mandy Jackson for all the advice and useful comments thoughout my PhD.

It has been almost 4 years in this lab and I want to say a big thank you to my colleagues who helped me with my project and my experiments. Thank you Konstanze Simbriger, Inês Amorim, Gilliard Lach and Agniete Kampaite. Also, former members of the Gkogkas lab who during their stay made my smile bigger, Stavroula Charilaou and Georgia Petrou.

Importantly, I would like to thank from the bottom of my heart, my former colleague and good friend, Theoklitos Amvrosiadis firstly for his love and interest for my project. Secondly, for always being there to help me and stand by me, regardless of the time or day. Lastly, I would like to thank him for always motivating me for being a better scientist and human as well.

I would also like to thank my dearest friend, Athanasia Arnokourou, for being there for me from the 1st day that we met in Edinburgh. This PhD and my whole life experience here would be indifferent if she was not so present and active in my life. Thank you for the love and for caring me.

A warm thank you to my colleague, Tian Tian, for all the hugs that we shared daily during our PhDs and my flatmates and friends, Klára Zsófia Gerlei and Daniel Marcu, for being like a second family for me here in Edinburgh.

I also want to thank my life friends back home for believing in me and loving me, no matter the distance between us, Ermioni Mantziorou, Eleni Liakou, Asimina Dimara, Elena Mavraeidopoulou, Pantelis Floukarakis, Aris Papatheodorou, Margarita Petropoulou and especially Eleni Kytinou for inspiring me throughout my life and for all the hours that she stayed awake just to talk with me. I also want to thank John Dafnis and Areti Strati because if they were not in my life at a crucial moment, I wouldn't have been in Edinburgh for my PhD and my former supervisor Penelope Ioannou for sharing all her passion about science and being a great mentor for me.

This thesis and especially me would be completely different if I was not a member of this beloved family. I can't express with words the strength of the bond and all the love, compassion and protection that I had all these years from my parents, Alexandros and Argentoula and my siblings Maria and Christos. A special thank you to my twin brother, Konstantinos, for all the moments that we shared from our day of birth till now and for all the guidance, advice, unforgettable support through my PhD. A big thank you to my grandparents Konstantinos, Asimina, Stelios, Maria and Ploumi who had a great impact on my life and personality. I will never forget my grandpa, Stelios, for being a scientist without even knowing himself, always curious and interested about biology, having suffered a lot from rheumatoid arthritis.

This thesis is dedicated to my inspiration, Vaggelis Giampazolias who makes me smile, think, love, live every day of my life. You squeeze life out of me, feeling blessed for having you in my life and having shared all this journey with you. I can't wait for the next ones.

Let us avoid death in soft doses,
always remembering that to be alive requires a strength much greater
than the simple act of breathing.
Only ardent patience will allow us to conquer
a splendid happiness.

Martha Medeiros

Abstract

Translational control is a powerful means to alter gene expression and regulates synaptic plasticity, learning and memory. 4E-BP2 (*Eif4ebp2,* Eukaryotic Initiation Factor 4E-Binding Protein 2) is the predominantly expressed 4E-BP in the mammalian brain and represses cap-dependent translation initiation, by binding to eIF4E (*Eif4e*, eukaryotic Initiation Factor 4E). As a master regulator of protein synthesis in the mammalian brain, 4E-BP2 has been implicated in learning, memory and Autism Spectrum Disorder (ASD).

Upon phosphorylation by mTOR (mammalian Target Of Rapamycin, mTOR) which occurs in most tissues, 4E-BP2 cannot bind to eIF4E, failing to repress translation initiation. However, in early postnatal brain development, 4E-BP2 undergoes brain-specific post-translational deamidation on asparagines N99 and N102, which are converted to aspartic acid. Asparagine deamidation is not catalysed by enzymes but can occur spontaneously and is induced by alkaline pH. Deamidated 4E-BP2 was shown to regulate the kinetics of excitatory synaptic transmission in early postnatal brain development, suggesting that it may be important for synaptic function during that crucial developmental period. N99/N102 deamidation decreases the affinity of 4E-BP2 for eIF4E and increases its binding to the mTORC1 protein Raptor. The significance of enhanced Raptor binding to deamidated 4E-BP2 is yet unclear because 4E-BP2 phosphorylation is very low in adult brain. Moreover, the role of deamidated 4E-BP2 and the downstream effects of deamidated 4E-BP2 translational control in the mammalian brain are not known but of cardinal importance given the pervasive role of 4E-BP2 in regulating brain function.

In this thesis, we describe a previously unidentified mechanism during early postnatal brain development, whereby the constitutively deamidated form of the cardinal brain translation initiation repressor 4E-BP2 is more susceptible to ubiquitin proteasomal degradation (as compared to unmodified, WT protein) because it binds with higher affinity to a complex, comprising the mTORC1 protein Raptor and the ubiquitin E3 ligase CUL4B. Deamidated 4E-BP2 (2D) stability is regulated by mTORC1 and AMPAR activity but not NMDARs. We also showed that 4E-BP2 deamidation is neuron-specific and occurs in human brain. We explored whether deamidated and WT 4E-BP2 have a similar subcellular distribution in neurons, indicating that there is very low co-localization of them in both soma and dendrites. We studied WT and 2D structures, with Synchrotron radiation circular dichroism

(SCRD), Small angle X-ray scattering (SAXS) and Nuclear magnetic resonance (NMR) spectroscopy of full-length recombinant 4E-BP2 (WT or 2D) expressed in *E. Coli* and purified, and we identified that they share a similar structure, with only minor differences in a few residues. Moreover, using unbiased translatome mapping, we discovered that overexpression of deamidated 4E-BP2 represses the translation of a distinct pool of mRNAs linked to cerebral development, mitochondria and chiefly NF-κB activity. Collectively, these data describe a previously unidentified brain-specific translational control mechanism that could be crucial for postnatal brain development in neurodevelopmental disorders such as ASD.

Lay summary

Complex behaviours such as perception, memory or emotions are the result of complicated computations carried out by our brains. Neurons in our brains carry out the processing and transmission of information through electrochemical connection structures called synapses. Information processing between neurons through synapses requires synthesis of specific proteins in neurons and the process controlling this synthesis spatially and temporally is called protein synthesis. Therefore, protein synthesis is indispensable for maintenance of synaptic structure and function since imbalance of this process has been linked to the development of neuropsychiatric diseases, such as Autism Spectrum Disorders (ASD). A master repressor of protein synthesis is *Eukaryotic initiation factor 4E-binding protein 2* (*Eif4ebp2*-4E-BP2). Genetically modified mice in which 4E-BP2 is inactivated were characterised by impaired memory and learning, underlying the importance of this protein in these complex behaviours.

The role as well as the activity of most proteins is controlled by specific chemical modifications that occur on them and can either activate, inactivate or even change their function inside the cells. In most tissues, 4E-BP2 is regulated by a chemical modification called phosphorylation. When 4E-BP2 is phosphorylated, it cannot inhibit protein synthesis. Interestingly, only in the brain and after birth, apart from phosphorylation, 4E-BP2 undergoes another chemical modification, called asparagine deamidation. In this thesis, we describe how this modification, deamidation, enables 4E-BP2 to control synthesis of specific proteins that are required for neuronal function after birth. Firstly, we studied whether the two protein forms, deamidated and unmodified 4E-BP2, are located in the same compartments/areas in neuronal cells and discovered that they do not have the exact same distribution, indicating a different role of the deamidated protein compared to the unmodified. Moreover, we characterised the three-dimensional protein structure called secondary structure of deamidated 4E-BP2 and identified a few residues that exhibit local variations compared to the unmodified 4E-BP2 but overall the secondary structure of the protein is not altered by deamidation. Interestingly, we showed that deamidated 4E-BP2, is more susceptible to degradation by a specific protein complex, consisted of two proteins, CUL4B and DDB1. Therefore, after CUL4B-DDB1 complex breaks down deamidated 4E-BP2 to its constituent amino acids, deamidated 4E-BP2 can no longer repress protein synthesis, allowing this process to promote the

synthesis of specific proteins. What is the role of these newly synthesized proteins by this novel mechanism that involves deamidated 4E-BP2? Importantly, we identified that these newly synthesized proteins regulate the activity of another protein in neurons called NF-κB and the development of the cerebral cortex in the brain. NF-κB is a crucial factor that can either promote or inhibit axonal growth depending on the chemical modifications that occur on its subunits. Thus, 4E-BP2 undergoes deamidation to promote synthesis of specific proteins that regulate probably major postnatal neuronal processes such as axonal growth through NF-κB. Collectively, these data describe a previously unidentified mechanism, specific to the brain, which regulates protein synthesis and could be crucial for postnatal brain development in neurodevelopmental disorders such as ASD.

Abbreviations

AAV	Adeno-associated viruses
AKT/PKB	Protein kinase B
AMPA	A-amino-3-hydroxy-5-methyl-4-isoxazolepropionic acid
Ara-C	Cytosine arabinoside
Arc	Activity-regulated cytoskeleton-associated protein
ASD	Autism Spectrum Disorder
Asn	Asparagine
Asp	Aspartyl
Bcl-xL	B-cell lymphoma-extra large
BDNF	Brain-derived neurotrophic factor
BP	Biological Pathways
bp	Base pairs
CA	Carbonic Anhydrases
CaMKII	Ca2+ / calmodulin – dependent protein kinase II
CC	Cellular Compartment
c-GAS	Cyclic GMP-AMP Synthase
CNS	Central Nervous System
CPEB	Cytoplasmic Polyadenylation Element Binding protein
CPEs	Cytoplasmic polyadenylation elements

CREB	Transcription factor Camp-responsive element binding protein
CUL3	Cullin 3
CUL4B	Cullin 4B
DAG	Diacylglycerol
DHPG	(RS)-3-5-dihydroxyphenylglycine
DRP1	GTPase Dynamin-Related Protein 1
DTGs	Differentially translated Genes
ED	Three-dimensional structure
eEF1A	Eukaryotic Elongation Factor 1A
eEF2	Eukaryotic Elongation Factor 2
eIF4E	Eukaryotic Initiation Factor 4E
eIF4E – BP2	Eukaryotic Initiation Factor 4E – Binding Protein 2
ER	Endoplasmic Reticulum
eRF1	Eukaryotic Release Factor 1
eRF3	Eukaryotic Release Factor 3
FCCP	Carbonylcyanide p-trifluoromethoxyphenylhydrazone
FMRP	Fragile X Mental Retardation Protein
GC	Guanine-Cytosine
GFAP	Glial fibrillary acidic protein
GFRs	Growth factor receptors
Gln	Glutamine
Glu	Glutamyl

GluA1	A-amino-3-hydroxy-5-methyl-4-isoxazolepropionic acid receptor subunit 1
GluA2	A-amino-3-hydroxy-5-methyl-4-isoxazolepropionic acid receptor subunit 2
GO	Gene Ontology
GPCRs	G protein–coupled receptors
HEKs	Human Embryonic Kidney cells
Hsc70	Heat shock cognate 71 kDa protein
hSyn	Human Synapsin I
IDPs	Intrinsically disordered proteins
IDRs	Intrisically disordered regions
IFN	Interferon
Insp3	Inositol trisphosphate
IRES	Internal Ribosome Entry Site
LB	Luria-Bertani
LKB1/AMPK	Serine/threonine kinase 11/LKB1/AMP-kinase
LTD	Long-Term Depression
LTM	Long-term memory
LTP	Long-Term Potentiation
mEPSCs	Miniature Excitatory Postsynaptic Currents
mGluR1	Metabotropic glutamate receptors 1
miRNAs	MicroRNAs
mLST8	mTOR Associated Protein, LST8 Homolog
MNKs	MAPK signal–integrating kinases 1 and 2

MAP	Molecular Activity Predictor
MF	Molecular Function
MTFP1	Mitochondrial Fission Process 1
mTOR	Mammalian/mechanistic Target Of Rapamycin
mTORC1	Mammalian/mechanistic Target Of Rapamycin Complex 1
mTORC2	Mammalian/mechanistic Target Of Rapamycin Complex 2
ncRNAs	Non-coding RNAs
NF-κB	Nuclear Factor kappa-light-chain-enhancer of activated B cells
Nlgn1	Neuroligin 1
NMDA	N-methyl-D-aspartate
NMR	Nuclear Magnetic Resonance
NSD	Normalized spatial discrepancy
ODC	Ornithine Decarboxylase
PABP	Poly(A)Binding Protein
PAIP2B	Polyadenylate-binding protein-interacting protein 2B
PAMPs	Pathogen associated molecular patterns
PDK1	Phosphoinositide-dependent protein kinase1
PFAS	PhosphoribosylFormylglycinAmidineSynthetase
PI3K	Phosphoinositide-3-Kinase
PIMT	Protein Isoaspartate Methyltransferase
PIP2	Phosphatidylinositol 4,5-bisphosphate

PIP3	Phosphatidylinositol-3,4,5-triphosphate
PKC	Protein kinase C
PRAS40	Proline-Rich AKT substrate 40kDa
PSD	Postsynaptic density
PSD95	Postsynaptic density protein 95
PTEN	Phosphatase and tensin homolog
Rheb	Ras homolog enriched in brain
RIG-I	Retinoic acid-Induced Gene I
rpS6	Ribosomal protein S6
rRNA	Ribosomal RNA
RT	Room temperature
RTKs	Receptor Tyrosine Kinases
S6K1 and S6K2	S6 kinases
SAXS	Small angle X-ray scattering
SCAPPER	F-box/LRR-repeat protein 20
SCRD	Synchrotron radiation circular dichroism
SEC-MALS	Size exclusion chromatography-multi angle light scattering
Ser	Serine
SGK1	Serum/glucocorticoid-regulated kinase
SHANK3	SH3 And Multiple Ankyrin Repeat Domains 3
siRNA	Small interfering Ribonucleic Acid
SPRCs	Synapse–associated polyribosomes complexes
STM	Short-term memory

Thr	Threonine
TOP	Terminal Oligopyrimidine Tract
TPRC	Transient Receptor Potential-Canonical
RBPs	*trans* RNA – Binding Proteins
TSC2	Tuberous Sclerosis Complex 2
TTX	Tetratodoxin
UbcH7/UBE2L3	Ubiquitin-conjugating enzyme E2 L3
UBE1	Ubiquitin activating enzyme E1
uORF	Upstream Open Reading Frame
VEFG	Vascular Endothelial Growth Factor
vGAT	Herpes viral homolog of Glutamine 4 AmidoTransferase
WT	Wild Type
XLID	X-linked intellectual disability

Contents

List of Figures

List of tables

1. Introduction

Prologue

During the past 15 years, the sequencing of different genomes has enabled us to unravel the genetic content of different cell types within organisms. Moreover, it has provided invaluable information, hence estimating that 20,000-25,000 genes encode proteins within each human cell (International Human Genome Sequencing, 2004). Protein synthesis is the last stage of gene expression, following transcription. During this process, the coding sequence of each mRNA is translated into amino acids and polypeptides are assembled (Hershey et al., 2012). Posttranslational modifications can occur in response to various stimuli, allowing each cell to regulate and modify the functions of its proteins in an energy-efficient way and according to the environmental conditions. Posttranslational modifications increase the possible molecular variations of proteins in cells by many orders of magnitude (Walsh et al., 2005). The mechanisms by which specific residues of proteins undergo these modifications involves about 5% of human enzymes that catalyse these chemical reactions (Venne et al., 2015). Understanding these modifications is challenging if one considers that the human proteome is 10-100 times more complex than the genome (Cho, 2007). The present thesis examines the regulatory mechanisms associated with the posttranslational asparagine deamidation of Eif4ebp2 (eukaryotic Initiation Factor 4E-Binding Protein 2, 4E-BP2). The *Eif4ebp2* gene encodes for the 4E-BP2 protein, an inhibitor of cap-dependent translation in higher eukaryotes, fundamental for the regulation of protein synthesis (translational control). For simplicity, we will refer to eIF4E-Binding Proteins as 4E-BPs in the remainder of this thesis.

1.1 Translation

1.1.1 Overview of translational machinery

The translational machinery that catalyses protein synthesis in higher eukaryotes consists of the following essential components for efficient translation: the mRNA, the 80S ribosome (40S and 60S ribosomal subunits), various eIFs (eukaryotic Initiation Factors), the aminoacyl-tRNAs and ATP (Hershey et al., 2012). The mRNA contains the genetic information that will be translated into protein sequence by ribosomes. Translating ribosomes are composed of two subunits (small-40S, large-60S), each subunit includes ribosomal RNA (rRNA) and proteins (Hershey et al., 2012). eIFs are indispensable for the initiation of translation. These are multi-protein complexes composed of many subunits, required for regulating translation (Hershey et al., 2012), the role of most eIFs will be outlined in section 1.1.2). Aminoacyl-tRNAs have undergone aminoacylation catalysed by the enzyme aminoacyl-tRNA synthetase and carry amino acids to the ribosome (Pang et al., 2014). Another unique characteristic of aminoacyl-tRNAs is the presence of the anticodon loop. This structure is required for binding to the mRNA and is complementary to mRNA codons (Hershey et al., 2012). All these components render translation a highly regulated process, divided into three major steps: initiation, elongation and termination/recycling (Hershey et al., 2012).

1.1.2 Initiation of Translation

Eukaryotic mRNAs are translated via different mechanisms of initiation of translation dependent on their structural elements. The predominant mechanism for most eukaryotic mRNAs is cap-dependent initiation. Nascent mRNAs which harbour the structure m7GpppN (where m is a methyl group and N is any nucleotide) at their 5’ end are called ‘’capped’’. The cap plays multiple roles throughout the life cycle of an mRNA (Gingras et al., 1999). Regarding protein synthesis it marks the 5' terminus, hence it can be recognized by eIF4E (Marcotrigiano et al., 1997; Sonenberg et al., 1979). Mature eukaryotic mRNAs also possess a poly (A) tail at their 3' terminus of 50-300 adenylates, responsible for the interaction with PABP [poly(A)Binding Protein] (Hershey et al., 2012). However, there is a number (5%-10%) of cellular and viral

mRNAs that are translated via a different mechanism involving the non-cap mediated recruitment of the 40S ribosomal subunit, called IRES (Internal Ribosome Entry Site)-dependent initiation (Gingras et al., 1999). These mRNAs have a specific IRES structure in which the 40S ribosomal subunit binds directly, avoiding the recognition step of the m7GpppN cap (Hershey et al., 2012).

Cap-dependent initiation is regulated by twelve or more initiation factors (Hershey et al., 2012). The first step is formation of the ternary complex, composed by Met-tRNA, eIF2 and GTP. Following its assembly, ternary complex associates with the 40S ribosomal subunit, on which factors eIF1A and eIF3 are already bound and form the 43S preinitiation complex. The consequent step is binding of mRNA to the preformed 43S complex, thus 48S preinitiation complex is now assembled. The formation of the 48S complex requires also translation factors eIF4E, eIF4G, eIF4A and eIF4B. The factors eIF4E, eIF4G and eIF4A form eIF4F complex: eIF4E binds to the cap of mRNA and associates with eIF4G. The latter forms a bridge between the 40S ribosomal subunit and mRNA by binding to eIF3 (Clemens et al., 2013). eIF4A is a helicase that unwinds the secondary structure of mRNA (Svitkin et al., 2001). At this phase, the downstream scanning begins until an initiation codon (AUG) is recognized (Hershey et al., 2012). As soon as the codon AUG is recognized, the 60S ribosomal subunit is added to the initiation complex in an eIF5-dependent step concomitant with hydrolysis of GTP and removal of eIF3 from the ribosome. Therefore, the 80S initiation complex is assembled and starts the protein synthesis by entering the elongation phase (Clemens et al., 2013). Figure 1.1 illustrates the mechanism of initiation, presenting the complexes that are formed in each stage.

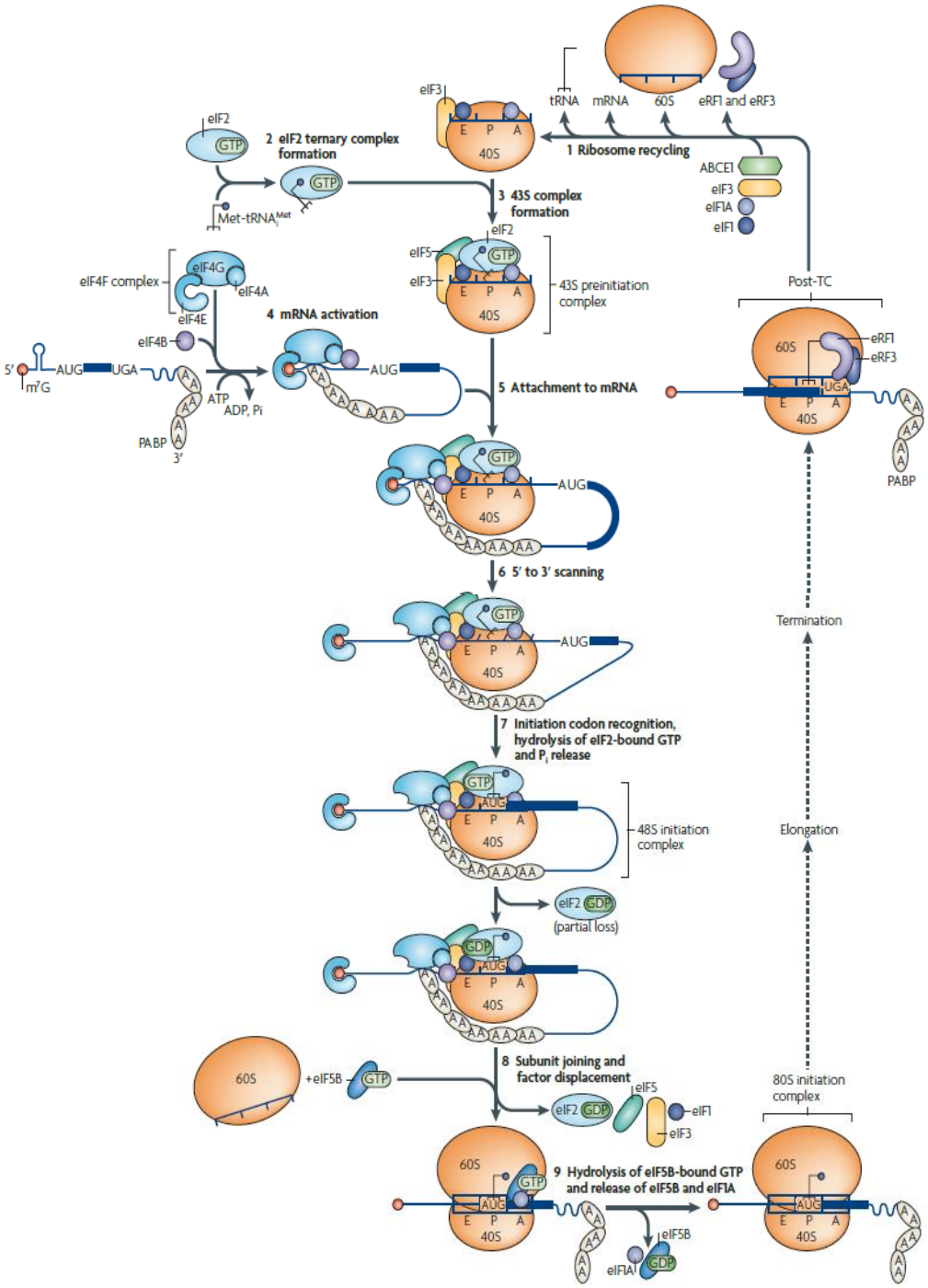

Figure 1.1 Initiation of Protein Synthesis in Eukaryotes.

Each complex is assembled in the presence of specific eIFs. As soon as the AUG initiation codon is recognized, the 60S ribosomal subunit binds to the 48S pre-formed complex, forming the 80S complex that enters the elongation phase (Jackson et al., 2010).

1.1.3 Elongation

Elongation is strongly conserved from bacteria to higher organisms. The main steps that are required to occur during each cycle of elongation are : a) the correct tRNA binds to the ribosome A (Aminoacyl) site (Hershey et al., 2012) and recognizes the corresponding codon of mRNA (Spiegel et al., 2007); b) a new peptide bond is formed between the polypeptide chain and the new amino acid; c) the newly formed peptidyl-tRNA and the mRNA translocate from A to P (peptidyl) which is the second binding site for tRNA, leaving the A binding site unoccupied for the next cycle (Hershey et al., 2012). After each cycle, the polypeptide chain continues to elongate one amino acid at a time (Spiegel et al., 2007). Each cycle requires two GTPases: eEF1A (eukaryotic Elongation Factor 1A) and eEF2. eEF1A provides the aminoacyl-tRNA to the A site as a component of the complex eEF2-GTP. eEF2 catalyses the translocation step of elongation with consequent GTP hydrolysis. Translocation will leave the A site empty, P site occupied by peptidyl-tRNA and E site occupied by deacetylated tRNA. The next codon will be presented in the A site since the movement of tRNA is concomitant with the movement of mRNA by three bases (Frank et al., 2007).

1.1.4 Termination/Recycling

Termination of translation occurs when the ribosome reaches the end of the coding sequence. Therefore, an aminoacyl-tRNA combined with a stop codon (UAA, UGA, UAG) enters the A site. In the termination process, two factors are essential in eukaryotes, eRF1 (eukaryotic Release Factor 1) and eRF3. eRF1 recognizes the stop codon with high-fidelity and also hydrolyses the peptidyl-tRNA whereas eRF3 is a translation GTPase that is released after the hydrolysis of GTP (Dever and Green, 2012).

1.2 Regulation of Protein Synthesis

Regulation of protein synthesis takes place mainly at the initiation step (Hershey et al., 2012). Global regulation of protein synthesis depends on the phosphorylation state of one or more initiation factors, reflecting their activation or inhibition. There are

many mechanisms of translational control; three of them are predominant in higher eukaryotes. The first mechanism acts on the formation of the ternary complex (eIF2, GTP, Met-tRNA). eIF2 hydrolyses GTP to GDP and dissociates from the mRNA, allowing binding of 60S ribosomal subunit. eIF2α upon phosphorylation at Ser51 acts as a negative regulator of initiation of translation by inhibiting the exchange of GDP for GTP and thus formation of ternary complex (Costache et al., 2012).

A second regulatory mechanism involves PABP. PABP enhances translation as it bridges the 3'-terminal poly (A) tail of mRNA and eIF4G by binding to both and thereby circularizing mRNA (Kahvejian et al., 2001). In mammals, two proteins interact with PABP: PAIP2A (PABP Interacting Protein 2A) and PAIP2B. Both proteins inhibit translation by removing PABP from the poly (A) tail (Berlanga et al., 2006).

A third level of regulation of protein synthesis occurs through a family of inhibitory proteins, 4E-BPs. This family is composed of three members, 4E-BP1, 4E-BP2 and 4E-BP3. 4E-BPs are capable of inhibiting cap-dependent initiation (Raught and Gingras, 1999). They compete with eIF4G for binding to eIF4E and hinder the assembly of eIF4F complex (Haghighat et al., 1995). The activity of 4E-BPs is determined by their phosphorylation state. Hypophosphorylated 4E-BPs bind to eIF4E and inhibit translation initiation. Upon phosphorylation on several sites, they dissociate from eIF4E, a functional eIF4F complex is assembled and initiation is promoted (Raught and Gingras, 1999).

Control of protein synthesis is also achieved by *trans* RNA–Binding Proteins (RBPs) or non-coding RNAs (ncRNAs), microRNAs (miRNAs) which bind to the structural elements of mRNAs such UTRs and can either repress or activate translation of these transcripts (Fabian et al., 2010; Imig et al., 2012). Furthermore, *cis*–acting elements of the transcripts such as upstream open reading frames (uORFs) can directly repress the translation of the mRNAs that they belong to, by interacting with ribosomes (Somers et al., 2013).

1.3 eIF4E-Binding Proteins (4E-BPs)

1.3.1 Activity and tissue distribution of 4E-BPs

4E-BP1 and 4E-BP2 were identified as eIF4E-binding proteins by Far-Western interactions (Pause et al., 1994) whereas 4E-BP3 was identified later (Poulin et al., 1998). The three members of the family specifically inhibit eIF4E-dependent translation *in vitro* and *in vivo* by impeding the formation of eIF4F complex, which is essential for the recruitment of ribosome to the mRNA (Pause et al., 1994). Particularly, they compete with eIF4G for binding to the convex dorsal surface of eIF4E (Mader et al., 1995). Interestingly, the interaction of 4E-BPs and eIF4E is based on two motifs instead of one that is required for eIF4E-eIF4G interaction. These motifs are the canonical ^{54}YXXXXLΦ^{60} and the ^{78}IPGVT^{82} site (Lukhele et al., 2013). Figure 1.2 (A) shows the percentage of sequence identity between 4E-BPs. Despite the fact that all three 4E-BPs repress cap-dependent translation (Pause et al., 1994), they exhibit different tissue expression levels, as Figure 1.2 (B) indicates. 4E-BP1 is highly expressed in adipose tissue and muscle whereas 4E-BP2 is abundant in the brain (Banko et al., 2005; Tsukiyama-Kohara, 2001). Moreover, RNA and protein expression of 4E-BP1 and 4E-BP2 differs within different brain structures, as Figure 1.2 (C) shows, indicating that 4E-BP2 is the prevailing isoform in the brain (Banko et al., 2005; Tsukiyama-Kohara, 2001).

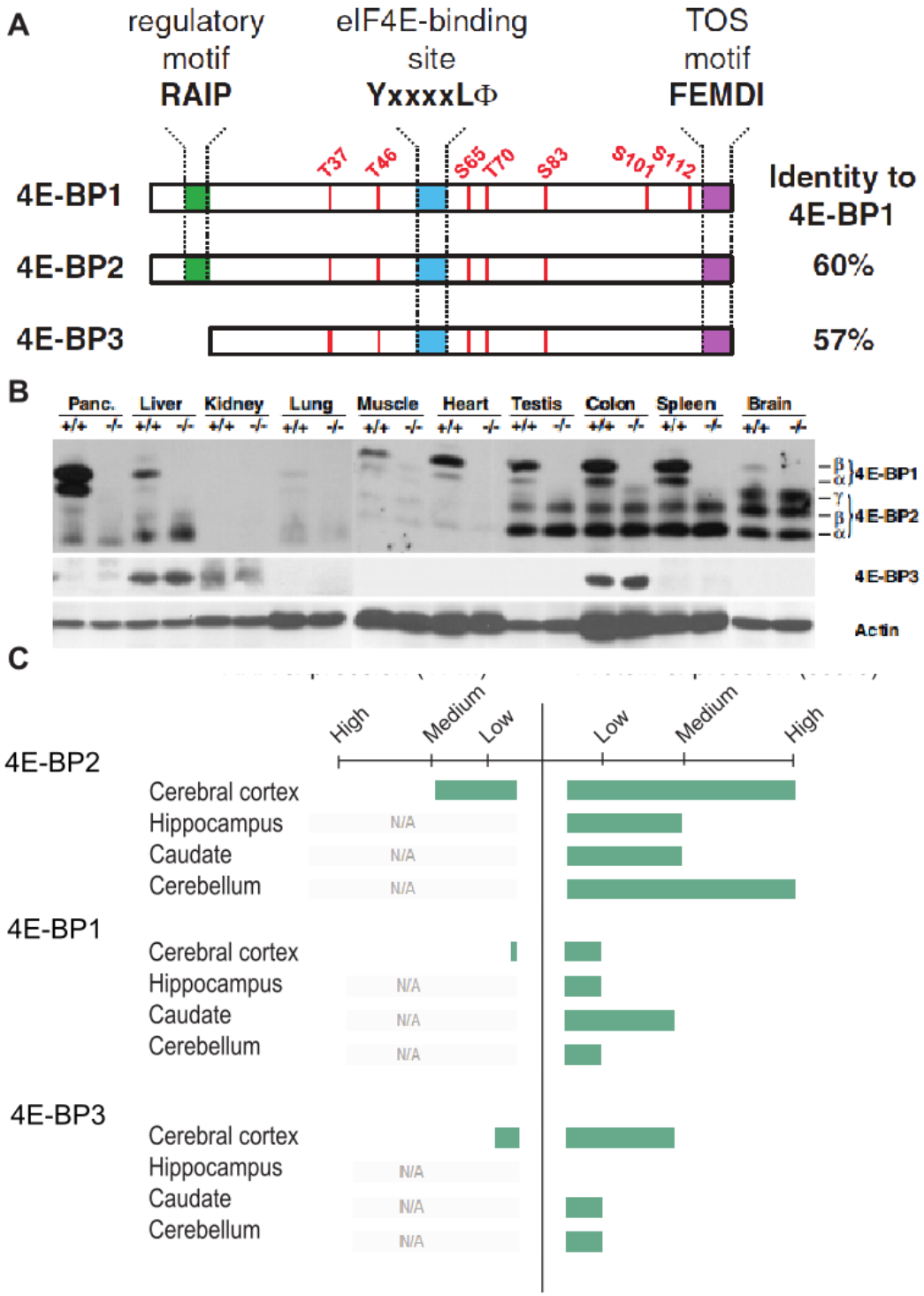

Figure 1.2 The three 4E-BPs show a high percentage (more than 50%) of primary sequence but differ in their RNA and protein tissue expression.

A. Schematic of the major domains in 4E-BPs: regulatory domains (RAIP), mTOR phosphorylation sites [Threonine (T), Serine (S) residues], eIF4E binding site and Raptor binding domain [containing the TOS (TOR signalling) motif] (Martineau et al., 2013). B. Western blot of 4E-BPs in different tissues from *Eif4ebp1* (+/+) and (-/-) mice (Tsukiyama-

Kohara, 2001). C. RNA and protein expression of 4E-BP1 and 4E-BP2 in different brain structures (The Human Protein Atlas).

1.3.2 Structure of 4E-BPs

4E-BPs belong to the family of intrinsically disordered proteins (IDPs), thus they lack stable secondary and tertiary structure and contain intrisically disordered regions (IDRs). They form dynamic interactions to mediate their biological role and may undergo a disorder-to-order transition when they interact with proteins (Lukhele et al., 2013). 4E-BPs are small polypeptides (100-120 amino acids) unstructured in solution. However, they gain alpha helical structure when they are tethered to eIF4E (Tomoo et al., 2005). Furthermore, they are remarkably stable to heat or acid as their original name denotes (PHAS, phosphorylated heat and acid-stable protein regulated by insulin) (Blackshear et al., 1982). Structure of 4E-BPs is discussed in more detail in Chapter 4.

1.3.3 Regulation of activity

Different extracellular stimuli affect translation by changing the phosphorylation state of specific serine/threonine residues of 4E-BPs. Figure 1.2 (A) illustrates the phosphorylation sites (red) that are present in each form and the major domains/motifs on their sequences. Insulin stimulation of rat adipocytes evokes phosphorylation of 4E-BP1 (Blackshear et al., 1982; Wang et al., 2007). Moreover, hormones, growth factors, cytokines, G-protein coupled receptor ligands and adenovirus infection induce phosphorylation of 4E-BP1 whereas heat shock in certain cell types and infection with poliovirus decrease its phosphorylation (Kleijn et al., 1998). Similarly, various stress stimuli differently affect phosphorylation of 4E-BP2 and thereby initiation of translation. Cerebral ischemia and ischemia-reperfusion injury induce phosphorylation and dephosphorylation of 4E-BP2 in Thr37/46, respectively (Ayuso et al., 2015).

1.3.4 Phosphorylation of 4E-BPs

The phosphorylation of 4E-BPs is regulated by an evolutionarily conserved Ser/Thr kinase termed mTOR (mammalian/mechanistic Target Of Rapamycin). mTOR has a vital role in regulating protein synthesis as well as cell growth and metabolism through control of anabolic and catabolic processes in response to

nutrients and growth factors (Laplante and Sabatini, 2013). mTOR forms two functional complexes, mTORC1 and mTORC2. Each complex consists of different components and has different activity (mTOR signalling pathway is discussed in detail in section mTOR).

Upon activation through different stimuli, mTORC1 phosphorylates residues Thr37 and Thr46 in human 4E-BPs. Interestingly, the phosphorylation of these sites acts as a priming event for the phosphorylation of Ser65 and Thr70. These phosphorylation sites are conserved between the three mammalian 4E-BPs and the lower eukaryotes (Gingras et al., 2001) and exhibit different sensitivity to stimulation. The Thr37/Thr46 residues can be phosphorylated even upon serum starvation, thus absence of growth factors. Conversely, serum-stimulation evokes phosphorylation of residues Thr70 and subsequently Ser65 which are proximal to C-terminus and close to the eIF4E-binding site (Gingras et al., 2001). Alterations on the phosphorylation levels of 4E-BPs do not affect levels of global protein synthesis but only translation of ‘’eIF4E-sensitive’’ mRNAs (Colina et al., 2008; Dowling et al., 2010; Lynch et al., 2004; Petroulakis et al., 2009). Those mRNAs encode proteins that play major roles in proliferation and survival and their translation is selectively stimulated by the mTORC1 complex (Dowling et al., 2010).

Phosphorylated 4E-BPs dissociate from eIF4E, allowing the formation of eIF4F complex (Pause et al., 1994). The hierarchical phosphorylation of 4E-BPs is critical for their activity (Gingras et al., 2001). Hypophosphorylated 4E-BP1 at Ser65 and/or Thr70 is still bound to eIF4E, implying that only hyperphosphorylated 4E-BPs dissociate from eIF4E (Gingras et al., 2001). Importantly, hypophosphorylated 4E-BPs preferably inhibit the translation of mRNAs with unstructured 5’ UTRs and are GC-rich (Gingras et al., 1999). For efficient phosphorylation of 4E-BPs, two motifs are required in their protein sequence, the RAIP (Arg-Ala-Ile-Pro) in the NH_2- and the TOR signalling motif (TOS, Phe-Glu-Met-Asp-Ile) in the COOH- terminus region of protein (Choi et al., 2003). Figure 1.2 (A) indicates the position of both motifs on the primary sequence of 4E-BPs. 4E-BP3 lacks RAIP motif. The TOS motif is essential for binding and interaction with Raptor, a component of mTORC1 complex, that recruits substrates to mTOR for phosphorylation (Nojima et al., 2003). Figure 1.3 delineates the activity of hypophosphorylated 4E-BP2, inhibiting the initiation of translation (left panel) and hyperphosphorylated 4E-BP2, allowing the assembly of eIF4F complex and translation initiation (right panel).

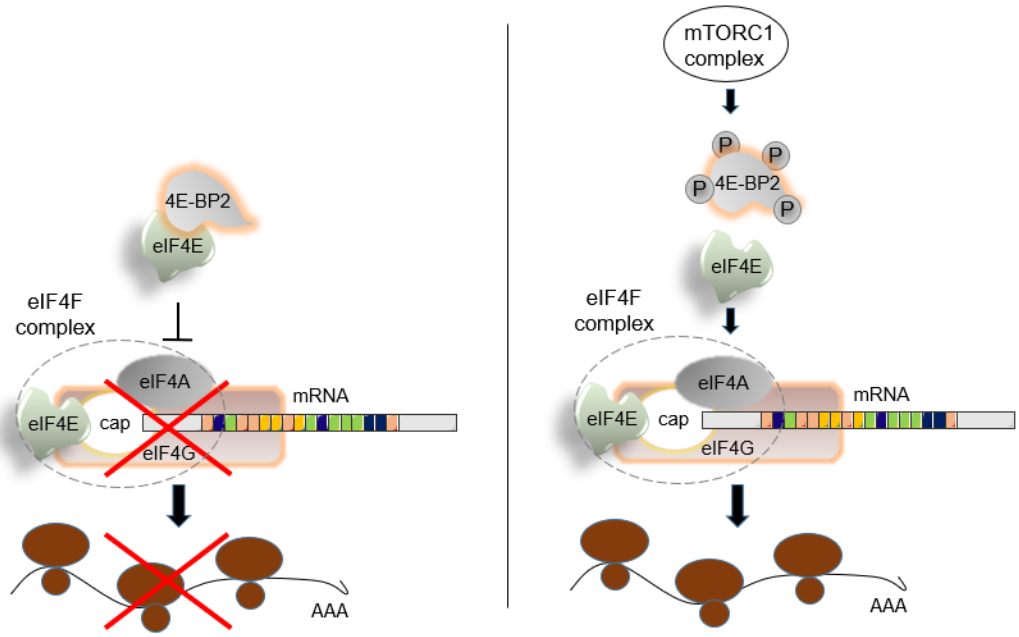

Figure 1.3 4E-BP2 is a repressor of cap-dependent translation in the brain.

Hypophosphorylated 4E-BP2 binds to eIF4E and prevents the assembly of eIF4F complex, thus inhibiting the initiation of protein synthesis. Upon mTOR phosphorylation, 4E-BP2 dissociates from eIF4E, allowing the formation of eIF4F complex and initiation of protein synthesis.

1.4 mTOR

1.4.1 mTORC1 and mTORC2

The mTOR kinase forms two distinct complexes, mTORC1 and mTORC2. mTORC1 complex is composed of mTOR; Raptor which acts as a scaffolding protein by recruiting substrates to the complex; PRAS40 (Proline-Rich AKT substrate 40kDa) and Deptor, both inhibiting the complex; mLST8 with yet unknown function; and tti1 and tel2, both scaffolding proteins, controlling the stability of the complex. mTORC2 consists of mTOR; Rictor that is another scaffolding protein; mSin1 which regulates the assembly of the complex and interaction with SGK1; protor1/2 that increases mTORC2 – dependent activation of SGK1 and mLST8; Deptor, tti1 and tel2 (Laplante and Sabatini, 2012). mTORC1 regulates various cellular processes such as growth, cell cycle, metabolism; is responsive to amino acids, energy levels, growth factors, oxygen and is blocked by rapamycin. On the contrary, mTORC2 controls metabolism, cell survival and cytoskeletal organization; is responsive to growth factors but is not inhibited by rapamycin (Laplante and Sabatini, 2013).

1.4.2 Upstream and downstream of mTOR

The activation of mTORC1 is dependent on various stimuli (they are described in the previous paragraph). In response to these stimuli, RTKs (Receptor Tyrosine Kinases) are activated which in turn activate PI3K (Phosphoinositide-3-Kinase). PI3K converts PIP2 (Phosphatidylinositol 4,5-bisphosphate) into PIP3 (Phosphatidylinositol-3,4,5-triphosphate) whereas PTEN (Phosphatase and tensin homolog) catalyzes the opposite reaction. PDK1 (Phosphoinositide-dependent protein kinase1) and AKT/PKB (Protein kinase B) bind to PIP3, allowing phosphorylation and activation of AKT. In addition, mTORC2 complex acts on the hydrophobic motif of AKT by phosphorylating it. Three successive events are part of the cross-talk between mTORC1 and mTORC2 complexes. Firstly, phosphorylated AKT inhibits TSC2 (Tuberous Sclerosis Complex 2) by phosphorylating it in various sites. The inhibition of TSC2 allows activation of Rheb (Ras homolog enriched in brain) which in turn activates mTORC1. Active mTORC1 complex phosphorylates 4E-BPs, allowing their dissociating from eIF4E and initiation of translation (Topisirovic and Sonenberg, 2011). A second target of mTORC1 complex are S6 kinases (S6K1

and S6K2). Upon activation, they phosphorylate ribosomal protein S6 (rpS6) which has been associated with enhanced rate of translation (Topisirovic and Sonenberg, 2011). mTORC1 preferentially regulates the translation of mRNAs that possess extensive secondary structure at their 5' UTR or are rich in pyrimidine bases at their 5' UTR (TOP mRNAs) (Ruvinsky and Meyuhas, 2006).

The PI3K/Akt pathway is not the only pathway that can stimulate mTORC1 complex. Other kinases that can also activate mTORC1 complex are the serine/threonine kinase 11/LKB1/AMP-kinase (LKB1/AMPK) (Topisirovic and Sonenberg, 2011).

The other pathway that plays a fundamental role in translational control is the Ras/MAPK pathway. This pathway can be activated through G protein–coupled receptors (GPCRs), protein kinase C (PKC) and RTKs (Topisirovic and Sonenberg, 2011), and encompasses two different signaling pathways that result in the phosphorylation of eIF4E. Firstly, stimuli such as growth factors, hormones and phorbol-esters activate Ras GTPase which in turn stimulates Raf kinase, an initial GTPase-regulated kinase (MAPKKK). Then, a subsequent activation of intermediate kinases occurs that activate the effector extracellular signal-regulated kinases 1 and 2 (ERK 1 and 2). Conversely, upon stimulation of Ras due to different cellular stresses, a cascade of successive activation events engenders activation of p38 MAPKs. Both ERK1 and 2 and p38 MAPKs activate MNKs (MAPK signal–integrating kinases 1 and 2) that phosphorylate eIF4E (Topisirovic and Sonenberg, 2011).

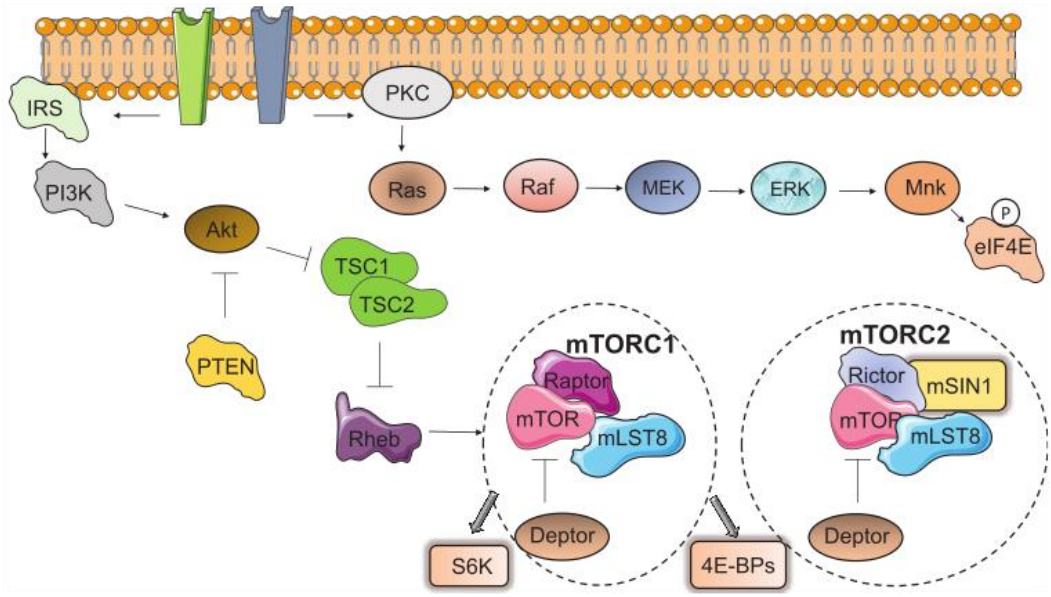

Figure 1.4 The mTOR signalling pathway.

mTOR kinase is part of two distinct complexes with different components: mTORC1 and mTORC2. Various stimuli such as amino acids and growth factors activate mTORC1 complex through PI3K/AKT pathway (Huber et al., 2011).

1.5 Translational Control in learning and memory

Translational control refers to changes in the rate of translation of mRNA (Gkogkas et al., 2010). The different mechanisms of translational control can induce rapid changes in protein amounts, according to the needs of a cell at a specific time (Schwanhausser et al., 2011). Furthermore, translational control endows spatially distinct protein synthesis since many physiological processes require specific proteins to be synthesized at specific sites (e.g. dendritic neuronal translation) (Rangaraju et al., 2017). Translational control in neurons is fundamental for controlling mnemonic processes through modification of synaptic connections named as synaptic plasticity. Therefore, complex behaviours such as learning and memory are dependent on protein synthesis. Specifically, long-term memory requires *de novo* protein synthesis, underlying the active role of translation in the mechanisms of memory storage (Gkogkas et al., 2010).

Since this thesis is focused on a key modulator of protein synthesis, 4E-BP2, it is important to outline the characteristics of knock out models for 4E-BP2. *Eif4ebp2* -/- mice display normal spontaneous locomotor activity compared to *Eif4ebp2* +/+ mice when tested in an open field test (Banko et al., 2007). However, checking the overall activity on the rotating rod task, *Eif4ebp2 -/-* mice exhibit reduced performance regarding motor coordination, balance and learning compared to *Eif4ebp2* +/+ mice (Banko et al., 2007). Moreover, after testing their anxiety-like behaviour using a light/dark test and a step-through passive avoidance task, *Eif4ebp2 -/-* mice show a significant longer latency to cross into the dark chamber on the training day, albeit overall there are no differences in the number of crosses compared to *Eif4ebp2* +/+ mice (Banko et al., 2007). Interestingly, after checking working memory on a T-maze of spontaneous alternation, *Eif4ebp2 -/-* mice exhibit a reduced alternation rate, choosing left or right arms with equal frequency compared to their WT counterparts, denoting that working memory requires 4E-BP2 (Banko et al., 2007). Moreover, 4E-BP2 KO mice demonstrated enhanced memory for conditioned taste aversion, avoiding in a higher frequency saccharin and NaCl solutions than WT mice (Banko et al., 2007). Thereby, 4E-BP2 is a key mediator of translational control in the brain and, thus of memory formation and learning processes (Banko et al., 2007; Banko et al., 2005). Formation of memory requires new protein synthesis which is pivotal for synaptic plasticity. Two major forms of synaptic plasticity, LTP (Long-Term Potentiation) and LTD (Long-Term Depression) are different *in Eif4ebp2* -/- mice

compared to Wild Type (WT). Specifically, *Eif4ebp2* -/- mice show increased DHPG-induced mGluR-LTD compared to WT mice (Banko et al., 2006). Furthermore, rapamycin inhibited DHPG-induced eIF4E complex formation in WT slices but not in slices from 4E-BP2 KO mice (Banko et al., 2006). This finding underlines the importance of 4E-BP2 during mGluR-LTD. In contrast to LTD, LTP-inducing stimulation increases assembly of eIF4F complex in both WT and 4E-BP2 KO mice, distinguishing the engagement of 4E-BP2 and cap-dependent translation between LTP and DHPG-LTD (Banko et al., 2006). Although basal synaptic transmission levels are not differentiated between *Eif4ebp2* -/- and WT mice, stimuli that induce early-phase LTP to WT mice, elicit late-phase LTP to *Eif4ebp2* -/- mice (Banko et al., 2005). Lastly, Eif4ebp2 -/- mice display deficits in spatial learning and memory on a Morris water maze and a conditioned fear paradigm (Banko et al., 2005). Importantly, 4E-BP2 KO mice exhibit autistic-like behaviours since they are characterized by social interaction deficits on a three-chamber social test, a self-grooming test and a marble-burying test (Gkogkas et al., 2013). Also, this autistic-like behaviour was associated with increased translation of neuroligins in 4E-BP2 KO mice compared to WT mice and is rescued after inhibiting eIF4E-eIF4G interaction (Gkogkas et al., 2013). Therefore, there is increasing evidence to support the importance of 4E-BP2 in multiple brain functions.

1.5.1 Translational control and synaptic plasticity

Short-term memory (STM) endures for seconds or minutes whereas long-term memory (LTM) can last for hours, days or years. LTM depends on protein synthesis to such an extent that synthesis of specific proteins determines if a mnemonic process will be stored transiently or permanently in the brain (Buffington et al., 2014). In *ex vivo* hippocampal slices, induction of late-phase LTP was dependent on protein synthesis but early-phase LTP was not (Kandel, 2001). In agreement with this finding, in hippocampal slices from mice with reduced phosphorylation of eIF2α [either lacking GCN2 (General Control Nonderepressible 2) kinase that phosphorylates eIF2α or lacking the phosphorylation site of eIF2α which was converted to alanine], the threshold in which the late-LTP was inducted was reduced in many behavioural tasks compared to slices from WT mice (Morris water maze, associative fear conditioning, conditioned taste aversion) (Costa-Mattioli et al., 2005; Costa-Mattioli et al., 2007). Therefore, changes in key regulators of translational control such as eIF2α have an

impact on long-lasting modifications of synaptic strength (Costa-Mattioli et al., 2009). Similarly, activation of metabotropic glutamate receptors induced LTD which also required protein synthesis (Huber et al., 2000). This translation – dependent memory storage will either strengthen existing synapses (LTP) or form new synaptic connections. Interestingly, certain types of memory are associated with weakening synaptic connections (LTD) (Malenka and Bear, 2004). Thus, induction of late–phase LTP and metabotropic GluRs–dependent induced LTD, both require protein synthesis.

1.5.2 Local protein synthesis and synaptic plasticity

The presence of the components of translational machinery in dendrites and dendritic spines (Steward and Schuman, 2001; Sutton and Schuman, 2006) was crucial for the discovery that long–lasting plasticity could be induced by local protein synthesis independently from transcription in the soma (Costa-Mattioli et al., 2009). Specifically, BDNF (Brain-derived neurotrophic factor) could engender LTP in pre- or postsynaptic pyramidal neurons that were de-attached from their somas and translation inhibitors could inhibit that LTP (Kang and Schuman, 1996). Another process that is regulated by local protein synthesis is stabilisation of new synapses during learning in *Aplysia* (Casadio et al., 1999; Martin et al., 1997). 5 min application of serotonin activates local translation and promotes stabilisation of new synapses even 72 h after the signal. Inhibition of translation 24 h after the serotonin application can remove new synapses (Miniaci et al., 2008). It is not clear yet whether this mechanism responsible for the stabilisation involves CPEB (Cytoplasmic Polyadenylation Element Binding protein) and/or increased translation of TOP mRNAs (Costa-Mattioli et al., 2009). Therefore, long-term synaptic plasticity and stabilisation of new synaptic connections is strongly dependent on local protein synthesis at synapses.

1.5.3 Local protein synthesis and glutamate receptors

Glutamate is the predominant excitatory neurotransmitter in the mammalian CNS (Central Nervous System) and is involved in the developmental mechanisms that drive the growth, branching, chemotropic turning, filopodial motility of axons and synaptogenesis that occurs when axons reach their target areas (Hsu et al., 2015; Schmitz et al., 2009; Tashiro et al., 2003; Zheng et al., 1996). During development,

glutamate mediates all these effects through activation of AMPA (α-amino-3-hydroxy-5-methyl-4-isoxazolepropionic acid) receptors and upregulation of protein synthesis in whole neurons and axons disconnected from their somas (local protein synthesis). Similarly, BDNF can also increase translation in these axons (Hsu et al., 2015).

Upon glutamate stimulation, AMPA receptors get activated in axons and Ca^{2+} can flow through AMPA Ca^{2+}- permeable receptors and voltage-gated Ca^{2+} channels, entailing their involvement in the upregulation of protein synthesis (Hsu et al., 2015). Moreover, metabotropic glutamate receptors 1 (mGluR1) and subsequent activation of TPRC (Transient Receptor Potential-Canonical) channels as well as group 2 mGluRs, play also a role in this glutamate–stimulated enhancement of local protein synthesis. Interestingly, increased translation in axons upon glutamate stimulation was abolished by EGTA that chelates extracellular Ca^{2+} and was partly inhibited by W7 treatment or rapamycin, blocking calmodulin or mTOR signalling, respectively. Thus, extracellular Ca^{2+}, calmodulin and mTOR signalling also participate in the mechanism of enhancement of translation in axons upon glutamate and BDNF stimulation (Hsu et al., 2015).

However, in whole neurons, global translation is affected by NMDA (N-methyl-D-aspartate) but not AMPA receptors but the reasons for this difference are still unclear. It could be due to the presence of extrasynaptic glutamate receptors in severed axons whereas in whole neurons there are both synaptic and extrasynaptic receptors. Moreover, the difference could be due to artificial effects of the chip–assay used in these experiments or it can be an indication that the mechanisms for increase of protein synthesis in whole neurons and axons differ significantly. Figure 1.5 shows the activated signalling pathways upon glutamate and BDNF stimulation (Hsu et al., 2015).

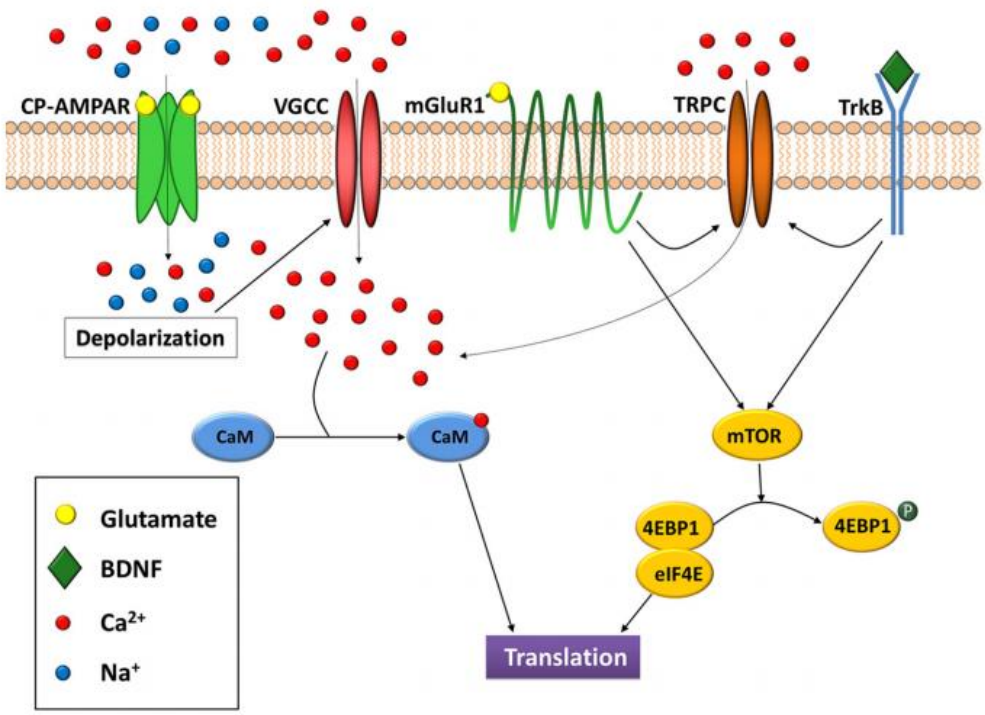

Figure 1.5 Glutamate and BDNF stimulation increase translation through specific signalling pathways.

AMPA receptors get activated in axons and Ca^{2+} can flow through AMPA Ca^{2+}- permeable receptors and voltage-gated Ca^{2+} channels. Moreover, metabotropic glutamate receptors 1 (mGluR1), TPRC channels and group 2 mGluRs are activated upon glutamate stimulation, (Hsu et al., 2015).

AMPA receptors are also involved in another mechanism responsible for upregulation of local protein synthesis through activation of D1/D1 dopaminergic receptors in hippocampal dendrites (Smith et al., 2005). Specifically, GluR1 is one protein upregulated through this mechanism along with enhanced incorporation of GluR1 receptors at synaptic sites and increased frequency of miniature synaptic events, relating local translation with synaptic plasticity after activation of dopamine receptors (Smith et al., 2005). Another subunit of AMPA receptors, GluR2, is also translated in isolated hippocampal dendrites and incorporated into the plasma membrane (Rebola et al., 2008) upon stimulation with DHPG [(RS)-3-5-dihydroxyphenylglycine] (Kacharmina et al., 2000).

NMDA receptors belong to the family of ionotropic glutamate receptors as AMPA receptors and are also key regulators of long-term synaptic plasticity at the synapses (Derkach et al., 2007; Santos et al., 2009). They are composed of two GluN1 (1A-4A) and two GluN2 (2A-2D) subunits and their expression is differentially regulated during development (Traynelis et al., 2010). Their expression and insertion into the membrane (surface expression) is dependent on synaptic activity similarly to AMPA receptors (Grosshans et al., 2002; Kwon and Castillo, 2008). GluN2A mRNA is localized to the dendrites along with the protein complex that regulates its expression: CPEB [(Cytoplasmic Polyadenylation Element)–Binding protein] which binds to CPE of 3' UTR of the mRNA, Gld2, a poly(A) polymerase, and Ngd (neuroguidin), an eIF4E-binding protein (Udagawa et al., 2012). Synaptic stimulation with glycine induces CPEB complex-dependent local translation of GluN2A mRNA and insertion of GluN2A–containing NMDA receptors into the dendritic membrane of hippocampal neurons (Swanger et al., 2013).

NMDA receptors are associated with activity–dependent Ca^{2+} entry into neurons and activation of different signalling pathways through generation of secondary messengers such as cAMP, IP_3 and DAG (Diacylglycerol) (Dell'Acqua et al., 2006; Sabatini et al., 2002; Vanhouttey and Bading, 2003). Depending on which signalling pathway gets activated, the outcome of NMDA receptor activation on protein synthesis is different. cAMP, IP_3 and DAG will activate cAMP–dependent kinase (PKA) and protein kinase C (PKC) and subsequently the MAPK pathway (Coogan et al., 1999; Cullen and Lockyer, 2002) that will result in phosphorylation of eIF4E whose function on translation is not clear (Kleign et al., 1998; Raught and Gingras, 1999; Scheper and Proud, 2002). PKA will also activate eEF2 kinase which will inhibit general translation elongation by phosphorylating eEF2, and concomitantly will increase translation of TOP mRNAs (Scheetz et al., 2000; Sutton et al., 2007). Influx of Ca^{2+} will also activate Ca^{2+}/calmodulin–dependent protein kinase II (CaMKII) and Aurora kinase. These kinases phosphorylate CPEB that will result in translation of specific mRNAs that contain CPEs along with the involvement of PABP and eIF4G (Cao and Richter, 2002). Therefore, NMDA receptors also play a major role in regulating local protein synthesis that is dependent on synaptic activity.

1.6 The Ubiquitin Proteasome system

1.6.1 Overview of the Ubiquitin Proteasome system

Protein are continuously synthesized and degraded to maintain cellular function and survival and this process is named ‘’protein turnover’’ (Alvarez-Castelao and Schuman, 2015). Local regulation of protein content can be achieved either through activation of different signalling pathways that generate protein–protein interactions, protein trafficking and posttranslational modifications or with precise regulation of protein turnover though local translation and degradation (Tsai, 2014). The Ubiquitin–Proteasome System is a key mediator of intracellular protein degradation (Hamilton and Zito, 2013). It has also been characterised as an indispensable molecular event for critical neuronal processes such as long–term potentiation, homeostatic plasticity and acute regulation of neurotransmitter release (Hamilton and Zito, 2013) that require fast information processing. Protein degradation is adapted rapidly to changes of synaptic plasticity, positioning proteasome directly dependent on neural activity state (Hamilton and Zito, 2013). Stimulation or inhibition of synaptic activity precisely regulates proteasome activity (Bingol and Schuman, 2006; Bingol et al., 2010; Djakovic et al., 2009) and its subcellular localization (Bingol and Schuman, 2006; Shen et al., 2007) within minutes.

Ubiquitination is the process where ubiquitin, a 76-residue molecule, is tagged on proteins as single moieties or polyubiquitin chains, targeting these substrates for protein degradation by a large protease complex, the 26S proteasome (Ding and Shen, 2008; Hamilton and Zito, 2013). However, ubiquitination also regulates other major cellular events such as intracellular trafficking, endocytosis, regulation of protein activity and lysosomal degradation (Nandi et al., 2006; Woelk et al., 2007) depending on which specific lysine residues of ubiquitin will create a polyubiquitin chain and the subsequent three–dimensional structure (Woelk et al., 2007). The minimal requirement for proteasomal degradation is a ubiquitin chain of four molecules linked at the lysine at position 48 (K48)(Thrower et al., 2000).

1.6.2 Structure of the Proteasome

In mammals, proteasomes are mainly cytosolic but can also be found in the plasma membrane, ER, cytoskeletal elements and nucleus where they also degrade

proteins (Nandi et al., 2006). The 26S proteasome is composed of a 20S core particle surrounded by at least one 19S regulatory particle (van Tijn et al., 2008). The 20S core subunit consists of four stacked rings, two inner and two outer, forming a barrel structure that has proteolytic activity. Each inner ring is composed of seven β-subunits and each outer of seven α–subunits (van Tijn et al., 2008). The proteolytic activity is designated into chymotrypsin-like, trypsin-like and peptidyl-glutamyl-peptide, hydrolysing activity in the β 5, β 2 and β 1 subunits, respectively (van Tijn et al., 2008). The 19S regulatory complex is composed of a structure attached to the 20S core, forming the base part, and another structure on top of the base made up of eight different subunits at least. The base structure consists of ATPases and non-ATPase subunits. The 19S regulatory complex is responsible for substrate recognition and removal of ubiquitin chain, each one attributed to specific subunits (van Tijn et al., 2008). Other functions that have been attributed to this regulatory complex are unfolding of substrates and opening of orifices to enable the entrance of the substrates into the barrel structure (Ciechanover; and Brundin, 2003).

1.6.3 The mechanism of the Ubiquitin Proteasome System

Ubiquitination takes place in three steps along with the active participation of three enzymes, each one catalysing a different reaction. Firstly, an E1–activating enzyme is charged with ubiquitin, hydrolysing ATP (Ding and Shen, 2008; Hamilton and Zito, 2013). A covalent bond is shaped between the C-terminal glycine of ubiquitin and active–site cysteine of the enzyme, activating ubiquitin (Ding and Shen, 2008). Then, Ubiquitin is transferred and coupled to an E2 ubiquitin conjugating enzyme through a new thioester bond with G76 of Ubiquitin (Ding and Shen, 2008). The newly formed Ub–E2 complex charges the attached Ubiquitin through its carboxy–terminal glycine to the target protein, interacting with an E3 ubiquitin ligase (Hamilton and Zito, 2013).

There are only two E1 (Ding and Shen, 2008), 30 E2 and hundreds of E3 enzymes that constitute the largest family of ubiquitin ligases (Hamilton and Zito, 2013; Pickart, 2001), conferring ubiquitination specificity (Hamilton and Zito, 2013; Pickart, 2001) and positioning the third ubiquitination step as the rate – limiting one (Tsai, 2014). Specifically, there are two categories of E3 enzymes (Pickart, 2001) based on the structural motifs that they share (Ciechanover; and Brundin, 2003): HECT (Homologous to E6-associated protein C-Terminus) and RING (Really

Interesting New Gene) domain (Pickart, 2001). A third class of E3 enzymes was identified, named U-box-containing E3 enzymes (van Tijn et al., 2008).

Although addition of single molecules of ubiquitin is catalysed by a similar mechanism as polyubiquitination, these substrates are mostly catalysed by the lysosome/vacuole (Ciechanover; and Brundin, 2003). Polyubiquitin chains will stem from additional ubiquitin moieties that may be bound to one of the 7 internal lysines of ubiquitin (Hamilton and Zito, 2013). The targeting motif usually is exposed to enable binding of a specific ligase and can be a single amino acid, a sequence or a domain. Sometimes, recognition of the substrate by E3 enzymes is not sufficient to enable ubiquitination and either the substrate or the E3 ligase must undergo specific posttranslational modifications in response to external cues to be active and allow substrate recognition (Ciechanover; and Brundin, 2003). Modifications on either the enzyme, changing its stability, or on the substrate, modulating its binding affinity for other ligases, occur through Ubiquitin-Like (UBL) proteins. UBLs require E1, E2 and possibly E3 enzymes that catalyse a similar mechanism to ubiquitination. The specificity of ubiquitination depends also on the stability of other auxiliary proteins. Molecular chaperones, transcription factors, kinases, DNA sequences all play a critical role in the recognition of the substrate (Ciechanover; and Brundin, 2003).

Ubiquitylated substrates need to come to proximity with the proteasome using different mechanisms since the E3 enzymes do not reside at the proteasome (Tai and Schuman, 2008). The 19S subunits RPT5 and RPN10 can act as scaffolding proteins to bring together the proteasome and the substrate as they can bind polyubiquitin (Hartmann-Petersen et al., 2003). In PSDs (Postsynaptic densities), molecular chaperones such as HSP40, HSP70 and chaperone – associated E3, CHIP, have been identified, implying that they serve as docking sites for ubiquitylated postsynaptic proteins (Li et al., 2004).

Apart from the addition of ubiquitin, the ubiquitination process is also regulated by the removal of ubiquitin moieties or chains by deubiquitinases (Hamilton and Zito, 2013). Specifically, while the ubiquitinated substrate is degraded by the proteasome, cleaving it in short peptides, deubiquitinases release ubiquitin which then reuse for new ubiquitination cycles (Ding and Shen, 2008). Deubiquitinases confer many functions by recycling ubiquitin moieties. They can rescue target proteins from degradation by removing the polyubiquitin chain at the entrance of proteasome or recycling ubiquitin molecules by disassembling free polyubiquitin chains (van Tijn et al., 2008).

Following proteasomal degradation, either short peptides are released from the proteasome and further processed by cytosolic amino- and carboxypeptidases or truncated products are generated that are then active like in the case of NF-κB (Nuclear Factor kappa-light-chain-enhancer of activated B cells) (Ciechanover; and Brundin, 2003). Moreover, a small fraction of these released peptides is transferred through the endoplasmic reticulum (ER) membrane and presented to cytotoxic T cells, following binding to the MHC class I molecules (Ciechanover; and Brundin, 2003). The 26S proteasome recognises and destructs only ubiquitinated substrates. Only in the case of the polyamine synthesizing enzyme ornithine decarboxylase (ODC), it degrades the substrate without prior ubiquitination but after its association with another protein, named antizyme (Ciechanover; and Brundin, 2003).

Proteasome degradation has different regulatory mechanisms acting on different steps of the process: subunit composition, proteolytic activity, subcellular localization and interactions of UPS with other proteins, all dependent on neuronal activity (Alvarez-Castelao and Schuman, 2015). Intriguingly, NMDA activation disassembled the 26S proteasome and lowered its proteolytic activity (Tai et al., 2010). Moreover, after TTX inhibition of voltage – gated sodium channels, the degradation of a chimeric proteasome substrate decreased whereas after bicucculine degradation increased (Djakovic et al., 2009). On the other hand, proteasome inhibitors recruited CamKII to phosphorylate the proteasome in response to glutamate with the concomitant block of spine outgrowth (Hamilton et al., 2012).

1.7 Protein synthesis and Proteasome degradation – Half-life of proteins

Protein turnover is highly dynamic, even when neurons are under basal activity, with both protein synthesis and protein degradation working concomitantly to achieve a fine-tuned renewal of the protein pool (Alvarez-Castelao and Schuman, 2015). Protein synthesis and proteasome degradation of synaptic proteins have been characterized as indispensable components of synaptic plasticity (Alvarez-Castelao and Schuman, 2015). Proteasomal inhibition with Lactacystin (Fonseca et al., 2006) or inhibition of protein synthesis with Anisomycin (Krug et al., 1984) disrupted hippocampal late LTP (Fonseca et al., 2006; Krug et al., 1984). Intriguingly, LTP was rescued after concomitant inhibition of both protein synthesis and degradation

(Fonseca et al., 2006). On the other side, synaptic activity can change the distribution of proteasomes within neurons. Specifically, increased synaptic activity leads to accumulation of proteasomes in dendritic spines (Bingol and Schuman, 2006). Apart from the proteasome, ubiquitination is also dependent on neuronal activity. Blockage of activity leads to decrease of polyubiquitinated protein in the PSD and induction of activity to an increase (Ehlers, 2003). Therefore, there are specific mechanisms that confer bidirectional control of protein content in local neuronal domains as in dendrites and axons (Steward and Schuman, 2003).

Key components of these regulatory mechanisms are polyribosomes that are synthesized in synapses (SPRCs, synapse – associated polyribosomes complexes), and signalling pathways, responsible for the regulation of local translation (Steward and Schuman, 2003). SPRCs have been found in non-spine and spine synapses, accosting postsynaptic sites and docking at the spine base, respectively (Steward et al., 1996). Activation of these signalling pathways is activity – dependent and can lead to translocation of the polyribosomes from the base to the spine head (Ostroff et al., 2002). The postsynaptic spine head is biochemically isolated from the dendrites and the translocation of molecules from the base to the head is activity – dependent (Bloodgood and Sabatini, 2005). In addition, after LTP stimulation, apart from the number of the polyribosomes, the size of the PSDs is larger, suggesting that local protein synthesis causes growth of PSDs (Ostroff et al., 2002). The number of SPRCs depends on the cell type and the developmental stage, reaching a high number during maximal synaptogenesis periods (Steward and Falk, 1986).

Local translation can be triggered after NMDA, mGluR, glutamate activation, activation of growth factor receptors (GFRs) and depolarization depending on the mRNAs (Steward and Schuman, 2003). Furthermore, regulation of dendritic translation can also be regulated by key signalling pathways as mTOR since major components as 4E-BP1 and 4E-BP2 have been found in dendrites (Steward and Schuman, 2003). Conversely, local degradation is also triggered by NMDA activation since recruitment of proteasomes is increased into spines after NMDA activation (Bingol and Schuman, 2006). Therefore, activity or neuronal stimulation does not have one whole effect on protein turnover but affects differently each process. Interestingly, even a single biological process is not affected towards one direction only (Alvarez-Castelao and Schuman, 2015).

Protein synthesis and degradation work together to maintain the required protein pool quantitatively and qualitatively (Alvarez-Castelao and Schuman, 2015).

Furthermore, their crosstalk is sometimes required for translational control of some protein. UPS degrades proteins – components of the translational machinery, regulating in this way protein synthesis (Alvarez-Castelao and Schuman, 2015).

Protein turnover and renewal of the proteome is also crucial for other neuronal functions apart from the main maintenance of proteins concentration in the cells (Alvarez-Castelao and Schuman, 2015). UPS also affects presynaptic neurotransmitter release by regulating the size of the vesicle pool and the Ca^{2+}-dependent vesicle release through SCAPPER (F-box/LRR-repeat protein 20), an E3 enzyme and its substrate RIM1 (Yao et al., 2007).

Brain proteome has been characterized with very slow protein half–lives, having an average lifetime of 9 days. This slow protein turnover rate emerges from stable brain–specific proteins and proteins expressed also in other tissues but exhibiting a slow turnover rate only in the brain (Price et al., 2010). However, a protein half–life can also be modified by the subcellular localization of the protein, the activity state and the developmental stage of the cell. Moreover, posttranslational modifications play a fundamental role in modulating protein stability (Alvarez-Castelao and Schuman, 2015).

Specifically, subcellular localization of the protein plays a critical role in determining its half – life (Dörrbaum et al., 2018). Membrane proteins associated with plasma membrane, ER and Golgi were characterized as short–lived proteins compared to mitochondrial proteins that were characterized as long–lived (Dörrbaum et al., 2018). Thus, different degradation mechanisms might be responsible for degradating cytosolic and membrane proteins (Tai and Schuman, 2008). Furthermore, molecular function also affects protein half–lives. Receptors and signalling molecules were shown to have short half–lives to endow rapid and fine–tuned regulation of synaptic plasticity (Dörrbaum et al., 2018).

1.7.1 Dendritic and axonal mRNAs

mRNAs that have been found to exhibit extensive dendritic localization encode for cytoplasmic, cytoskeletal, integral membrane and membrane–associated proteins. The subcellular localization varies between different cell types and different developmental periods. Some mRNAs are present during early development and absent from mature neurons (Steward and Schuman, 2003). Moreover, this dendritic localization is enhanced after depolarisation by KCl (Tiruchinapalli et al., 2003) or

neurotrophin treatment (Knowles and Kosik, 1997), denoting its dependence from neuronal activity and major signalling pathways that mediate synaptic responses (Steward and Schuman, 2003). Therefore, since the dendritic branch is capable of synthesizing and degrading proteins, owing translational machinery and UPS (Alvarez-Castelao and Schuman, 2015), and can be individually regulated by synaptic activity along with the associated synapses (Branco and Hausser, 2010), this cluster may be the fundamental computational neuronal unit (Alvarez-Castelao and Schuman, 2015).

Proteins encoded by dendritic mRNAs are components of key protein complexes for mediating postsynaptic responses such as CAMKII, Shank, Insp3 (Inositol trisphosphate), Arc (Activity-regulated cytoskeleton-associated**)**, assembling the NMDA receptor complex (Husi et al., 2000). However, it is not known whether the components (Knowles and Kosik, 1997) are synthesized and the complex is formed away from the synapse and then translocates into synaptic areas or the components replace molecules in existing synaptic complexes (Steward and Schuman, 2003). Different half-lives that have been found for protein components of the same complex (Ehlers, 2003) and presence of ribosomes–associated with the postsynaptic density (Asaki et al., 2003) support the second theory. Furthermore, activity–mediated translocation of ribosomes to the spine head (Ostroff et al., 2002) suggest that newly synthesized protein can stem from mRNAs being translated in these areas, closely to the PSD (Steward and Schuman, 2003).

Dendritic mRNAs are not concomitantly axonal mRNAs, implying the existence of precise but different mechanisms of mRNAs transportation and protein synthesis in dendrites and axons. Specifically for the dendritic mRNAs, it has been demonstrated that *cis*–acting elements in the 3' UTR play the role of ''zip–codes'' for dendritic delivery (Tiedge and Brosius, 1996) through granules that consist of mRNAs and translocate in dendrites (Knowles and Kosik, 1997). There are many other regulatory elements located in either the 3'or 5' UTR, controlling the translocation, localization, stabilization and translation of the mRNAs (Andreassi and Riccio, 2009). RNA – binding proteins bind to these elements and attach the RNAs to cytoskeletal motor or adaptor proteins that drive their localization (Czaplinski, 2014). Alternative polyadenylation plays an important role to this process since it will provide the diversity of the 3' UTRs of the mRNAs (Tian and Manley, 2017). Regarding local translation, mRNAs containing cytoplasmic polyadenylation elements (CPEs), have

been found to exhibit increased translation after neuronal stimulation (Wells et al., 2001).

1.8 Posttranslational Modifications

The activation of many Initiation Factors relies on their phosphorylation. However, other posttranslational modifications have also been identified. Even though many of these modifications target factors whose function is clear, their effects on these proteins and consequently on translation are unknown. Recently, it was discovered that 4E-BP2 is the only isoform of 4E-BPs which undergoes asparagine deamidation in two sites only in the brain (Bidinosti et al., 2010b). However, the role of deamidated 4E-BP2 in translation remains to be elucidated.

1.8.1 Deamidation

Deamidation is a post-translational modification that can take place *in vivo* and *in vitro*. It is the spontaneous conversion of asparagine (Asn) and glutamine (Gln) residues to aspartyl (Asp) and glutamyl (Glu) residues (Robinson and Robinson, 2001). After each deamidation event, each of the following products can be produced: L-aspartic acid, D-aspartic acid, L-iso-aspartic acid and Disoaspartic acid residue (Hipkiss, 2006). The rate of the reaction depends on multiple factors such as primary sequence, three-dimensional (ED) structure, pH, temperature, ionic strength, buffer ions and other solution properties. Deamidation introduces a negative charge at the residue that takes place at neutral pH (Robinson and Robinson, 2001) and increases the mass of protein 1Da (Washington et al., 2013). Therefore, many biological and structural differences can occur in proteins due to deamidation (Hipkiss, 2006; Robinson and Robinson, 2001).

The two residues, Asn and Gln exhibit different susceptibility in deamidation. Asparagine residues are more prone to deamidation than glutamine and the reaction on Asn is faster than on Gln residues (Hipkiss, 2006). There is evidence that the motif NGxG (where N is any nucleotide, G is a Glycine on the carboxyl-terminus and a second Glycine in the position x+3) exhibits increased susceptibility to deamidation of Asn residues *in vivo* (Mikkat et al., 2013). For many years deamidation was thought as non-specific but there is evidence that it is a highly regulated process in some

proteins. Deamidation in Gln residues can occur enzymatically and nonenzymatically (Robinson and Robinson, 2004). Regarding deamidation in Asn residues, no enzyme was known to catalyse deamidation until recently where PFAS (PhosphoribosylFormylglycinAmidineSynthetase) was found to be the first protein deamidase. PFAS is recruited after specific viral infections. RIG-I (Retinoic acid-Induced Gene I) is a pattern recognition receptor which can recognize pathogen associated molecular patterns (PAMPs). After the detection of PAMPs and IFN (Interferon) stimulation, it exhibits increased expression. Following infection with gamma herpesviruses, vGAT, (herpes viral homolog of Glutamine 4 AmidoTransferase) recruits cellular PFAS for deamidation of RIG-I, thus the virus evades cytokine production and immune response (He et al., 2015).

Deamidation has been characterized in a variety of proteins and has been associated with many biological processes. The heterotrimeric G protein Go is the most abundant G protein in mammalian brain with its α subunit undergoing deamidation (Kim et al., 1997). Moreover, Bcl-xL (B-cell lymphoma-extra large), an important anti-apoptotic protein, becomes deamidated *in vivo* and probably *in vitro* (Aritomi et al., 1997). Deamidation can also change the intracellular localization and the interactions of proteins (Pepperkok et al., 2000) . Interestingly, deamidated PKA exhibited different intracellular localization and associated with decreased phosphorylation of CREB (transcription factor Camp-responsive element binding protein) compared to the WT PKA (Pepperkok et al., 2000). Non-specific deamidation can take place spontaneously especially in aged proteins that are targeted for degradation (Reissner and Aswad, 2003). Deamidation in these aged proteins results in accumulation of IsoAsp residues in their sequence (Reissner and Aswad, 2003). These examples of deamidation indicate that this modification has pivotal biological effects on proteins, therefore, it is important to identify its precise effects on various cellular processes.

1.8.2 Mechanism of Asn deamidation

The deamidation mechanism is spontaneous and includes formation of a short-lived intermediate product, succinimide. The formation of succinimide can arise from deamidation on Asn residues or dehydration of aspartate (final deamidation product) (Reissner and Aswad, 2003).

The first step of the mechanism is rearrangement of the peptide bond in Asn or Asp residues. The α-amino group of the C-terminal peptide bond is responsible for nucleophilic attack on the amide of Asn- or Asp-side chain group. Subsequently, the linkage of the peptide bond through the β-carboxyl group of Asn- or Asp occurs and succinimide is formed, which is quickly hydrolysed to a mixture of aspartyl (30%) and isoaspartyl (70%) linkages. In a protein sequence, Asn is replaced by Asp (Reissner and Aswad, 2003). Many studies support the idea that levels of isoAp in proteins may provide a novel regulating mechanism for protein function. Therefore, isoAsp levels may be a way to regulate protein function (Robinson and Robinson, 2004). Figure 1.6 shows a simple model of the basic mechanism of Asn deamidation.

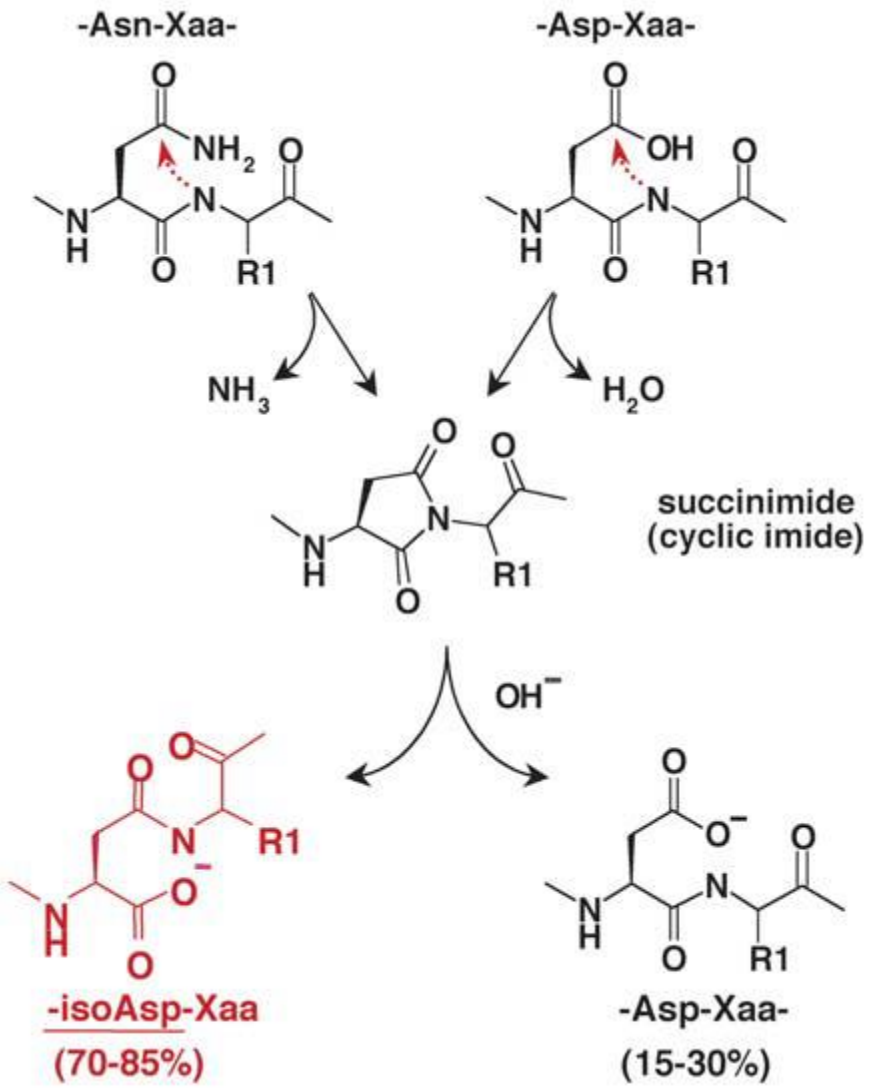

Figure 1.6 Mechanism of Asn deamidation.

The first product is a metastable succinimide which hydrolyses to a mixture of products isoAsp and Asp residues in a ratio 70:30 (Adapted from Reissner and Aswad, 2003).

The change of the amino acid composition that arises from deamidation of asparagines can be repaired partially by an enzyme called PIMT (Protein Isoaspartate Methyltransferase) (Hipkiss, 2006). The α-carboxyl group at an isoAsp site is the target of PIMT. PIMT facilitates reformation of the intermediate product which again hydrolyses to Asp and isoAsp (ratio 30:70) (Geiger and Clarke, 1987; Stephenson and Clarke, 1989). PIMT -/- mice have shown the importance of this enzyme in the brain. They exhibited accumulation of abnormal polypeptides mostly in their brains

and decreased lifespan (Kim et al., 1997). Furthermore, after silencing of PIMT in the brain, many proteins such as synapsins, dynamins and α/β tubulins are prone to Asp isomerization and deamidation (Qin et al., 2013). Thus, PIMT exhibit important protective effect on proteins with high isoAsp levels (Reissner and Aswad, 2003).

1.8.3 Deamidation of 4E-BP2

The aim of this thesis is to investigate the role of deamidated 4E-BP2 in the regulation of translation in the mammalian brain. 4E-BP2 undergoes postnatal posttranslational deamidation in two sites, N99 and N102, only in brain tissue. Deamidated 4E-BP2 exhibited enhanced interaction with Raptor and reduced association with eIF4E (Bidinosti et al., 2010b). Apart from protein-protein interactions, deamidation also altered synaptic activity. Upon genetic deletion of 4E-BP2, mice exhibited increased excitatory synaptic activity. In more detail, mEPSCs (miniature Excitatory Postsynaptic Currents) of 4E-BP2-/- neurons expressing deamidated 4E-BP2 displayed slower rise and decay time compared to those expressing WT 4E-BP2. This may facilitate increased signal integration and, therefore plasticity (Bidinosti et al., 2010b). However, there is also evidence that deamidated 4E-BP2 may have a different role than the WT protein. Interestingly, the expression of deamidated 4E-BP2 in post-synaptic pyramidal neurons of 4E-BP2-/- mice restored the increased charge transfer of mEPSCs whereas the expression of WT protein did not (Bidinosti et al., 2010b). Thus, deamidated 4E-BP2 is associated with translation and probably with synaptic responses. Since deamidation is brain specific and spontaneous (not regulated enzymatically), it is important to elucidate the regulatory mechanisms downstream of 4E-BP2 deamidation to facilitate our understanding of translational control in the brain.

1.9 Thesis Aim

Given the established role of 4E-BP2 in learning, memory, synaptic plasticity, and its implication in Autism Spectrum Disorders, the aim of this thesis was to investigate the role of a brain-specific posttranslational modification of 4E-BP2, asparagine deamidation, in protein synthesis. To achieve this goal, the presented thesis was divided into four main aims, resulting in four results chapters:

- Aim 1 (Chapter 3): Study the mechanism of regulation of deamidated 4E-BP2. Furthermore, examine whether it is a cell-specific modification and whether it is present in humans
- Aim 2 (Chapter 4): Study the subcellular localization of WT and deamidated 4E-BP2 in neurons
- Aim 3 (Chapter 5): Identify translated mRNAs that are regulated by WT and deamidated 4E-BP2
- Aim 4 (Chapter 6): Examine the tertiary structure of WT and deamidated 4E-BP2

2. Materials and Methods

2.1 Animals

All procedures were in accordance with UK Home Office on Animal Care regulations and were approved by the University of Edinburgh. C57Bl/6J background animals were used (backcrossed for more than 10 generations; pregnant dams to collect E16-18 embryos and P56 males). Food and water were provided *ad libitum*, and mice were kept on a 12 h light/dark cycle. Pups were kept with their dams until weaning at postnatal day 21. After weaning, mice were group housed (maximum of 6 per cage) by sex. Cages were maintained in ventilated racks in temperature (20-21 ^{o}C) and humidity (~55%) controlled rooms, on a 12-hour circadian cycle (7am-7pm light period).

2.2 Human tissue

Post – mortem human brains were acquired from the MRC Edinburgh Brain & Tissue Bank. Information about sex, age, brain area and MRC brain bank number can be found in Table 2.1.

Table 2.1 Post-mortem human brains

ID	Sex	Age	Area	MRC BRAIN BANK NUMBER
SD038/15	Male	44	Posterior Cyngulate Gyrus BA23	BBN 26313
SD034/15	Male	69	Posterior Cyngulate Gyrus BA23	BBN 26308

2.3 Table of materials

Unless otherwise stated, chemicals were from Merck and tissue culture reagents were from Thermo Fisher Scientific. The list of primary and secondary antibodies, plasmids, chemicals, commercial assays, softwares and algorithms used can be found in Table 2.2. Links for softwares and algorithms can be found in Appendix.

Table 2.2 Table of materials

REAGENT or RESOURCE	SOURCE	IDENTIFIER
Primary and Secondary Antibodies		
4E-BP2	Cell Signalling Technologies	2845S
4E-BP1 (53H11)	Cell Signalling Technologies	9644S
Phospho-4E-BP1 (Thr37/46) (236B4)	Cell Signalling Technologies	2855S
Phospho-S6 Ribosomal Protein (Ser240/244)	Cell Signalling Technologies	2215S
Ribosomal Protein S6 Antibody (C-8)	Santa Cruz Biotechnology	sc-74459
c-Myc Antibody (9E10)	Santa Cruz Biotechnology	sc-40
Anti-Cullin 4B antibody	Abcam	ab67035
DDB1	Cell Signalling Technologies	5428S
HA Tag Monoclonal Antibody (2-2.2.14), DyLight 680	ThermoFisher Scientific	26183-D680
Anti-rabbit IgG, HRP-linked Antibody	Cell Signalling Technologies	7074S
HSC 70 Antibody (B-6)	Santa Cruz Biotechnology	sc-7298

DYKDDDDK Tag Monoclonal Antibody (L5), Alexa Fluor 488	ThermoFisher Scientific	MA1-142-A488
Anti-mouse IgG, HRP-linked Antibody #7076	Cell Signalling Technologies	7076S
p44/42 MAPK (Erk1/2) (137F5) Rabbit mAb	Cell Signalling Technologies	4695S
GAPDH (14C10) Rabbit mAb	Cell Signalling Technologies	2118S
Monoclonal Anti-β-Actin antibody produced in mouse	Merck	A5316-100UL
Monoclonal ANTI-FLAG® M2 antibody produced in mouse	Merck	F1804-200UG
Phospho-p44/42 MAPK (Erk1/2) (Thr202/Tyr204) Antibody	Cell Signalling Technologies	9101S
Anti-mouse IgG for IP (HRP)	Abcam	ab131368
Ubiquitin	Cell Signalling Technologies	3933S
α-Tubulin	Sigma-Aldrich	T9026
Phospho-Threonine-Proline	Cell Signalling Technologies	9391S
Anti-HA.11 Epitope Tag (Formerly Covance MMS-101R-500)	Cambridge Bioscience	901514
PSD95 (D27E11) XP® Rabbit mAb	Cell Signalling Technologies	3450S

Monoclonal Anti-Glial Fibrillary Acidic Protein (GFAP) antibody produced in mouse - 100UL	Merck	G3893-100UL
Histone H3 (D1H2)	Cell Signalling Technologies	12648S
Synaptophysin - 1	Synaptic Systems	101 011
Raptor (24C12) Rabbit mAb	Cell Signalling Technologies	2280S
His-Tag Antibody	Cell Signalling Technologies	2365S
UBE2L3 Antibody	Cell Signalling Technologies	3848S
Experimental models: Cell Lines		
Human Embryonic Kidney cells (HEK-293H ATCC® CRL-1573	Thermo Fisher Scientific	11631017
Plasmids		
pCDNA3-3HA–*4E-BP2* WT	Bidinosti et al., 2010b	N/A
pCDNA3-3HA–*4E-BP2* N99D/N102D	Bidinosti et al., 2010b	N/A
pCDNA3-3HA–*4E-BP2* ΔTOS	Bidinosti et al., 2010b	N/A
pCDNA3-3HA–*4E-BP2* N99A/N102A	Bidinosti et al., 2010b	N/A
pGEX-6P-1-*4E–BP2* WT	Bidinosti et al., 2010b	N/A
pGEX-6P-1-*4E–BP2* N99D/N102D	Bidinosti et al., 2010b	N/A
Myc-Raptor	Addgene	1859

mCerulean3-*4E-BP2* WT	This thesis	N/A
mCerulean3-*4E-BP2* N99D/N102D	This thesis	N/A
mCerulean3-*4E-BP2* N99A/N102A	This thesis	N/A
4E-BP2 WT–mCerulean3	This thesis	N/A
4E-BP2–N99D/N102D mCerulean3	This thesis	N/A
4E-BP2 N99A/N102A–mCerulean3	This thesis	N/A
mCherry2–*4E-BP2* WT	This thesis	N/A
mCherry2–*4E-BP2* N99D/N102D	This thesis	N/A
mCherry2–*4E-BP2* N99A/N102A	This thesis	N/A
4E-BP2 WT–mCherry2	This thesis	N/A
4E-BP2 N99D/N102D–mCherry2	This thesis	N/A
4E-BP2 N99A/N102A–mCherry2	This thesis	N/A
AAV9-hSyn1-3XFlag-4E-BP2 WT-IRES-GFP-WPRE	This thesis	Vector Biolabs
AAV9-hSyn1-3XFlag-4E-BP2 N99D/N102D-IRES-GFP-WPRE	This thesis	Vector Biolabs
His-Ubiquitin	(Hock et al., 2011)	N/A
Chemicals		

Cycloheximide	Merck	C7698-1G
Lactacystin	Merck	L6785-.2MG
MG132 (Z-Leu-Leu-Leu-al)	Merck	C2211-5MG
Homoharringtonine (HHT)	Merck	SML1091-10MG
Torin1	Tocris Bioscience	4247
U0126	Tocris Bioscience	1144
Betullinic acid	Merck	B8936
NBQX	Abcam	ab120046
D-AP5	HelloBio	HB0225
Rapamycin	LC Laboratories	R-5000
Critical Commercial Assays		
TriFECTa DsiRNA Kit for hs.Ri.RPTOR.13	IDT	N/A
TriFECTa DsiRNA Kit for hs.Ri.CUL4B.13	IDT	N/A
Clarity Western ECL Substrate	Biorad	1705061
Pierce™ ECL Western Blotting Substrate	ThermoFisher Scientific	32106
TruSeq Ribo Profile (Mammalian) Kit	Illumina	RPHRM12126
Ribo-Zero Gold (Human/Mouse/Rat) Kit	Illumina	MRZG126

Agilent Small RNA Kit	Agilent Technologies	5067-1549
NEXTflex™ Small RNA Sequencing Kit v3	Bioo Scientific	NOVA-5132-06
Software and Algorithms		
Adobe Illustrator	Adobe	
GraphPad PRISM	Graphpad	
Fiji ImageJ software	Open source	
Imaris software	Bitplane	
NIS-Elements-v4.13 software	Nikon	
Huygens Software 4.5.1p3	Scientific Volume Imaging	
ImageStudio Software	LI-COR	
ATSAS software suite	(Konarev et al., 2003)	
DAMMIN	(Svergun, 1999)	
GASBOR	(Svergun et al., 2001)	
Multifastats	-	
UTRdb/UTRscan	(Grillo et al., 2010).	
Ingenuity Pathway Analysis (IPA)	Qiagen	
Database for Annotation, Visualization and Integrated Discovery (DAVID)	(Huang da et al., 2009)	

2.4 Protocols

2.4.1 Adeno-associated viruses (AAV) and infection of cortical cultures

All AAVs were from Vector Biolabs. AAV vectors were cloned by Vector Biolabs: AAV9-hSyn1-3Xflag-4E-BP2 WT-IRES-GFP-WPRE and AAV9-hSyn1-3Xflag-4E-BP2 N99D/N102D-IRES-GFP-WPRE and were used to generate ~$3.5x10^{13}$ GC/ml for each AAV. Primary dissociated cortical neuronal cultures were infected at DIV10 with $7x10^{11}$ GC/ml of each virus and collected at DIV25.

2.4.2 Transfection in Human Embryonic Kidney cells

Human Embryonic Kidney cells (HEKs) were transfected with 1-2ug DNA (the amount of DNA was balanced to get equal protein expression for each plasmid) and 1ul of Lipofectamine 3000 (L3000008, Thermo Fisher Scientific) in Opti-MEM (31985070, Thermo Fisher Scientific). The mix was added directly on the cells.

2.4.3 Primary dissociated cortical neuronal cultures

All reagents for cell culture were from Thermo Fisher Scientific unless stated otherwise. E16-18 mouse embryos were collected from pregnant dams and cortices were dissected from the brain and immersed in ice cold HBSS solution (14170146) supplemented with 1x Antibiotic/antimycotic mix (15240062) and HEPES solution at concentration 10 mM (15630106). Cells were dissociated after addition of 1 mg/ml Trypsin (LS003702, Lorne Laboratories) and incubation for 15 min at 37 ^{o}C. Then, 0.05 mg/ml Dnase I (D5025-15KU, Merck) was added and cells were incubated for 5 min at 37 ^{o}C. After the incubation, Neurobasal media (21103049) was added twice, supplemented with 1x Antibiotic/antimycotic mix, 1x Glutamax (35050038), B-27 (17504044) and 10% Horse Serum (26050088) to inhibit Trypsin. Then, DNAse I was re-added and tissue was triturated. Cells were plated on dishes that were coated with 0.05 mg/ml Poly-D-Lysine (P7886, Merck) for 2 h the day before tissue dissection. 5 h after plating, the media was removed and replaced by new media without serum. Half of the media was replaced every 3 days, supplemented with 1 μM Cytosine β–D–arabinofuranoside hydrochloride (Ara-C, C6645-25MG, Merck). To obtain glial

cultures, Ara-C-free DIV10 neuronal cultures were trypsinised with Trypsin-EDTA (25300054). Cells were washed twice in 1x PBS and re-plated in DMEM (11995065) supplemented with 10% fetal bovine serum (10500064) and 1% Pen/Strep (15140148).

2.4.4 Protein stability assay

HEK-293H cells were transfected with 1-2 μg DNA (or 10 nM siRNA). Pilot experiments were carried out to calculate the required μg for each plasmid construct to ensure equal starting amounts of protein. For protein stability assays, after 48 h, transfected HEK-293H cells, (non-transfected cultured neurons or isolated synaptoneurosomes) were treated with 100 μg/ml Cycloheximide (C7698-1G, Merck), 5 μM Lactacystin (L6785-.2MG, Merck), 20 μM MG132 (Z-Leu-Leu-Leu-al, C2211-5MG, Merck), 2 μg/ml HHT (SML1091-10MG, Merck), 10 μg/ml Anisomycin, 250 nM Torin1 (4247, Tocris Bioscience), 20 μM U0126 (1144, Tocris Bioscience), 2.5 μg/ml Betullinic acid (B8936, Merck), 10 μM NBQX (ab120046, Abcam) and 50 μM D-AP5 (HBO225, HelloBio) for the indicated period of time.

2.4.5 *In vivo* ubiquitination assay

HEK-293H cells were transfected with 5-10 μg of 3xHA-plasmids expressing either WT or 2D 4E-BP2 [pilot experiments were carried out to determine the required amount (μg) for each plasmid construct to ensure equal starting amounts of protein] and 10 μg His-Ubiquitin (Hock et al., 2011). After 48 h of transfection, cells were treated with 20 μM MG132 for 6 h. Cells were lysed in urea buffer (8 M Urea, 0.1 M NaH_2PO_4, 0.1 M Tris-HCl [pH 8.0], 0.05% Tween 20, and 10 mM imidazole [pH 8.0]). 5 mg of total protein was incubated with Ni-NTA Agarose beads (30210, Qiagen) overnight to pull down ubiquitinated proteins. The beads were washed twice with denaturing wash buffer (8 M Urea, 0.1 M NaH_2PO_4, 0.1 M Tris-HCl [pH 8.0], 0.05% Tween 20, 20 mM imidazole [pH 8.0]) and then with native wash buffer (0.1 M NaH_2PO_4, 0.1 M Tris-HCl [pH 8.0]. Protein was dissolved in Laemmli sample buffer (50 mM Tris, pH 6.8, 100 mM DTT, 2% SDS, 10% glycerol, 0.1% bromophenol blue) and resolved by SDS-PAGE. Monoclonal antibody HA.11 (901514, Cambridge Bioscience) was used to detect ubiquitinated 4E-BP2.

2.4.6 *In vitro* ubiquitination assay

In vitro ubiquitination assay was performed in 100 µl reaction mixture at 37 °C for 2 h. The reaction mixture included 100 ng purified human recombinant 4E-BP2 WT and N99D/N102D, 100 ng purified human recombinant UBE1 (E1 enzyme, E-304, BostonBiochem), 500 ng UbcH7/UBE2L3 (E2 enzyme, E2-640, BostonBiochem), 10 µg ubiquitin (U-530, BostonBiochem), 2.5 µg purified human recombinant CUL4B (E3 enzyme, H00008450-P01, Novus Biologicals), 50 ng purified human recombinant DDB1 (ab114333, abcam), purified human recombinant Raptor (H00057521-P01, Novus Biologicals) in an ATP-regenerating system [50 mM Tris-HCl, pH 7.6, 10 mM $MgCl_2$, 2 mM ATP (R0441, ThermoFisher Scientific) 10 mM creatine phosphate (10621714001, Merck), 3.5 U/mL creatine kinase (10127566001, Merck) and 0.6 U/mL inorganic pyrophosphatase (M0361S, New England Biolabs)], in the presence of 5 µM ubiquitin aldehyde (U-201, BostonBiochem) and 50 µM MG132. Proteins were dissolved in Laemmli buffer and resolved by SDS-PAGE.

2.4.7 Immunoprecipitation

HEK-293H cells were transfected with 5 µg DNA of the HA plasmids expressing either WT or 2D (the amount of DNA was balanced to achieve the same intensity/protein expression for each plasmid) and 10 µg of Myc – Raptor. After 48 h of transfection, cells were rapidly homogenized in ice cold lysis buffer (50mM HEPES pH 7.5, 1% CHAPS, 150mM NaCl, protease and phosphatase inhibitors), on ice. Homogenates were incubated at 4 °C with constant rotation and centrifuged at 15,000 x *g* for 10 min at 4 °C. Supernatants were collected and precleared with 100 µl of protein G agarose beads (37478S, Cell Signalling Technologies). 7 mg of precleared supernatant was incubated with 3 µg of c-myc antibody [(9E10), sc-40, Santa Cruz] for 30 min at 4 °C, followed by incubation with protein G agarose beads overnight at 4 °C. Beads were then centrifuged at 3,500 x *g* for 1 min at 4 °C and washed three times with lysis buffer for 10 min. Immunoprecipitates were dissolved in 2X Laemmli buffer, resolved by SDS-PAGE and probed with anti-myc and anti-HA antisera.

2.4.8 Immunoblotting

HEK-293H cells, dissociated cortical neuronal cultures or mouse/human tissue were lysed in RIPA buffer (150 mM sodium chloride, 1.0% NP-40, 0.5% sodium

deoxycholate, 0.1% SDS, 50 mM Tris, pH 8.0) supplemented with protease and phosphatase inhibitors (Roche) unless otherwise specified, in a Dounce glass homogeniser by applying ~30 strokes, on ice. Samples were further incubated on ice for 15 min, with occasional vortexing, and cleared by centrifugation for 20 min at 16,000 x *g* at 4 °C. The supernatant was used for Western blotting after protein concentration of each sample was determined by measuring A_{280} absorbance on a NanoDrop (ThermoFisher Scientific). 50 μg of protein per lane was prepared in Laemmli sample buffer, heated to 98 °C for 2 min, and resolved on 10%–16% polyacrylamide gels. Proteins were transferred to 0.2 μm nitrocellulose membrane (Bio-Rad), blocked in 5% milk in TBS-T (10mM Tris, pH 7.6, 150mM NaCl, 0.1% Tween20) for 1 h at room temperature, incubated with primary antibodies 1:1000 (1% BSA in TBS-T containing 0.02% Na azide) overnight at 4 °C and with secondary antibodies 1:5000 for 1 h at room temperature (5% milk in TBS-T). Between incubations, membranes were washed three times in TBS-T. For re-probing, membranes were stripped by incubation with 0.2 M NaOH for 10 min and blocked with 5% milk in TBS-T for 1 h. Proteins were visualized using enhanced chemiluminescence (1705061, Biorad and 32106, ThermoFisher Scientific) after exposing on X-ray films (34089, ThermoFisher Scientific) processed with an Ecomax Film Processor (ProTec).

2.4.9 Quantification of Immunoblotting

The intensity of each protein band was measured from original images (no brightness or contrast adjustments) with ImageStudio Software (Li-COR Biosciences) in triplicate and averaged to minimize measuring variability. Loading controls were used in each experiment. Data are shown as protein expression (arbitrary units) after normalization to control. For quantification of endogenous 4E-BP2 in brain, the intensity of the bottom band was measured for WT 4E-BP2 and the intensity of both, middle and top band, corresponding to single and double deamidated 4E-BP2 respectively, was measured for 2D 4E-BP2. Figure legends include information about band sizes on all blots.

2.4.10 Phosphatase Treatment

Whole brains or cortical neuronal cells at the indicated ages were homogenized as described previously (2.4.8) in 1X phosphatase buffer [PMP Buffer, B0761S, New England Biolabs, (50 mM HEPES, 100 mM NaCl, 2 mM DTT, 0.01 % Brij 35, pH 7.5)] supplemented with protease inhibitors (Roche) and 1 mM $MnCl_2$ (B1761S, New England Biolabs). The protein concentration of supernatant was determined by measuring A_{280} absorbance on a NanoDrop (Thermo Fisher Scientific). Extracts were diluted to 2 μg/μl in a total volume of 90 μl. 9 μl of the phosphatase (P0753S, New England Biolabs) was added per sample and the samples were incubated at 30 ^{o}C for 45 min. The reactions were stopped by addition of Laemmli sample buffer and samples were analysed by Immunoblotting (2.4.8).

2.4.11 Isolation of purified synaptoneurosomes

Purified synaptoneurosomes were prepared from fresh mouse brain tissue. Cortices were isolated from WT mice aged 8-12 weeks, and each hemisphere was homogenized in 5 ml of ice–cold sucrose buffer (320mM Sucrose, 5mM Tris, 1mM EDTA, pH 7.4) and the homogenates were centrifuged for 10min, at 1000 x *g*, 4 ^{o}C. For each tube, the supernatant was transferred on a new tube and kept on ice (part of the supernatant was used as a control sample to compare the purity of synaptoneurosomes and labelled as crude) and the pellet was resuspended in 10 ml sucrose buffer and centrifuged again for 10 min, 1000 x *g* at 4 ^{o}C. The supernantants were combined and the pooled supernatant was then centrifuged for 10 min, at 21,000 x *g* at 4 ^{o}C to pellet out synaptoneurosomes. The pellet was resuspended in 3% Percoll (GE Healthcare) of sucrose buffer and layered on top of a discontinuous Percoll gradient (layers of 24% and 10% Percoll in sucrose media, preparation of Percoll gradients is described in Table 2.3). The gradients were centrifuged at 30750 x *g*, for 9 min at 4 ^{o}C with minimum acceleration and no deceleration on JA-25.50 fixed angle rotor in a Beckman Avanti JA-25 centrifuge. The material between layers 24% and 10% was collected, resuspended in 10 ml Ionic Media (20mM HEPES, 10 mM Glucose, 1.2mM Na_2HPO4, 1 mM $MgCl_2$, 5mM NaHCO3, 5mM KCl, 140mM NaCl, pH 7.4) and centrifuged at 21,000 x *g*, for 15 min at 4 ^{o}C. The pellets from the duplicate preparations from the same animal were combined, resuspended in 2 ml Ionic Media and centrifuged at 21,000 x *g*, for 15 min at 4 ^{o}C. The protein

concentration of the samples was determined by measuring A_{280} absorbance using Nanodrop.

Table 2.3 Preparation of Percoll gradients

% (v/v)	100% Percoll (ml)	5XSET (ml)	H_2O (ml)
24%	7.2	6	16.8
10%	3	6	21
3%	1.2	6	22.8

2.4.12 Stimulation of synaptoneurosomes

The pellet of purified synaptoneurosomes was resuspended in 200ul Ionic Media and vortex briefly. Then, the resuspended volume was shared in tubes depending on the number of different treatments and stimulations that would be performed. All the treatments of resuspended synaptoneurosomes were performed at 37 ºC for 1h. Then, resuspended synaptoneurosomes were lysed in RIPA buffer and protein concentration was determined by measuring A_{280} absorbance on a NanoDrop. Proteins were dissolved in Laemmli sample buffer and resolved by SDS-PAGE electrophoresis.

2.4.13 Proteasome activity assay

The chymotrypsin-like activity of the proteasome was determined using a specific proteasome substrate (Proteasome Substrate III, Fluorogenic, Suc-Leu-Leu-Val-Tyr-AMC, 539142-5MG, Calbiochem). Total lysates or the synaptoneurosome fractions (10 µg) were incubated with the substrate (40 µM) in 100 µl of proteasome assay buffer [0.05 M Tris-HCl (pH 8.0), 0.5 mM EDTA, 1 mM ATP, and 1 mM dithiothreitol (DTT)] at 37 °C for 1h. After the incubation, proteasome activity was measured every 20 min and the plate was kept at 37 °C. The fluorescence of the released AMC was detected using a fluorescence microplate reader system (GloMax Explorer Multimode Microplate Reader, Promega) at 380-nm excitation and 460-nm emission wavelengths.

2.4.14 Cohesive-End restriction cloning of *eif4ebp2* WT and mutants in fluorescent vectors

GeneBlocks eif4ebp2 fragments (encoding for WT, double deamidated and Alanine mutant protein) were designed according to the Consensus Coding Sequence Database (https://www.ncbi.nlm.nih.gov/projects/CCDS/CcdsBrowse.cgi) (CCDS ID for *eif4ebp2* WT sequence, *Homo sapiens*: 7303.1) and were from IDT. Fluorescent vectors were from Addgene [mCherry2-C1 (54563), mCherry2-N1 (54517), mCerulean3-C1 (54605), mCerulean3-N1 (54730)]. (See Appendix for sequences of geneblock fragments)

Geneblocks were resuspended in 20ul of buffer (10 mM Tris pH 8.0, 1 mM EDTA) to a final concentration of 10 ng/µl. Then, the following reaction of restriction digestion (Table 2.4) was set up for each geneblock:

Table 2.4 Restriction digestion on geneblocks

Component	µl per 1 reaction
CutSmart Buffer 10X (B7204S, New England Biolabs)	3
DNA	10 (100 ng)
EcoRI (R0101S, New England Biolabs)	1 (20 units)
XhoI (R0146S, New England Biolabs)	1 (20 units)
BSA 10 µg/µl	0.3
ddH_2O	14.7
Total	30

The reactions were incubated at 37 ^{o}C for 1 h. DNA was purified using QIAquick Gel Extraction Kit (28704, QIAGEN), according to the manufacturer's instructions and DNA concentration was measured using a Nanodrop (A260).

Fluorescent vectors were linearized by restriction digestion and the following reaction (Table 2.5) was set up for each vector:

Table 2.5 Restriction digestion on vectors

Component	µl per 1 reaction
CutSmart Buffer 10X	3
DNA	2 (1 µg)
EcoRI	1
XhoI	1
BSA 10 µg/µl	0.3
ddH_2O	22.7
Total	30

The reactions were incubated at 37 ^oC for 1 h. Then, linearized vectors were dephosphorylated with alkaline phosphatase using the following reaction (Table 2.6):

Table 2.6 Dephosphorylation of vectors

Component	µl per 1 reaction
CIAP Buffer 10X (M1821, Promega)	5
DNA	2 (1 µg)
CIAP (M1821, Promega)	1 (0.01 units)
ddH_2O	42
Total	50

The reactions were incubated at 37 ^oC for 30 min and were stopped by addition of 300 µl CIAP stop buffer (M1821, Promega). Then, linearized and dephosphorylated vectors were mixed with SYBR Safe DNA Gel Stain (S33102, ThermoFisher Scientific), were resolved with TAE buffer (40mM Tris base, 40mM acetate, 1mM EDTA) on a 1.5 % agarose gel and purified (QIAquick Gel Extraction Kit), according to the manufacturer's instructions.

Ligation reactions of geneblocks and vectors were set up in a molar ratio 4:1, respectively. To calculate the amount of DNA of geneblocks needed for the ligation reaction with each vector (50 ng) according to the ratio 4:1, we used the following formula:

$$\frac{ng\ (vector) \times molar\ ratio \times geneblock\ length\ (bp)}{vector\ length\ (bp)} = ng\ geneblock$$

For mCerulean3-C1 (4750 bp) and mCherry2-C1 vectors (4750 bp) and geneblocks (384 bp):

16.168 ng of geneblock needed for ligation reaction

For mCerulean3-N1 (4750 bp) and mCherry2-N1 vectors (4750 bp) and geneblocks (381 bp):

16.042 ng of geneblock needed for ligation reaction

Table 2.7 shows all the different combinations of geneblocks and vectors that were constructed. Table 2.8 and Table 2.9 describe the ligation reactions that were prepared.

Table 2.7 Geneblocks cloned in fluorescent vectors

vector	Geneblock (CCDS)	ng geneblock
mCherry2-C1	4E-BP2 WT	16.168
mCherry2-C1	4E-BP2 N99D/N102D	16.168
mCherry2-C1	4E-BP2 N99A/N102A	16.168
mCherry2-N1	4E-BP2 WT	16.168
mCherry2-N1	4E-BP2 N99D/N102D	16.168

mCherry2-N1	4E-BP2 N99A/N102A	16.168
mCerulean3-C1	4E-BP2 WT	16.042
mCerulean3-C1	4E-BP2 N99D/N102D	16.042
mCerulean3-C1	4E-BP2 N99A/N102A	16.042
mCerulean3-N1	4E-BP2 WT	16.042
mCerulean3-N1	4E-BP2 N99D/N102D	16.042
mCerulean3-N1	4E-BP2 N99A/N102A	16.042

The following ligation reactions were set up:

Table 2.8 Ligation reaction for geneblocks with mCerulean3-C1 and mCherry2-C1

Component	**µl per 1 reaction**
Quick Ligase Reaction Buffer 2X	10
Linearized vector	2.75
geneblock	1.6168 (16.168 ng)
Quick Ligase	1
ddH_2O	4.6332
Total	20

Table 2.9 Ligation reaction for geneblocks with mCerulean3-N1 and mCherry2-N1

Component	µl per 1 reaction
Quick Ligase Reaction Buffer 2X	10
Linearized vector	2.75
geneblock	1.604 (16.1042 ng)
Quick Ligase	1
ddH_2O	4.646
Total	20

The reactions were incubated at Room Temperature (25 ^oC, RT) for 5 min. Then, XL1blue Cells (200236, Agilent technologies) were used for transformation of the cloned geneblocks. 2 µl of ligation mixture was added in 25 µl of competent cells and cells were incubated at 4^oC for 30 min. Heat shock was performed at 42^oC for 45 s and then, cells were kept for at 4 ^oC for 2 min. 250 µl of pre-warmed SOC (Super Optimal Broth) medium was added to each transformation reaction and reactions were incubated at 37 ^oC for 1 h in a shaking incubator. Lastly, 125 µl of transformation reactions were plated on LB (Luria-Bertani) plates with 100 µg/ml ampicillin.

Single bacterial colonies were picked and incubated in 5 ml LB at 37 ^oC in a shaking-incubator for 16 h. DNA was isolated using QIAprep Spin Miniprep Kit (QIAGEN), according to the manufacturer's instructions. DNA concentration was measured using a Nanodrop (A260). All samples were sequenced using Source BioScience DNA sequencing service.

3 x HA-4E-BP2 expressing plasmids (WT, double deamidated, Alanine mutant) have been described and FLAG-4E-BP2 expressing plasmids were constructed from Vector Biolabs.

2.4.15 Immunofluorescence and Confocal Imaging

Primary cortical neuronal cultures were prepared from E17 mouse embryos. Cells were plated on coverslips, previously coated with 0.05 mg/ml poly-D-lysine (P7886, Merck) for 2 h and 10 μg/ml laminin (23017-015, Invitrogen) for 1 h, at a density of 80,000 cells/well in 24-well dishes. Four days after plating, neurons were co-transfected with 0.25 μg of HA-4E-BP2 WT plasmid and 0.25 μg of FLAG – 4E-BP2 N99D/N102D using 0.5 μl of Lipofectamine 3000 in pre-warmed Opti-MEM supplemented with 1x Glutamax. Following 1 h of transfection, neurons were returned to conditioned media. Neurons were fixed at DIV16 in 4% PFA in phosphate-buffered saline (PBS) for 8 min and washed three times for 5 min in PBS. Cells were permeabilised with 0.1% Triton-X 100 for 5 min and blocked with 2.5% BSA in 1x PBS for 30 min. Then, cells were incubated with 1:50 anti-FLAG Tag Monoclonal Antibody (L5), Alexa Fluor 488 (MA1-142-A488, Thermo Fisher Scientific) and 1:25 anti-HA Tag Monoclonal Antibody (2-2.2.14), DyLight 680 (26183-D680, Thermo Fisher Scientific) for 2 h. Coverslips were incubated with DAPI 1:10000 (4',6-Diamidino-2-Phenylindole, Dihydrochloride, D1306, Thermo Fisher Scientific) for 5 min. Then, the coverslips were washed and mounted with Lab Vision PermaFluor Aqueous Mounting Medium (TA-030-FM, Thermo Fisher Scientific). Images of co-transfected neurons were acquired on a Nikon A1R microscope using a 60X objective. For the quantification and colocalization analysis experiments, z-stack images were taken with a pixel size of 60×60 nm^2 and z-step size of 150 nm. Excitation laser wavelengths for the different samples were: 488 nm for FLAG tag, 680 nm for HA tag, and 401.5 nm for DAPI. Microscope control and image acquisition were done using the NIS-Elements-v4.13 software.

2.4.16 Imaging analysis

Deconvolution of confocal images was performed using Huygens Essential (Huygens Software 4.5.1p3) before subsequent analysis. Co-localization analysis was performed on 3D, deconvolved images and quantified using ImarisColoc (Imaris v8.2.1, Bitplane Inc, software available at http://bitplane.com). All image analysis and quantification of images acquired with confocal microscopy were performed on

deconvolved images without any additional processing. Brightness and contrast settings were adjusted in Imaris for presentation purposes only.

2.4.17 Cell lysis for Ribosome Profiling

Primary dissociated cortical neurons were prepared according to the protocol described previously (section 2.4.3). Similarly, infection of cortical neurons with AAVs, overexpressing either WT or deamidated 4E-BP2 was described in previous section (2.4.1). Cells were treated with CHX (100 µg/ml) for 5 min and then, they were washed with ice-cold PBS twice. Then, cells were collected by scraping and lysis was performed as described previously (section 2.4.8) in Mammalian Polysome Buffer (20 mM NaCl, 150 mM Tris pH 7.5, 5 mM MgCl2, 100 µg/ml CHX, 2 mM DTT, 0.5 % Triton X-100, 0.5 % NP-40), supplemented with protease inhibitors. The supernatant was collected, and RNA concentration was measured on a Nanodrop (A260).

2.4.18 Ribosome Profiling

For ribosome footprinting samples, 5 units of TruSeq Ribo Profile Nuclease (RPHRM12126, Illumina) were added per A260/ml and then, samples were kept at 4 °C for 45 min with constant agitation. Nuclease digestions were quenched by adding 300 units SUPERase In RNase Inhibitor (AM2696, ThermoFisher Scientific). RPFs were purified using Illustra MicroSpin S-400 columns (27514001, Scientific Laboratory Supplies). Columns were equilibrated with Mammalian Polysome Buffer and were centrifuged at 600 *x g* for 4 min at room temperature (RT). 100 µl of the nuclease-digested sample were added immediately and columns were centrifuged at 600 *x g* for 2 min at RT, collecting the flow-through. SDS was added to both the nuclease-digested sample and undigested lysate to a final concentration of 1% and RNA was extracted using the RNA Clean & Concentrator™-25 Kit (R1017, Zymo Research).

All samples were quantified using a Nanodrop, to calculate input for the rRNA depletion reaction using the Ribo-Zero Gold Kit (MRZG12324, Illumina). rRNA depletion was followed by a purification using the RNA Clean & Concentrator™-5 Kit (R1016, Zymo Research). RPFs were size selected on a 15% TBE-Urea Polyacrylamide gel (EC68852BOX, ThermoFisher Scientific) and purified. Total RNA samples were randomly heat-fragmented and both samples were end-repaired using a Polynucleotidekinase (Illumina), following the manufacturer's instructions. cDNA

libraries for sequencing were generated from fragmented RNA with NEXTflex® Small RNA Sequencing Kit v3 for Illumina Platforms (NOVA-5132-06, Bioo Scientific).

After the end-repair, samples were quantified using the Agilent Small RNA Kit (5067-1548, Agilent Technologies). Input was balanced between samples to ensure similar output. The manufacturer's protocol was followed, using the lowest input option, due to total sample quantities below 1 ng. Briefly, an adenylated 3' adapter was ligated, followed by an adenylated 5' adapter ligation. The RNA fragments were then, reverse transcribed into cDNA and amplified using PCR (18 cycles). During the PCR, individual samples were barcoded for multiplex sequencing using the barcoding primers compatible with Illumina sequencing, included in the kit. Indexing primers used are summarised in Table 2.10. The PCR products were size selected on an 8% native TBE-PAGE gel (EC62152BOX, ThermoFisher Scientific) and purified from the gel according to the manufacturer's instructions. The cDNA libraries were then analysed for size, quantity and quality using the Agilent High Sensitivity DNA kit (5067-4626, Agilent Technologies). Samples were balanced and pooled for sequencing with Edinburgh Genomics on NovaSeq S1/2 flow cells yielding 50 bp paired-end reads. All sequencing was performed with Edinburgh Genomics.

Ribosome Profiling was performed by Konstanze Simbriger.

2.4.19 Bioinformatics Analysis

Bioinformatic and statistical consulting was provided by omics2view.consulting GbR, Kiel (Germany). All bioinformatic analysis was performed by omics2view, using a customised pipeline, adapted for ribosome profiling results. In summary, the FASTX Toolkit v0.0.14 (Gordon and J. Hannon, 2010) was used to trim adapter sequences from raw reads of both RPF and total RNA samples and RPF reads below 18 bp removed from the data. Next, undesired sequences (ribosomal RNAs and tRNAs) were removed from the datasets using Bowtie v1.1.2 (Langmead et al., 2009). The Filtered RPFs and total reads were then aligned to an indexed reference genome (built from GRCm38 primary genome assembly and the corresponding gene structure information, retrieved from GENCODE), using STAR v2.5.2b (Dobin et al., 2013). Only uniquely mapped reads were considered for the output. Data, including counts was summarised in a table including several columns:

- Ensembl gene ID
- Gene symbol
- Gene type
- Chromosome
- Gene length
- Non-coding or coding sequence
- Pseudogene
- Entrez gene ID
- Official gene ID (gene description)

Furthermore, the table included RPKM and TE values for each gene/condition and were calculated as:

$$RPKM_i = \frac{n_i}{\frac{l_i}{10^3} \cdot \frac{\sum_{i=1}^{k} n_i}{10^6}}$$

where n_i is the number of reads mapped to a gene i of length l_i. $\sum_{i=1}^{k} n_i$ is the sum of read counts for the given sample over all k genes in the reference genome. Results were rounded to 4 decimal places.

For each gene i in a given sample, the translational efficiency (TE_i) was calculated as:

$$TE_i = \frac{\frac{RPF_i}{\sum_{i=1}^{k} n_i \ RPF_i}}{\frac{total \ mRNA_i}{\sum_{i=1}^{k} n_i total \ mRNA_i}}$$

RPF_i and $total \ mRNA_i$ is the respective number of reads mapped to gene i for the ribosome protected fragments and total mRNA. $\sum_{i=1}^{k} n_i \ RPF_i$ and $\sum_{i=1}^{k} n_i \ total \ mRNA_i$ are the sums of the read counts, respectively, over all genes

in the reference genome. Again, results were rounded to four decimal places. Both these values were added to table summarising the results. Further, the pipeline produces graphical outputs summarising the data:

Table 2.10 NEXTflex™ Indexing Primers

NEXTflex™	Index Sequence	Reverse Complement
PCR Primer 1	CGTGAT	ATCACG
PCR Primer 2	ACATCG	CGATGT
PCR Primer 3	GCCTAA	TTAGGC
PCR Primer 4	TGGTCA	TGACCA
PCR Primer 5	CACTGT	ACAGTG
PCR Primer 6	ATTGGC	GCCAAT
PCR Primer 7	GATCTG	CAGATC
PCR Primer 8	TCAAGT	ACTTGA
PCR Primer 9	CTGATC	GATCAG
PCR Primer 10	AAGCTA	TAGCTT
PCR Primer 11	GTAGCC	GGCTAC
PCR Primer 12	TACAAG	CTTGTA
PCR Primer 13	TTGACT	AGTCAA
PCR Primer 14	GGAACT	AGTTCC
PCR Primer 15	TGACAT	ATGTCA
PCR Primer 16	GGACGG	CCGTCC
PCR Primer 17	CTCTAC	GTAGAG
PCR Primer 18	GCGGAC	GTCCGC
PCR Primer 19	TTTCAC	GTGAAA
PCR Primer 20	GGCCAC	GTGGCC
PCR Primer 21	CGAAAC	GTTTCG
PCR Primer 22	CGTACG	CGTACG
PCR Primer 23	CCACTC	GAGTGG
PCR Primer 24	GCTACC	GGTAGC
PCR Primer 25	ATCAGT	ACTGAT
PCR Primer 26	GCTCAT	ATGAGC

PCR Primer 27	AGGAAT	ATTCCT
PCR Primer 28	CTTTTG	CAAAAG

Histogram of translational efficiencies The translational efficiencies across all replicates are averaged for each protein coding gene. 0 values are excluded and all remaining values are log_2-transformed and plotted as superimposed histograms.
Violin plots of translational efficiencies the same values as for the histograms are plotted in violin plots. Changes in TE and transcription were analysed for pairwise comparisons, based on experimental design, using microarray normalisation methods (Quackenbush, 2002). For each treatment, an average across replicates was calculated for TE/RPKM values, using the geometric mean on a per-gene basis. Two statistics were then derived from these averages, for each gene:

Ratio which is calculated by dividing the value for the transgenic (deamidated 4E-BP2) by the value for the WT 4E-BP2.
Intensity which is calculated by multiplying the afore-mentioned values Data was ordered by increasing *log_{10}(Intensity).* Along this ordered set of values, mean *log_{10}(Intensity)* as well as mean and standard deviation of *log_2(Ratio)* were calculated within a sliding window of 100 genes at steps of 50 genes. Each gene was assigned to the window with a mean *log_{10}(Intensity)* closest to the gene's *log_{10}(Intensity)*. A z-score was calculated for each gene *i* using the respective window's *log2(Ratio)* mean and standard deviation as follows:

$$z_i = \frac{log_2(Ratio_i) - \mu^{window}_{log_2(Ratio)}}{\sigma^{window}_{log_2(Ratio)}}$$

p-values were derived for each gene i from the z-score by treating it as a quantile of the standard normal distribution:

$$p_i = 2 \times (1 - \Phi(|z_i|))$$

The sliding window was used to adequately represent the inherent structure of the data. Similar to microarray data, TE ratios and particularly – transcription ratios are more variable at low intensities. With z-scores simply calculated from the overall mean and standard deviation of the data, one might misidentify extreme $log_2(Ratio)$ values as significant at low intensities. At higher intensities, on the other hand, genes with significant $log_2(Ratio)$ values might not be identified. The intensity-dependent z-score is calculated with a subset of data from genes with similar intensity. This takes local data structure into account, allowing a more accurate determination of differential TE and transcription. For TE values, we further used the R package Xtail v1.1.5 (Xiao et al., 2016), a tool that has been specifically developed for analysing ribosome profiling data. For both the z-score-based p-values and the p-values derived with Xtail, false-discovery-rates (FDR) were calculated (Benjamini and Hochberg, 1995),
according to three (adjustable) parameters:

• Low TE/RPKM ratio threshold (generally pre-set to 0.666)
• High TE/RPKM ratio threshold (generally pre-set to 1.5)
• Minimum across all samples (generally pre-set to 40)

2.4.20 UTR analysis

UTRs were obtained from Biomart ENSEMBL (Yates et al., 2016) using the GRCm38.p6 version of the mouse genome. 5′ UTR motifs were predicted using UTRscan, pooling data from UTRdb (Grillo et al., 2010). Length in bp (base pairs) and %GC (Guanine-Cytosine) content were calculated using free Python-based scripts (Multifastats; https://github.com/davidrequena/multifastats).

2.4.21 Gene Ontology and Pathway Analysis

Gene Ontology (GO) and Pathway Analysis were performed using, respectively, the online tool DAVID version 6.8 (Huang da et al., 2009), and the Ingenuity Pathway Analysis Software (IPA; Qiagen; version 42012434). Differentially translated genes were submitted to IPA and subjected to Core Analysis with analysis parameters set to include Direct and Indirect Interactions and Experimentally Observed data only. Networks data was obtained for all datasets and a Molecular

Activity Predictor (MAP) analysis was applied based on the differentially regulated genes belonging to each individual network. For GO analysis, filtered gene lists set to highlight genes differentially repressed by WT or 2D were individually submitted to DAVID and GO annotation gathered for Biological Function, Molecular Function and Cellular Component.

IPA analysis was performed by Ines Amorim.

2.4.22 Protein expression and purification

pGEX-6P-1 vectors expressing the human 4E-BP2 WT and 4E-BP2 N99D/N102D protein with a N-terminal Glutathione S-transferase (GST) tag (Bidinosti et al., 2010a) were used for transformation in *Escherichia coli* BL21(DE3) (C600003, ThermoFisher Scientific). A 3C protease cleavage site is located between the GST tag and the protein, allowing tag removal and only two N-terminal residues (Gly-Pro) on the N-terminal side of the protein. Recombinant proteins were expressed in *Escherichia coli* BL21(DE3) by growing transformed cells in LB medium at 37 °C, inducing with 1 mM isopropyl β-D-1 thiogalactopyranoside (IPTG, I6758, Merck). After 3 h of induction at 28 °C, the cells were harvested, washed with 100 mM Tris-HCl (pH 7.5), 170 mM NaCl and lysed in 20 mM PBS, (pH 7.4), 270 mM NaCl, 5 mM KCl, 1 mM DTT, 0.1 mg/ml lysozyme (L6876, Merck) by one freeze-thaw cycle, followed by sonication. Lysed cells were centrifuged at 16,000 x *g* for 30 min at 4 °C and the supernatant was loaded onto a glutathione-sepharose resin (GE17-0756-01, GE Healthcare), allowing the protein to bind for 4 h at 4 °C. The resin was then washed with 10mM PBS, (pH 7.4), 140 mM NaCl, 3 mM KCl and 1 mM DTT. Recombinant His-tagged 3C protease was added to the resin and incubated for 18 h at 4 °C. Tagless protein was collected and loaded onto a Ni-NTA resin (30230, Qiagen) to bind the 3C protease. Tagless protein was eluted with 20 mM imidazole. Eluted fractions were loaded onto a Superdex S200 16/600 column (GE Healthcare), equilibrated with 20 mM Tris-HCl pH 7.4 and 150 mM NaCl. 4E-BP2 gave one monodisperse peak, which was collected and 1 mM DTT was added. Protein samples were then concentrated using a 3 kDa MWCO spin concentrator to 4-11 mg/ml. Protein concentration was determined by absorbance measurements at 280 nm on a Nanodrop and protein identity was confirmed by tryptic in-gel digestion and mass spectrometry using the method described previously (Raasakka et al., 2015). (See Appendix for recombinant protein sequences)

Protein samples used for NMR were prepared as stated above but expressed in M9 minimal medium supplied with N^{15} labeled ammonium chloride. The buffer used in the final SEC purification step consisted of 20 mM PBS pH 7.4 and 150 mM NaCl.

2.4.23 Size exclusion chromatography-multi angle light scattering

The molecular mass of 4E-BP2 was determined with SEC-MALS, using a miniDAWN Treos MALS detector (Wyatt). Protein concentration was measured with an online RI detector. The SEC column, Superdex S200 Increase 10/300 (GE Healthcare), was equilibrated with 20 mM Tris-HCl (pH 7.4), 150 mM NaCl at 4 °C. The SEC-MALS system was calibrated using ovalbumin, and the concentration of the injected 4E-bP2 was 1.2 mg/ml.

2.4.24 Synchrotron radiation circular dichroism

Recombinant purified proteins were either diluted into a buffer (20 mM PBS pH 7.4, 150 mM NaF and 0.5 mM DTT) just before the measurement or dialyzed against 20mM phosphate pH 7.5 for 20 h at 4 °C. The ellipticity of each sample was measured between 170 and 280 nm in a quartz cuvette with a pathlength of 0.1 mm on the AU-CD beamline at ASTRID2 (ISA, Aarhus, Denmark) at 10 °C. Sample concentrations were between 0.3-1.0 mg/ml and the same protein concentration was used, when different samples were compared.

2.4.25 Small angle X-ray scattering

SAXS data were collected on the BM29 beamline (Pernot et al., 2013) of the European synchrotron radiation facility (ESRF, Grenoble, France), using a wavelength of 0.9919 Å. For batch measurements, 20 frames were collected with 0.5 seconds of exposure per frame at a temperature of 10 °C. Sample concentrations were within a range of 0.5-10 mg/ml. SEC-SAXS was also performed using an Agilent BioSEC-3 HPLC column, equilibrated with 20 mM Tris-HCl (pH 7.4), 150 mM NaCl, collecting one frame/s. Data were processed and analyzed using the ATSAS software suite (Konarev et al., 2003). The radius of gyration was calculated either based on the

Guinier region or using the Debye formula (Calmettes et al., 1994). 3D *ab initio* models were generated using DAMMIN (Svergun, 1999) and GASBOR (Svergun et al., 2001).

2.4.26 Nuclear magnetic resonance

Purified ^{15}N labelled proteins (9 mg/ml) were measured in a buffer consisting of 20 mM PBS (pH 7.4), 150 mM NaCl and 1 mM DTT with 10% D_2O and 2,2-dimethyl-2-silapentane-5-sulfonate (0.1 mM), using an 850 MHz Bruker BioSpin 850 Ascend sepctrometer at 27 ^oC.

SRCD and SAXS were performed by Erik Ingmar-Hallin (University of Bergen, Norway) and NMR was performed by Erik Ingmar-Hallin in collaboration with J. Underhaug at the Norwegian NMR platform in Bergen.

2.4.27 Statistical Analysis and Experimental Design

All data are presented as mean ±S.E.M. (error bars) and individual experimental points are illustrated in bar graphs. Statistical significance was set *a priori* at 0.05 (n.s.: non-significant). The age of animals that were used for dissociated mouse cortical cultures and synaptoneurosomal preparations is mentioned in the description of the methods. The n number denotes biological replicates. For all experiments, the minimum number of biological replicates was 3, apart from Ribosome Profiling where 2 biological replicates were processed. Quantification of Western Blot and specifically of 4E-BP2 was carried out by quantifying the intensity of both, the middle and slowest migrating bands for deamidated 4E-BP2 and by quantifying the intensity of fastest migrating band for WT (non-deamidated) 4E-BP2. Both 4E-BP2 forms were normalised to the loading control. Most experiments that included Western Blot were design to identify whether there is an effect on deamidated 4E-BP2 compared to WT after a specific treatment. For these experiments, two-way repeated measures ANOVA was used. For quantification of data, two-way ANOVA was used to enable us to compare the mean differences between groups that have been split on two independent variables. The intensity is the dependent, continuous variable (corresponding to protein expression) of 4E-BP2. The first independent variable is treatment/time and consists of the following categorical groups: Vehicle-0 h, Treated-(1, 9, 48 h). The second independent variable is which specific 4E-BP2 form is affected and consists of two categorical groups (WT 4E-BP2, deamidated 4E-BP2).

Our main question is whether there is an interaction between treatment and specific 4E-BP2 form on 4E-BP2 expression. The interaction term in a two-way ANOVA informs us whether the effect of treatment on the intensity is the same for WT and deamidated 4E-BP2 (and vice versa). Bonferroni's posthoc does not assume that each comparison is independent of the others while Sidak method does. Thus, Bonferroni's correction is the appropriate and was used for our data, because it is more stringent. Details for statistical and post-hoc tests used were provided within figure legends; Data summaries and statistical analysis were carried out using Graphpad Prism 6 unless otherwise stated.

3. Investigating the Protein Turnover and Regulation of 4E-BP2

3.1 Introduction

Protein turnover is a crucial regulatory mechanism that enables cells to adapt to environmental changes by rapidly regulating their protein levels (Kristensen et al., 2013). It also allows cells to replace their damaged, misfolded proteins with newly synthesized functional copies (Toyama & Hetzer, 2013). The balance between protein synthesis and degradation determines the turnover rate of a protein (Price, Guan, Burlingame, Prusiner, & Ghaemmaghami, 2010);(Kristensen et al., 2013). It can vary from minutes to days depending on the protein function, localization (Toyama & Hetzer, n.d.), host cell (dividing, non-dividing) (Cambridge et al., 2011);(Yen, Xu, Chou, Zhao, & Elledge, 2008) and organism (Belle et al., 2006);(Toyama & Hetzer, 2013). Long-lived proteins evade protein turnover and are susceptible to accumulation of damage which may affect their physiological function (Toyama & Hetzer, 2013).

Posttranslational modifications such as deamidation affect protein stability, thus playing a major role in regulating protein half-lives. Deamidation is an age-dependent posttranslational modification of many aged proteins (Robinson and Robinson, 2001) such as crystallins, therefore promoting the formation of larger protein aggregates (Bloemendal et al., 2004). Consequently, the number of deamidated proteins increases with age *in vivo* in whole organisms and individual tissues (Robinson and Robinson, 2004). Protein degradation involves deamidation, according to the N-end rule pathway (Varshavsky, 2011). The N-end rule pathway denotes that the identity of N-terminal residue of a protein determines the *in vivo* half-life of the protein (Varshavsky, 2011). Specifically, N-terminal Asn or Gln deamidation acts as a

degradation signal called N-degron which destabilises these residues, targeting them for degradation by the Ubiquitin-proteasome pathway (Varshavsky, 2011).

Brain proteome has a long half-life compared to other tissues (Price et al., 2010). 4E-BP2, the abundant isoform of 4E-BPs in the brain, is a long half-life protein (Graber et al., 2013). Since deamidation labels many aged proteins, acting as a damage signal, but can also target proteins for degradation when it is present at N-terminal residues, we set out to determine whether and how deamidation of 4E-BP2 can affect the stability of the protein.

3.2 Experimental Aim

The main aim of this thesis is to investigate the role of deamidated 4E-BP2 in cap-dependent translation. To gain a further insight on the effect of deamidation on 4E-BP2, we examined the half-life of different 4E-BP2 forms in Human Embryonic Kidney cells (HEKs), in dissociated mouse cortical neuronal cultures and mouse isolated synaptoneurosomes. By blocking protein synthesis using different inhibitors, we investigated the degradation rate of different 4E-BP2 forms whereas by inhibiting proteasome activity, we studied the accumulation rate of these forms, indicating the sensitivity to proteasome degradation. To study whether there are different regulatory mechanisms for deamidated and WT 4E-BP2 and identify which signalling pathways are responsible for this regulation, we inhibited key molecules–regulators of cap-dependent translation in the brain. Moreover, we also investigated whether deamidation of 4E-BP2 is present in humans and different mouse models of Autism Spectrum Disorders. Overall, these experiments aim to shed light on the role of deamidated 4E-BP2 in the regulatory mechanisms of translational control in the mammalian brain that govern synaptic plasticity, learning and memory.

3.3 Results

Before any data presented and discussed, Figure 3.1 shows the migration of endogenous 4E-BP2, endogenous phospho-4E-BP1 and endogenous phospho-4E-BP2 on a SDS-PAGE gel from a murine +brain lysate.

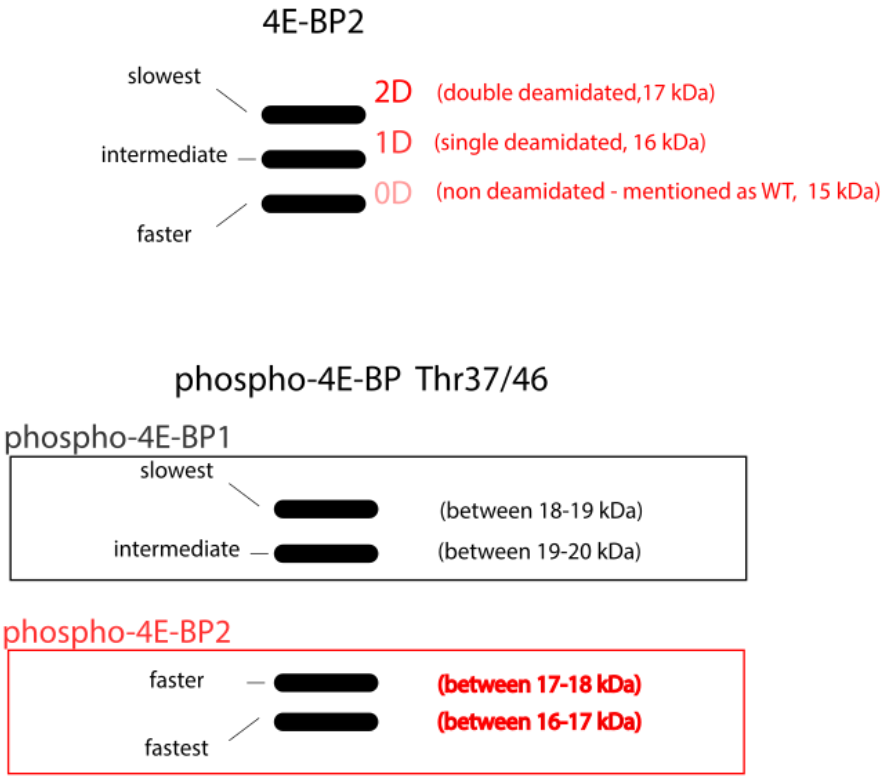

Figure 3.1 Schematic diagram of endogenous 4E-BP2, phospho-4E-BP1 and phospho-4E-BP2 migration on a SDS-PAGE gel from a murine brain lysate.

Top: Endogenous 4E-BP2 migrates as three bands on a SDS-PAGE gel. Bottom band (15 kDa) corresponds to non-deamidated 4E-BP2, referred to this thesis as WT. Middle (16 k Da) and top (17 kDa) slower migrating bands correspond to single and double deamidated 4E-BP2, respectively. **Bottom**: Phospho-4E-BP Thr37/46 recognizes endogenous 4E-BP1 forms (between 18-21 kDa) and endogenous 4E-BP2 forms (between 16-18 kDa) when phosphorylated at Thr37 and/or Thr46.

3.3.1 Deamidated 4E-BP2 undergoes accelerated degradation in Human Embryonic Kidney cells

Asn or Gln deamidation increases in aged-proteins (Robinson and Robinson, 2001). Moreover, deamidated Asn or Gln at N-terminal in proteins determine the half-life of them, acting as destabilising residues (Varshavsky, 1997). To examine the stability of 4E-BP2, we transfected plasmids that encode the following different forms of 4E-BP2: 4E-BP2 WT and 4E-BP2 N99D/N102D (encodes for the double deamidated protein), both present in mammalian brain; and 4E-BP2 N99A/N102A which was used as negative control of deamidation since the two asparagine sites are replaced by alanine and thus it cannot undergo deamidation. Specifically, in HEKs we transfected the following plasmids [(pcDNA3.1-3 x HA -*Eif4ebp2* (WT), pcDNA3.1-3 x HA-*Eif4ebp2* N99D/N102D (double deamidated), pcDNA3.1-3 x HA-*Eif4ebp2* N99A/N102A (alanine mutant)]. 48 h posttransfection, we treated the cells with 100 µg/ml Cycloheximide (CHX) (Dai et al., 2013), a protein synthesis inhibitor that impedes elongation of the peptide chain (Balinga et al., 1969) for 0, 1, 2 and 6 h. Cells were lysed, followed by western blotting for HA (Figure 3.2).

Using western blotting, we detected a significantly faster degradation of deamidated 4E-BP2 compared to WT 4E-BP2 or Alanine mutant ($p < 0.05$, Figure 3.2). Moreover, Alanine mutant displays the slowest degradation of all 4E-BP2 forms (Figure 3.2). Interestingly, after 6 h of Cycloheximide treatment, we observed that protein levels of both deamidated 4E-BP2 and Alanine mutant increase by 20% compared to 2 h whereas 4E-BP2 WT remains stable (Figure 3.2). At the same indicated time point, 6 h, a slower migrating band >15kDa, which is the size of HA-4E-BP2, is apparent on each blot of 4E-BP2, WT, deamidated and Alanine mutant. This slower migrating band denotes a posttranslational modification that has taken place, probably phosphorylation, after 6 h of Cycloheximide treatment (Figure 3.2). Taken together, these data suggest that 4E-BP2 N99D/N102D is prone to enhanced degradation.

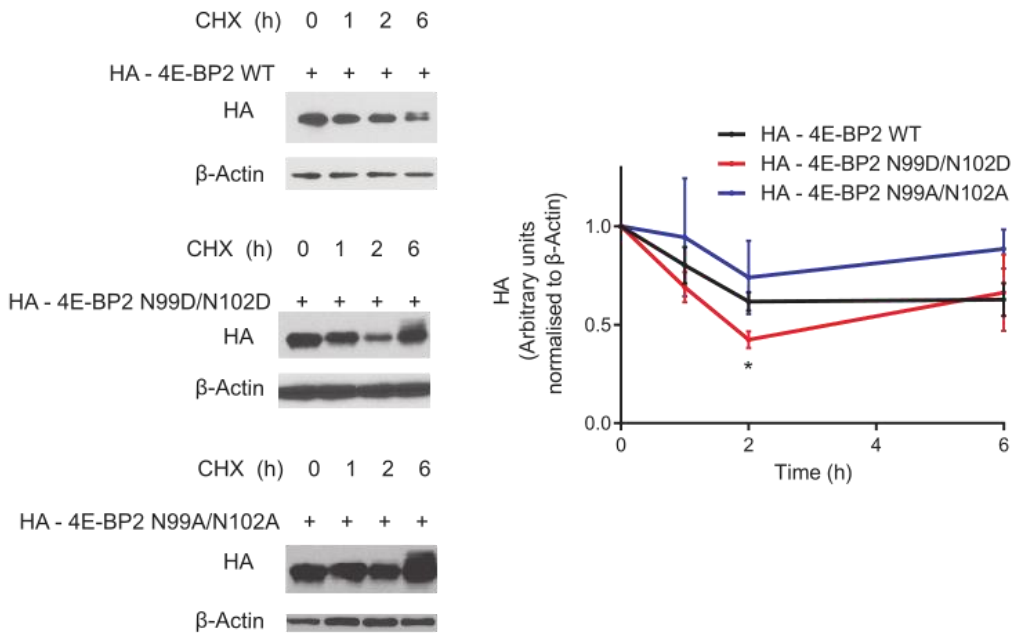

Figure 3.2 Protein stability assay of 4E-BP2 Wild Type, 4E-BP2 double deamidated and 4E-BP2 Alanine mutant.

A. Representative immunoblots of lysates from transfected HEKs probed for HA. HA 4E-BP2 WT and HA 4E-BP2 N99A/N102A appeared at 15 kDa whereas HA 4E-BP2 N99D/N102D appeared at 17 kDa. β-Actin was used as a loading control and appeared at 42 kDa. HEKs were transfected with 3 x HA–4E-BP2 plasmids that express three different forms of 4E-BP2 [WT, Double deamidated (N99D/N102D), Alanine mutant (N99A/N102A]. After 48 h of transfection, cells were treated with CHX (100 µg/ml) for 0, 1, 2, 6 h. Cells were lysed, followed by western blotting for HA. **B**. Quantitative analysis of the different 4E-BP2 amounts in (A). The intensities of the bands were measured using Image Studio Lite Ver 5.2 and normalised against β-Actin. The intensity of the band at 0 h (lane 1) is set as 1. The data shown in (A) are representative of three independent experiments. Quantitative data with mean ± SEM are shown in (B). *$p < 0.05$ using Bonferroni-corrected two-way ANOVA.

3.3.2 Hypophosphorylated 4E-BP2 forms are unstable in Human Embryonic Kidney cells

Apart from deamidation, phosphorylation can also have an impact on protein half-lives. Specifically, the first isoform of 4E-BPs, 4E-BP1, upon phosphorylation at sites 37/46 by the mammalian kinase mTOR, concurrently undergoes (Elia et al., 2008). Additionally, phosphorylated 4E-BP1 is unstable when it is unbound to eIF4E and gets degraded after being ubiquitinated (Yanagiya et al., 2012). Therefore, we asked whether phosphorylation of 4E-BP2 affects protein stability. To answer this question, we transfected the same plasmids mentioned above that express three different 4E-BP2 forms (WT, double deamidated, Alanine mutant) in HEKs and 24 h after transfection, we treated them with 250 nM Torin1, a selective active-site mTOR inhibitor, for 12 h, thus inhibiting phosphorylation of 4E-BP2 (Thoreen et al., 2009). After 12 h of Torin1 treatment only hypophosphorylated 4E-BP2 forms are present (Figure 3.3). Then, we treated the cells with 100 µg/ml CHX for 0, 1, 2 and 6 h, to examine the stability of hypophosphorylated 4E-BP2. Cells were lysed, followed by western blotting for HA as shown in Figure 3.3.

After 12 h of Torin1 and 1 h of CHX treatment, the protein amounts of all three 4E-BP2 forms reduce to a level that is not detectable by western blotting, implying an accelerated degradation for all three hypophosphorylated 4E-BP2 forms (Figure 3.3). Blots were also probed for phospho-4E-BP2 37/46 but protein levels could not be detected even at 0 h of CHX treatment, showing that 12 h of Torin1 treatment effectively inhibits phosphorylation of 4E-BP2 (Figure 3.3). Thus, prolonged inhibition of phosphorylation reduces protein stability of 4E-BP2 in HEKs.

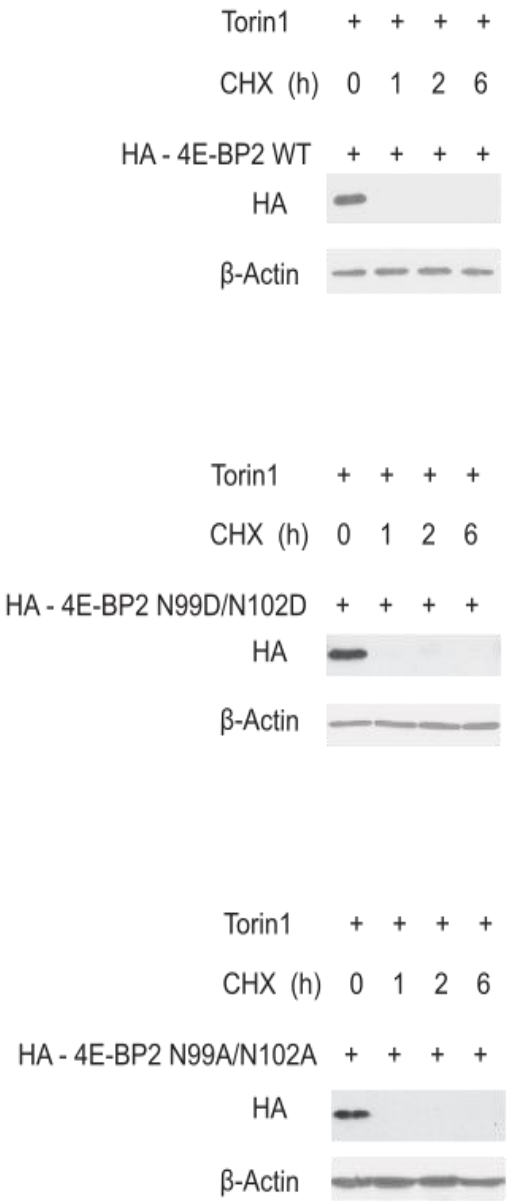

Figure 3.3 Protein stability assay of hypophoshorylated 4E-BP2 Wild Type, 4E-BP2 double deamidated and 4E-BP2 alanine mutant.

Representative immunoblots of lysates from transfected HEKs probed for HA. β-Actin was used as a loading control. HEKs were transfected with 3 x HA–4E-BP2 plasmids that express three different forms of 4E-BP2 [WT, Double deamidated (N99D/N102D), Alanine mutant (N99A/N102A)]. After 24 h of transfection, cells were treated with Torin1 (250nM) for 12 h and then with CHX (100 µg/ml) for 0, 1, 2 and 6 h. Cells were lysed, followed by western blotting for HA. The data shown are representative of three independent experiments.

To test the stability of endogenous 4E-BP2 and compare it with the stability of transfected HA–4E-BP2 WT in HEKs, we treated untransfected HEKs with 100 µg/ml CHX for 0, 1, 2, 6 h. The cells were lysed, followed by western blotting and probed for 4E-BP2 to test the protein stability of endogenous protein (Figure 3.4). For investigating the stability of hypophosphorylated endogenous 4E-BP2, we treated untransfected HEKs with 250nM Torin1 for 12 h and then, with 100 µg/ml CHX for 0, 1, 2, 6 h (Figure 3.4). Figure 3.4 depicts immunoblots from a protein stability assay of endogenous 4E-BP2 WT and endogenous hypophosphorylated 4E-BP2 WT.

Endogenous 4E-BP2 is stable and inhibition of protein synthesis with CHX does not affect its protein levels, even after 6 h of treatment (Figure 3.4). Transfected 4E-BP2 WT is also stable after CHX treatment, as shown in Figure 3.2, denoting that both transfected and endogenous 4E-BP2 display comparable degradation rates. 4E-BP1 exhibits a faster degradation rate as compared to 4E-BP2 (Figure 3.4). Furthermore, after 2 h and 6 h of CHX treatment, we detected only slower migrating forms (>17kDa), corresponding to hyperphosphorylated 4E-BP1, showing that CHX induce phosphorylation of 4E-BP1 (Figure 3.4). After Torin1 treatment for 12 h, we observed lower molecular weight bands (<15kDa) for 4E-BP2 and 4E-BP1, indicating that Torin1 effectively inhibits phosphorylation of both proteins (Figure 3.4). Hypophosphorylated endogenous 4E-BP2 and 4E-BP1 are also stable after inhibition of protein synthesis with CHX (100 µg/ml), displaying a different stability pattern compared to the transfected hypophosphorylated 4E-BP2 forms (Figure 3.3). Therefore, these data suggest that endogenous 4E-BP2 WT displays a similar stability compared to transfected HA–4E-BP2 WT apart from its hypophosphorylated form. Lastly, 4E-BP1 follows a different stability pattern than 4E-BP2.

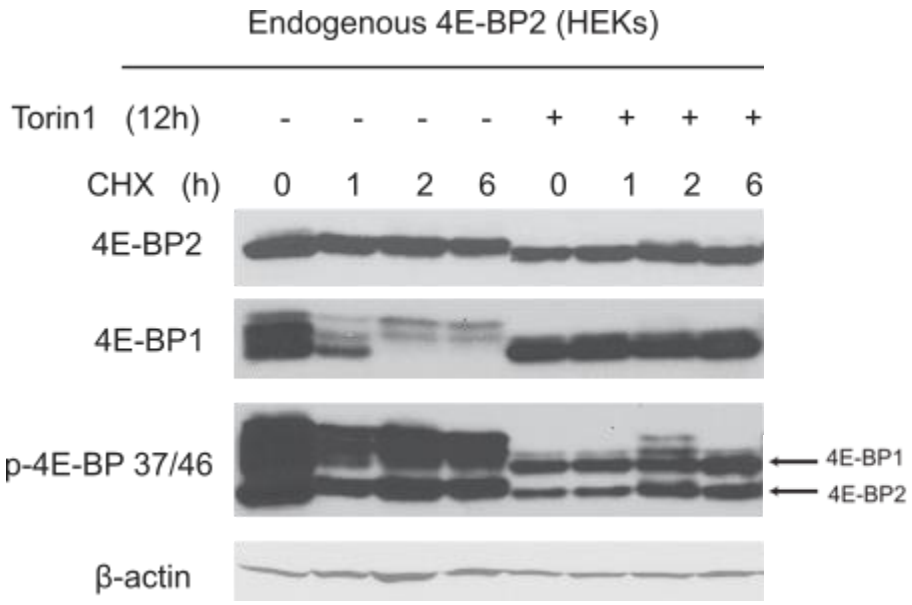

Figure 3.4 Protein stability assay of endogenous 4E-BP2 Wild Type, endogenous hypophoshorylated 4E-BP2 WT and endogenous 4E-BP1.

Representative immunoblots of lysates from untransfected HEKs probed for 4E-BP2, 4E-BP1, phospho – 4E-BP 37/46. β-Actin was used as a loading control. Cells were treated with Torin1 (250nM) for 12 h and then with CHX (100 μg/ml) for 0, 1, 2, 6 h. Cells were lysed, followed by western blotting. The data shown are representative of three independent experiments.

3.3.3 Deamidated 4E-BP2 is degraded by the proteasome

Since deamidation is responsible for targeting proteins for degradation according to N-end rule pathway (Varshavsky, 1997), we asked whether 4E-BP2 deamidation plays a similar role. A number of proteins that undergo deamidation are then targeted by the Ubiquitin Proteasome pathway (Dho et al., 2013). For example, deamidation of Bcl-xL has been conserved from metazoan to human, denoting its crucial role in regulating protein levels (Dho et al., 2013). To study the proteasome sensitivity of each 4E-BP2 form, we transfected the aforementioned plasmids, which express the three different 4E-BP2 forms (WT, double deamidated, Alanine mutant) in HEKs and 48 h after transfection, we treated them with 5 μM Lactacystin, a

proteasome inhibitor (Fenteany et al., 1995), for 0 and 6 h. Then, cells were lysed, followed by western blotting for HA. Representative blots are shown in Figure 3.5.

After 6 h of Lactacystin treatment, deamidated 4E-BP2 protein abundance significantly increases, as compared to WT 4E-BP2 or Alanine mutant [$p < 0.001$, Figure 3.5(A), (B)]. Inhibition of the proteasome with Lactacystin does not affect endogenous 4E-BP2 WT [Figure 3.5(C)], displaying a similar pattern as transfected 4E-BP2 WT.

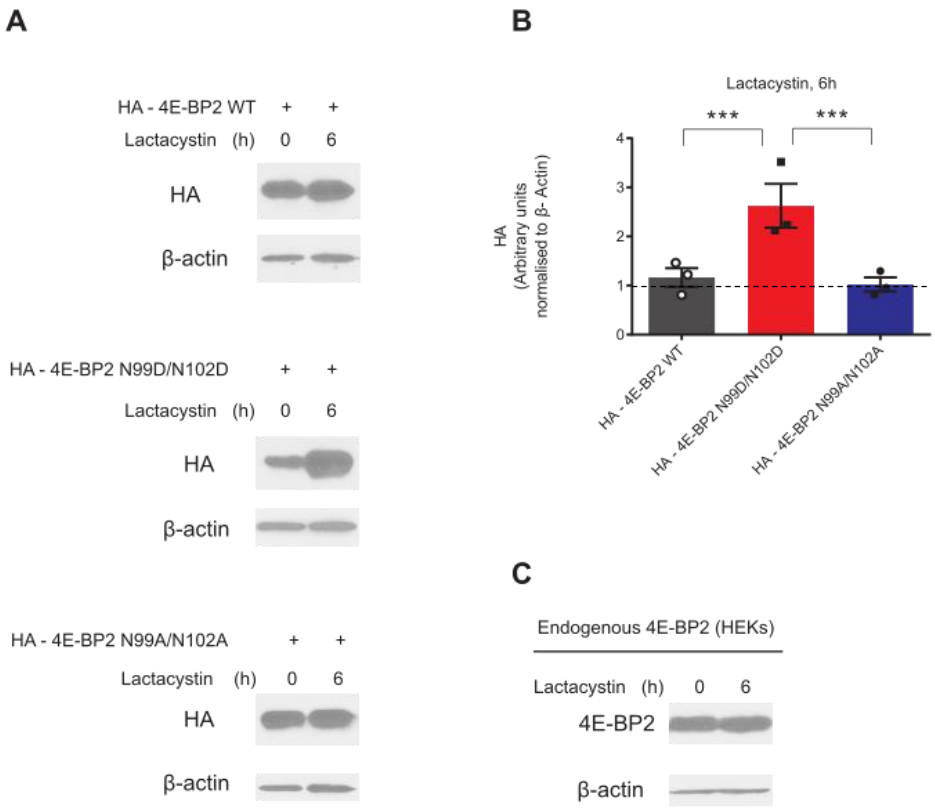

Figure 3.5 Deamidated 4E-BP2 accumulates after inhibition of proteasome with Lactacystin in HEKs.

A. Representative immunoblots of lysates from transfected HEKs probed for HA. HA 4E-BP2 WT and HA 4E-BP2 N99A/N102A appeared at 15 kDa whereas HA 4E-BP2 N99D/N102D appeared at 17 kDa. β-Actin was used as a loading control and appeared at 42 kDa. HEKs were transfected with 3 x HA – 4E-BP2 plasmids that express three different forms of 4E-BP2 [(WT, Double deamidated (N99D/N102D), Alanine mutant (N99A/N102A)]. After 48 h of transfection, cells were treated with Lactacystin (5 µM) for 0, 6 h. Cells were lysed, followed by western blotting for HA. **B**. Quantitative analysis of the different 4E-BP2 amounts in (A). The intensities of the bands were measured using Image Studio Lite Ver 5.2 and normalised against β-Actin. The intensity of the band at 0 h (lane 1) is set as 1 (dotted line on graph). The data shown in (A) are representative of three independent experiments. Quantitative data with mean ± SEM are shown in (B). ***$p < 0.001$ using Bonferroni-corrected two-way ANOVA. **C.** Representative immunoblot of lysate from untransfected HEKs probed for 4E-BP2. β-Actin was used as a loading control. Cells were treated with Lactacystin (5 uM) for 0, 6 h, then were lysed, followed by western blotting for 4E-BP2. The data shown are representative of independent three independent experiments.

To further confirm the accumulation of deamidated 4E-BP2 in HEKs after inhibition of the proteasome, we used a different proteasome inhibitor, MG132 (Hayashi et al., 1992). We transfected HEK cells with the following plasmids [(pcDNA3.1-3 x HA-*Eif4ebp2* (WT), pcDNA3.1-3 x HA-*Eif4ebp2* N99D/N102D (double deamidated), pcDNA3.1-3 x HA-*Eif4ebp2* N99A/N102A (alanine mutant)], and 48 h after transfection, we treated them with 20 μM MG132 for 0 and 6 h. The cells were lysed, followed by western blotting for HA. Representative blots are presented in Figure 3.6.

After inhibition of proteasome with MG132, deamidated 4E-BP2 protein levels accumulate, as compared to WT or Alanine mutant ($p < 0.05$, $p < 0.01$, Figure 3.6). Moreover, we observed lower migrating bands (<15kDa) of deamidated protein, which appear only after proteasome inhibition, possibly these smaller species are present due to ubiquitin-induced fragmentation of the protein since they cannot be degraded after MG132 treatment (Figure 3.6). Therefore, these data suggest that N99D/N102D mutation in 4E-BP2 leads the protein to accelerated proteasomal degradation.

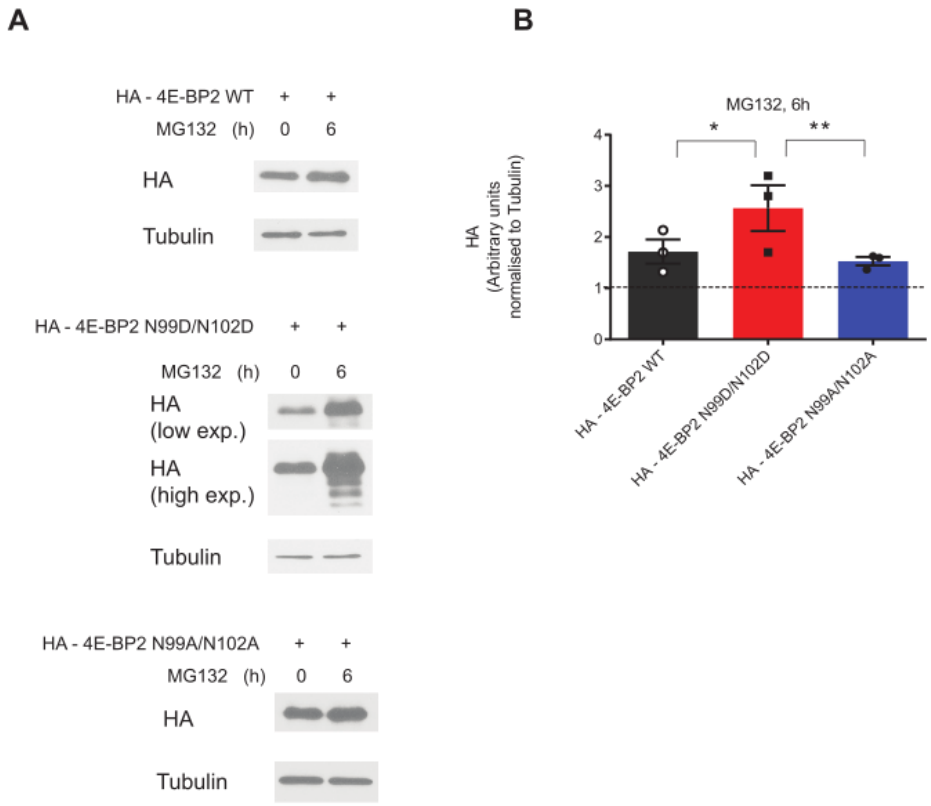

Figure 3.6 Deamidated 4E-BP2 accumulates after inhibition of the proteasome with MG132 in HEKs.

A. Representative immunoblots of lysates from transfected HEKs probed for HA. HA 4E-BP2 WT and HA 4E-BP2 N99A/N102A appeared at 15 kDa whereas HA 4E-BP2 N99D/N102D appeared at 17 kDa. Tubulin was used as a loading control and appeared at 50 kDa. HEKs were transfected with 3 x HA–4E-BP2 plasmids that express three different forms of 4E-BP2 [WT, Double deamidated (N99D/N102D), Alanine mutant (N99A/N102A)]. After 48 h of transfection, cells were treated with MG132 (20 uM) for 0, 6 h. Cells were lysed, followed by western blotting for HA. Low exposure of film corresponds to 1-3 min. High exposure of films corresponds to 15-20 min. **B**. Quantitative analysis of the different 4E-BP2 amounts in (A). The intensities of the bands were measured using Image Studio Lite Ver 5.2 and normalised against Tubulin. The intensity of the band at 0 h (lane 1) is set as 1 (dotted line on graph). The data shown in (A) are representative of three independent experiments. Quantitative data with mean ± SEM are shown in (B). *$p < 0.05$, **$p < 0.01$ using Bonferroni-corrected two-way ANOVA. For quantification, only films that were exposed for 1-3 min (low exposure) were used.

3.3.4 Deamidated 4E-BP2 is highly ubiquitinated in HEKs

Since deamidated 4E-BP2 is rapidly degraded by the proteasome compared to WT 4E-BP2 or Alanine mutant, we proceeded to examine the ubiquitination status of 4E-BP2, using an *in vivo* ubiquitination assay. In HEKs, we transfected each of the three different plasmids that express WT, deamidated and Alanine mutant 4E-BP2 along with His-Ubiquitin plasmid, and 48 h after transfection we treated cells with 20 μM MG132 for 6 h. Then, we performed a pull-down assay using Ni-NTA agarose on a column to purify His-tagged ubiquitinated proteins, followed by western blotting for HA to detect ubiquitinated 4E-BP2 forms as Figure 3.7 indicates. Deamidated 4E-BP2 immunoprecipitates with a greater amount of His-Ubiquitin than WT protein or Alanine mutant (Figure 3.7), supporting that this increased ubiquitination leads the protein to degradation by the Ubiquitin proteasome pathway.

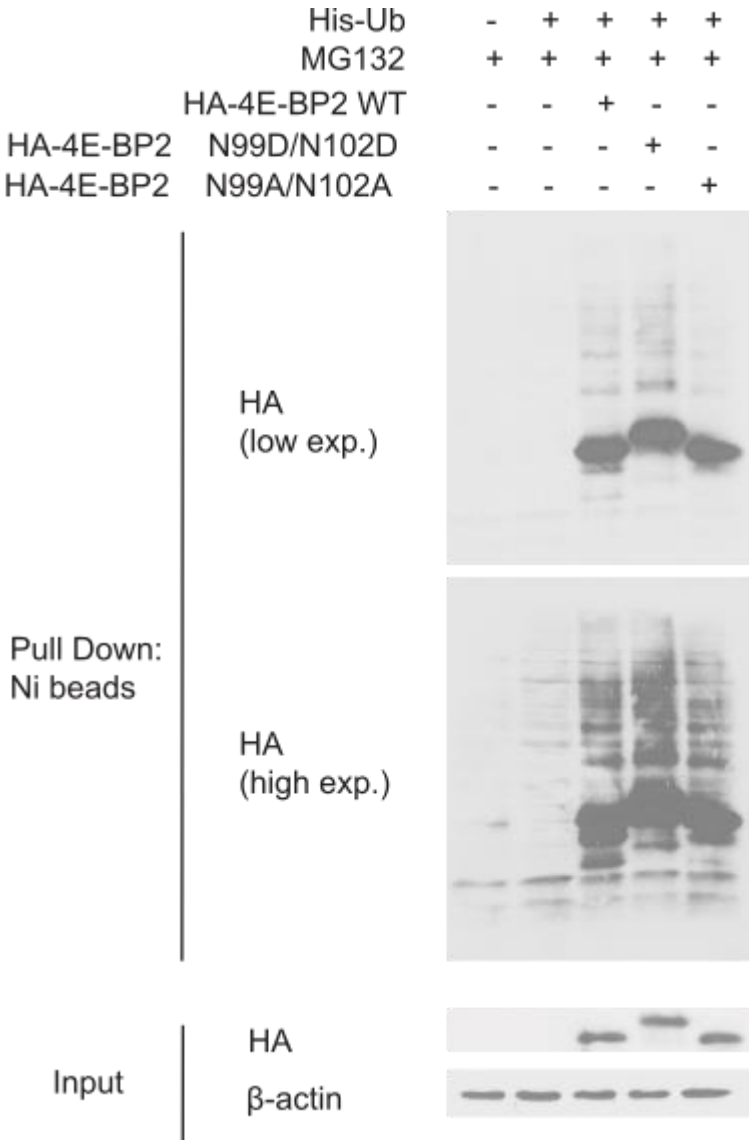

Figure 3.7 Deamidated 4E-BP2 is highly ubiquitinated in HEKs.

HA-4E-BP2 WT, deamidated and Alanine mutant plasmids were transfected in HEKs along with His-Ubiquitin, and cells were treated with 20 µM MG132 for 6 h, followed by *in vivo* ubiquitination assay. Proteins that were pulled-down were then analyzed by western blotting and probed for HA. HA 4E-BP2 WT appeared at 15 kDa whereas HA 4E-BP2 N99D/N102D appeared at 17 kDa in the total lysates (input). Expression of each 4E-BP2 form is shown in lysates/input that were used for the pull-down assay. β-Actin was used as a loading control and appeared at 42 kDa. Low exposure of film corresponds to 1-3 min. High exposure of films corresponds to 15-20 min.

3.3.5 Raptor affects the stability of 4E-BP2 Wild Type and Alanine mutant

3.3.5.1 Raptor co-expression reduces the stability of wild type 4E-BP2

Regulation of 4E-BPs and consequently, of protein synthesis is mediated through mTOR kinase. mTOR phosphorylates 4E-BPs in a hierarchical manner, thus abrogating their affinity for eIF4E and allowing initiation of protein synthesis (Ma and Blenis, 2009). Deamidated 4E-BP2 displays increased association with Raptor, a component of mTORC1 complex (Bidinosti et al., 2010b). Raptor is a large scaffolding protein, responsible for recruiting substrates to the mTOR kinase for phosphorylation (Ma and Blenis, 2009). Therefore, we asked whether the enhanced interaction of deamidated 4E-BP2 with Raptor plays a role in regulating the stability of the protein. To study the stability of all 4E-BP2 forms along with the interaction with Raptor, we transfected each of the three different 4E-BP2 plasmids that encode different protein forms (WT, deamidated, Alanine mutant) along with Myc-Raptor in HEKs and 48 h after transfection we treated the cells with 100 µg/ml CHX for 0, 1 and 2 h. Cells were lysed, followed by western blotting for HA and Myc. Representative blots and a graph for 4E-BP2 WT are shown in Figure 3.8.

After co-expression of Raptor and inhibition of protein synthesis with CHX for 2 h, 4E-BP2 WT protein amounts significantly decrease ($p < 0.05$, right blot, Figure 3.8), denoting a rapid degradation compared to the exhibited slow degradation of transfected 4E-BP2 WT with empty vector (left blot, Figure 3.8). Thus, Myc-Raptor plays a major role in regulating the stability of 4E-BP2 WT in HEKs, since co-expression of Myc-Raptor provokes 4E-BP2 WT to behave similarly as deamidated 4E-BP2.

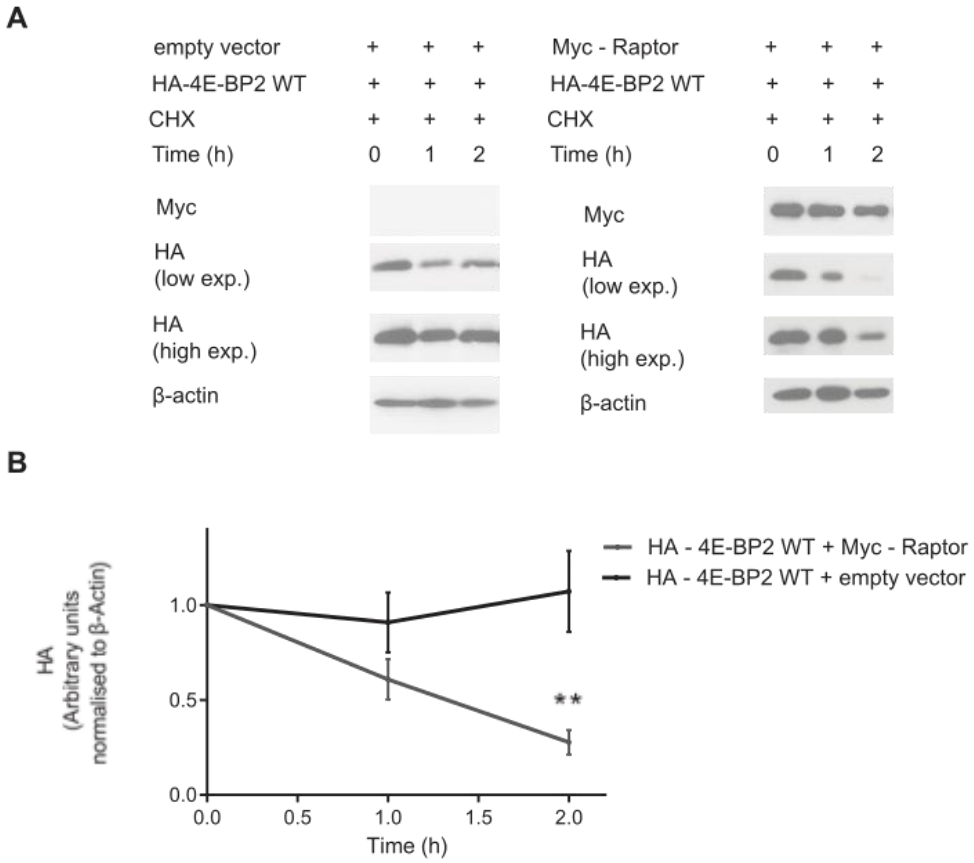

Figure 3.8 Protein assay stability of 4E-BP2 WT after co-transfection with Myc-Raptor.

A. Representative immunoblots of lysates from transfected HEKs probed for HA and Myc. HEKs were transfected with HA – 4E-BP2 plasmid that express 4E-BP2 WT and Myc – Raptor or empty vector. After 48 h of transfection, cells were treated with CHX (100 µg/ml) for 0, 1, 2 h. Cells were lysed, followed by western blotting for HA. HA 4E-BP2 WT appeared at 15 kDa and Myc-Raptor appeared at 151 kDa. β-Actin was used as a loading control and appeared at 42 kDa. Low exposure of film corresponds to 1-3 min. High exposure of films corresponds to 15-20 min. **B.** Quantitative analysis of 4E-BP2 WT amount (A). The intensities of the bands were measured using Image Studio Lite Ver 5.2 and normalised against β-Actin. The intensity of the band at 0 h (lane 1) is set as 1. The data shown in (A) are representative of three independent experiments. Quantitative data with mean ± SEM is shown in (B). *$p < 0.05$ using Bonferroni-corrected two-way ANOVA. For quantification, only films that were exposed for 1-3 min (low exposure) were used.

3.3.5.2 Raptor co-expression does not affect the degradation rate of deamidated 4E-BP2

Since deamidated 4E-BP2 displays enhanced interaction with Raptor (Bidinosti et al., 2010b), we asked whether overexpression of Myc–Raptor in HEKs will affect the stability of deamidated 4E-BP2. Therefore, we co-transfect HEKs with plasmids expressing double deamidated 4E-BP2 and Myc-Raptor. After 48 h of transfection, cells were treated with CHX 100 µg/ml (0, 1, 2 h). Then, cells were lysed, followed by western blotting for HA and Myc (Figure 3.9).

Co-transfection with Myc-Raptor does not affect deamidated 4E-BP2 degradation rate, as compared to empty vector transfected cells (Figure 3.9). It is possible that increased association with endogenous Raptor has already decreased the stability of the protein to a level that is very unstable, thus overexpression of Raptor cannot further reduce the stability of deamidated 4E-BP2. Furthermore, after co-transfection with Myc-Raptor, protein levels of deamidated 4E-BP2 reduce (0 h, right blot), independent of CHX treatment, as compared to the levels after co-transfection with empty vector (0 h, left blot), (Figure 3.9). Therefore, expression of Myc-Raptor might reduce protein levels of deamidated 4E-BP2 very quickly prior to CHX treatment.

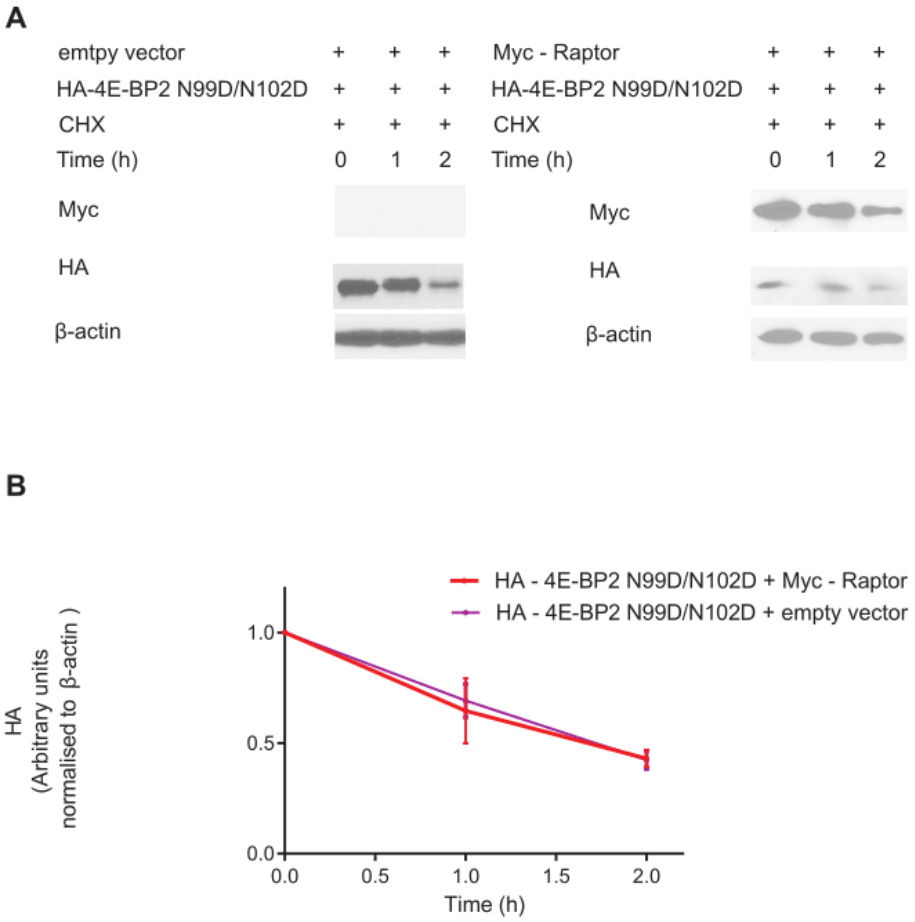

Figure 3.9 Protein stability assay of 4E-BP2 N99D/N102D after co-transfection with Myc-Raptor.

A. Representative immunoblots of lysates from transfected HEKs probed for HA and Myc. HEKs were transfected with HA–4E-BP2 plasmid that express deamidated 4E-BP2 and Myc–Raptor or empty vector. After 48 h of transfection, cells were treated with CHX (100 µg/ml) for 0, 1, 2 h. Cells were lysed, followed by western blotting for HA. HA 4E-BP2 N99D/N102D appeared at 17 kDa and Myc-Raptor appeared at 151 kDa. β-Actin was used as a loading control and appeared at 42 kDa **B.** Quantitative analysis of deamidated 4E-BP2 amount (A). The intensities of the bands were measured using Image Studio Lite Ver 5.2 and normalised against β-Actin. The intensity of the band at 0 h (lane 1) is set as 1. The data shown in (A) are representative of three independent experiments. Quantitative data with mean ± SEM is shown in (B). Bonferroni-corrected two-way ANOVA.

3.3.5.3. Raptor co-expression reduces the stability of 4E-BP2 Alanine mutant

Alanine mutant 4E-BP2 is a protein form than cannot undergo deamidation, thereby we questioned if Raptor will affect its stability since this specific form does not display increased interaction with Raptor as deamidated 4E-BP2 (Bidinosti et al., 2010b). Specifically, Alanine mutant 4E-BP2 exhibits similar level of interaction with Raptor in HEKs as 4E-BP2 WT protein (Bidinosti et al., 2010b). We co-transfected 4E-BP2 Alanine mutant and Myc–Raptor in HEKs and after 48 h, we treated the cells with 100 μg/ml CHX for 0, 1, 2 h. HEKs were lysed and proteins were resolved on an SDS-PAGE gel, followed by western blotting for HA and Myc. The stability of 4E-BP2 Alanine mutant is depicted in one representative blot and graph in Figure 3.10.

As expected, overexpression of Raptor has the same effect on the stability of the protein as in 4E-BP2 WT, making the protein very unstable (Figure 3.10). Specifically, after 1 h of CHX, protein amounts remarkably decrease ($p < 0.05$, Figure 3.10) and are detectable only after long exposure of the film. Moreover, after 2 h of treatment, a band of higher molecular weight (>15kDa) is apparent on the blot (Figure 3.10), possibly due to phosphorylation of the protein, induced by CHX treatment. Thus, these data suggest that interaction of 4E-BP2 with Raptor has a key role in determining the stability of 4E-B P2 protein.

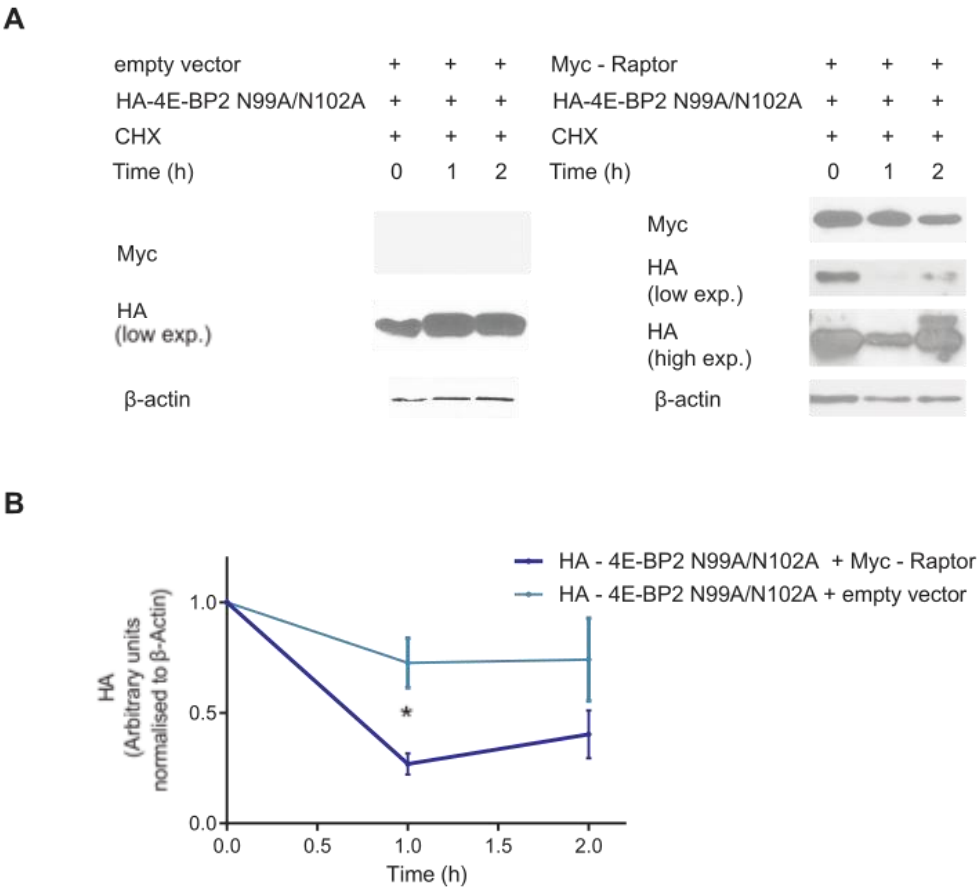

Figure 3.10 Protein stability assay of 4E-BP2 N99A/N102A after co-transfection with Myc-Raptor.

A. Representative immunoblots of lysates from transfected HEKs probed for HA and Myc. HEKs were transfected with HA–4E-BP2 plasmid that express Alanine mutant 4E-BP2. After 48 h of transfection, cells were treated with CHX (100 µg/ml) for 0, 1, 2 h. Cells were lysed, followed by western blotting for HA. HA 4E-BP2 N99A/N102A appeared at 15 kDa and Myc-Raptor appeared at 151 kDa. β-Actin was used as a loading control and appeared at 42 kDa. Low exposure of film corresponds to 1-3 min. High exposure of films corresponds to 15-20 min. **B.** Quantitative analysis of deamidated 4E-BP2 amount (A). The intensities of the bands were measured using Image Studio Lite Ver 5.2 and normalised against β-Actin. The intensity of the band at 0 h (lane 1) is set as 1. The data shown in (A) are representative of three independent experiments. Quantitative data with mean ± SEM is shown in (B). *$p < 0.05$ using Bonferroni-corrected two-way ANOVA. For quantification, only films that were exposed for 1-3 min (low exposure) were used.

3.3.5.4 Raptor does not affect the stability of a 4E-BP2 mutant lacking the ΔTOS motif

4E-BPs interact with Raptor through the TOS motif (TOR Signalling Motif) at the C-terminus (FEMDI) of 4E-BPs and is indispensable for phosphorylation of all

three 4E-BPs by the mTOR kinase (Schalm and Blenis, 2002). Furthermore, TOS motif is also crucial for regulation of cell growth through the mTOR signalling pathway (Schalm et al., 2003). Therefore, to study further the role of Raptor in regulation of stability of 4E-BP2, we questioned the stability of 4E-BP2 form in which TOS motif has been deleted, thus the interaction with Raptor has also been abolished (Bidinosti et al., 2010b). To answer this question, we co-transfected HEKs with a plasmid that expresses 4E-BP2 without the ΔTOS motif either with empty vector or with Myc–Raptor and 48 h later we treated the cells with 100 μg/ml CHX for 0, 1 and 2 h. Cells were lysed, followed by western blotting for HA and Myc. Representative blots and graphs are shown in Figure 3.11.

Overexpressing Myc–Raptor in HEKs does not affect the stability of 4E-BP2 ΔTOS (Figure 3.11), demonstrating that the TOS motif is crucial for interaction with Raptor and thus regulation of stability of 4E-BP2 from Raptor. Since the TOS motif has been abolished, Raptor probably cannot bind to 4E-BP2 and consequently affect the stability of this protein form.

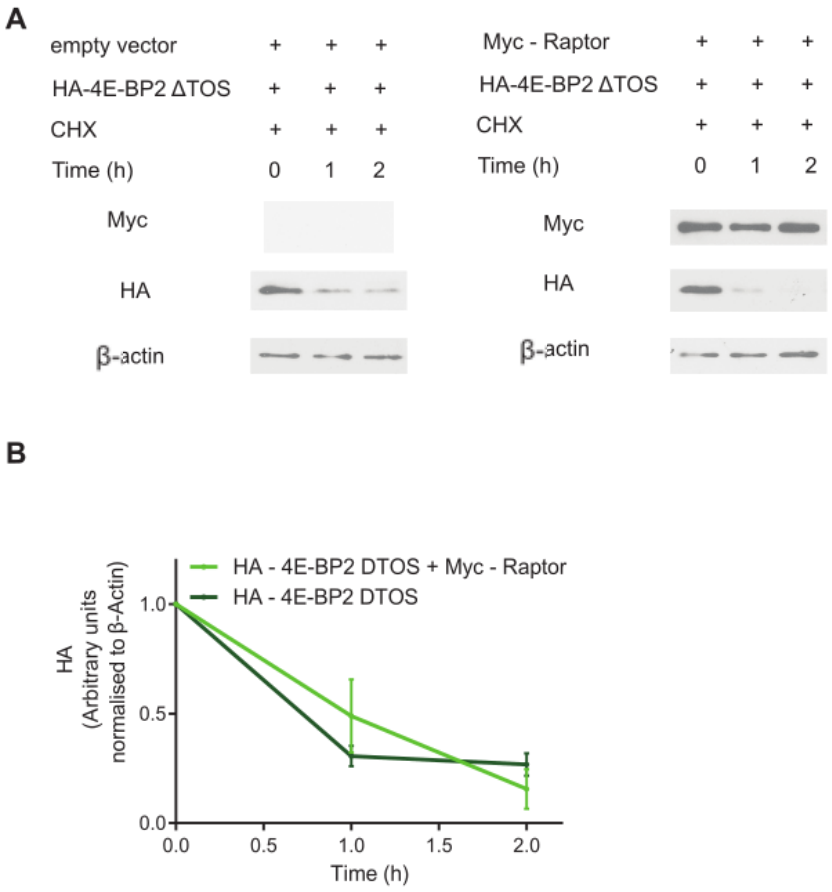

Figure 3.11 Protein stability assay of 4E-BP2 ΔTOS after co-transfection with Myc-Raptor.

A. Representative immunoblots of lysates from transfected HEKs with probed for HA and Myc. HEKs were transfected with HA–4E-BP2 plasmid that express 4E-BP2 without ΔTOS motif. After 48 h of transfection, cells were treated with CHX (100 µg/ml) for 0, 1, 2 h. Cells were lysed, followed by western blotting for HA and Myc. HA 4E-BP2 ΔTOS appeared at 13 kDa and Myc-Raptor appeared at 151 kDa. β-Actin was used as a loading control and appeared at 42 kDa **B.** Quantitative analysis of 4E-BP2 ΔTOS amount (A). The intensities of the bands were measured using Image Studio Lite Ver 5.2 and normalised against β-Actin. The intensity of the band at 0 h (lane 1) is set as 1. The data shown in (A) are representative of three independent experiments. Quantitative data with mean ± SEM is shown in (B). *$p < 0.05$ using Bonferroni-corrected two-way ANOVA.

3.3.6 Knockdown of *Raptor* increases the stability of deamidated 4E-BP2 in HEKs

Overexpression of Raptor in HEKs does not affect stability of deamidated 4E-BP2 as we observed in Figure 3.9. To confirm the vital role of Raptor in regulating the stability of deamidated 4E-BP2, we questioned the effect of down-regulation of endogenous Raptor in HEKs on the stability of deamidated 4E-BP2. To answer this question, we transfected HEKs with a plasmid encoding double deamidated 4E-BP2 and concomitantly we used siRNA to knockdown endogenous *Raptor* from the cells. After 48 h of transfection, we treated the cells with CHX (100 µg/ml) for 0, 1 and 2 h. Cells were lysed, followed by western blotting for HA and Raptor. Figure 3.12 (A) shows the pilot experiment where we transfected HEKs either with scramble siRNA or siRNAs for Raptor, trying different concentrations of two siRNAs (0, 1, 10 nM), each one targeting Raptor. Efficient knockdown of *Raptor* is achieved after transfection of siRNA2 (10nM). Therefore, we used siRNA2 at 10 nM to investigate the stability of deamidated 4E-BP2 after down-regulating Raptor. Figure 3.12 (B), (C) illustrates one representative blot and graph, respectively.

Our previous findings suggest that overexpression of Raptor does not affect the degradation rate of deamidated 4E-BP2, since CHX treatment does not change protein levels of deamidated 4E-BP2 even after 2h (Figure 3.9). Nevertheless, transient knockdown of *Raptor* using siRNA rescued the rapid degradation of deamidated 4E-BP2 since protein levels are stable ($p < 0.05$), as compared to scramble-transfected HEKs [Figure 3.12 (B), (C)]. Thereby, Raptor plays an important role in regulating the stability of deamidated 4E-BP2 and enhanced interaction of 4E-BP2 with Raptor is causal for decreased protein stability.

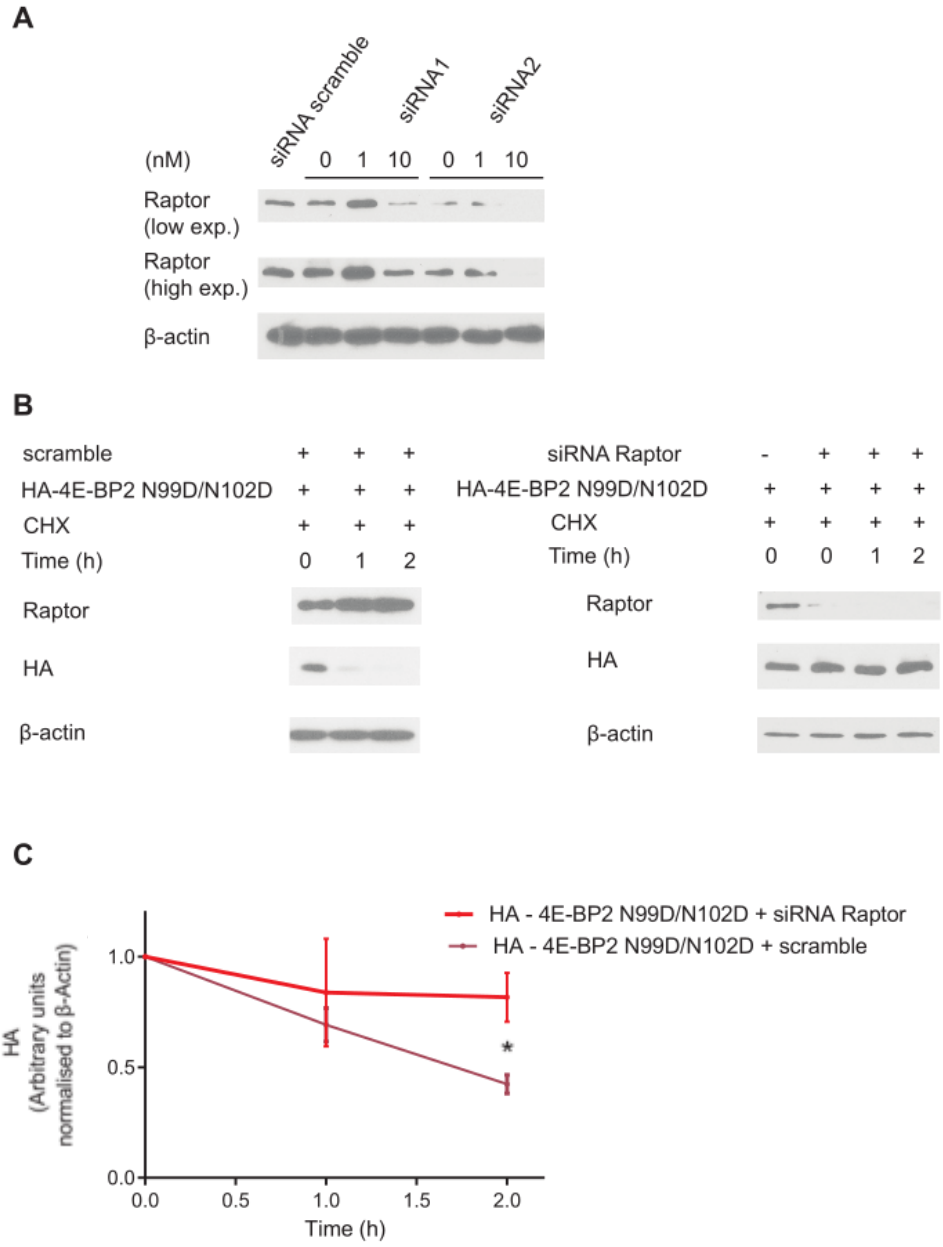

Figure 3.12 Protein stability assay of deamidated 4E-BP2 after down-regulating Raptor.

A. Representative immunoblots of lysates from transfected HEKs with a non-target control siRNA (scramble) or siRNA targeting Raptor, probed for Raptor. siRNA1 and siRNA2 were used in the following concentrations:0, 1, 10 nM. HA 4E-BP2 N99D/N102D appeared at 17 kDa and Raptor appeared at 150 kDa. β-Actin was used as a loading control and appeared at 42 kDa. **B.** HEKs were transfected with HA–4E-BP2 plasmid that express deamidated 4E-BP2 and siRNA2 (10nM) targeting endogenous Raptor. After 48 h of transfection, cells were treated with CHX (100 µg/ml) for 0, 1, 2 h. Cells were lysed, followed by western blotting for HA and Raptor. **C.** Quantitative analysis of deamidated 4E-BP2 amount (B). The intensities of the bands were measured using Image Studio Lite Ver 5.2 and normalised against β-Actin. The intensity of the band at 0 h (lane 1) is set as 1. The data shown in (A) are representative of

three independent experiments. Quantitative data with mean ± SEM is shown. *p < 0.05 using Bonferroni-corrected two-way ANOVA.

3.3.7 Raptor regulates the stability of deamidated 4E-BP2 through interaction with CUL4B-DDB1 E3 Ubiquitin ligase

Our previous findings demonstrate that Raptor plays a major role in controlling the stability of deamidated 4E-BP2 since down–regulation of endogenous Raptor increases protein stability, showing a slow degradation (Figure 3.12). Raptor is a WD40 repeat-containing protein and interacts and binds to CUL4B (Cullin 4B)–DDB1 (DNA Damage Binding Protein 1) complex, which is a Ubiquitin E3 ligase (Ghosh et al., 2008). Like others, WD40 proteins, Raptor acts as an adaptor protein, endowing CUL4B–DDB1 complex with substrate specificity (Ghosh et al., 2008). Loss of this complex displays similar effects as Raptor inactivation, setting the interaction of Raptor with CUL4B–DDB1 crucial for mediating Ubiquitin–dependent proteolysis of different proteins (Ghosh et al., 2008). For elucidating further the involvement of other proteins, apart from Raptor, in the regulation of stability of deamidated 4E-BP2, we asked whether deamidated 4E-BP2 apart from exhibiting increased interaction with Raptor also binds to the CUL4B – DDB1 complex. To answer this question, we co-transfected each of the plasmids expressing different 4E-BP2 form along with Myc–Raptor and 48 h after, we performed anti–Myc immunoprecipitation followed by western blotting for HA, Myc, CUL4B and DDB1 as shown in Figure 3.13 (A).

We confirmed that deamidated 4E-BP2 binds to Raptor with a higher affinity than WT, as evidenced by the increased HA-tagged deamidated protein amounts measured by immunoblotting in the myc immunoprecipitated samples [Figure 3.13 (A)]. Probing these samples with CUL4B and DDB1 antisera reveals increased binding of CUL4B to Raptor in the presence of deamidated but not WT 4E-BP2 [Figure 3.13 (A)]. DDB1 binding does not change between all samples [Figure 3.13 (A)]. Moreover, 4E-BP2 ΔTOS displays no interaction with Raptor but increased interaction with CUL4B [Figure 3.13 (A)]. We did not observe any differences in protein expression in input lysates regarding myc-tagged Raptor, CUL4B or DDB1, showing that all differences in the immunoprecipitated samples emerge from actual differences in protein-protein interactions and not due to different protein expression between samples [Figure 3.13 (A)]. In conclusion, these data strongly suggest that decreased

stability of deamidated 4E-BP2 is mediated by increased binding to the Raptor-CUL4B-DDB1 complex.

To confirm that CUL4B-DDB1 complex is responsible for ubiquitination of deamidated 4E-BP2, we performed an *in vitro* ubiquitination assay with recombinant proteins of Ubiquitin Proteasome pathway [UBE1 (E1) enzyme, UBE2L3 (E2) enzyme, CUL4B (E3) enzyme] along with recombinant Raptor, DDB1, WT and double deamidated 4E-BP2. After 2 h incubation, samples were lysed, followed by western blotting. Figure 3.13 (B) shows a representative blot. Deamidated 4E-BP2 exhibits increased ubiquitination levels from CUL4B-DDB1 complex compared to WT protein [Figure 3.13 (B)].

To determine the role of CUL4B to the stability of deamidated 4E-BP2, we also transfected HEKs with plasmid encoding double deamidated 4E-BP2 and concomitantly we used siRNA to knockdown endogenous *CUL4B*. After 48 h of transfection, we treated the cells with CHX (100 µg/ml) for 0, 1 and 2 h. Figure 3.13 (C) presents a representative blot and graph. Transient knockdown of *CUL4B* from HEKs using siRNA rescued the rapid degradation of deamidated 4E-BP2 as protein levels do not change after CHX treatment [Figure 3.13 (C)]. Thereby, CUL4B, similarly to Raptor, plays a pivotal role in regulating the stability of deamidated 4E-BP2 and is responsible for driving deamidated 4E-BP2 to the Ubiquitin Proteasome pathway.

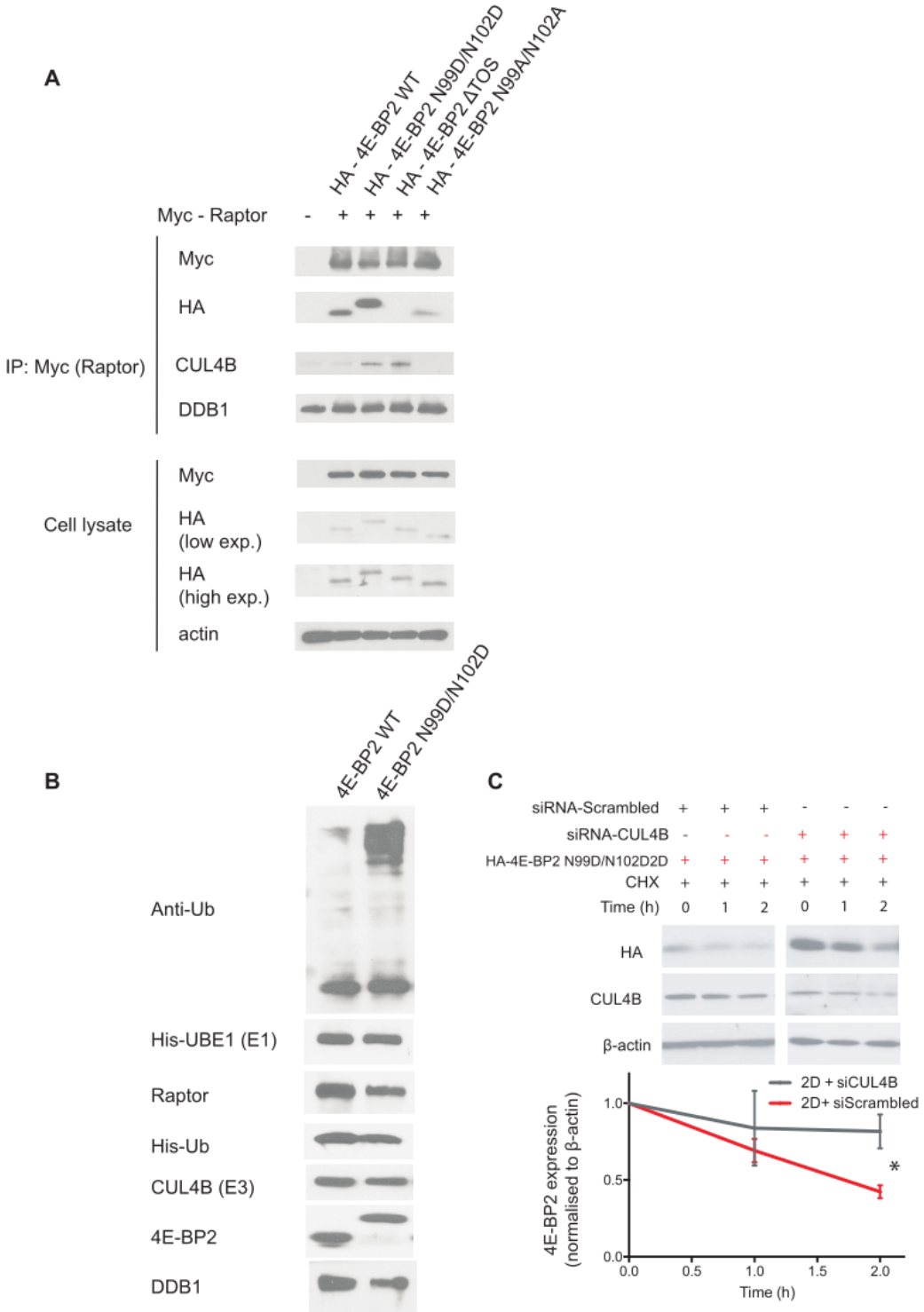

Figure 3.13 Raptor regulates the stability of deamidated 4E-BP2 through increased interaction with CUL4B-DDB1 E3 Ubiquitin ligase.

A. HEKs were co-transfected with Myc–Raptor and each one of plasmids that express different 4E-BP2 forms. Anti–Myc immunoprecipitation was performed on the lysates after they were checked for equal HA, Myc, CUL4B and DDB1 expression (input). β-Actin was used as a loading control and appeared at 42 kDa. Pulled down lysates were probed for Myc, HA, CUL4B and DDB1. Myc-Raptor appeared at 151 kDa, HA 4E-BP2 WT and HA 4E-BP2 N99A/N102A appeared at 15 kDa, HA 4E-BP2 N99D/N102D at 17 kDa, HA 4E-BP2 ΔTOS at 13 kDa, CUL4B at 100 kDa and DDB1 at 127 kDa. Low exposure of film corresponds to 1-3 min. High exposure of films corresponds to 15-20 min. **B**. *In vitro* ubiquitination assay of purified GST-4E-BP2 WT or 2D. The reactions were performed in the presence of purified CUL4B, Raptor, DDB1, His-Ubiquitin, UBE2L3 and UBE1 proteins and probed with the antisera against the indicated proteins. His-UBE1 appeared at 121 kDa, Raptor appeared at 150 kDa, CUL4B at 100 kDa, DDB1 at 127 kDa, 4E-BP2 WT and 4E-BP2 N99D/N102D appeared at 15 kDa and 17 kDa, respectively and His-Ub appeared at 10 kDa. **C**. Representative immunoblots from HEKs that were co-transfected with siRNA (scrambled or against *CUL4B)* and 2D HA-tagged 4E-BP2. Experiment was carried out in the presence of 100 μg/ml cycloheximide (CHX) for 0, 1 or 2 h. β-actin is the loading control and appeared at 42 kDa. HA 4E-BP2 N99D/N102D appeared at 17 kDa and CUL4B at 100 kDa. Bottom: Quantification of HA-expression (corresponding to WT or 2D) measured by immunoblotting, normalised to β-actin. For (C), data are shown as mean ±S.E.M. *$p < 0.05$ using Bonferroni-corrected two-way ANOVA.

3.3.8 Overexpression of 4E-BPs does not alter cell cycle progression in HEKs

3.3.8.1 Overexpression of 4E-BPs does not change cell cycle progression in HEKs

Apart from regulation of translation, 4E-BPs also regulate progression of cell cycle through mTORC1 signalling and interaction with Raptor without affecting cell survival or size (Dowling et al., 2010). Therefore, we asked whether a specific 4E-BP2 form is responsible for regulation of the cell cycle. To test this hypothesis, we transfected each plasmid, that express different 4E-BP2 forms, in HEKs (WT, N99D/N102D, N99A/N102A) and checked the cell cycle distribution after each single transfection of 4E-BP2 plasmid using propidium iodide DNA staining. Figure 3.14 (A)–(D) show the cell cycle distributions (left graphs) after transfecting different 4E-BP2 forms and the gating of single cells (right plots) in each cell population. Figure 3.14 (E) indicates the percentage of cells in each stage of cell cycle (G0/G1, S, G2/M).

In all cell cycle distribution graphs [left graphs, Figure 3.14 (A-D)], the number of cells in G0/G1 phase is very high compared to the number of cells in phases S and G2/M. However, there is no significant difference between them.

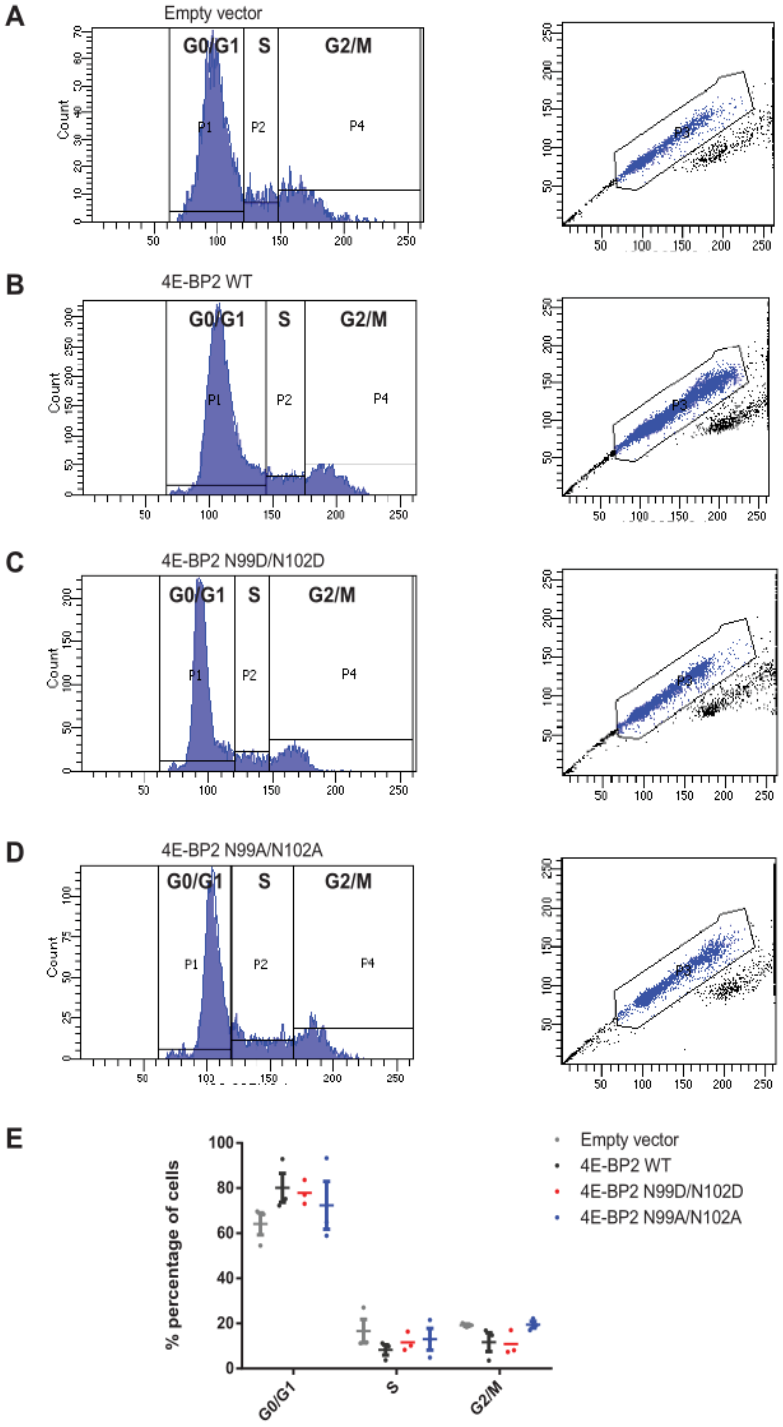

Figure 3.14 Cell cycle distributions after overexpression of different 4E-BP2 forms.

Cell cycle profiles (left graphs) and plots of single cell gating (right plots) from transfected HEKs with empty vector (A), 4E-BP2 WT (B), 4E-BP2 N99D/N102D (C), 4E-BP2 N99A/N102A (D). (E) Graph illustrating % percentage of cells in each phase of cell cycle after single

transfection. The data shown are representative of three independent experiments. Quantitative data with mean ± SEM is shown in (E). Bonferroni-corrected two-way ANOVA

3.3.8.2 Overexpression of Raptor concomitant with 4E-BPs does not change cell cycle progression in HEKs

Various stimuli such as serum and growth factors mediate proliferative events through 4E-BPs (Dowling et al., 2010). Specifically, in conditions where 4E-BPs are hypophoshorylated, they inhibit the progression from G1 to S phase stage of the cell cycle by suppressing the translation of eIF4E-sensitive mRNAs, required for cell cycle progression, such as cyclin D3, VEFG (Vascular Endothelial Growth Factor) and ODC (Ornithine Decarboxylase) (Dowling et al., 2010). Thus, we wondered whether overexpression of each 4E-BP2 form along with Raptor will influence cell cycle distribution using propidium iodide DNA staining. Figure 3.15 (A)–(D) depicts cell cycle distributions (left graphs) after transfecting each 4E-BP2 form along with Myc–Raptor and the gating of single cells (right plots) in each cell population. Figure 3.15 (E) indicates percentage of cells in each stage of the cell cycle (G0/G1, S, G2/M).

After co–transfecting Myc–Raptor with deamidated 4E-BP2, there is a significantly lower number of cells in G0/G1 phase ($p < 0.05$), as compared to the number after co–transfecting Myc–Raptor with empty vector [Figure 3.15 (C), (E)]. However, there are no differences between deamidated 4E-BP2 and WT or deamidated 4E-BP2 and Alanine mutant. Therefore, we cannot conclude that overexpression of deamidated 4E-BP2 along with Raptor leads to increased cell cycle progression. [Figure 3.15 (C),(E)].

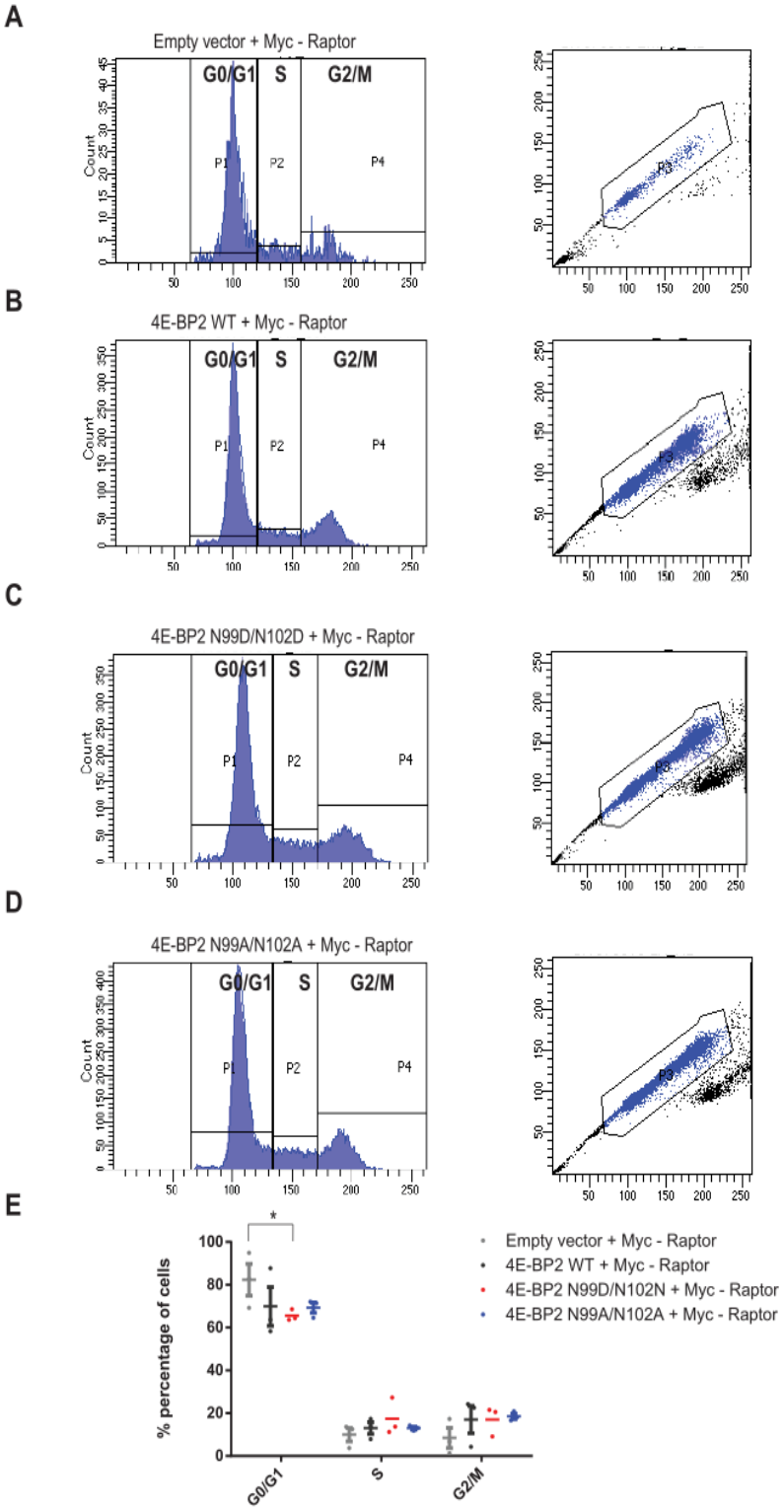

Figure 3.15 Cell cycle distributions after overexpression of different 4E-BP2 form and Myc-Raptor.

Cell cycle profiles (left graphs) and plots of single cell gating (right plots) from co – transfection of Myc – Raptor in HEKs with empty vector **(A)**, 4E-BP2 WT **(B)**, 4E-BP2 N99D/N102D **(C)**, 4E-BP2 N99A/N102A **(D)**. **(E)** Graph illustrating % percentage of cells in each phase of cell cycle after co-transfection. The data shown are representative of three independent experiments. Quantitative data with mean ± SEM is shown in **(E)**. *$p < 0.05$ using Bonferroni-corrected two-way ANOVA.

Figure 3.16 illustrates the cell cycle profile after overexpression of each 4E-BP2 form either alone or after co–transfection with Myc–Raptor. Overexpression of Myc–Raptor along with deamidated 4E-BP2 leads to increased cell cycle progression since a lower percentage of cells are in G0/G1 stage ($p < 0.05$), as compared to the percentage of cells after overexpressing only deamidated 4E-BP2 [Figure 3.16(C)].

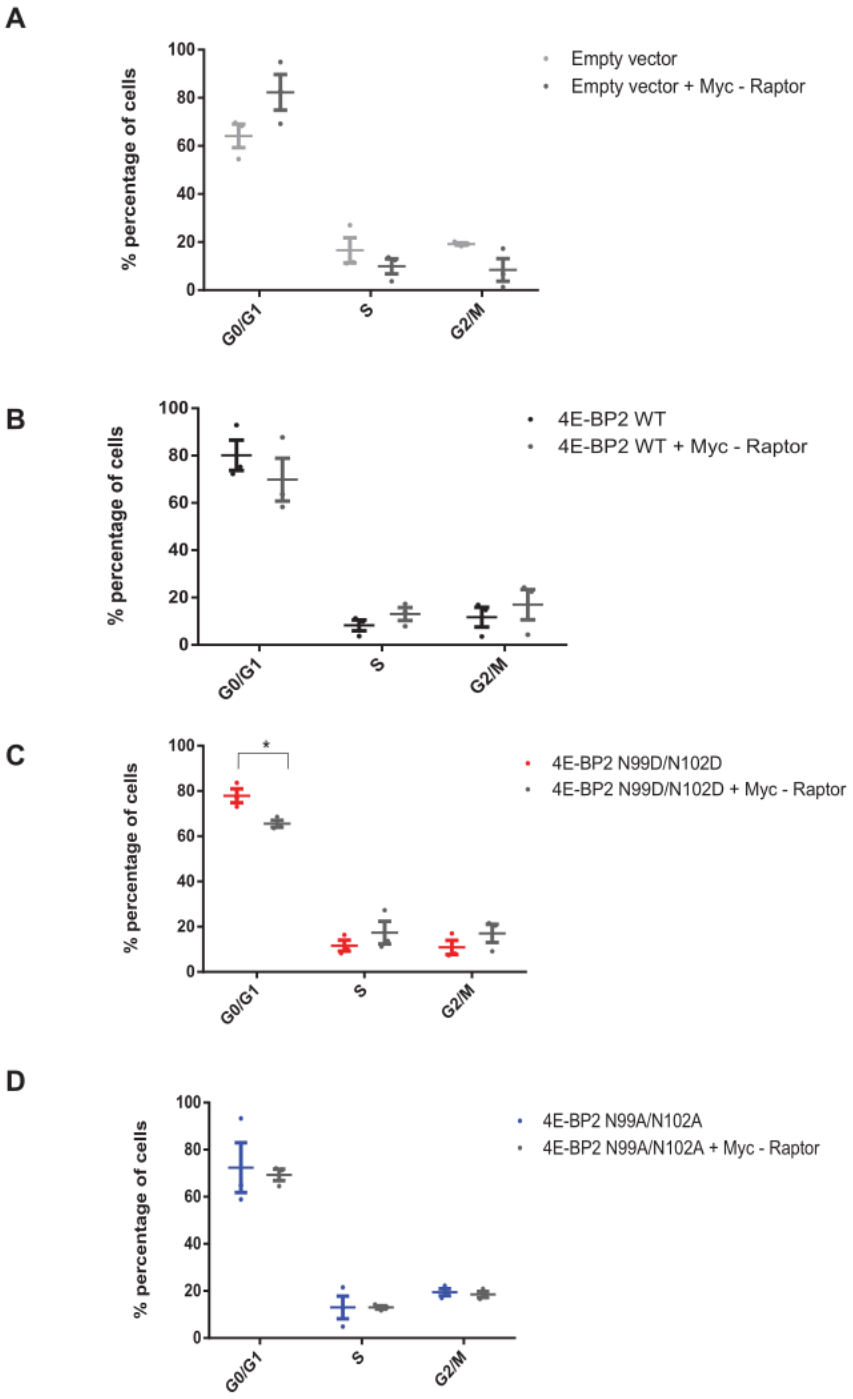

Figure 3.16 Cell cycle distributions after overexpression of different 4E-BP2 form either alone or with co–transfection with Myc-Raptor.

Graph illustrating % percentage of cells in each phase of cell cycle after transfection of (A) Empty vector, (B) 4E-BP2 WT, (C) deamidated 4E-BP2, (D) Alanine mutant 4E-BP2 with or

without Myc – Raptor in HEKs. The data shown are representative of three independent experiments. Quantitative data with mean ± SEM is shown. *p < 0.05 using Bonferroni-corrected two-way ANOVA.

3.3.9 4E-BP2 is also deamidated in human brain

4E-BP2 from murine brain migrates as three forms with different electrophoretic mobility on an SDS-PAGE gel (Banko et al., 2005; Tsukiyama-Kohara, 2001) with the slower migrating forms (>15kDa) corresponding to double deamidated 4E-BP2 (Bidinosti et al., 2010b). This unique migration pattern is brain–specific (Bidinosti et al., 2010b). We asked whether 4E-BP2 undergoes asparagine deamidation also in humans. To investigate this, we treated post mortem human lysates and mouse lysates from different tissues: brain, liver and spleen with λ phosphatase, followed by western blotting for 4E-BP2 and phospho-Threonine-Proline. Figure 3.17 (A) shows treated and untreated lysates with λ phosphatase, probed for 4E-BP2.

Three 4E-BP2 forms are apparent in all human and mouse brain lysates [Figure 3.17 (A)], even after treatment with λ phosphatase [Figure 3.17 (A), (B)], thus implying that the slower migrating forms are not due to phosphorylation. Moreover, double deamidated 4E-BP2 corresponding to the slowest migrating form, exhibits increased expression in human lysates compared to mouse lysates [Figure 3.17 (A)]. Regarding the other tissues that were studied, 4E-BP2 is expressed in mouse, liver and spleen lysates, indicating one band, but is not detectable in human liver and spleen lysates [Figure 3.17 (A)]. Figure 3.17 (B) indicates human and brain lysates treated with λ phosphatase probed for 4E-BP2 and phospho–Threo – Proline antibody that determines phosphatase treatment efficacy. Taken together, these data suggest that deamidation of 4E-BP2 is brain–specific in mice and occurs in humans.

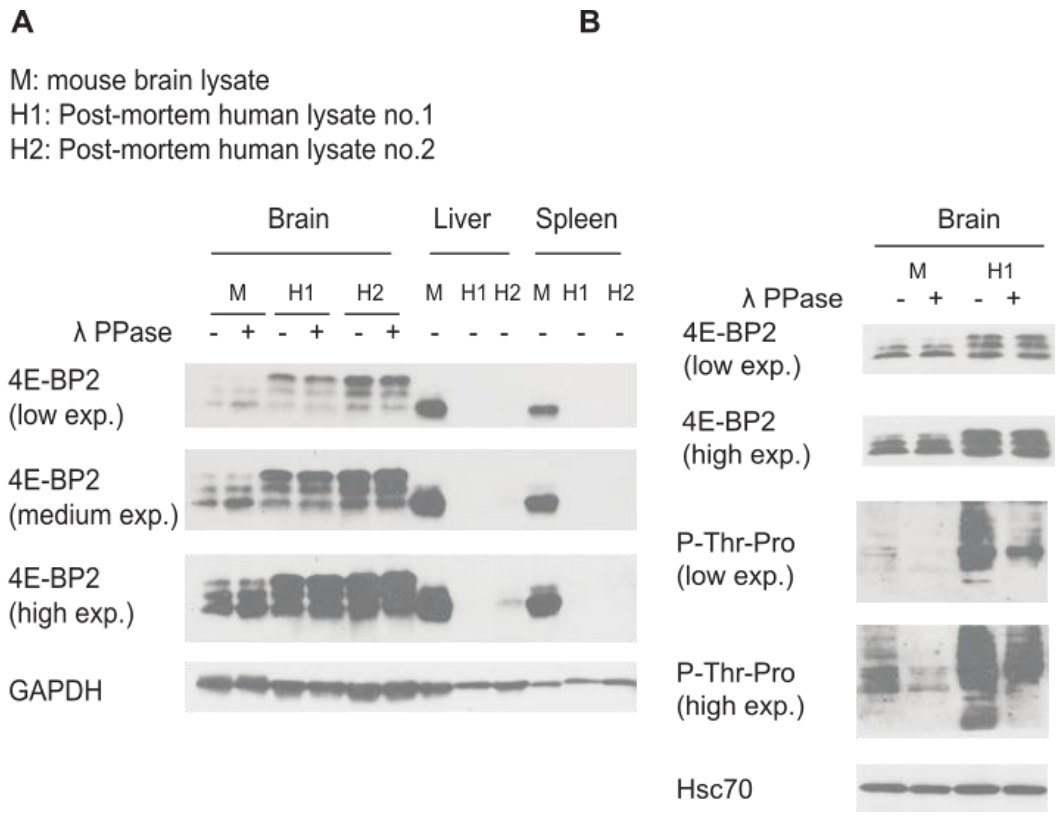

Figure 3.17 4E-BP2 is also deamidated in human brain.

A. Adult mouse lysates and post mortem human lysates from brain, liver and spleen were treated with λ phosphatase and analysed by western blotting. Membranes were probed for 4E-BP2. GAPDH was used as a loading control and appeared at 37 kDa. 4E-BP2 appeared as three bands (bottom band: 15 kDa, middle band: 16 kDa and top band: 17 kDa). Low exposure films for 4E-BP2 correspond to 1-3 min of exposure, medium exposure films correspond to 5-10 min and high exposure films to 15-20 min. For P-Thr-Pro signal, low exposure of films corresponds to 5 min and high exposure to 20 min. **B**. Adult mouse brain and post mortem human brain lysates were treated with λ phosphatase and analysed by western blotting. Membranes were probed for 4E-BP2 and phospho–Threo–Proline. Hsc70 was used as a loading control and appeared at 70 kDa. 4E-BP2 appeared as three bands (bottom band: 15 kDa, middle band: 16 kDa and top band: 17 kDa).

3.3.10 Deamidated 4E-BP2 is neuron-specific

Deamidation of 4E-BP2 occurs postnatally in mouse brain (Bidinosti et al., 2010b). Our previous findings also indicate that deamidated 4E-BP2 also occurs in human brain (Figure 3.17). However, it is not known whether deamidation of 4E-BP2 is cell–type specific. To identify the cells in which 4E-BP2 undergoes deamidation, we prepared two primary dissociated cortical neuronal cultures from mice, growing under different conditions: one mixed culture which after confluency was passaged, re-plated and labelled as Glia passage 1 and one Neuronal culture. In mixed culture, neuronal cells were grown in Neurobasal Medium supplemented with B-27, 1x Glutamax and Horse Serum until DIV 10 and then, we used trypsin to dissociate cells from culture and re-plated them, thus effectively removed all neuronal cells. After passaging and re-plating, this culture is labelled as Glia passage 1. In the second culture, named neuronal (N), neuronal cells were grown until DIV 25 in Neurobasal Media supplemented with B-27, 1x Glutamax and Ara-C (cytosine arabinoside), which limits astrocyte proliferation. Lysates from different days from both cultures were analysed by western blotting as Figure 3.18 (A) shows.

4E-BP2 migrates as three bands in the neurons on the gel from DIV 16 and this pattern is apparent until DIV 25 [Figure 3.18 (A)]. Moreover, the middle slower band starts being visible from DIV 12, denoting that deamidation starts occurring from this day [Figure 3.18 (A)]. In Glia culture passage 1, 4E-BP2 appears as one band that corresponds to 4E-BP2 WT and one band of lower molecular weight (<15kDa), probably corresponding to hypophosphorylated 4E-BP2 [Figure 3.18 (A)]. Thus, deamidation of 4E-BP2 is neuron–specific [Figure 3.18 (A)]. Phosphorylated 4E-BP1 expression increases in mixed culture at DIV 10 and in Neuronal culture at DIV 12 since in later days its expression decreases [Figure 3.18 (A)]. Phosphorylated 4E-BP2 follows a similar expression pattern as phosphorylated 4E-BP1 with enhanced expression at DIV 10 for mixed and DIV 12 for Neuronal culture [Figure 3.18 (A)]. In later days as DIV 25 of Neuronal culture, hyperphosphorylated 4E-BP2 is apparent whereas in glia culture hypophoshorylated 4E-BP2 is present [Figure 3.18 (A)]. Moreover, 4E-BP1 is highly expressed in the Glia culture, as compared to Neuronal culture that is present but not in the same levels [Figure 3.18 (A)].

Figure 3.18 (B) indicates that three bands, corresponding to deamidated and WT 4E-BP2, are still present after λ phosphatase treatment in neuronal lysates

(DIV25), implying that slower migrating forms do not stem from phosphorylation of 4E-BP2. In Glia culture, 4E-BP2 is apparent as one band in treated and untreated lysates [Figure 3.18 (B)]. Phospho–4E-BP1 is expressed in both neurons and glia but phospho-4E-BP2 is detectable in neurons and not glia [Figure 3.18 (B)]. Phospho-Threo–Proline antibody was used to determine the phosphatase efficacy [Figure 3.18 (B)]. Therefore, deamidation of 4E-BP2 is postnatal and neuron–specific [Figure 3.18 (B)]. Phosphorylated 4E-BP2 and 4E-BP1 levels decrease from early (DIV 10) to late (DIV 25) postnatal development [Figure 3.18 (A)] whereas hyperphosphorylated 4E-BP2 is present in neurons (DIV25) and hypophosphorylated 4E-BP2 is present in Glia [Figure 3.18 (A)]. Furthermore, 4E-BP1 exhibits a high expression pattern in glia, as compared to neuronal cells (DIV 25) during late postnatal development [Figure 3.18 (A)].

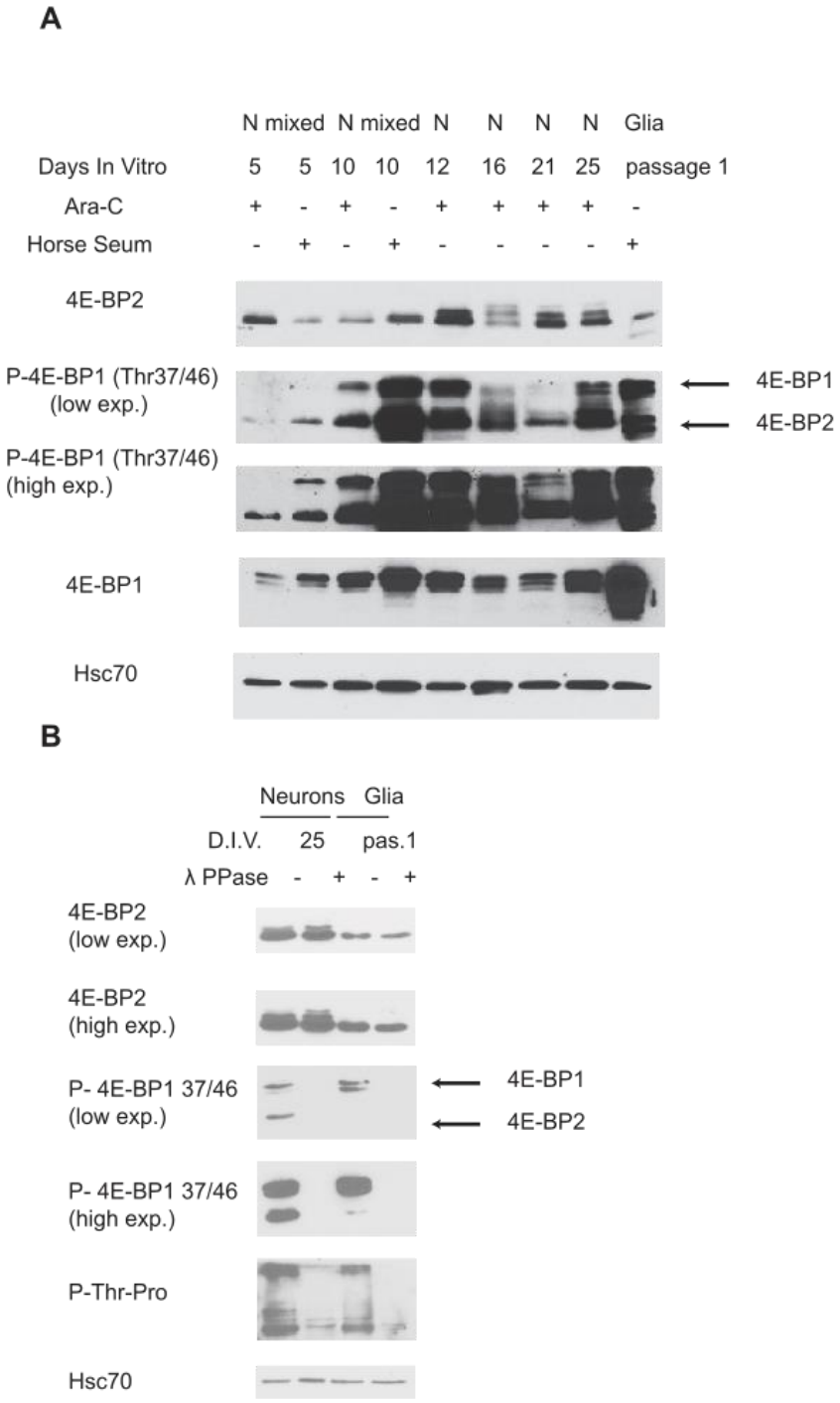

Figure 3.18 4E-BP2 is deamidated in neurons and not in glia after DIV 12 in dissociated cortical neuronal cultures.

A. Deamidated 4E-BP2 is neuron-specific and occurs postnatally since three bands are apparent after DIV 16 in mouse cultured neurons. Mixed culture was grown until DIV 10 and then was passaged for having a glia culture. Neuronal (N) culture was grown until DIV 25. Lysates were analysed by western blotting and probed for 4E-BP2, p – 4E-BP 37/46 and 4E-BP1. Hsc70 was used as a loading control and appeared at 70 kDa. 4E-BP2 appeared as three bands (bottom band: 15 kDa, middle band: 16 kDa and top band: 17 kDa). 4E-BP1 appeared as three bands between 18-20 kDa. Phospho-4E-BP1 appeared between 18-21 kDa and phospho-4E-BP2 appeared between 16-18 kDa. Low exposure films of 4E-BP2 correspond to 1-3 min of exposure and high exposure to 15-20 min. For p-4E-BP1 37/46, low exposure of films corresponds to 10 min and high exposure to 30-40 min. **B.** Mouse cortical neuronal and glia lysates were treated with λ phosphatase, followed by western blotting and probed for 4E-BP2, p – 4E-BP1 37/46, 4E-BP1 and p-Threo–Pro. Hsc70 was used as a loading control. appeared at 70 kDa. 4E-BP2 appeared as three bands (bottom band: 15 kDa, middle band: 16 kDa and top band: 17 kDa). Phospho-4E-BP1 appeared between 18-21 kDa and phospho-4E-BP2 appeared between 16-18 kDa

3.3.11 Expression of deamidated 4E-BP2 is not altered in mouse models of autism

4E-BP2 has been implicated with Autism spectrum disorders because *Eif4ebp2* -/- mice exhibit deficits in social interactions, altered communication between dams and pups and repetitive/stereotyped behaviours due to dysregulated protein synthesis (Gkogkas et al., 2013). Another mouse model of autism, *Tsc2* -/+, display also impaired communication between dams and pups (Young D., 2010). It is not known whether there is a link between deamidation of 4E-BP2 and autism and if deamidation of 4E-BP2 is impaired in mouse models of autism. Therefore, we investigated 4E-BP2 pattern expression in different mouse models of autism. We lysed brains from *Fmr1* +/- (encoding for FMRP, Fragile X Mental Retardation Protein, B6.129P2-*Fmr1*^{tm1Cgr}/J, Stock No: 003025), *Shank3* +/- (encoding for SH3 and Multiple Ankyrin Repeat domains 3, B6.Cg-*Shank3*$^{tm2.1Bux}$/J, Stock No:032169 |Shank3$^{\Delta 4\text{-}22}$), *Tsc2* +/- (B6;129S4-*Tsc2*^{tm1Djk}/J, Stock No:004686) and BTBR (BTBR *T*$^{+}$ *Itpr3*^{tf}/J, Stock No:002282 |BTBR) mice which exhibit a 100% absence of the corpus callosum and a severely reduced hippocampal commissure (Wahlsten et al., 2003) and analysed them with western blotting for 4E-BP2. Figure 3.19 shows 4E-BP2 expression in these transgenic mice.

Protein amounts of WT and deamidated 4E-BP2 for *Fmr1* +/- mice do not differentiate significantly [Figure 3.19 (A)], as compared to *Fmr1* +/+mice. We also observed that there are no significant differences between protein levels of WT and deamidated 4E-BP2 in *Shank3* +/-, as compared to *Shank3* +/+ mice [Figure 3.19 (B)]. *Tsc2* +/- and BTBR mice display no difference in expression of WT and deamidated 4E-BP2, as compared to *Tsc2*+/+ and WT mice, respectively [Figure 3.19

(C), (D)]. To conclude, deamidated 4E-BP2 is not altered in these mouse models of autism that we studied.

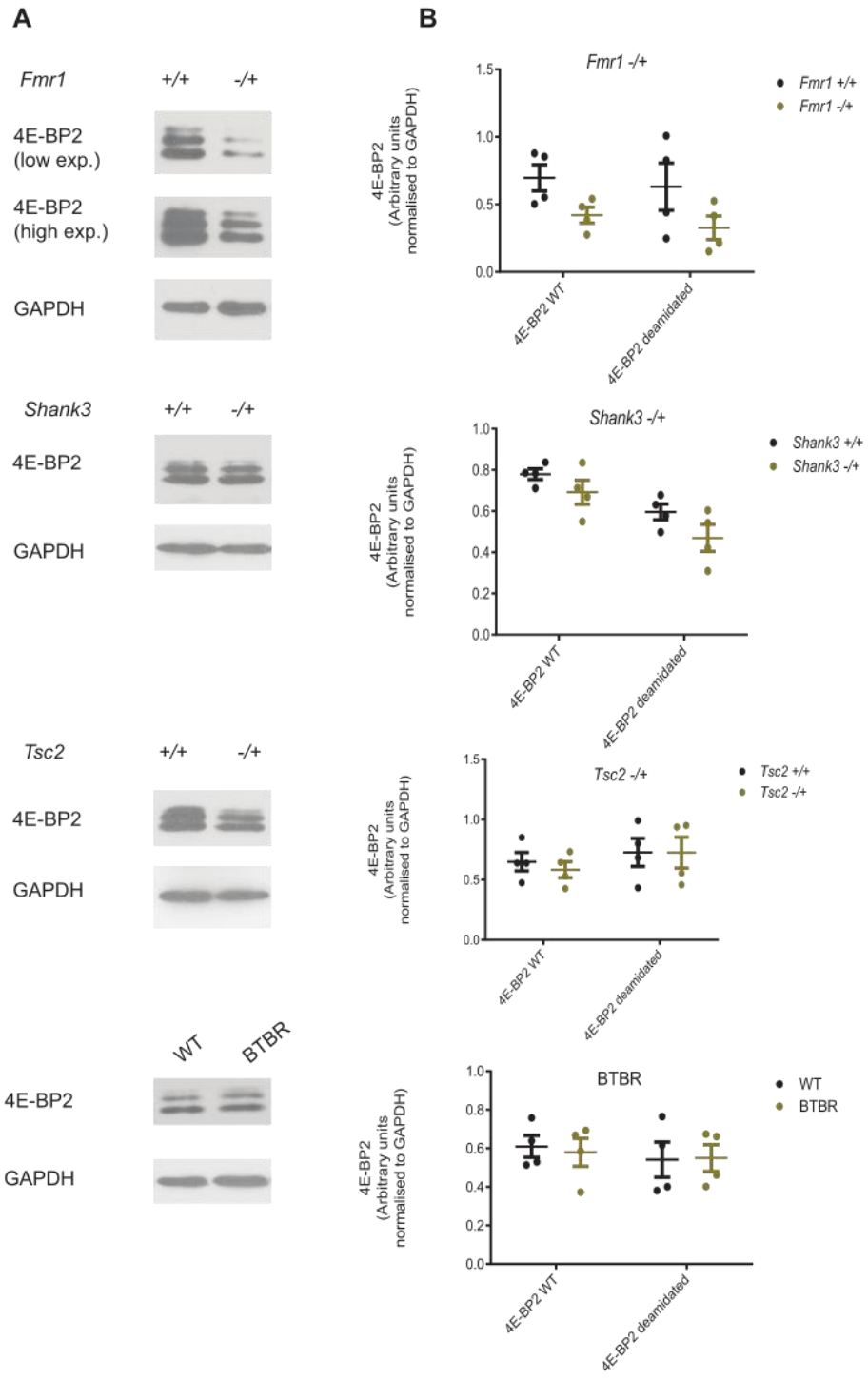

Figure 3.19 4E-BP2 pattern in transgenic mice.

A. Representative immunoblots brain lysates from FMRP, SHANK3, TSC2 heterozygous and BTBR mice were analysed by western blotting and probed for 4E-BP2. GAPDH was used as a loading control and appeared at 37 kDa. 4E-BP2 appeared as three bands (bottom band: 15 kDa, middle band: 16 kDa and top band: 17 kDa). **B.** Quantitative analysis of 4E-BP2 WT (bottom band) and deamidated (intermediate and top bands) amount (A). The intensities of the bands were measured using Image Studio Lite Ver 5.2 and normalised against GAPDH. The data shown in (A) are representative of three independent experiments. Quantitative data with mean ± SEM is shown in (B). Bonferroni-corrected two-way ANOVA. For the comparison of BTBR mice, C57Bl/6J background animals were used.

3.3.12 Endogenous deamidated 4E-BP2 is a long-lived protein in neurons and is degraded by the proteasome

Deamidated 4E-BP2 displays a faster degradation rate in HEKs, as compared to WT or Alanine mutant 4E-BP2 (Figure 3.2) and gets degraded by the proteasome since inhibition of the proteasome with Lactacystin (Figure 3.5) or MG132 (Figure 3.6) leads to its significant accumulation. However, in the brain, 4E-BP2 has a long half-life as most proteins (Graber et al., 2013). Since deamidated 4E-BP2 is brain-specific in mice (Bidinosti et al., 2010b), we asked whether the stability of deamidated 4E-BP2 is different from WT 4E-BP2 in the brain where deamidation takes place *in vivo* and *in vitro*. To test this hypothesis, we treated primary dissociated cortical neurons with inhibitors of protein synthesis and proteasome as in HEKs: CHX (100 µg/ml) for 0, 2, 9 h, Lactacystin (5 µM) for 0, 9 h and MG132 (20 µM) for 0, 9 h but also with other elongation inhibitors of translation such as Homoharringtonine (HHT, 2 µg/ml) and Anisomycin (10 µg/ml). The duration of each treatment was longer compared to HEKs due to the long half-life of brain proteome (Graber et al., 2013). We used inhibitors of translation or proteasome degradation in concentration where neurons were still healthy and did not die, following the treatment. Figure 3.20 (A) and (B) present representative blots and quantitative graph respectively, of neuronal lysates treated with CHX, Lactacystin and MG132, followed by western blotting for 4E-BP2.

Deamidated and WT 4E-BP2 protein amounts do not change after 2, 9 h of CHX [Figure 3.20 (A), (B)], thus implying that both 4E-BP2 forms have a long half-life in neurons. Inhibition of proteasome with Lactacystin for 9 h does not alter deamidated 4E-BP2 or WT protein levels [Figure 3.20 (A), (B)]. Nevertheless, upon inhibition of proteasome with MG132 for 9 h, we detected a significantly higher accumulation of deamidated 4E-BP2 ($p < 0.05$), as compared to WT 4E-BP2 [Figure 3.20 (A), (B)].

Figure 3.20 (C) displays blots from neuronal lysates, treated with CHX for 0, 2, 9 h, in which Puromycin (5 µg/ml) was added 30 min before cell collection and lysis. Puromycin gets incorporated in the elongating peptides, giving an indication of *de novo* protein synthesis in these neuronal cells. Figure 3.20 (C) displays that CHX does not change 4E-BP2 deamidated or WT protein levels, similarly to Figure 3.20 (A), and concomitantly, decreases Puromycin incorporation, denoting the efficacy of inhibition of protein synthesis with CHX. Figure 3.20 (D) illustrates western blotting from neuronal lysates treated with HHT for 0, 2 and 9 h. Similarly to CHX, HHT treatment does not change protein amounts of deamidated 4E-BP2 or WT [Figure 3.20 (D)], confirming that 4E-BP2 forms are stable in neurons. Figure 3.20 (E) shows western blotting from lysates treated with Anisomycin for the same duration of 0, 2 and 9 h, and Puromycin was added 30 min before cell collection. Protein levels of 4E-BP2 forms do not change after treatment and Puromycin incorporation diminishes after 2 and 9 h of Anisomycin, implying the efficient inhibition of translation [Figure 3.20 (E)]. Figure 3.20 (F) shows proteasome enzymatic activity of neuronal lysates that were analysed by western blotting in Figure 3.20 (A). The graph illustrates proteasome activity assay of 20S proteasome in control (0 h), MG132-treated (9 h) or Lactacystin-treated (9 h) cortical neurons [Figure 3.20 (F)]. The graph reveals that MG132 treatment decreases proteasome activity assay but Lactacystin does not decrease efficiently proteasome enzymatic activity [Figure 3.20 (F)], therefore a higher concentration of Lactacystin in neuronal cells is probably required. To conclude, these data suggest that deamidated and WT 4E-BP2 are stable in neurons and deamidated 4E-BP2 gets degraded by the proteasome.

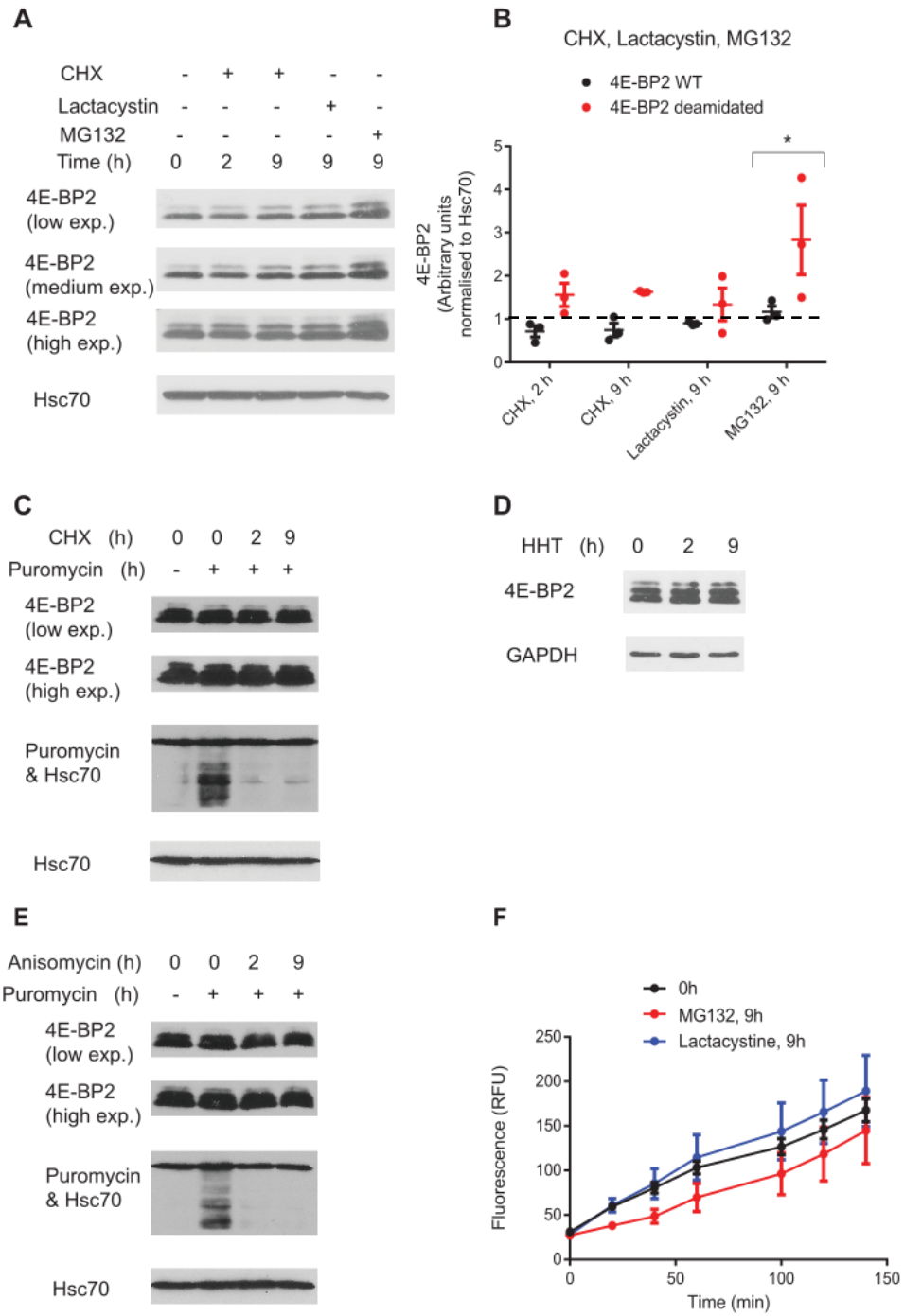

Figure 3.20 Protein stability assays of endogenous 4E-BP2 in dissociated cortical neurons.

Representative immunoblots of mouse cortical neuronal lysates treated with different protein synthesis inhibitors or proteasome inhibitors, analysed by western blotting and probed for 4E-BP2. Hsc70 appeared at 70 kDa and GAPDH appeared at 37 kDa and were used as loading controls. **A.** Dissociated cortical neurons were treated with Cycloheximide (100 µg/ml) for 0, 2, 9 h, Lactacystin (5 µM) for 0, 9 h and MG132 (20 µM) for 0 and 9 h. **B.** Quantitative analysis of the deamidated and WT 4E-BP2 amounts in (A). The intensities of the bands were measured using Image Studio Lite Ver 5.2 and normalised against Hsc70. The intensity of the band at 0 h (lane 1) is set as 1 (dotted line on graph). Quantitative data with mean ± SEM is shown in (B). *$p < 0.05$ using Bonferroni-corrected two-way ANOVA. **C.** Dissociated cortical neurons were treated with Cycloheximide (100 µg/ml) for 0, 2, 9 h and Puromycin (5 µg/ml) was added 30 min before cell lysis. Lysates were probed for 4E-BP2 and Puromycin. **D.** Dissociated cortical neurons were treated with HHT (2 µg/ml) for 0, 2 and 9 h, followed by western blotting and probed for 4E-BP2. **E.** Dissociated cortical neurons were treated with Anisomycin (10 µg/ml) for 0, 2 and 9 h and Puromycin (5 µg/ml) was added 30 min before cell lysis. Lysates were probed for 4E-BP2 and Puromycin. **F.** Proteasome enzymatic activity was measured in treated lysates that were analysed by western blotting in (A). Proteasome activity is shown in RFU/min (+ s.e.m., $n = 3$). Bonferroni-corrected two-way ANOVA. The data shown in (A), (C), (D), (E) are representative of three independent experiments. 4E-BP2 appeared as three bands (bottom band: 15 kDa, middle band: 16 kDa and top band: 17 kDa). Low exposure films for 4E-BP2 correspond to 1-3 min of exposure, medium exposure films correspond to 5-10 min and high exposure films to 15-20 min. For quantification, only films that were exposed for 1-3 min (low exposure) were used.

3.3.13 Deamidated 4E-BP2 protein amounts are regulated by mTOR but not by MAPK signalling

Deamidated 4E-BP2 exhibits enhanced interaction with Raptor and decreased affinity for eIF4E compared to WT 4E-BP2 in HEKs (Bidinosti et al., 2010b). Based on this finding, we hypothesize that there might be a different regulatory mechanism of stability of deamidated 4E-BP2, as compared to WT protein in neurons. To investigate this hypothesis and elucidate the pathways that are responsible for regulating deamidated 4E-BP2, we treated cortical neuronal cultures with Torin1 (250 nM), a selective active-site mTOR inhibitor (Thoreen et al., 2009) and U0126 (20 µM), a MEK/ERK inhibitor (Favata et al., 1998), for 9 h (short-term treatment) and 48 h (long-term treatment). Furthermore, we also activated these two major pathways of translational control in the brain by treating cortical neurons with Insulin (10 µM) for 9 h and 48 h. Figure 3.21 (A) and (B) illustrates representative blots and graphs respectively, from Torin1-, U0126- and Insulin-treated neurons that were analysed by western blotting.

After 9 h of Torin1 treatment, we discovered significantly higher protein levels of deamidated 4E-BP2 ($p < 0.05$), as compared to WT protein levels [Figure 3.21 (A),

(B)]. Torin treatment also inhibits phosphorylation of ribosomal protein S6, 4E-BP1 and 4E-BP2 [Figure 3.21 (A)], thus showing efficient inhibition of mTOR by Torin1. Furthermore, total S6 levels are not different after Torin1 treatment [Figure 3.21 (A)] whereas 4E-BP1 levels are not detectable due to complete inhibition of phosphorylated 4E-BP1 [Figure 3.21 (A)]. After 9 h treatment with U0126, protein levels of WT and deamidated 4E-BP2 do not differentiate [Figure 3.21 (A), (B)]. However, phosphorylation of MAPK (ERK1/2) is also blocked, therefore showing U0126 treatment efficacy [Figure 3.21 (A)]. Total ERK1/2 levels do not change after 9 h of U0126 treatment [Figure 3.21 (A)]. Moreover, activation of both pathways by Insulin does not alter protein levels of deamidated from WT 4E-BP2 [Figure 3.21 (A), (B)]. Moreover, higher intensity of the bands corresponding to phosphorylated 4E-BP2, 4E-BP1 as well as total levels of 4E-BP1 after Insulin treatment is also apparent [Figure 3.21 (A)]. Thus, the stability of deamidated 4E-BP2 is regulated by the mTOR but not MAPK pathway.

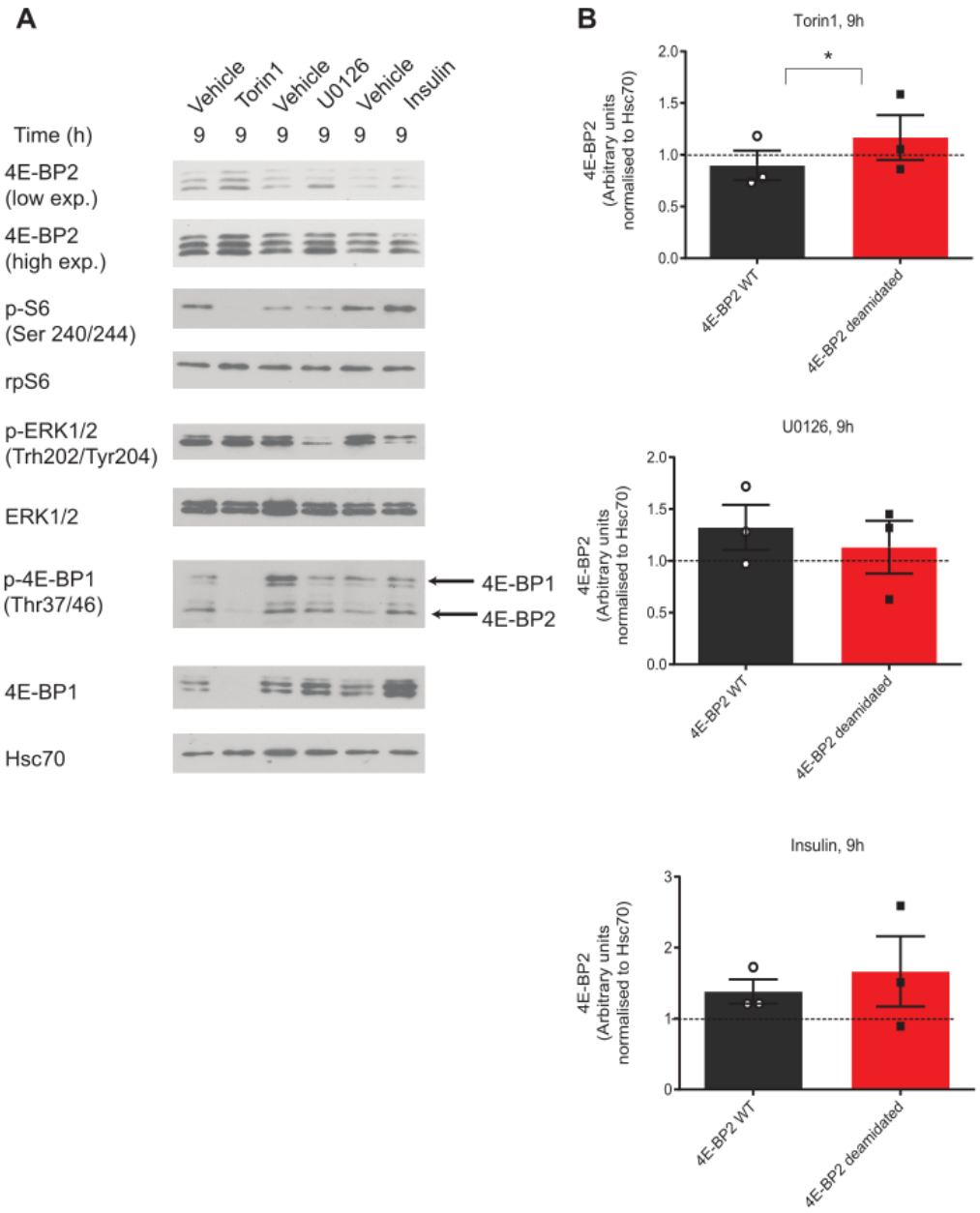

Figure 3.21 Short-term inhibition of mTOR signalling for 9 h leads to accumulation of deamidated 4E-BP2 but inhibition of MAPK signalling or activation of both pathways with Insulin do not alter deamidated or WT 4E-BP2.

A. Cortical neurons were treated with Torin1 (250 nM), U0126 (20 µM), Insulin (10 µM) for 9 h and were analysed by western blotting. Hsc70 was used as a loading control and appeared at 70 kDa. 4E-BP2 appeared as three bands (bottom band: 15 kDa, middle band: 16 kDa and top band: 17 kDa). 4E-BP1 appeared as three bands between 18-20 kDa. Phospho-4E-BP1 appeared between 18-21 kDa and phospho-4E-BP2 appeared between 16-18 kDa. ERK1/2 and phospho-ERK1/2 appeared at 42, 44 kDa. rpS6 and phospho-S6, both appeared at 32 kDa. Low exposure of films for 4E-BP2 corresponds to 1-3 min and high exposure to 15-20 min. For quantification, only films that were exposed for 1-3 min (low exposure) were used. **B.**

Quantitative analysis of the different 4E-BP2 amounts in (A). The intensities of the bands ere measured using Image Studio Lite Ver 5.2 and normalised against Hsc70. The intensity of the bands at 9 h corresponding to Vehicle (lane 1, lane 3, lane 5) is set as 1 (dotted line on graph). The data shown in (A) are representative of three independent experiments. Quantitative data with mean ± SEM is shown in (B). *$p < 0.05$ using Bonferroni-corrected two-way ANOVA.

Then, we asked whether long-term inhibition of these pathways will have the same effect on the stability of 4E-BP2. Figure 3.22 (A) depicts representative blots and Figure 3.22 (B) presents quantitative graphs of protein amounts from Torin1-, U0126- and Insulin-treated neuronal lysates for 48 h to test the effect of long-term inhibition of the same pathways on deamidated and WT 4E-BP2.

After inhibition of mTOR signalling for 48 h, we detected a significantly higher accumulation of deamidated 4E-BP2 ($p < 0.001$), as compared to WT 4E-BP2 protein amounts [Figure 3.22 (A), (B)]. Moreover, Torin1 treatment completely blocks phosphorylation of S6, 4E-BP1 and 4E-BP2 whereas it does not change total levels of S6 [Figure 3.22 (A)]. 4E-BP1 levels are still detectable after 48 h of Torin1 but only hypophosphorylated forms are present [Figure 3.22 (A)]. After 48 h of U0126, there are no significant differences between the protein amounts of deamidated from WT 4E-BP2 [Figure 3.22 (A), (B)]. U0126 treatment also inhibits phosphorylation of MAPK (ERK 1/2) but total levels of protein do not change [Figure 3.22 (A)]. Activation of both pathways with Insulin does not change protein levels of any of 4E-BP2 forms [Figure 3.22 (A), (B)]. Thereby, the mechanism of regulation of neuronal stability of deamidated 4E-BP2 is mTOR- and not MAPK–dependent.

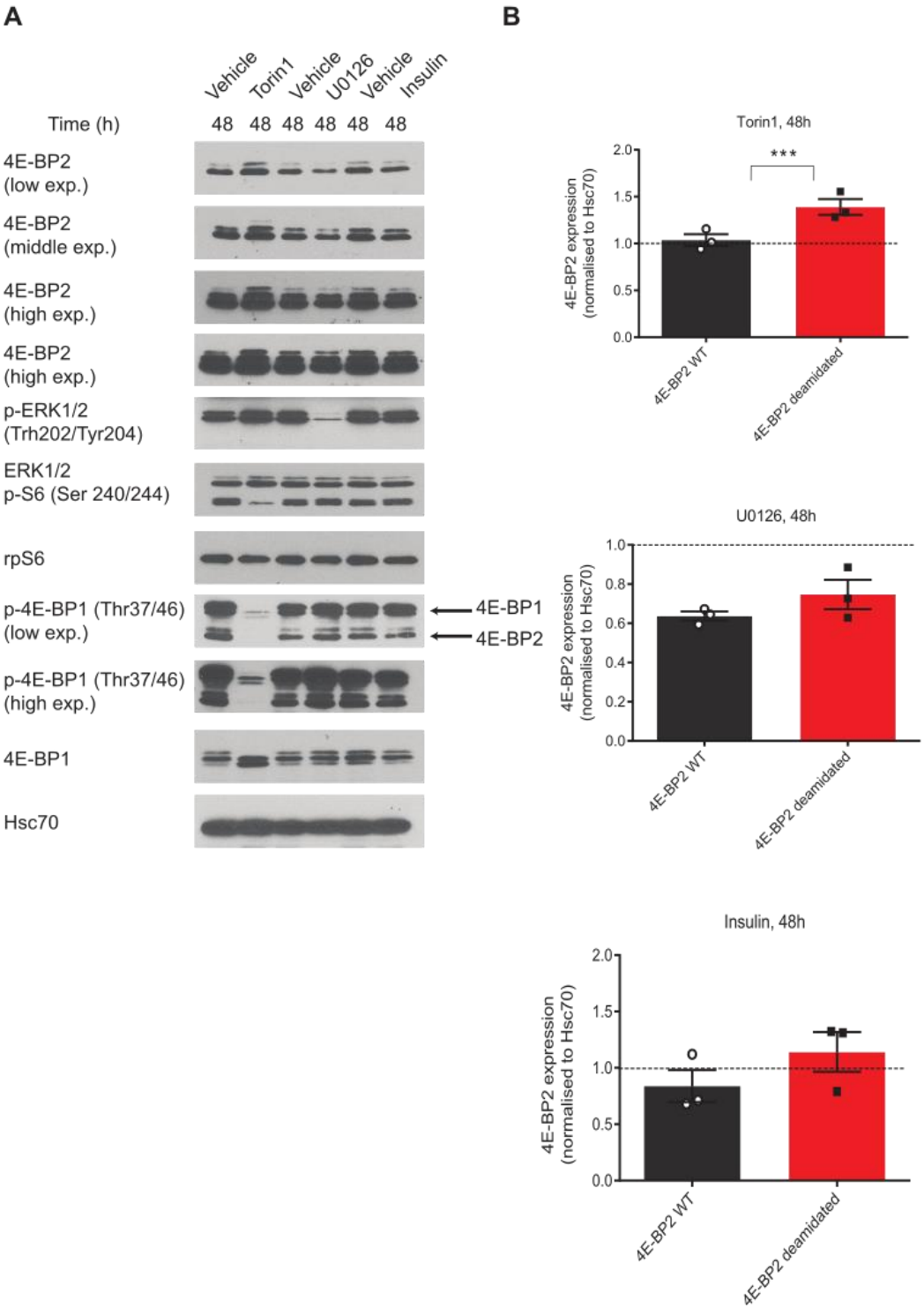

Figure 3.22 Long-term inhibition of mTOR signalling for 48 h leads to accumulation of deamidated 4E-BP2.

A. Cortical neurons were treated with Torin1 (250 nM), U0126 (20 µM), Insulin (10 µM) for 48 h and were analysed by western blotting. Hsc70 was used as a loading control and appeared at 70 kDa. 4E-BP2 appeared as three bands (bottom band: 15 kDa, middle band: 16 kDa and top band: 17 kDa). 4E-BP1 appeared as three bands between 18-20 kDa. Phospho-4E-BP1 appeared between 18-21 kDa and phospho-4E-BP2 appeared between 16-18 kDa. ERK1/2 and phospho-ERK1/2 appeared at 42, 44 kDa. rpS6 and phospho-S6, both appeared at 32 kDa. Low exposure films of 4E-BP2 correspond to 1-3 min of exposure, medium corresponds to 10-15 min and high exposure corresponds to 15-20 min. For p-4E-BP1 37/46, low exposure of films corresponds to 10 min and high exposure to 30-40 min**. B.** Quantitative analysis of the different 4E-BP2 amounts in (A). The intensities of the bands were measured using Image Studio Lite Ver 5.2 and normalised against Hsc70. The intensity of the bands at 48 h corresponding to Vehicle (lane 1, lane 3, lane 5) is set as 1 (dotted line on graph). The data shown in (A) are representative of three independent experiments. Quantitative data with mean ± SEM are shown in (B). ***$p < 0.001$ using Bonferroni-corrected two-way ANOVA. For quantification, only films that were exposed for 1-3 min (low exposure) were used.

3.3.14 mTOR or MAPK inhibition in glia does not alter stability of 4E-BP2

We demonstrated that deamidated 4E-BP2 is present in neurons and not in glia (Figure 3.18). Moreover, we discovered that the regulatory mechanism of deamidated 4E-BP2 is mTOR–dependent and MAPK–independent (Figure 3.21, Figure 3.22). To confirm that the mTOR–dependent mechanism, responsible for regulating the stability of deamidated 4E-BP2 is specific to neurons, we performed an experiment of inhibition and activation of mTOR and MAPK pathways with Torin1 (250 nM), U0126 (20 µM) and Insulin (10 µM) for 48 h in pure glia cells. Figure 3.23 shows representative blots from treated-glia lysates with the inhibitors.

After 48 h of Torin1, 4E-BP2 WT protein amounts do not change [Figure 3.23 (A), (B)]. Torin1 also inhibits phosphorylation of S6, 4E-BP1 and 4E-BP2, implying efficient inhibition of mTOR signalling [Figure 3.23 (A)]. Total 4E-BP1 levels decrease, denoting inhibition of expression of hyperphosphorylated 4E-BP1 forms since only bands of lower molecular weight (<17kDa) are detectable [Figure 3.23 (A)]. Interestingly, phosphorylation of ERK 1/2 also increases after 48 h of Torin1 treatment [Figure 3.23 (A)]. Similarly to Torin1 treatment, inhibition of MAPK pathway with U0126 for 48 h in glia does not change 4E-BP2 WT protein amounts [Figure 3.23 (A), (B)]. Phosphorylated MAPK levels are barely detectable, proving U0126 treatment efficacy [Figure 3.23 (A)]. Moreover, phosphorylated 4E-BP2 and 4E-BP1 and similarly, total ERK1/2 or 4E-BP1 levels do not change after U0126 treatment [Figure 3.23 (A)]. Finally, as in neurons, insulin treatment for 48 h does not alter 4E-BP2 WT expression [Figure 3.23 (A), (B)]. Taken together, these data suggest that the mTOR–dependent regulation of stability of deamidated 4E-BP2 is also a neuron–specific mechanism.

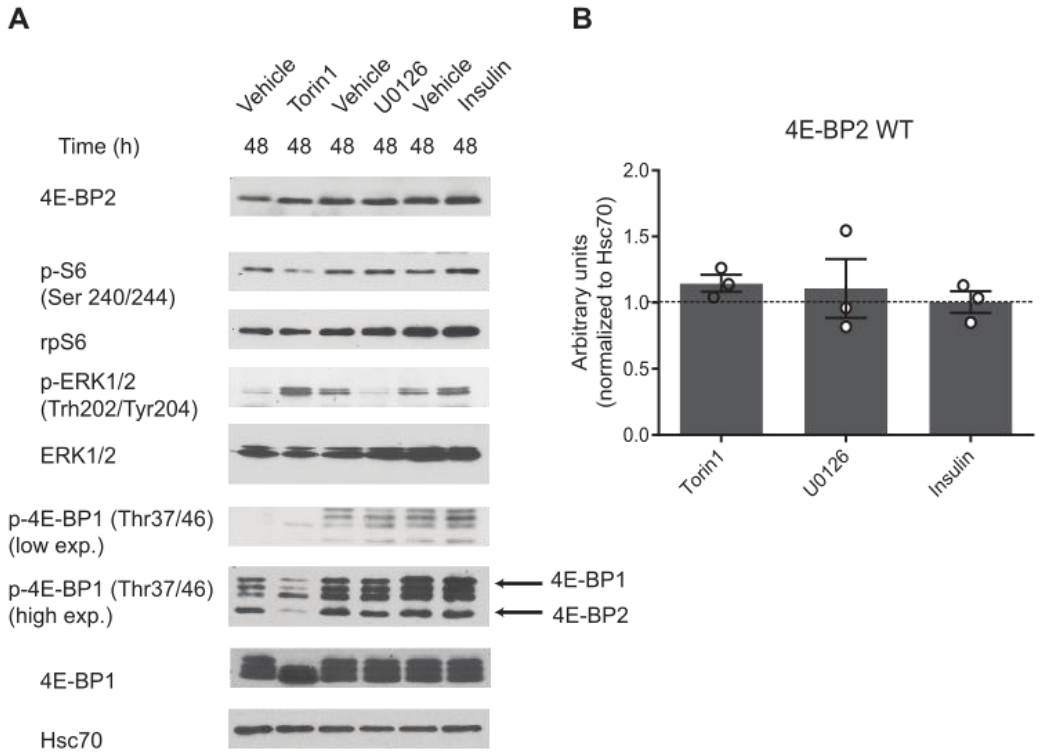

Figure 3.23 Inhibition of mTOR or MAPK signalling for 48 h does not alter 4E-BP2 WT in glia cells. Similarly, activation of both pathways with Insulin does not change 4E-BP2 WT expression.

Mixed neurons and glia culture were grown (as it was described in section 3.3.10 Deamidated 4E-BP2 is neuron-specific) and was trypsinised and passaged. **A.** The passaged glia culture was treated with Torin1 (250 nM), U0126 (20 µM), Insulin (10 µM) for 48 h and analysed by western blotting. Hsc70 was used as a loading control and appeared at 70 kDa. 4E-BP2 appeared as three bands (bottom band: 15 kDa, middle band: 16 kDa and top band: 17 kDa). 4E-BP1 appeared as three bands between 18-20 kDa. Phospho-4E-BP1 appeared between 18-21 kDa and phospho-4E-BP2 appeared between 16-18 kDa. ERK1/2 and phospho-ERK1/2 appeared at 42, 44 kDa. rpS6 and phospho-S6, both appeared at 32 kDa. For p-4E-BP1 37/46, low exposure of films corresponds to 10 min and high exposure to 30-40 min. **B.** Quantitative analysis of 4E-BP2 amount in (A). The intensities of the bands were measured using Image Studio Lite Ver 5.2 and normalised against Hsc70. The intensity of the bands at 48 h corresponding to Vehicle (lane 1, lane 3, lane 5) is set as 1 (dotted line on graph). The data shown in (A) are representative of three independent experiments. Quantitative data with mean ± SEM is shown in (B). Bonferroni-corrected two-way ANOVA.

3.3.15 Short-term inhibition of AMPA receptors leads to accumulation of deamidated 4E-BP2 in dissociated cortical neurons whereas long-term inhibition of AMPA and NMDA receptors concomitantly decreases deamidated 4E-BP2

Deletion of *Eif4ebp2* in mice leads to augmented synthesis of glutamate receptors GluA1 and GluA2 and facilitation of AMPA–mediated synaptic activity (Ran et al., 2013). Contrarily, deletion of *Eif4ebp2* in mice does not affect NMDA–dependent miniature excitatory postsynaptic currents (mEPSCs) (Ran et al., 2013). Therefore, we asked whether inhibition of glutamate receptors (AMPAR or NMDAR) will affect differently the stability of deamidated and WT 4E-BP2. To investigate this, we inhibited AMPA and NMDA receptors with 10 µM NBQX and 50 µM AP5 respectively, in dissociated cortical neurons for 9 h and 48 h, and treated lysates were analysed by western blotting. Figure 3.24 (A) shows representative blots of treated neuronal lysates with AMPA and NMDA receptor inhibitors separately for 9 h and then together with both inhibitors for 9 h. Figure 3.24 (B) illustrates quantitative graphs of representative blots.

After 9 h of NBQX treatment, deamidated 4E-BP2 protein amounts exhibit a significant increase ($p < 0.05$), as compared to WT protein levels [Figure 3.24 (A), (B)]. Conversely, inhibition of NMDA receptors with AP5 for 9 h does not differentiate WT and deamidated protein levels [Figure 3.24 (A), (B)]. Lastly, inhibition of both AMPA and NMDA receptors shows a similar effect as inhibition of NMDA receptors [Figure 3.24 (A), (B)]. Specifically, inhibition of both receptors does not differentiate significantly deamidated protein levels from WT 4E-BP2 levels [Figure 3.24 (A), (B)]. Membranes were also stripped and probed for phospho – 4E-BP 37/46 [Figure 3.24 (A)]. Phosphorylated 4E-BP2 does not follow the same direction as total 4E-BP2 since it does not change after any treatment [Figure 3.24 (A)]. On the other hand, phosphorylated 4E-BP1 increases after 9 h of NBQX treatment and decreases after 9 h of AP5 treatment [Figure 3.24 (A)]. Inhibition of both AMPA and NMDA receptors does not change phosphorylation of 4E-BP1 [Figure 3.24 (A)].

Figure 3.24 (C) illustrates representative blots of neuronal lysates that were treated with 10 µM NBQX and 50 µM AP5 for 48 h to check the effect of long-term

inhibition of AMPA and NMDA receptors on the stability of deamidated and WT 4E-BP2. Figure 3.24 (D) shows quantitative graphs of 4E-BP2 protein amounts. Long-term inhibition of AMPA receptors with NBQX or NMDA with AP5 does not alter protein levels of deamidated from WT 4E-BP2 levels [Figure 3.24 (C), (D)]. However, after long-term inhibition of both receptors, we observed a significant decrease of deamidated 4E-BP2 protein amounts ($p < 0.05$), as compared to WT 4E-BP2 [Figure 3.24 (C), (D)]. Membranes were again stripped and probed for phospho–4E-BP 37/46 [Figure 3.24 (C)]. Levels of phosphorylated 4E-BP2 and 4E-BP1 decrease after AP5 treatment alone or along with NBQX [Figure 3.24 (C)]. To conclude, duration of inhibition of glutamate receptors determines the effect on the stability of deamidated 4E-BP2. Short-term inhibition of AMPA receptors increased protein amounts of deamidated 4E-BP2 whereas long-term inhibition of both AMPA and NMDA receptors

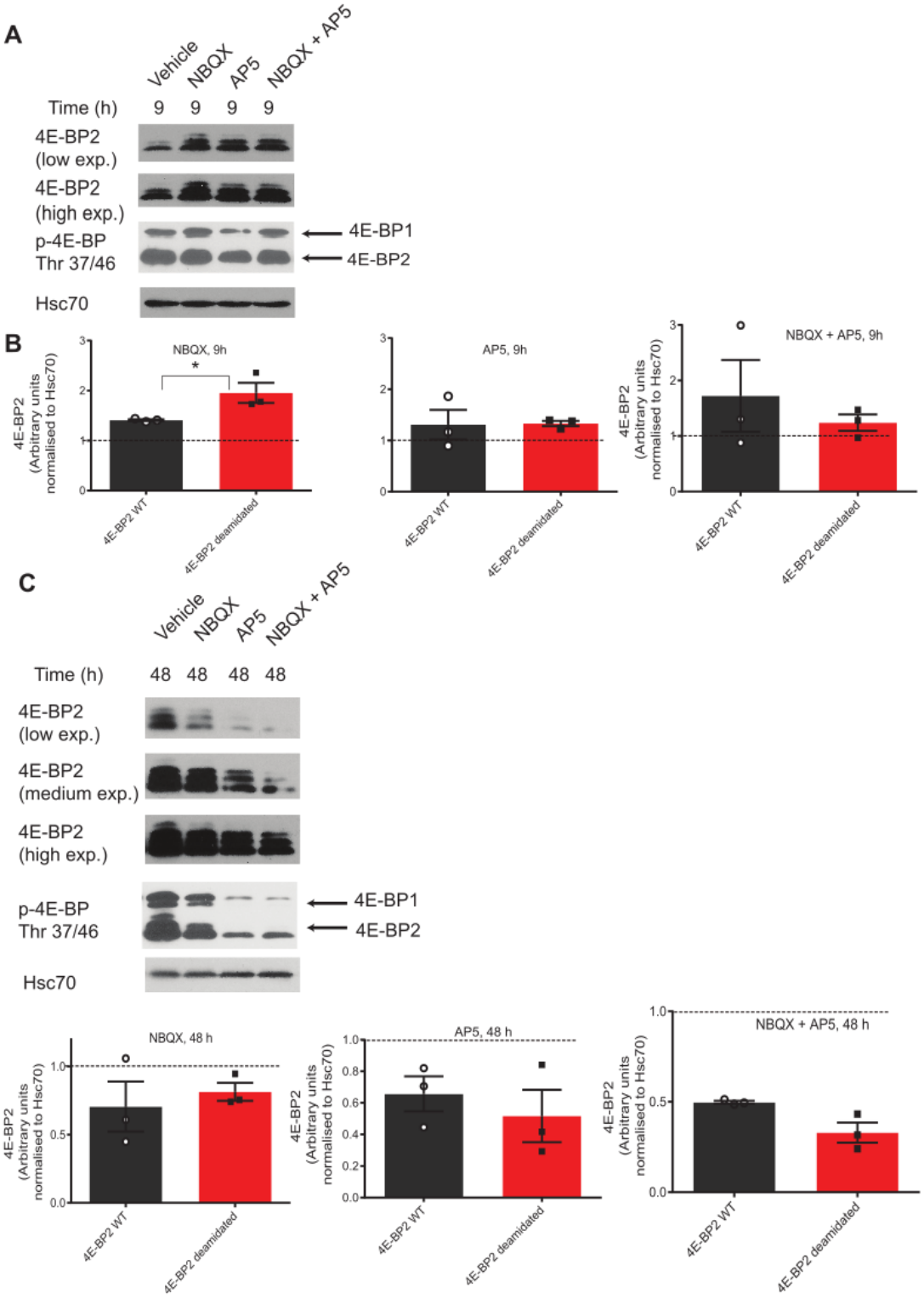

Figure 3.24 Inhibition of AMPA receptors for 9 h leads to accumulation of deamidated 4E-BP2 whereas inhibition of both AMPA and NMDA receptors for 48 h decreased deamidated 4E-BP2.

A. Cortical neurons were treated with NBQX (10 μM), AP5 (50 μM) and then together for 9 h and were analysed by western blotting and probed for 4E-BP2 and phospho – 4E-BP2 37/46. Hsc70 was used as a loading control and appeared at 70 kDa. 4E-BP2 appeared as three bands (bottom band: 15 kDa, middle band: 16 kDa and top band: 17 kDa). Phospho-4E-BP1 appeared between 18-21 kDa and phospho-4E-BP2 appeared between 16-18 kDa. Low exposure of films for 4E-BP2 correspond to 1-3 min, medium exposure to 10-15 min and high exposure to 15-20 min. **B**. Quantitative analysis of the different 4E-BP2 amounts in (A). The intensities of the bands were measured using Image Studio Lite Ver 5.2 and normalised against Hsc70. The intensity of the band at 9 h (Vehicle, lane 1) is set as 1 (dotted line on graph). The data shown in (A) are representative of three independent experiments. Quantitative data with mean ± SEM is shown in (B). *$p < 0.05$ using Bonferroni-corrected two-way ANOVA. **C**. Cortical neurons were treated with NBQX (10 μM), AP5 (50 μM) and then together for 48 h and were analysed by western blotting and probed for 4E-BP2 and phospho – 4E-BP2 37/46. Hsc70 was used as a loading control and appeared at 70 kDa. 4E-BP2 appeared as three bands (bottom band: 15 kDa, middle band: 16 kDa and top band: 17 kDa). Phospho-4E-BP1 appeared between 18-21 kDa and phospho-4E-BP2 appeared between 16-18 kDa. **D**. Quantitative analysis of the different 4E-BP2 amounts in (A). The intensities of the bands were measured using Image Studio Lite Ver 5.2 and normalised against Hsc70. The intensity of the band at 48 h (Vehicle, lane 1) is set as 1 (dotted line on graph). Bonferroni-corrected two-way ANOVA. The data shown in (A) are representative of three independent experiments. Quantitative data with mean ± SEM is shown in (B). For quantification, only films that were exposed for 1-3 min (low exposure) were used.

3.3.16 Inhibition of action potential firing does not affect deamidated 4E-BP2 degradation

We show that inhibition of AMPA receptors for 9 h increases deamidated 4E-BP2 protein amounts, but not WT 4E-BP2 [Figure 3.24 (A), (B)]). However, long-term inhibition of both AMPA and NMDA receptors decreases deamidated 4E-BP2 protein levels ([Figure 3.24 (C), (D). To further study the relation between synaptic activity and deamidated 4E-BP2, we inhibited action potential firing in dissociated cortical neuronal cultures by using TTX (Tetratodoxin) for 48 h. Firstly, we used 1 μM TTX at an early age DIV 12, and then we treated the lysates with λ phosphatase to be able to distinguish between phosphorylation and deamidation of 4E-BP2. Moreover, we also resolved on the gel a non-treated lysate from DIV 8 as a negative control for deamidation pattern. Then, we used 1 μM TTX at DIV 25 and we treated the lysates with λ phosphatase. For this age, we resolved on the gel one non-treated neuronal lysate collected at DIV 21 where we were not sure if would get the full deamidation pattern as with lysates at DIV 25. Figure 3.25 presents representative blots of treated dissociated neuronal cells with TTX.

On DIV 12, TTX treatment does not modify 4E-BP2 WT protein levels whereas phosphatase treatment completely abolishes the slower migrated band (>15kDa),

implying that this band corresponds to phosphorylated 4E-BP2 (Figure 3.25). On DIV 25, TTX treatment does not change deamidated 4E-BP2 protein amounts which correspond to the slower migrating form (>15 kDa) that is still present after phosphatase treatment (Figure 3.25). At the same age, DIV 25, TTX treatment does not alter 4E-BP2 WT protein amounts, as we show at DIV 12 (Figure 3.25). Therefore, long-term inhibition of action potential firing does not affect proteasomal degradation of deamidated 4E-BP2.

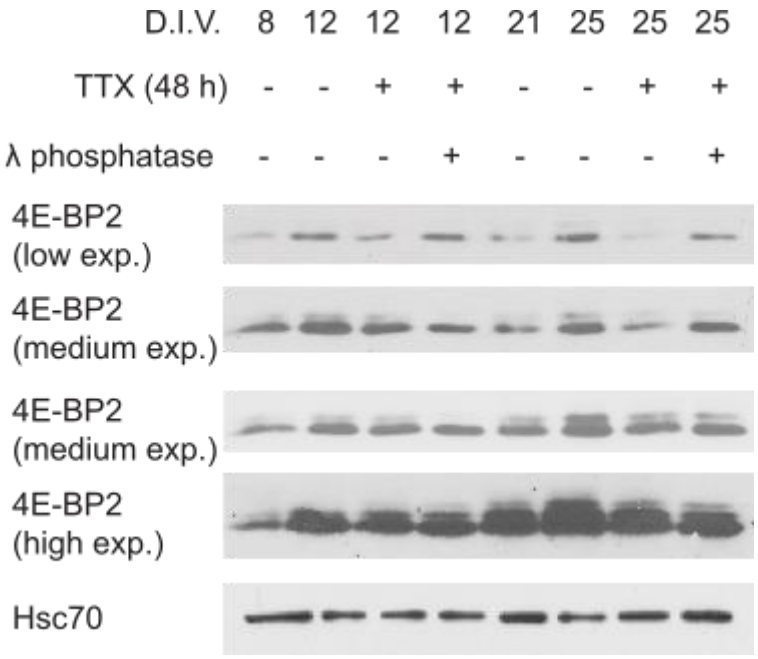

Figure 3.25 Inhibition of synaptic activity for 48 h does not affect deamidated 4E-BP2 protein levels.

Cortical neurons were treated with TTX (1 µM), then lysed and treated with λ phosphatase, followed by western blotting and probed for 4E-BP2. Hsc70 was used as a loading control and appeared at 70 kDa. 4E-BP2 appeared as three bands (bottom band: 15 kDa, middle band: 16 kDa and top band: 17 kDa). Low exposure of films for 4E-BP2 correspond to 1-3 min, medium exposure to 10-15 min and high exposure to 15-20 min. The data shown are representative of three independent experiments.

3.3.17 Deamidated 4E-BP2 gets degraded by the proteasome and is regulated by mTOR signalling in isolated synaptoneurosomes

3.3.17.1 Deamidated 4E-BP2 is also expressed in isolated synaptoneurosomes and gets degraded by the proteasome

Deamidated 4E-BP2 affects synaptic transmission since expression of deamidated 4E-BP2 in *Eif4ebp2* -/- neurons alters charge transfer of mEPSCs (Bidinosti et al., 2010b). Therefore, we asked whether 4E-BP2 is also deamidated in synaptic fractions. To answer this question, we isolated synaptoneurosomes from adult mice, and then we lysed and analysed them with western blotting. Brain lysed homogenate in sucrose buffer before centrifugation is labelled as crude. Figure 3.26 (A) shows representative blots of lysed crude and synaptoneurosomes that were probed for 4E-BP2 and different synaptic, glial and nuclear proteins to study and compare the purity of synaptoneurosomes.

We detected deamidated 4E-BP2 in synaptoneurosomal fractions along with synaptic proteins such as Synaptophysin (presynaptic) and PSD95 (postsynaptic) [Figure 3.26 (A)]. GFAP (Glial fibrillary acidic protein) and Histone H3 protein levels are barely detectable in synaptoneurosomes, as compared to crude, indicating their purity [Figure 3.26 (A)]. Then, we examined the stability of 4E-BP2 in synaptoneurosomes. To investigate this, firstly, we performed a proteasome activity assay to check levels of activity of 20S proteasome in crude and synaptoneurosomal fractions. Figure 3.26 (B) graph presents levels of activity assay in 20S proteasome between crude and synaptoneurosomes. 20S proteasome activity levels decreases in synaptoneurosomes ($p < 0.001$), as compared to crude [Figure 3.26 (B)].

To focus on the study of stability of 4E-BP2 in synaptic fractions, we inhibited protein synthesis with 100 µg/ml CHX and proteasome with 20 µM MG132 or 10 µM Lactacystin in synaptoneurosomes for 1 h. Figure 3.26 (C) shows representative blots of treated synaptoneurosomes with different inhibitors. Unexpectedly, results from inhibiting protein synthesis with CHX for 1 h are inconclusive due to high variability between replicates [Figure 3.26 (C)]. Deamidated and WT 4E-BP2 increases after CHX treatment for 1 h [Figure 3.26 (C), representative left blot] in 3 replicates and decreases in other 2 replicates [Figure 3.26 (C), representative right blot]. The graph in Figure 3.26 (D) shows that on average both WT and deamidated 4E-BP2 protein

amounts exhibit no significant change after CHX treatment of synaptoneurosomes. Inhibition of proteasome with MG132 increases deamidated 4E-BP2 protein levels ($p < 0.01$), as compared to WT protein [Figure 3.26 (C, left and right blot), (D)], implying that deamidated 4E-BP2 gets degraded by the proteasome in synaptoneurosomes. Figure 3.26 (C) and (D) illustrate representative blots of treated synaptoneurosomes with Lactacystin and quantitative graph of protein amounts, respectively. Proteasome inhibition with Lactacystin (a higher concentration was used compared to total neuronal lysates) in synaptoneurosomes increases protein amounts of deamidated 4E-BP2 ($p < 0.05$), as compared to WT protein [Figure 3.26 (D)].

To confirm that the higher concentration of Lactacystin that was used in this experiment effectively blocked proteasome activity, we measured activity levels of 20S proteasome in treated synaptoneurosomes with Lactacystin for 1 h [Figure 3.26 (E)]. Lactacystin completely inhibits 20S proteasome activity ($p < 0.05$), as compared to 0h-treated synaptoneurosomes [Figure 3.26 (E)]. Thus, 4E-BP2 is also deamidated in synaptic fractions and gets degraded by the proteasome in synaptoneurosomes.

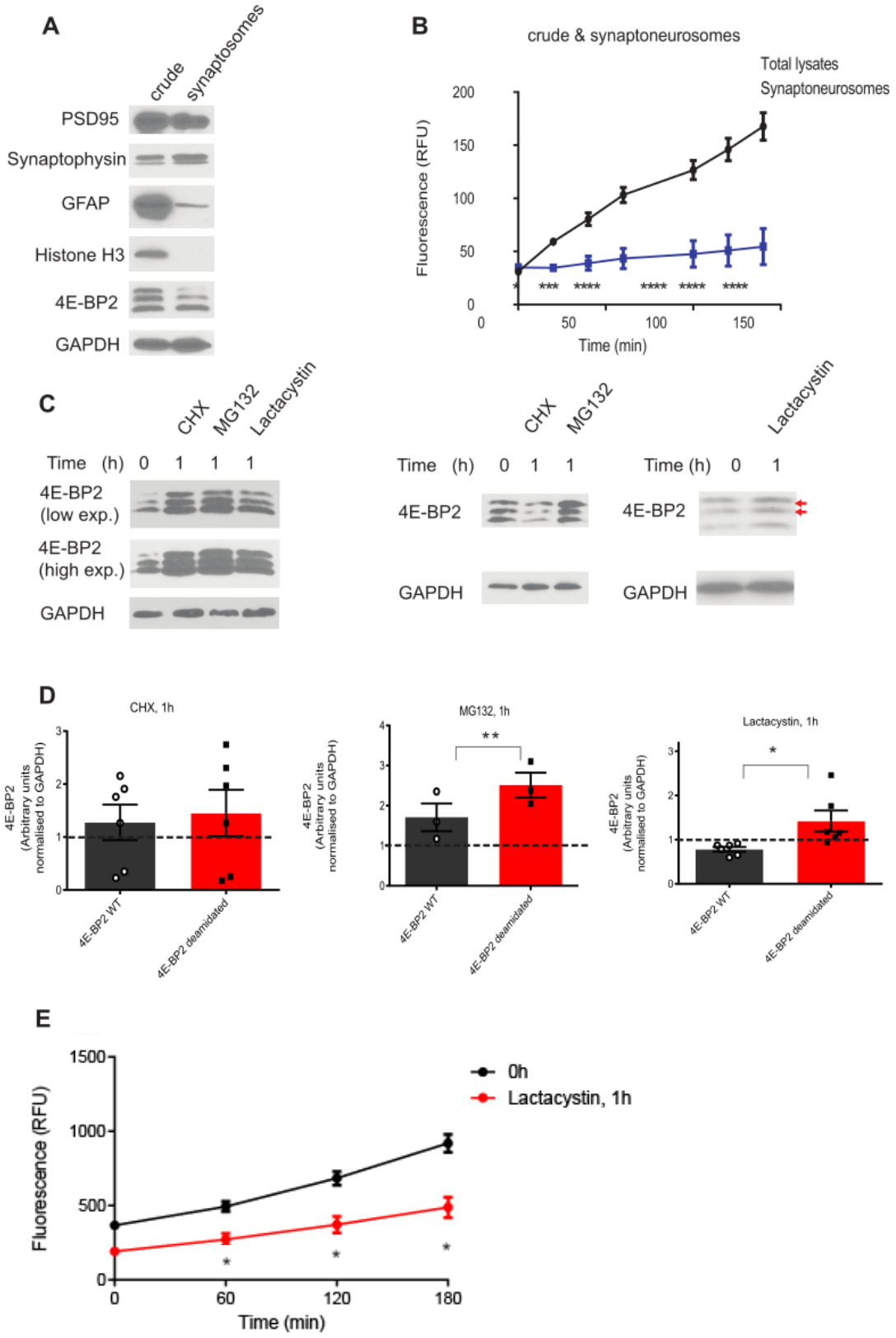

Figure 3.26 Deamidated 4E-BP2 is expressed in synaptoneurosomes and gets degraded by the proteasome.

A. Crude and synaptoneurosome lysates were analysed by western blotting and probed for PSD95 (95 kDa), Synaptophysin (38 kDa), GFAP (50 kDa), Histone H3 (15 kDa) and 4E-BP2. GAPDH was used as a loading control and appeared at 37 kDa. 4E-BP2 appeared as three bands (bottom band: 15 kDa, middle band: 16 kDa and top band: 17 kDa). **B.** Proteasome enzymatic activity was measured in treated lysates from crude and synaptoneurosomes that were analysed by western blotting in (A). Proteasome activity is shown in RFU/min (+ s.e.m., *n* = 3). **C.** Isolated synaptoneurosomes were treated with CHX (100 µg/ml), MG132 (20 µM) and Lactacystin (10 µM) for 1 h and were analysed by western blotting and probed for 4E-BP2. GAPDH was used as a loading control and appeared at 37 kDa. 4E-BP2 appeared as three bands (bottom band: 15 kDa, middle band: 16 kDa and top band: 17 kDa). Low exposure of films for 4E-BP2 correspond to 1-3 min and high exposure to 15-20 min. **D.** Quantitative analysis of the different 4E-BP2 amounts in (C). The intensities of the bands were measured using Image Studio Lite Ver 5.2 and normalised against GAPDH. The intensity of the band at 0 h (lane 1) is set as 1 (dotted line on graph). Quantitative data with mean ± SEM is shown in (B). **E.** Proteasome enzymatic activity was measured in treated synaptoneurosome lysates that were analysed by western blotting in (C). Proteasome activity is shown in RFU/min (+ s.e.m., *n* = 3). The data shown in (A), (B), (C), (D), (E) are representative of three independent experiments. *p < 0.05, **p < 0.01, ***p < 0.001, ****p < 0.0001, using Bonferroni-corrected two-way ANOVA. For quantification, only films that were exposed for 1-3 min (low exposure) were used.

3.3.17.2 Deamidated 4E-BP2 has a shorter half-life than WT in synaptoneurosomes

We show that deamidated 4E-BP2 has a short half-life in HEKs transfected with different 4E-BP2 forms (Figure 3.2). However, CHX treatment in dissociated cortical neurons (Figure 3.20) or synaptoneurosomes (Figure 3.26) does not affect protein levels of deamidated 4E-BP2 Therefore, we used different protein synthesis inhibitors to investigate the stability of 4E-BP2 in synaptoneurosomes. To study this, we treated synaptoneurosomes with 2 µg/ml HHT or 10 µg/ml Anisomycin for 1 h, and then lysed and analysed them by western blotting. Puromycin (5 µg/ml) was also added 30 min before the end of HHT or Anisomycin treatment. Figure 3.27 (A) shows representative blots of treated synaptoneurosomes with HHT or Anisomycin that were probed for 4E-BP2. Figure 3.27 (B) presents a quantitative graph of protein amounts of deamidated and WT protein.

After HHT treatment for 1 h, deamidated 4E-BP2 has a faster degradation rate ($p < 0.05$), as compared to WT protein in treated synaptoneurosomes [Figure 3.27 (A), (B)]. Deamidated 4E-BP2 protein amounts in Anisomycin-treated synaptoneurosomes also exhibit a significant decrease ($p < 0.05$), as compared to WT protein [Figure 3.27 (A), (B)]. HHT and Anisomycin treatment also diminishes

Puromycin incorporation [Figure 3.27 (A)], proving efficacy of HHT and Anisomycin treatment. Thereby, deamidated 4E-BP2 is unstable in synaptic fractions of neurons.

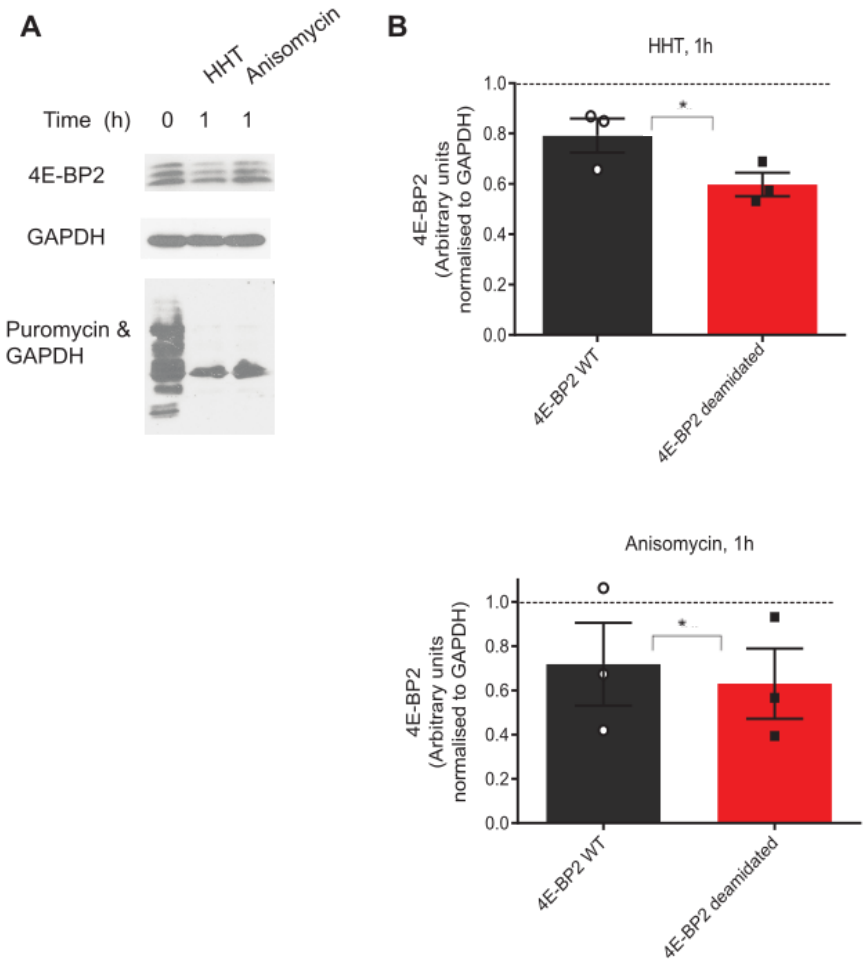

Figure 3.27 Protein stability assay in isolated synaptoneurosomes of deamidated 4E-BP2.

A. Isolated synaptoneurosomes were treated with 2 µg/ml HHT or 10 µg/ml Anisomycin for 1 h and were analysed by western blotting and probed for 4E-BP2 and Puromycin. GAPDH was used as a loading control and appeared at 37 kDa. 4E-BP2 appeared as three bands (bottom band: 15 kDa, middle band: 16 kDa and top band: 17 kDa). **B.** Quantitative analysis of the different 4E-BP2 amounts in (A). The intensities of the bands were measured using Image Studio Lite Ver 5.2 and normalised against GAPDH. The intensity of the band at 0 h (lane 1) is set as 1 (dotted line on graph). Quantitative data with mean ± SEM is shown in (B). *$p < 0.05$ using Bonferroni-corrected two-way ANOVA. The data shown in (A), (B) are representative of three independent experiments. For quantification, only films that were exposed for 1-3 min (low exposure) were used.

3.3.17.3 Deamidated 4E-BP2 accumulates after inhibition of mTOR in synaptoneurosomes and this accumulation is rescued by proteasome activation

We discovered that deamidated 4E-BP2 regulation in neurons is mTOR – dependent (Figure 3.21, Figure 3.22) and we wondered whether this regulation is also important in synaptic fractions where local protein synthesis is required for synaptic transmission, learning and memory (Cajigas et al., 2010). To answer this question, we treated synaptoneurosomes either with 250 nM Torin1 or 20 nM Rapamycin for 1 h, lysed and analysed them by western blotting. Figure 3.28 (A), (C) show representative blots of treated synaptoneurosomes probed for 4E-BP2 and (B), (D) quantitative graphs of 4E-BP2 protein amounts. Deamidated 4E-BP2 protein levels accumulate after inhibition of mTOR, either with Torin1 or Rapamycin for 1 h, in synaptoneurosomes ($p < 0.05$), as compared to WT protein [Figure 3.28 (A), (B), (C), (D)]. Figure 3.28 (E) presents measured 20S proteasome activity levels in treated synaptoneurosomes with Torin1 or Rapamycin. mTOR inhibition either with Torin1 or Rapamycin decreased 20S proteasome activity levels in synaptoneurosomes [Figure 3.28 (E)].

To confirm, that accumulation of deamidated 4E-BP2 after inhibition of mTOR is due to inhibition of proteasomal degradation of deamidated 4E-BP2 specifically, we used a proteasome activator, Betullinic acid, and check if we could rescue the accumulation of deamidated 4E-BP2. For this reason, we treated synaptoneurosomes with 2.5 µg/ml Betullinic acid, Torin1 and then, Betullinic acid and Torin1 together for 1 h. Figure 3.28 (G) depicts representative blot from treated synaptoneurosomes. Interestingly, inhibition of mTOR for 1 h and concomitantly, activation of proteasome with Betullinic acid, rescues increased protein levels of deamidated 4E-BP2, indicating that accumulation of deamidated 4E-BP2 after inhibition of mTOR is due to incomplete degradation of deamidated protein [Figure 3.28 (G)]. Therefore, inhibition of mTOR is causal for inhibition of proteasome that leads to accumulation of deamidated 4E-BP2.

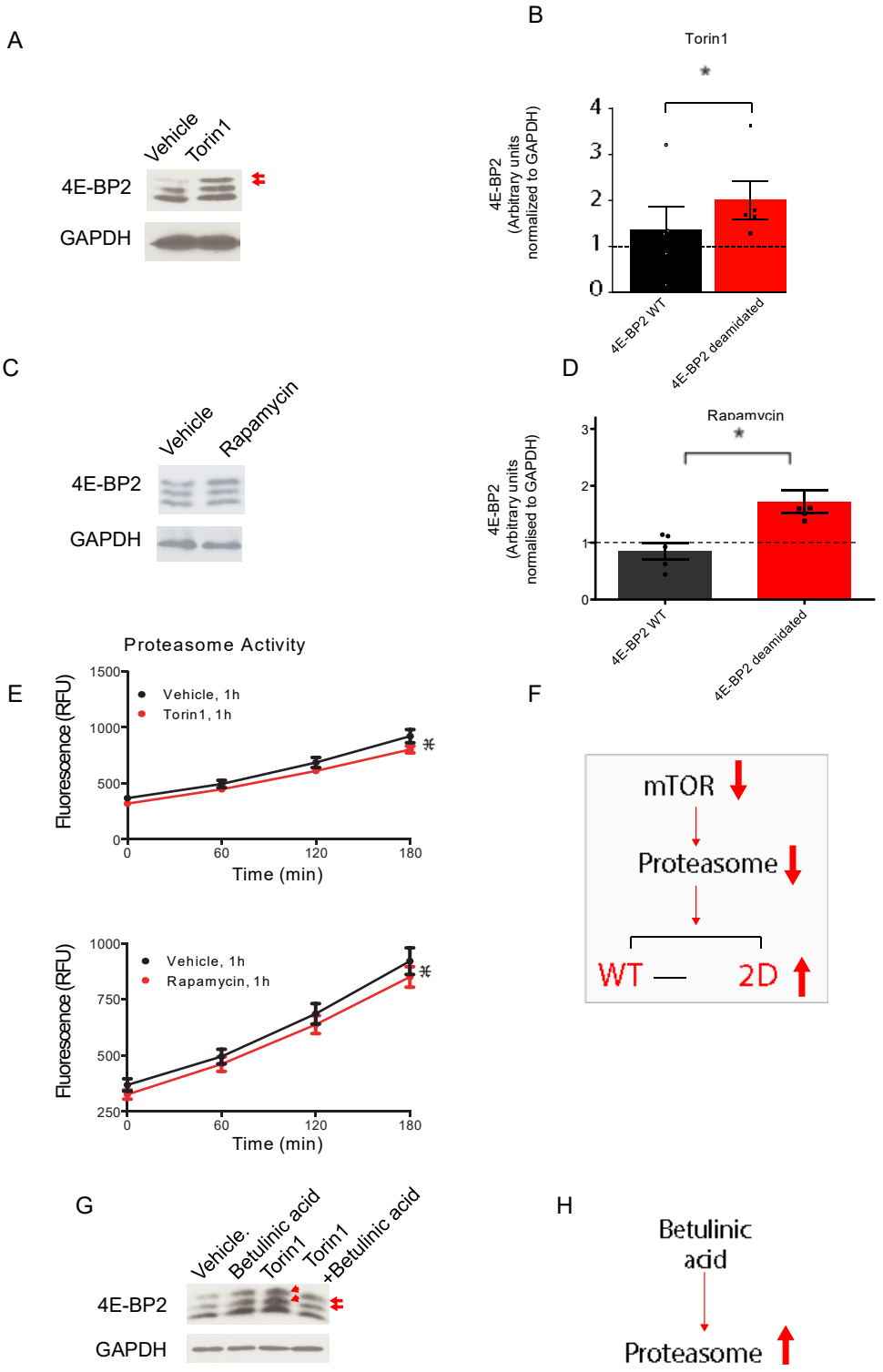

Figure 3.28 Inhibition of mTOR causes accumulation of deamidated 4E-BP2 which emerges from incomplete proteasomal degradation of the protein.

A. Isolated synaptoneurosomes that were treated with Torin1 (250 nM) for 1 h were analysed by western blotting and probed for 4E-BP2. GAPDH was used as a loading control and appeared at 37 kDa. 4E-BP2 appeared as three bands (bottom band: 15 kDa, middle band: 16 kDa and top band: 17 kDa). **B.** Quantitative analysis of the different 4E-BP2 amounts in (A). The intensities of the bands were measured using Image Studio Lite Ver 5.2 and normalised against GAPDH. The intensity of the band at Vehicle (lane 1) is set as 1 (dotted line on graph). Quantitative data with mean ± SEM is shown in (B). *p < 0.05 using Bonferroni-corrected two-way ANOVA.**C.** Isolated synaptoneurosomes that were treated with 20 nM Rapamycin were analysed by western blotting and probed for 4E-BP2. GAPDH was used as a loading control and appeared at 37 kDa. 4E-BP2 appeared as three bands (bottom band: 15 kDa, middle band: 16 kDa and top band: 17 kDa). **D.** Quantitative analysis of the different 4E-BP2 amounts in (C). The intensities of the bands were measured using Image Studio Lite Ver 5.2 and normalised against GAPDH. The intensity of the band at Vehicle (lane 1) is set as 1 (dotted line on graph). Quantitative data with mean ± SEM is shown in (D). *p < 0.05 using Bonferroni-corrected two-way ANOVA. **E.** Proteasome enzymatic activity was measured in Torin1- and Rapamycin-treated lysates from synaptoneurosomes that were analysed by western blotting in (A), (C). Proteasome activity is shown in RFU/min (+ s.e.m., *n* = 3). *p < 0.05 using Bonferroni-corrected two-way ANOVA. **F.** Schematic diagram, illustrating our hypothesis. Inhibition of mTOR decreases proteasomal activity and degradation of deamidated 4E-BP2, leading to its protein accumulation as it is shown in (A). **G.** Isolated synaptoneurosomes were treated with 2.5 µg/ml Betullinic acid, 250 nM Torin1, 2.5 µg/ml Betullinic acid and 250 nM Torin1 and were analysed by western blotting and probed for 4E-BP2. GAPDH was used as a loading control and appeared at 37 kDa. 4E-BP2 appeared as three bands (bottom band: 15 kDa, middle band: 16 kDa and top band: 17 kDa). **H.** Diagram indicates that Betullinic acid acts as a proteasomal activator. Red arrows on (A), (G) indicate the slower migrating bands that correspond to deamidated 4E-BP2. The data shown in (A), (B), (C), (D) are representative of three independent experiments.

3.3.17.4 Stimulation of synaptoneurosomes does not change stability of deamidated 4E-BP2

We showed that deamidated 4E-BP2 is a long half-lived protein in cortical neuronal cultures (Figure 3.20) but unstable in synaptoneurosomes where is also regulated by the mTOR and proteasome [(Figure 3.28 (A), (B), (G)]. These data indicate that deamidated 4E-BP2 might have a unique role in synaptic fractions of neurons. Thus, we asked whether stimulation of synaptoneurosomes will change the stability of the protein. To test this hypothesis, we treated synaptoneurosomes with KCl (50 mM) for 1 h with or without inhibiting translation and proteasome activity. The synaptoneurosomes were lysed after stimulation, followed by western blotting. Figure 3.29 (A) shows representative blots from stimulated synaptoneurosomes, treated with 100 µg/ml CHX, 20 µM MG132 and 5 µM Lactacystin. Figure 3.29 (C) illustrates quantitative graphs of deamidated and WT 4E-BP2 protein levels from the representative blots depicted in Figure 3.29 (A).

Inhibition of protein synthesis or proteasome in stimulated synaptoneurosomes [Figure 3.29 (A)] has similar effects as on unstimulated [Figure 3.26 (C)] synaptoneurosomes. After CHX treatment with concomitant KCl stimulation [Figure 3.29 (A), (C)], there are no significant differences between protein levels of deamidated 4E-BP2, as compared to WT protein. Inhibition of proteasome with MG132 and Lactacystin in stimulated synaptoneurosomes [Figure 3.29 (A), (C)] do not differentiate protein levels of deamidated from WT 4E-BP2.

Since inhibition of translation with CHX in vehicle and stimulated synaptoneurosomes does not reduce protein levels of deamidated or WT 4E-BP2, as [Figure 3.29 (A)], we asked whether CHX could effectively inhibit protein synthesis in synaptoneurosomes. To answer this question, we treated synaptoneurosomes with CHX and KCl, either each one alone or together and 30 min before stopping the treatments, we added Puromycin (5 μg/ml). Figure 3.29 (B) presents one representative blot of the CHX and KCl treatments. After KCl stimulation for 1 h [Figure 3.29 (B), (lane 3 on the gel)], protein synthesis levels decrease (Puromycin antibody), as compared to Vehicle (1 h). After 1 h of CHX treatment [Figure 3.29 (B), (lane 4 on the gel] or CHX along with KCl stimulation [Figure 3.29 (B), (lane 5 on the gel], translation levels (Puromycin antibody) reduce, as compared to 0 h and 1 h Vehicle, showing that CHX effectively blocks protein synthesis. Deamidated 4E-BP2 protein amounts do not differentiate, as compared to WT in any condition [Figure 3.29 (B)]. Taken together, our findings indicate that KCl stimulation does not affect stability of deamidated 4E-BP2.

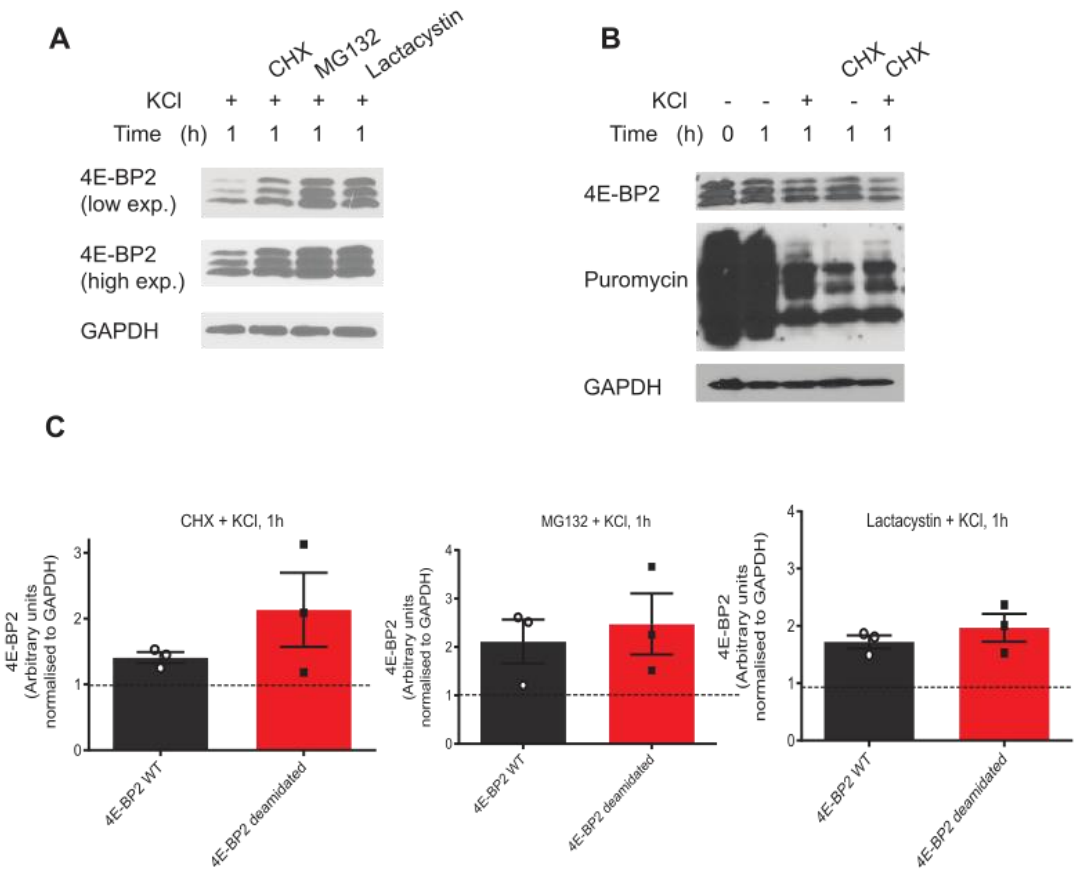

Figure 3.29 Stimulation of synaptoneurosomes does not affect the stability of deamidated 4E-BP2.

A. Isolated synaptoneurosomes were treated with 50 mM KCl along with 100 µg/ml CHX, 20 µM MG132, 5 µM Lactacystin for 1 h and were analysed by western blotting and probed for 4E-BP2. GAPDH was used as a loading control and appeared at 37 kDa. 4E-BP2 appeared as three bands (bottom band: 15 kDa, middle band: 16 kDa and top band: 17 kDa). Low exposure of films for 4E-BP2 correspond to 1-3 min and high exposure to 15-20 min. **B.** Isolated synaptoneurosomes were treated with 50 mM KCl and/or 100 µg/ml CHX for 1 h and were analysed by western blotting and probed for 4E-BP2. GAPDH was used as a loading control and appeared at 37 kDa. 4E-BP2 appeared as three bands (bottom band: 15 kDa, middle band: 16 kDa and top band: 17 kDa). Puromycin (5 µg/ml) was also added 30 min before stopping the treatment. **C.** Quantitative analysis of the different 4E-BP2 amounts in (A). The intensities of the bands were measured using Image Studio Lite Ver 5.2 and normalised against GAPDH. The intensity of the band at 1 h KCl stimulation (lane 1) is set as 1 (dotted line on graph). Quantitative data with mean ± SEM is shown in (C). The data shown in (A), (C), (D), (E), (F) are representative of three independent experiments. Bonferroni-corrected two-way ANOVA. For quantification, only films that were exposed for 1-3 min (low exposure) were used**.**

3.3.18 Inhibition of AMPA or NMDA receptors do not change stability of deamidated 4E-BP2 in synaptoneurosomes

We discovered that KCl stimulation does not change stability of deamidated 4E-BP2 (Figure 3.29). Previously, we showed that inhibition of AMPA receptors increases deamidated 4E-BP2 protein levels whereas inhibition of NMDA receptors does not alter 4E-BP2 protein levels. We asked whether inhibition of AMPA and NMDA receptors in synaptic fractions will affect deamidated 4E-BP2 on the same direction as in cortical neurons. Thus, we used 10 µM NBQX and 50 µM AP5 in isolated synaptoneurosomes for 1 h either alone or together and check the stability of deamidated and WT 4E-BP2. Figure 3.30 (A) shows representative blots of treated synaptoneurosomes with NBQX, AP5, NBQX + AP5 for 1 h and (B) presents quantitative graphs of each treatment of deamidated and WT protein levels.

After inhibition of AMPA receptors in synaptoneurosomes with NBQX, or NMDA receptors with AP5 or inhibition of both receptors, protein levels of deamidated 4E-BP2 do not alter from WT protein levels [Figure 3.30 (A), (B). Thus, inhibition of either AMPA or NMDA receptors in synaptoneurosomes does not change stability of deamidated 4E-BP2.

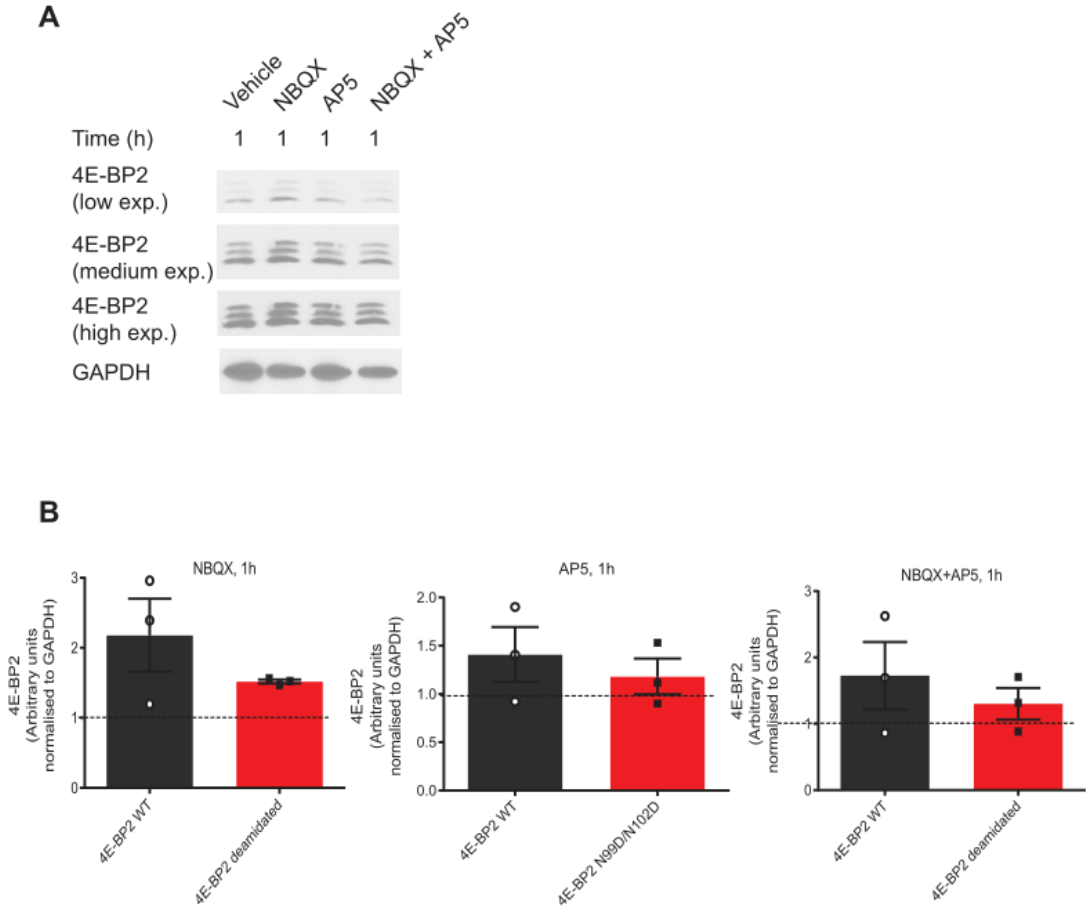

Figure 3.30 Inhibition of AMPA or NMDA receptors for 1 h does not affect stability of deamidated 4E-BP2.

A. Isolated synaptoneurosomes were treated with NBQX (10 µM), AP5 (50 µM) and then, together for 1 h and were analysed by western blotting and probed for 4E-BP2. GAPDH was used as a loading control and appeared at 37 kDa. 4E-BP2 appeared as three bands (bottom band: 15 kDa, middle band: 16 kDa and top band: 17 kDa). Low exposure of films for 4E-BP2 correspond to 1-3 min, medium exposure to 10-15 min and high exposure to 15-20 min. **B**. Quantitative analysis of the different 4E-BP2 amounts in (A). The intensities of the bands were measured using Image Studio Lite Ver 5.2 and normalised against GAPDH. The intensity of the band at 1 h (Vehicle, lane 1) is set as 1 (dotted line on graph). The data shown in (A) are representative of three independent experiments. Quantitative data with mean ± SEM is shown in (B). Bonferroni-corrected two-way ANOVA. For quantification, only films that were exposed for 1-3 min (low exposure) were used.

3.4 Discussion

Protein turnover enables neurons to change their proteome depending on the environmental changes and neural activity, maintaining flexible synapses and simultaneously, contributing to synaptic plasticity. For many proteins, deamidation is traditionally viewed as an “aging by-product”, which labels long-lived proteins for degradation (Robinson, 2002). Deamidation of Bcl-xL mediates its degradation and subsequently, inactivates Bcl-xL prosurvival activity (Dho et al., 2013). In accordance with this, we observe that double deamidated 4E-BP2 (2D) is unstable compared to WT 4E-BP2 (transfected and endogenous protein), dictating that deamidation reduces protein stability 4E-BP2. Only the deamidated form and not an Alanine mutant (2A) exhibits reduced protein stability, suggesting that this phenotype is specifically induced by the conversion of asparagines to aspartates and not by a non-specific mutation. We also discover that prolonged inhibition of phosphorylation decreases 4E-BP2 protein stability, regardless of the included mutations on 4E-B2 sequence. We then proceed to show that 2D stability is regulated through the Ubiquitin proteasome pathway as deamidated 4E-BP2 gets highly ubiquitinated and also accumulates after inhibition of proteasome compared to WT protein.

Deamidated 4E-BP2 exhibits increased interaction with Raptor (Bidinosti et al., 2010b), therefore we searched whether there is a causal relationship between increased affinity for Raptor and reduced protein stability of deamidated 4E-BP2. Indeed, overexpression of Raptor reduces significantly the stability of WT 4E-BP2 and Alanine mutant, denoting that association of 4E-BP2 with Raptor regulates 4E-BP2 protein stability. Furthermore, protein levels of 4E-BP2 ΔTOS, which lacks the TOS motif required for association with Raptor, do not change after overexpression of Raptor, dictating that binding of Raptor to 4E-BP2 through TOS motif regulates its protein stability. Conversely, reduced protein stability of deamidated 4E-BP2 is rescued after down-regulating Raptor, proving a Raptor-dependent regulatory mechanism of 4E-BP2 protein levels. We then discovered that the responsible complex for the ubiquitination and degradation of deamidated 4E-BP2 is Raptor-CUL4B-DDB1 complex as increased binding of Raptor and CUL4B is visible only in the presence of deamidated and not WT 4E-BP2. Moreover, increased ubiquitination levels of deamidated protein compared to WT 4E-BP2 by CUL4B and rescue of

decreased stability by downregulating CUL4B are indicative of the pivotal role of the CUL4B-DDB1 complex.

Interestingly, association of Raptor and deamidated 4E-BP2 also promotes cell cycle progression since, after overexpression of both proteins, more cells are in later stages S, G2/M of cell cycle compared to the number of cells on the S, G2/M stages after overexpression of Raptor and empty vector. Therefore, it is plausible that increased association of deamidated 4E-BP2 to Raptor and subsequent degradation of the protein by CUL4B-DDB1 complex might play a role in regulating cell cycle progression. Hypophosphorylated 4E-BPs inhibit cell cycle progression (Dowling et al., 2010). Therefore, overexpression of Raptor with deamidated 4E-BP2 might lead to increased phosphorylation of deamidated and WT 4E-BP2, allowing translation and thus, cell cycle progression.

To further characterise the potential role of deamidated 4E-BP2 in the brain, we sought to see whether 4E-BP2 is also deamidated in human brain. Indeed, deamidation of 4E-BP2 occurs also in human brains and is neuron-specific. Moreover, deamidated of 4E-BP2 occurs postnatally after DIV12 in cortical neurons, in accordance with previous studies (Bidinosti et al., 2010b). Brain proteome is characterised by a long half-life (Graber et al., 2013), thereby endogenous deamidated 4E-BP2 is stable in cortical neurons but unstable in isolated synaptoneurosomes, implying that deamidation of 4E-BP2 might play a specific role in synapses and local protein synthesis. Deamidated 4E-BP2 does not rescue increased charge transfer of mEPSCs in *Eif4ebp2* -/- mice (Bidinosti et al., 2010b), supporting the hypothesis that this posttranslational modification might confer a synaptic function to 4E-BP2. Moreover, stability of deamidated 4E-BP2 is regulated by mTOR signalling and this mechanism is also neuron-specific. Therefore, it remains to be elucidated which neuronal functions are regulated through proteasomal degradation of deamidated 4E-BP2 by this neuron-specific mechanism that involves Raptor-CUL4B-DDB1 complex and is mTOR- and AMPA-dependent.

4. Studying the Subcellular Localization of 4E-BP2

4.1 Introduction

Subcellular protein localization is tightly linked to protein function and activity (Geda et al., 2008). In eukaryotes, spatial compartmentalization of proteins is a highly dynamic process that allows cells to adapt to changes in the environment or stress conditions (Bauer et al., 2015; Geda et al., 2008). Thus, various stimuli activate signalling pathways which lead to efficient functional regulation of the proteome through control of protein localization (Geda et al., 2008). Therefore, proteins fluctuate between different subcellular compartments and this mechanism of regulating their precise distribution directly affects their activity (Geda et al., 2008). Furthermore, the subcellular distribution of a protein affects its activity by controlling access to that specific protein and determining its interaction partners (Scott et al., 2005). Therefore, refining protein localization often can provide invaluable information in characterising the role of newly discovered proteins (Scott et al., 2005).

Given the important role of 4E-BP2 in neurons, acting as a repressor of protein synthesis, we sought to study the subcellular distribution of endogenous 4E-BP2 in neurons. Regarding the subcellular distribution of 4E-BPs in cells, 4E-BP1 localizes in the cytoplasm with a fraction of 30% being in the nucleus in different cell lines and multiple tissues (Rong et al., 2008). 4E-BP2 follows a similar cytoplasm – nuclear localization as 4E-BP1 (Rong et al., 2008). Nuclear localization of 4E-BP1 is not dependent on the phosphorylation status of the protein or binding to eIF4E. On the contrary, 4E-BPs regulate eIF4E release from the nucleus since their interaction with eIF4E is indispensable for the nuclear localization of eIF4E (Rong et al., 2008). Moreover, inhibition of mTOR pathway is causal for nuclear accumulation of eIF4E through 4E-BPs (Livingstone et al., 2009). However, it is not known whether 4E-BP2,

which is the prevailing isoform in the brain, exhibits the same subcellular distribution in neurons as in other cells.

4.2 Experimental aim

The main aim of this thesis is to characterize the role of brain – specific deamidated 4E-BP2. To gain a further insight on the spatial distribution of 4E-BP2 in neurons, we set out to determine: 1) the subcellular localization of 4E-BP2 in neurons, 2) whether deamidated 4E-BP2 exhibits different intracellular distribution than WT 4E-BP2.

4.3 Results

4.3.1 4E-BP2 localizes in perinuclear puncta in the cytoplasm and dendrites

4E-BP2 is the abundant isoform of 4E-BPs in the brain. Moreover, 4E-BP2 is localized in the cytoplasm in most cells with a fraction of 30% being in the nucleus along with eIF4E. Furthermore, this nuclear accumulation of 4E-BPs is dependent on the mTOR pathway. However, the intracellular distribution of 4E-BP2 in neurons remains unknown. To study the subcellular localization of 4E-BP2 in neurons, we fixed DIV16 dissociated cortical mouse neurons and processed them for immunofluorescence with 4E-BP2 antibody. Figure 4.1 shows the subcellular distribution of endogenous 4E-BP2 in neurons.

4E-BP2 antibody recognises both 4E-BP2 forms, deamidated and WT, thereby the fluorescent signal denotes the subcellular localization of both 4E-BP2 forms (Figure 4.1). 4E-BP2 localizes in perinuclear puncta in the cell body of neurons but also in the dendrites (Figure 4.1). Moreover, we observe fluorescent puncta of 4E-BP2 in some distal dendrites (white arrows in Figure 4.1), supporting our previous findings that deamidated and WT 4E-BP2 are also expressed in synaptoneurosomes (Figure 3.26), probably playing a role in regulating local protein synthesis in these synaptic fractions.

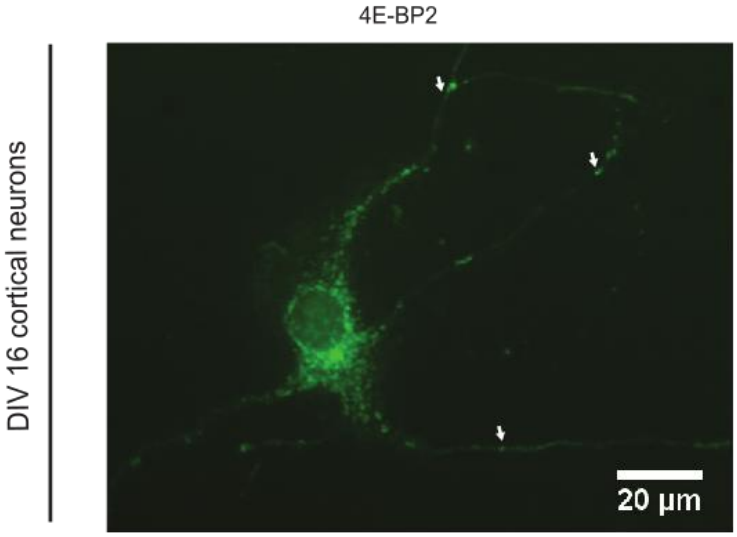

Figure 4.1 Intracellular distribution of endogenous 4E-BP2 in cortical neurons.

Dissociated DIV16 cortical mouse neurons probed first with antisera against 4E-BP2, followed by secondary antibody Alexa Fluor 488. Scale bars (20 µm) and arrows marking fluorescent puncta in distal dendrites are shown in white.

4.3.2 Fusion of fluorescent proteins to the C – terminal of 4E-BP2 affects 4E-BP2 expression

Posttranslational modifications influence enzymatic activity, protein turnover, protein – protein interactions and localization. Therefore, they play a pivotal role in modulating protein function, having a great impact on the cellular microenvironment (Karve and Cheema, 2011). Specifically, deamidation at neutral pH introduces a negative charge at the deamidation site, hence affecting properties of the proteins (Robinson, 2002). Thereby, we asked whether deamidation of 4E-BP2 changes the subcellular localization of 4E-BP2. To test this hypothesis, we cloned human *4E-BP2* (WT, double deamidated, Alanine mutant) in the mCerulean3-N1 and mCherry2-N1 vectors to have fused proteins, expressing N-terminal 4E-BP2 and C-terminal fluorescent (Cerulean, Cherry) protein. To test whether the expression and localization of 4E-BP2 is dependent on the orientation of subcloned *4E-BP2* in the

fluorescent vectors, we cloned human *4E-BP2* (WT, double deamidated, Alanine mutant) in the mCerulean3-C1 and mCherry2-C1 vectors to have fused proteins expressing N-terminal fluorescent proteins and C-terminal 4E-BP2. To test the expression level of each plasmid, we transfected HEKs with all plasmids expressing each 4E-BP2 form at N-terminal or C-terminal. 48 h post – transfection, cells were fixed and imaged at epifluorescence microscope. Figure 4.2 depicts fluorescent images from transfected HEKs expressing different fluorescent 4E-BP2-fusion proteins.

Figure 4.2 shows that the expression level of all 4E-BP2 forms is dependent on the orientation of *4E-BP2* in the cloned vector. In the plasmids that 4E-BP2 was expressed at the C-terminal of fused protein (top panel), fluorescent signal, depicting protein expression, is higher compared to the plasmids that 4E-BP2 was expressed at the N-terminal of fused protein (bottom panel) (Figure 4.2). Thus, when fluorescent tags are fused to the C- terminal of 4E-BP2, 4E-BP2 expression reduces as compared to N- terminal fusions (Figure 4.2). This finding is confirmed for all three 4E-BP2 forms (Figure 4.2). Specifically, for deamidated 4E-BP2, we did not detect any expression after transfecting fluorescent plasmid mCherry2, encoding N-terminal deamidated 4E-BP2 (Figure 4.2). Figure 1.2 (A) illustrates the human sequence of 4E-BP2 and conserved regions, important for interaction with eIF4E and Raptor. FEMDI is the TOS motif, essential for binding to Raptor and its position is at the end of C-terminal (Nojima et al., 2003). Therefore, binding of 4E-BP2 to Raptor may play a pivotal role on the expression and subcellular localization of 4E-BP2.

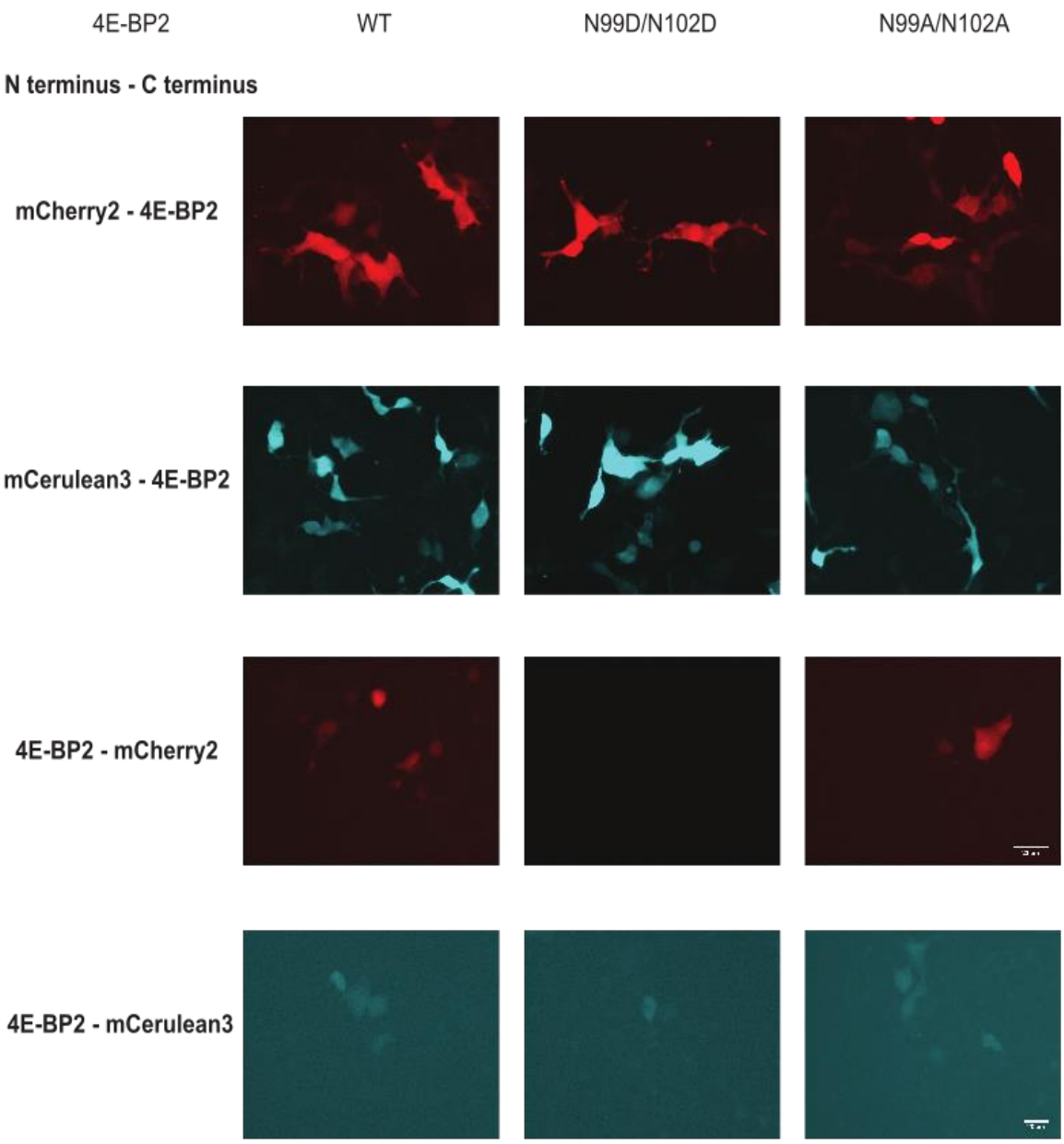

Figure 4.2 Fusion of fluorescent protein to C-terminal of 4E-BP2 affects 4E-BP2 expression levels.

Fluorescent microscopy of HEKs, transfected with 4E-BP2-mCherry2 (WT, 2D, Alanine mutant) (red) and 4E-BP2-mCerulean3 (WT, 2D, Alanine mutant) (blue) in both orientations. Scale bars (20 µm) are the same for all cells on this figure.

4.3.3 Deamidated 4E-BP2 colocalize in low levels with WT protein in neurons

Previously, we confirmed that deamidation of 4E-BP2 is neuron – specific (Figure 3.18), thus we asked whether deamidation of 4E-BP2 causes a different subcellular distribution than WT protein in neurons. To answer this question and considering that we lack a specific antibody recognising deamidated 4E-BP2, we co – transfected DIV4 dissociated mouse cortical neurons with plasmids expressing N – terminally HA tagged and N – terminally FLAG tagged WT or double deamidated 4E-BP2. On DIV16, we fixed transfected neurons and processed them for immunofluorescence and confocal imaging. Figure 4.3 depicts transfected dissociated cortical neurons, expressing both FLAG – 4E-BP2 WT (green) and HA – 4E-BP2 N99D/N102D (double deamidated, red). Merged images (yellow), illustrating colocalization of WT and deamidated signals (Figure 4.3).

The images indicate that both deamidated and WT 4E-BP2 exhibit a similar subcellular localization in the cell body and dendrites of neurons (Figure 4.3). Specifically, in the cell body there is a high number of colocalized puncta (yellow) of both 4E-BP2 forms (Figure 4.3). However, in distal dendritic areas (white arrows), we observed distinct fluorescent puncta of deamidated and WT 4E-BP2 (Figure 4.3). Thus, deamidated and WT 4E-BP2 appear to colocalize in the cell body but not in dendrites.

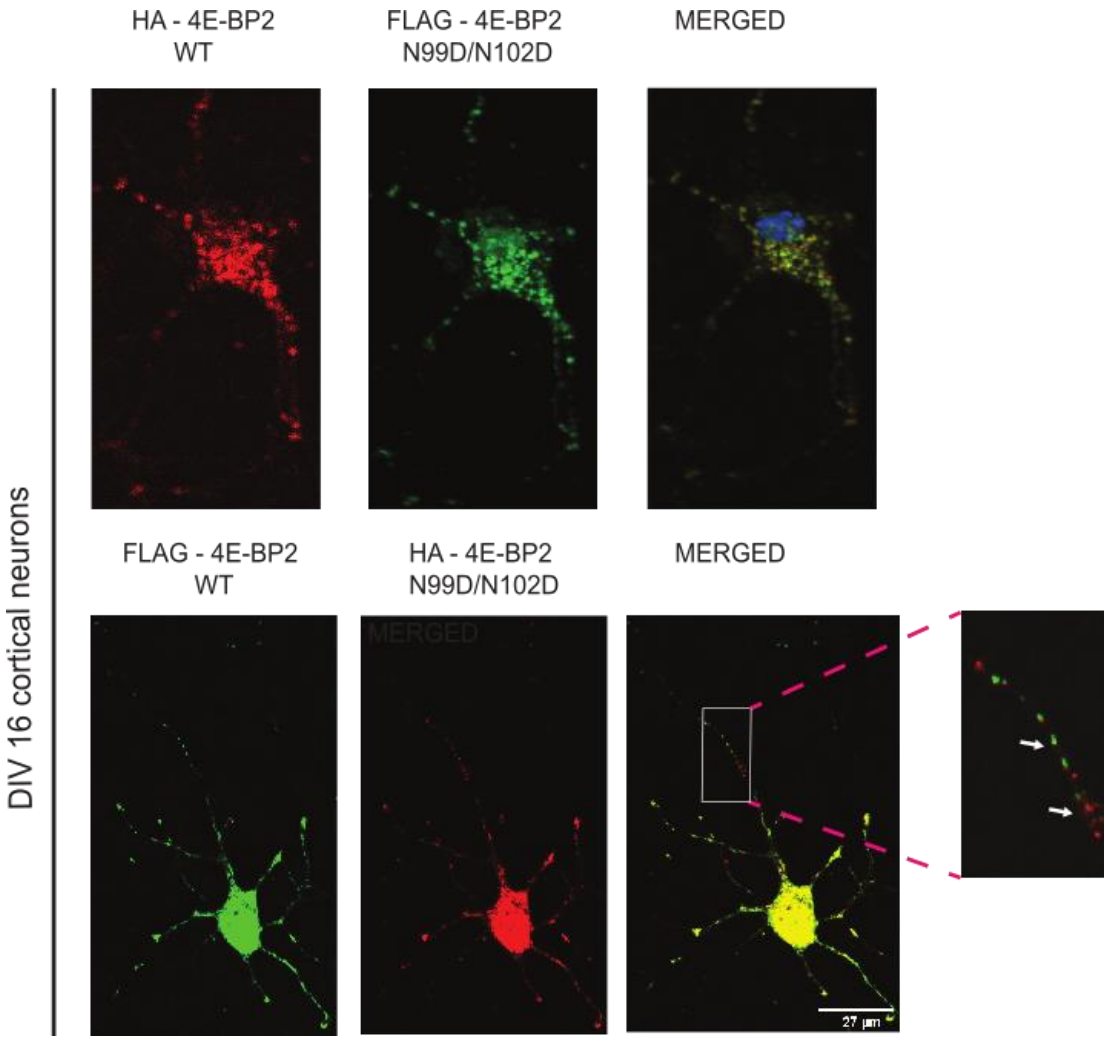

Figure 4.3 Dissociated DIV16 cortical mouse neurons transfected with either WT (FLAG-tag) or 2D (HA-tag) *4E-BP2*.

After fixation, neurons were probed first with antisera against FLAG- or HA- tags, followed by secondary antibodies (conjugated to: WT-green- Alexa Fluor 488; 2D-red- DyLight 680). Scale bars (27 µm) are the same for all cells in this figure and arrows marking distinct WT or 2D fluorescent puncta are shown in white.

To explore the localization of deamidated 4E-BP2 and test whether it colocalizes with WT 4E-BP2 in neurons, we transfected and overexpressed both 4E-BP2 forms in cortical neurons, but we increased the magnification and decreased the scan area to enable to zoom in the cell body and dendrites, separately. After image acquisition, we proceeded with colocalization analysis using Imaris software. Figure 4.4 (A) presents transfected dissociated cortical neurons, expressing both FLAG – 4E-BP2 WT (green) and HA – 4E-BP2 N99D/N102D (double deamidated, red).

Colocalization puncta are depicted in yellow [Figure 4.4 (A)]. Histograms of colocalization are also illustrated on the right panel [Figure 4.4 (B)].

The images illustrate cell bodies from DIV16 dissociated transfected cortical neurons [Figure 4.4 (A)]. Surprisingly, colocalization analysis reveals very low colocalization of WT and deamidated 4E-BP2 in the cell bodies [Figure 4.4 (B)], implying that each form displays a distinct intracellular distribution in neurons. Pearson correlation coefficient (r=0.1464, r=0.0777, r=0.2389) of the colocalized volume of red (deamidated) over green (WT) channel confirms the different subcellular expression of each 4E-BP2 form [Figure 4.4 (B)]. Therefore, deamidation of 4E-BP2 does not change the spatial expression pattern of the protein, albeit it colocalizes in low levels with WT protein in neuronal cell bodies.

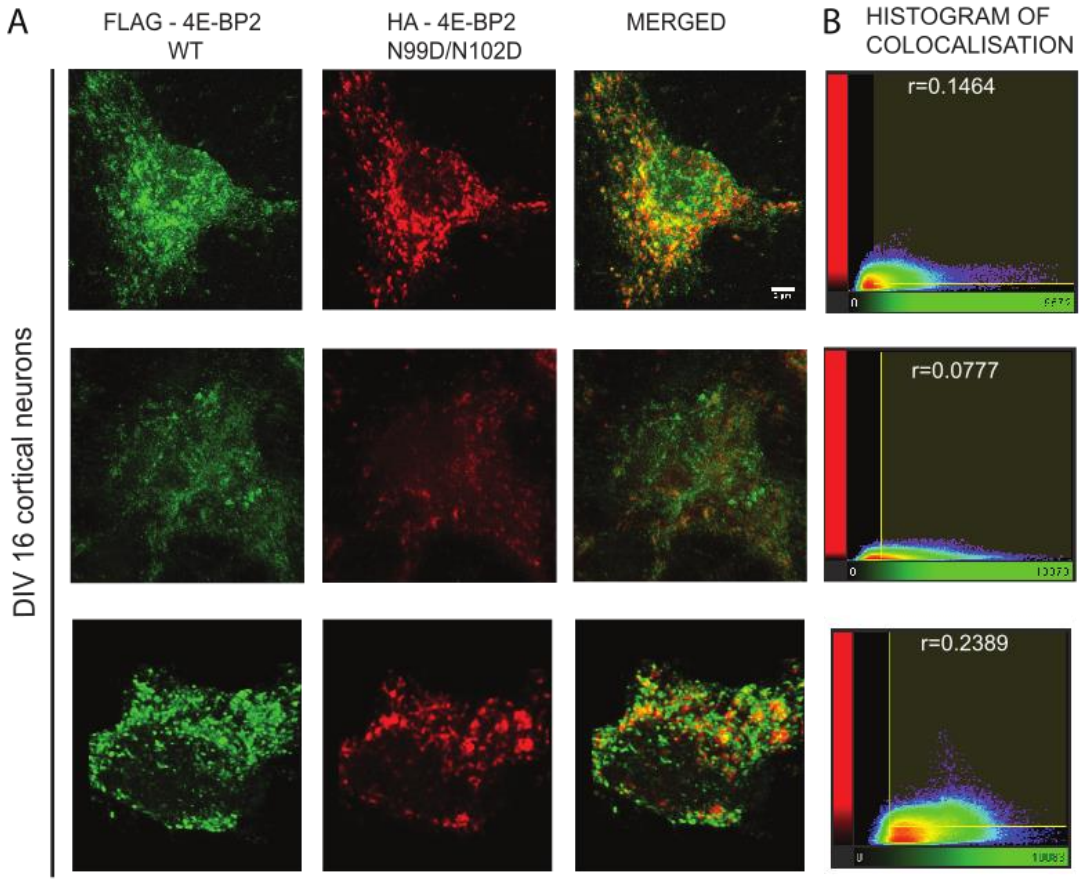

Figure 4.4 Deamidated 4E-BP2 colocalize in low levels with WT protein in cell bodies of neurons.

A. Soma from dissociated DIV16 cortical mouse neurons transfected with either WT (FLAG-tag) or 2D (HA-tag) *4E-BP2* and probed first with antisera against FLAG- or HA- tags, followed by secondary antibodies (conjugated to: WT-green- Alexa Fluor 488; 2D-red- DyLight 680). Scale bars (3 μm) are the same for all cell bodies in this figure. **B.** Imaris generated 2D histograms showing quantification of fluorescent intensity measured images from C (soma) and D (dendrites), displaying Pearson correlation coefficient of the colocalized volume of the red (2D) over green (WT) channel.

We discovered that deamidated 4E-BP2 colocalize in low levels with WT protein in the soma of cortical neurons. The first observation of different distribution of the two 4E-BP2 forms emerges from the first microscopy images (Figure 4.3) where we could distinguish red (deamidated) from green (WT) puncta in some distal dendrites. To test whether the low colocalization of fluorescent signals of 2D and WT 4E-BP2 characterizes also dendrites, we transfected the aforementioned plasmids, expressing both FLAG – 4E-BP2 WT (green) and HA – 4E-BP2 N99D/N102D (double deamidated, red), but we focused in individual dendrites as scan areas instead of the cell body of neurons. Figure 4.5 displays dissociated cortical neurons transfected, expressing both FLAG – 4E-BP2 WT (green) and HA – 4E-BP2 N99D/N102D (double deamidated, red). Colocalization puncta are depicted in yellow [Figure 4.5 (A)]. Histograms of colocalization are also presented on the right panel [Figure 4.5 (B)].

The images indicate dendrites from DIV16 transfected cortical neurons [Figure 4.5 (A)]. Apparently, we could recapitulate the different subcellular distribution of deamidated and WT 4E-BP2 in dendrites [Figure 4.5 (A), (B)]. Similarly, to cell bodies, there is very low colocalization of WT and deamidated 4E-BP2 in the dendrites, denoting that deamidated 4E-BP2 follows a different localization pattern from WT protein in neurons [Figure 4.5 (A), (B)]. Pearson correlation coefficient (r=0.4019, r=0.3232, r=0.0388) of the colocalized volume of red (deamidated) over green (WT) channel confirms the different subcellular expression of each 4E-BP2 form [Figure 4.5 (B)]. Taken together, these data suggest that deamidation of 4E-BP2 does not change the spatial expression of 4E-BP2, but it does not colocalize in high levels with WT protein in the cell bodies and dendrites of neurons. Thus, deamidated 4E-BP2 may have a distinct role in synapses compared to WT protein.

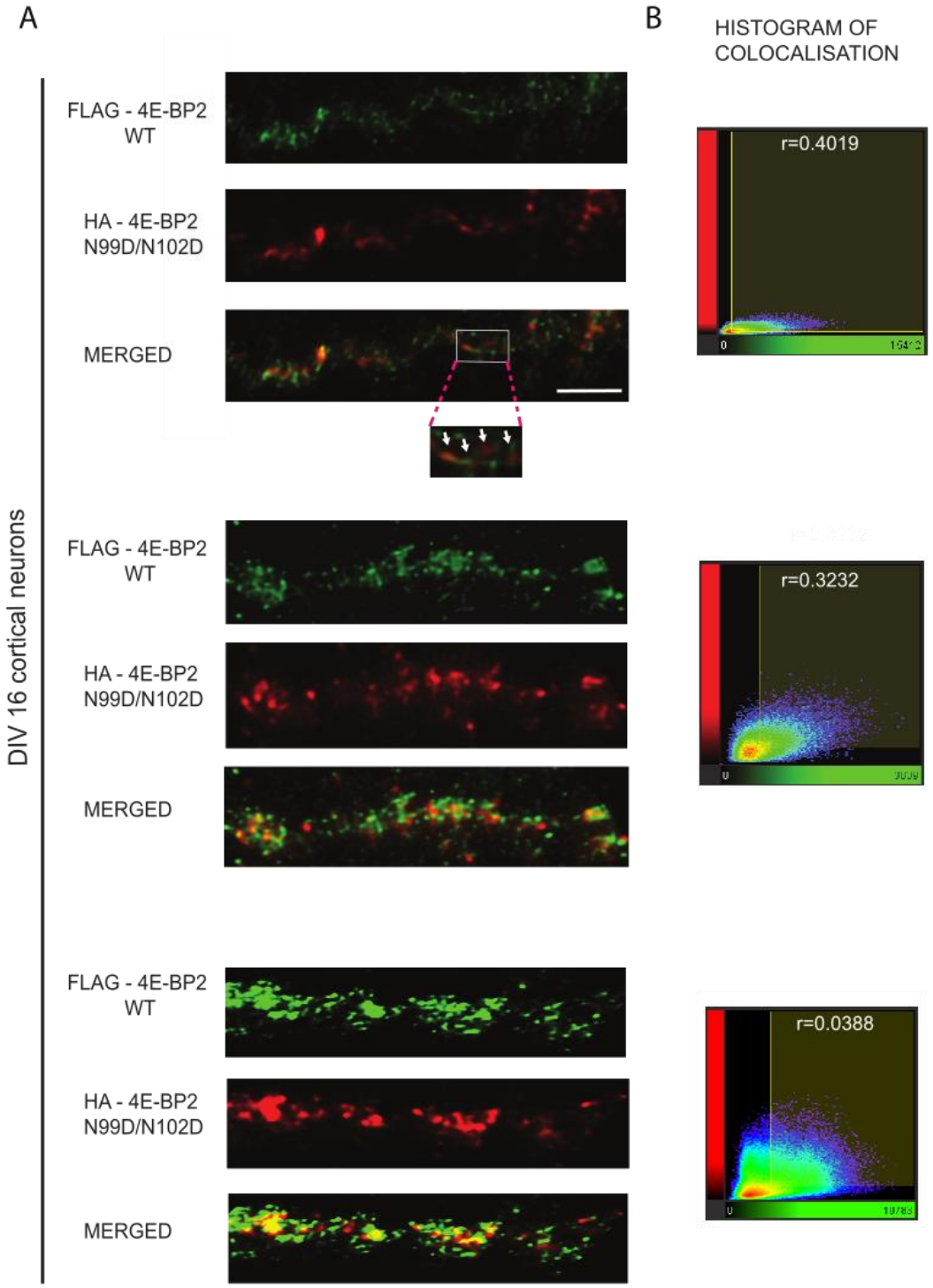

Figure 4.5 Deamidated 4E-BP2 does not colocalize in high levels with WT protein in dendrites.

Dendrites from dissociated DIV16 cortical mouse neurons transfected with either WT (FLAG-tag) or 2D (HA-tag) *4E-BP2* and probed first with antisera against FLAG- or HA- tags, followed by secondary antibodies (conjugated to: WT-green- Alexa Fluor 488; 2D-red- DyLight 680).

Scale bars (3 μm) are all the same for the dendrites shown in this figure. **B.** Imaris generated 2D histograms showing quantification of fluorescent intensity measured images from C (soma) and D (dendrites), displaying Pearson correlation coefficient of the colocalized volume of the red (2D) over green (WT) channel.

4.4 Discussion

Subcellular protein localization is firmly linked to protein function, especially in neurons where spatial and temporal compartmentalization of gene expression can confer invaluable information about protein function. Elucidation of protein intracellular localization can define their physiological role, depending on the compartments that they are localized to.

Given the important role of 4E-BP2 as a repressor of cap-dependent translation, we examined the intracellular distribution of 4E-BP2 in neurons. We discovered that endogenous 4E-BP2 localizes in the soma and dendrites of cortical neurons. To investigate separately the localization of WT and deamidated 4E-BP2, we constructed plasmids that encode 4E-BP2 with HA or FLAG tag or fused to a fluorescent protein. We discovered that the two 4E-BP2 forms (WT, double deamidated) exhibit similar distribution in neurons, albeit they do not colocalize in high levels in the soma or dendrites. Dendritic expression of both 4E-BP2 proteins indicates that they probably play a role in the regulation of local protein synthesis in synapses, apart from translation in the cell body of neurons. Low number of colocalized puncta between WT and deamidated 4E-BP2 support the hypothesis that both 4E-BP2 proteins might regulate different types of synapses (excitatory, inhibitory). Furthermore, low levels of expression of fluorescent 4E-BP2 proteins with 4E-BP2 fused at the N-terminal compared to other fluorescent proteins where 4E-BP2 is at the C-terminal, indicates that possibly interaction with Raptor, through TOS motif at the C-terminal of 4E-BP2, can affect expression and intracellular distribution of 4E-BP2. One explanation is that Raptor might drive 4E-BP2 to specific subcellular compartments. Therefore, colocalization analysis of WT and deamidated 4E-BP2 with Raptor would shed new light on the subcellular localization of 4E-BP2 and would determine whether this phenotype is Raptor–dependent or not.

5. Investigating the Subset of mRNAs that are regulated by 4E-BP2

5.1 Introduction

4E-BP2 is an inhibitor of protein synthesis and undergoes asparagine deamidation in the mammalian brain during postnatal development (Bidinosti et al., 2010b). We determined that deamidated 4E-BP2 is neuron-specific (Figure 3.18) and is regulated by a different mechanism than WT (Figure 3.21). Specifically, deamidated 4E-BP2 gets degraded by the proteasome and is unstable in isolated mouse synaptoneurosomes (Figure 3.26), as compared to WT protein. The stability of deamidated 4E-BP2 is regulated by mTORC1 and not MAPK signalling (Figure 3.28). Moreover, deamidated 4E-BP2 exhibits attenuated translational repression compared to WT, displaying decreased affinity for eIF4E, increased interaction with Raptor (Bidinosti et al., 2010b) and colocalize in low levels with WT protein in neurons (Figure 4.4, Figure 4.5). Therefore, we aim to discover what is the function of deamidated 4E-BP2 in the mammalian brain and whether it differs from WT 4E-BP2.

Translation is regulated through different signalling pathways. Key molecules of these pathways are main regulators of protein synthesis by stimulating or repressing translation of specific mRNAs (Kelleher and Bear, 2008). Therefore, depending on the state and the conditions that every cell is in (energy level, amino acid availability), protein synthesis is not always on or off at a global level, but certain mRNAs are preferentially regulated (Gilbert and Heng-Ye, 2014). eIF4E preferentially stimulates translation of mRNAs, harbouring extensive secondary structure at the 5' UTR or other elements on their sequence (Hay and Sonenberg, 2004; Koromilas et al., 1992). Interestingly, in mice knockout for 4E-BP2 and eIF4E-overexpressing mice, translation of mRNAs, encoding for synaptic adhesion molecules such as neuroligins, increases (Gkogkas et al., 2013). This preferential translation might be regulated through the 5' UTR of neuroligin mRNAs which possess a repeated structural element

(Gkogkas et al., 2013). These mice display autistic-like behaviours (social interaction deficits, altered communication and repetitive/stereotyped behaviours) and knockdown of *Nlgn*1 (Neuroligin1) improves social approach behaviour to wild-type levels, implying that selective translation of Neuroligin 1 is directly linked to the pathophysiology of ASD (Gkogkas et al., 2013).

Since 4E-BP2 is a major inhibitor of translation, we sought to identify which mRNAs are regulated by each 4E-BP2 form, and thus understand the role of deamidated 4E-BP2 in protein synthesis in the mammalian brain. To answer this question, we performed Ribosome Profiling in mouse cortical neuronal cultures that were infected with AAVs (Adeno-Associated Viruses) overexpressing either WT or deamidated 4E-BP2.

5.1.1 Methods of gene expression: RNA sequencing, Polysome Profiling, TRAP (Translating Ribosome Affinity Purification), Ribosome Profiling

Translation is the final step of gene expression, determining the proteomic content of each cell every moment along with protein degradation (Harper and Bennett, 2016). Methods such as RNA sequencing measure mRNA abundance without providing information about the rate of protein synthesis, thus focusing on studying the transcriptome and not the translatome (Ingolia et al., 2012). Recently, specific approaches have been developed to study the translatome and thus, understand the translational regulation events (King and Gerber, 2016). These approaches include all mRNAs undergoing translation: Polysome profiling, Ribosome Profiling and Ribosome-Affinity techniques (King and Gerber, 2016). Polysome Profiling separates mRNAs depending on the number of the bound ribosomes using a sucrose gradient. Ribosome Profiling identifies mRNAs that undergo translation by sequencing ribosome protected mRNA fragments named footprints (RPFs). Lastly, ribosome-affinity purification involves the isolation of affinity-tagged ribosomes, enabling cell-specific analysis of translatome (King and Gerber, 2016). The main advantages of Ribosome profiling over the other two methods are that it does not require specialised equipment as with Polysome Profiling or genetic manipulation, as with Ribosome affinity purification (King and Gerber, 2016), and it also provides information regarding the position of the ribosomes on the transcripts and exact measurement of ribosome densities (Ingolia et al., 2012).

5.1.2 Ribosome Profiling

Ribosome Profiling measures gene expression at the actual level of translation (Ingolia et al., 2012) and provides a quantitative measurement of the specific reading frames translated. The level of translation on these reading frames can be inferred from the density of footprints (Blair et al., 2017). Therefore, reading of ribosome density per mRNA corresponds to the level/rate of synthesis of specific protein (King and Gerber, 2016), indicating that ribosome profiling directly monitors translation and not transcriptional network (Ingolia et al., 2009). In more detail, each ribosome footprint corresponds to a translating ribosome and the number of footprints indicates the number of active ribosomes, synthesizing the encoded protein (Ingolia et al., 2012). The amount of protein produced is proportional to this number of active ribosomes. Since the speed of protein synthesis does not change among different genes, the density of ribosome footprints determines the rate of protein synthesis for this transcript (Ingolia et al., 2012). The identification of specific points where ribosomes are stalled can also be identified by the unusual increased number of footprints on this site (Ingolia et al., 2012). After proper consideration of confounding factors (for example, more abundant mRNAs will tend to produce more footprints), these measurements can be compared between different mRNAs, and for a given mRNA across different physiological conditions (McGlincy and Ingolia, 2017). To conclude, Ribosome footprint density encompasses mRNA abundance and translation because higher mRNA abundance or increased translation will yield more ribosome footprints (Blair et al., 2017).

Apart from quantitatively measuring translation, Ribosome profiling also provides positional information of the bound ribosomes, therefore shedding light on the mechanisms of translational regulation that are invisible to normal mRNA measurements (Blair et al., 2017). Positional information of ribosomes revealed unexpected ribosome occupancy in many parts of the transcriptome, reflecting substantial levels of non-AUG initiation, translation of cytosolic RNAs (Blair et al., 2017) and transcripts that contain short open ORFs, corresponding to extended or truncated forms of proteins. These different translated isoforms may stem from different mRNA isoforms and different initiation sites on the same mRNA transcript (Ingolia et al., 2012). By examining the frequency distribution of ribosome footprints along a given mRNA(s), we can understand the nature of ribosomal movement and the effect of mRNA sequence on this movement (McGlincy and Ingolia, 2017).

Moreover, variations in the density of ribosomes within a reading frame reflect differences in the speed of ribosomes, providing insights into the mechanisms of translation as well (Blair et al., 2017).

5.1.3 Brief description of Ribosome profiling method

A translating ribosome protects a 30nt mRNA fragment from nuclease digestion. This protected fragment, called ribosome footprint (RPF), and its sequence will define the synthesized protein. Ribosome profiling confers a quantitative gene expression measurement, relying on deep sequencing of these RPFs, indicating ribosome positions (Ingolia et al., 2012). Figure 5.1 designates the basic steps of the method. Briefly, cells are briefly treated with CHX to capture the translational status of unperturbed cells (Blair et al., 2017). Then cells are lysed and harvested under appropriate conditions to maintain the ribosomes on mRNAs *in vivo*. Lysates are treated by nuclease digestion (nuclease footprinting) with RNase I, and ribosomes are recovered and pelleted by ultacentrifigation. To isolate ribosome footprints, RNA from the ribosomal pellet is resolved by electrophoresis through a denaturing gel, and then fragments of the expected size range are extracted from the gel (Ingolia et al., 2012; McGlincy and Ingolia, 2017). To analyze ribosome positions by high-throughput sequencing, the ribosome-protected mRNA fragments must be converted into DNA libraries, flanked with constant priming sites required by these sequencing technologies (Ingolia et al., 2012). Therefore, ribosome footprints are purified and ligated to a single stranded-linker that acts as a priming site for reverse transcription. Products from reverse transcription are circularized, providing a second priming site flanking the captured footprint sequence, which is used for PCR amplification of a deep sequencing library (Ingolia et al., 2012). A double-stranded DNA library of suitable structure and concentration for Illumina sequencing is then constructed from the single-stranded cDNA circles by means of a PCR reaction (McGlincy and Ingolia, 2017). Total mRNA extraction and sequencing is performed in parallel, to normalize RPFs to mRNA abundance (King and Gerber, 2016).

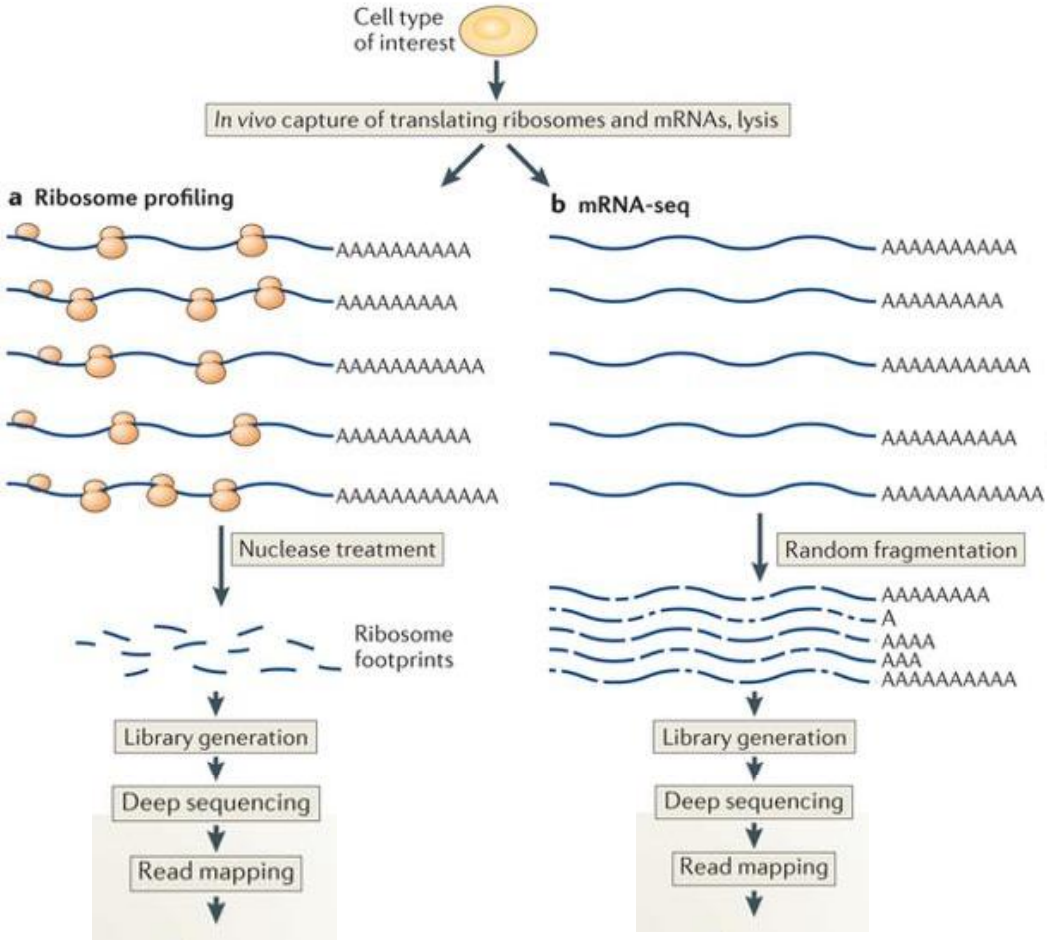

Translational Efficiency (TE) = RPKM footprints/RPKM total mRNA

Figure 5.1 Overview of Ribosome Profiling

Polysomes are extracted from cells and the prepared lysate is processed for RNase I digestion, leaving RPFs intact. These fragments are purified and size selected before cDNA library generation for next generation sequencing (left panel). The prepared lysate is also processed for RNA Sequencing by random fragmentation and library generation (total RNA sample), (right panel). After bioinformatic processing of the sequencing results, normalised count values for sequencing reads aligning to each gene (RPKM, Reads Per Kilobase of transcript per Million) are obtained. RPKM values for the total RNA sample can be used to assess transcriptional changes. Translational efficiency (TE) values, corresponding to the translational state of a gene, are calculated dividing RPKM values of RPFs by RPKM values of total RNA for each gene [Figure adapted from (Brar and Weissman, 2015)].

5.2 Experimental aim

4E-BP2 is a major regulator of cap-dependent translation. Deamidated 4E-BP2 is less stable than WT and its stability is regulated differently from the WT protein. To understand the role of deamidated 4E-BP2 in translation, it is vital to identify the mRNAs that are regulated by each 4E-BP2 form. We hypothesize that deamidated 4E-BP2 regulates a distinct pool of mRNAs that does not overlap with the mRNAs that are regulated by the WT protein, conferring a novel mechanism of translational regulation in the postnatal brain. Therefore, we will be able to link WT and deamidated 4E-BP2 with specific neuronal processes, depending on the mRNAs that each 4E-BP2 form preferentially regulates.

5.3 Results

5.3.1 Identification of mRNAs-targets of WT- or 2D-overexpressing neurons using Ribosome profiling

Deamidation of 4E-BP2 is a neuron-specific posttranslational modification that could constitute a novel regulatory mechanism of translation, targeting a distinct pool of mRNAs, required for specific neuronal functions of early postnatal development. To test this hypothesis, we performed an experiment that would enable us to map the neuronal translatome under conditions of overexpression of deamidated or WT 4E-BP2, thus mimicking conditions where deamidated 4E-BP2 is more active due to accumulation such as mTORC1 (Figure 3.21, Figure 3.22) or AMPAR inhibition (Figure 3.24). Therefore, we carried out unbiased translational profiling using ribosome footprinting coupled with RNA sequencing (Ingolia et al., 2012). Mouse cortical neuronal cultures were infected with AAV9 expressing FLAG-tagged WT or 2D 4E-BP2 driven by the neuron-specific human Synapsin (hSyn) promoter on DIV10 and were collected and lysed on DIV25 under conditions to maintain the ribosomes bound on mRNAs *in vivo*.

Figure 5.2 (A) indicates a simple graph, depicting the infection and collection days in mouse cortical cultures (top). The same figure [Figure 5.2 (A)] presents a representative blot of AAV-infected neuronal lysates at DIV25 that were probed for anti-FLAG and 4E-BP2 to confirm overexpression of each 4E-BP2 form. Indeed,

immunoblotting reveals robust expression of WT or 2D 4E-BP2 after infecting the cultures with AAV9-FLAG WT or 2D 4E-BP2, respectively [Figure 5.2 (A)]. The cultures were infected appropriately to give a similar expression of each 4E-BP2 form (FLAG expression) [Figure 5.2 (A)]. Figure 5.2 (B) illustrates the basic principle and steps of Ribosome Profiling. Using a hypotonic lysis buffer, we extracted polysomes and subsequently ribosome protected footprints by RNAse I nuclease digestion [Figure 5.2 (B)]. In parallel, we isolated total RNA from neuronal culture lysates [Figure 5.2 (B)]. From both ribosome protected footprints (a proxy for translation) and total mRNA (a proxy for transcription) we prepared libraries for RNA sequencing [Figure 5.2 (B)].

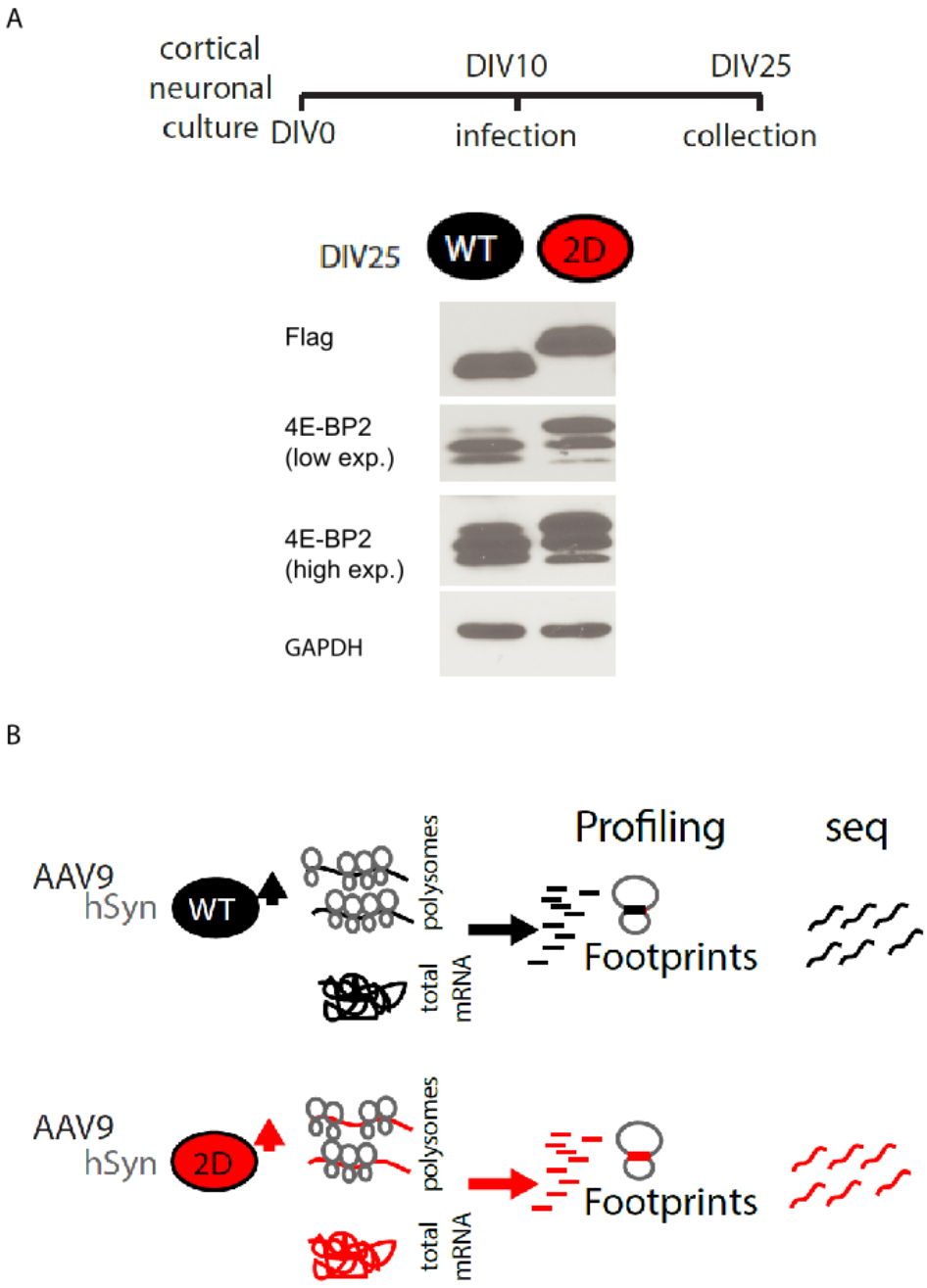

Figure 5.2 Overexpression of FLAG-tagged 4E-BP2 (WT or 2D) using AAV9 in mouse cortical neurons**.**

A. Representative immunoblots from DIV25 mouse cortical neuron lysates, infected at DIV10. GAPDH is a loading control and appeared at 37 kDa. 4E-BP2 appeared as three bands (bottom band: 15 kDa, middle band: 16 kDa and top band: 17 kDa). **B.** Diagrammatic depiction of the ribosome profiling experiment.

5.3.2 Novaseq produced high quality reads for footprint and mRNA libraries

To test the quality of footprint and mRNA libraries, the Bioinformatics pipeline workflow produces specific graphs, characterizing the quality of the data. These graphs are the following:

- **Reproducibility Plots** are pairwise plots between biological replicates, proving the reproducibility between replicates. The squared Pearson product-moment correlation coefficient r^2 is calculated as a coefficient of determination. These plots are generated from log_2-transformed RPKM and TE values (Figure 5.3).
- **Per-sample size distribution Plots** indicate the length (in nucleotides) of 100,000 randomly sub-sampled RPF and total mRNA, respectively, for each sample in the same plot, to compare (Figure 5.4).
- **Cumulative reading frame usage** plots show the relative abundance of respective reading frames within a sample. The reading frames are calculated as follows:

  ops mod 3

  ops stands for the offset 5' end position of a read, relative to the start codon (as determined for the cumulative footprint 5' end positions relative to all start and stop codons plots). *mod 3* is the modulo, also called the remainder, after Euclidean division by 3. 5' end positions are added up for each reading frame and converted to relative abundances. (Figure 5.5)
- **Cumulative footprint 5' end positions relative to all start and stop codons** plots are generated by mapping 5' end positions to positions in a window of ±30 nt around starting nucleotide of any start and stop codon, respectively. These mapped positions are then transformed into offset positions (relative to the start codon of the respective gene). These offset positions are combined for all genes and RPF positions are displayed as peaks, while total mRNA positions are visualised as a line in the background (Figure 5.6).

Novaseq produced high quality reads for footprint and mRNA libraries, as evidenced first by the r^2 of Reads Per Kilobase of transcript per Million mapped reads (RPKM) between biological replicates, which is >0.9 for both footprints and total

mRNA (Figure 5.3), second by the canonical distribution of footprint size (28-32nt) (Figure 5.4), third by the read distribution within the 3 frames (Figure 5.5) and fourth by the canonical periodicity of ribosomal footprints across mRNA coding and non-coding regions (Figure 5.6). The clear trinucleotide periodicity with peaks at the first nucleotide position stems from the ribosome movement along the mRNA in a stepwise fashion one codon at a time, beginning at the start codon (Ingolia, 2014; Ingolia et al., 2012; Michel and Baranov, 2013). This periodicity also allows assignment of the translation reading frame, distinguishing footprints arising from translating ribosomes from RNA fragments that are protected for any other reason (Jackson and Standart, 2015).

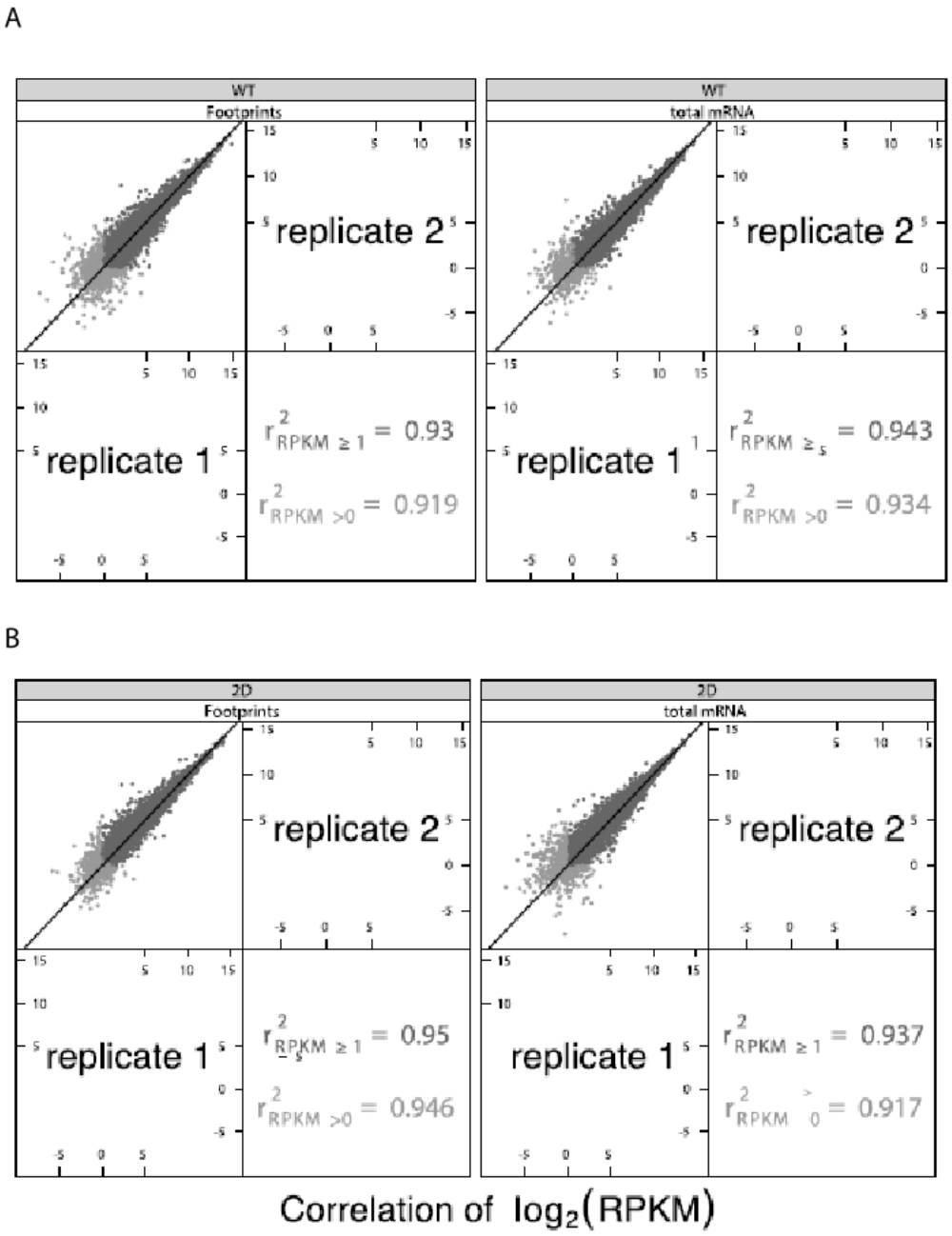

Figure 5.3 Reproducibility plot between biological replicates

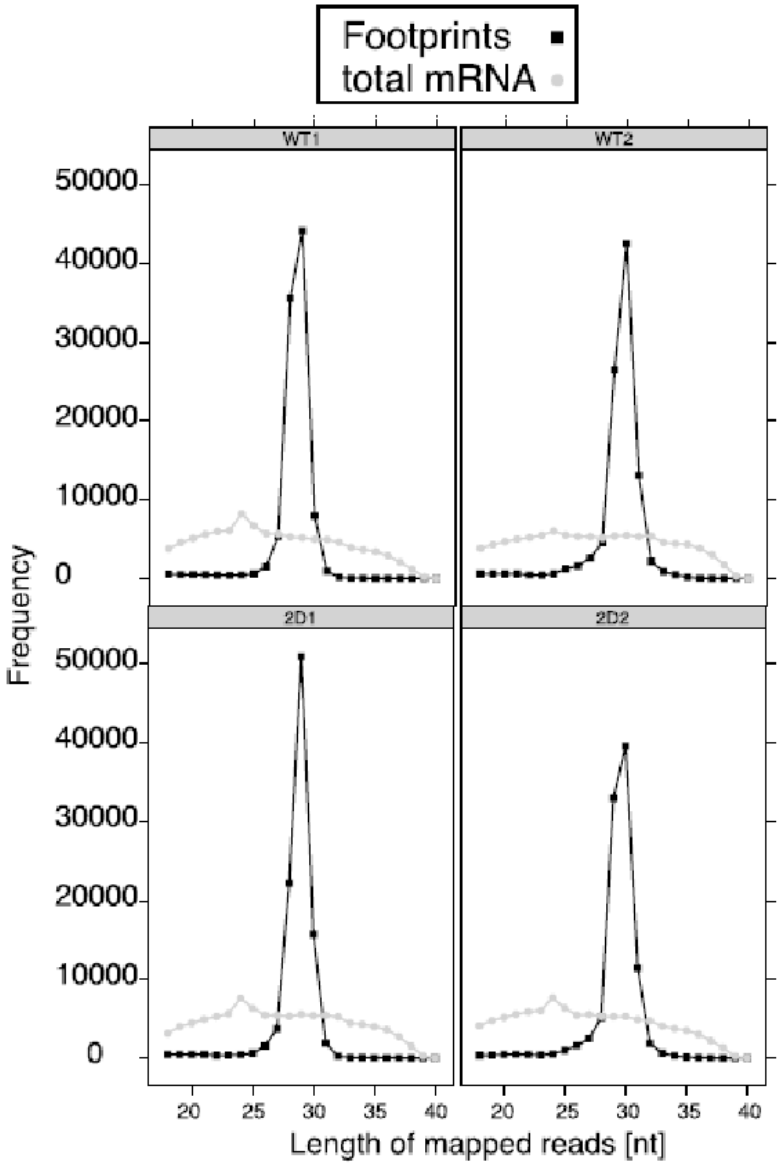

Figure 5.4 Per-sample size distribution Plots for each sample and each biological replicate.

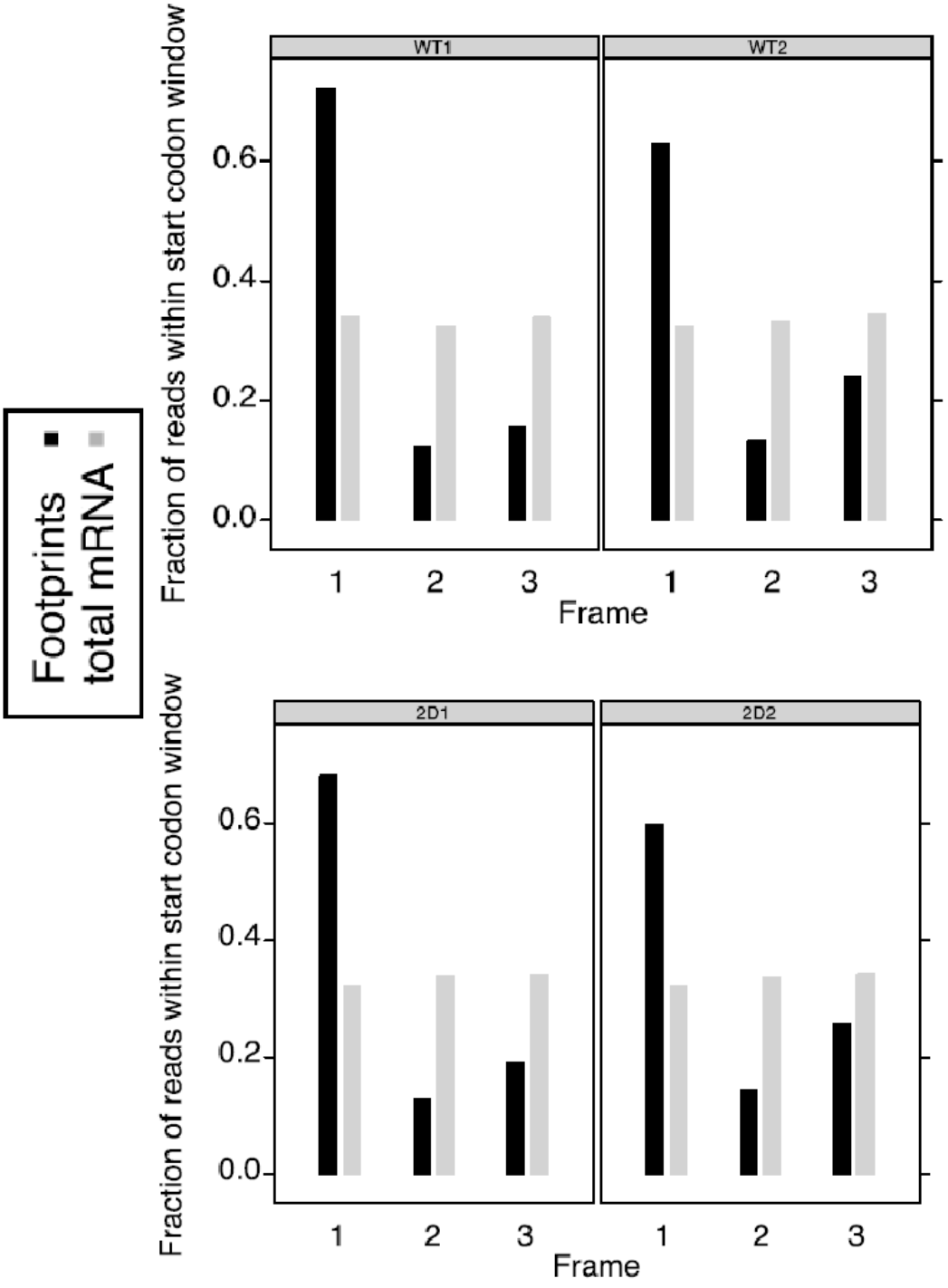

Figure 5.5 Cumulative reading frame usage plot in each sample and biological replicate.

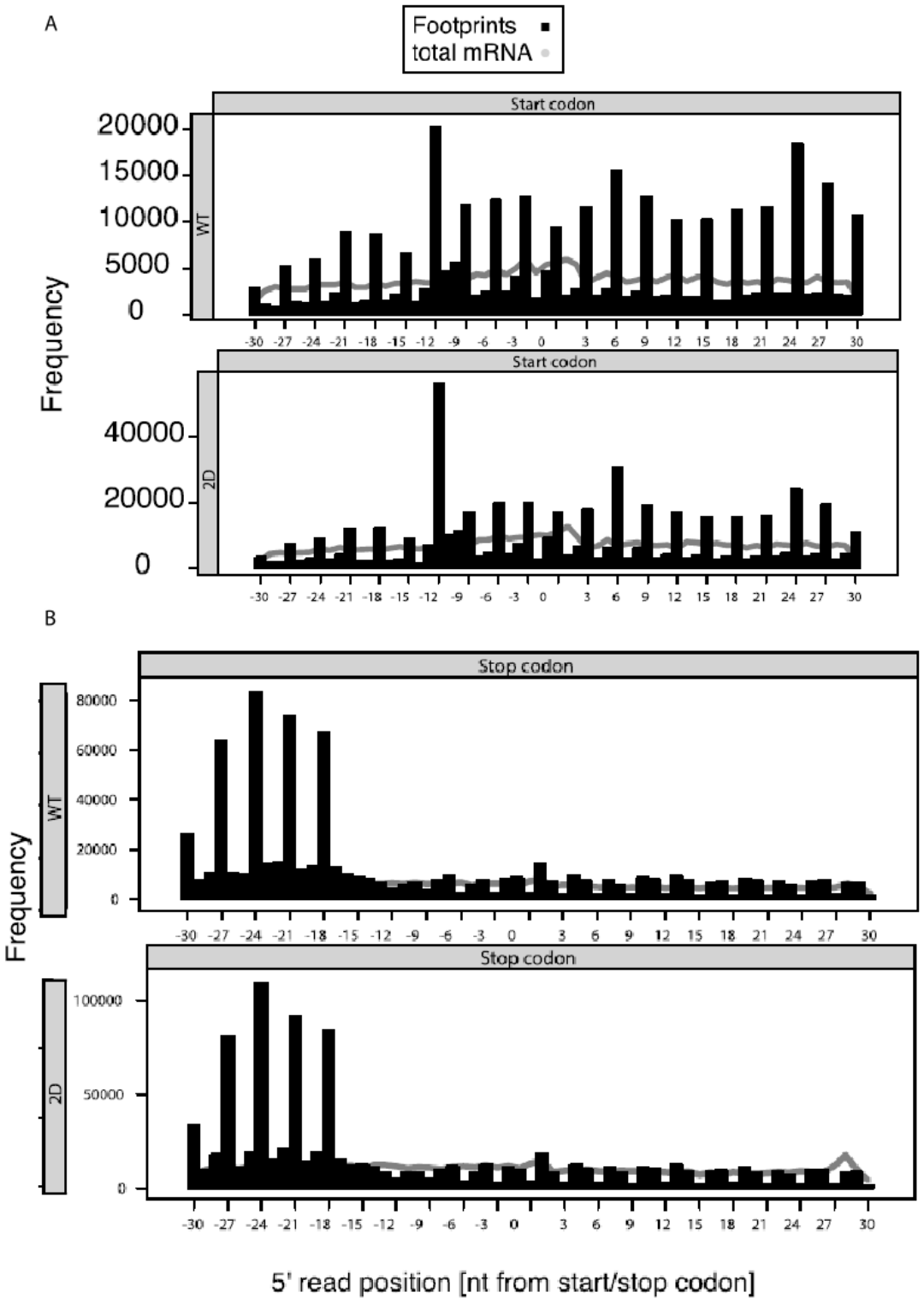

Figure 5.6 Cumulative footprint 5' end positions relative to all start and stop codons plots for each sample.

5.3.3 Overexpression of deamidated 4E-BP2 affects the neuronal translatome but not the transcriptome

To test whether overexpression of deamidated 4E-BP2 causes any changes to the transcriptome, we plotted Reads Per Kilobase of transcript per Million mapped reads (RPKM) of total mRNA of 2D 4E-BP2-overexpressed neurons and RPKM of total mRNA of WT 4E-BP2-overexpressed neurons [Figure 5.7 (A)]. Similarly, to check whether overexpression of deamidated 4E-BP2 alters neuronal translatome, we plotted translational efficiency [(TE): calculated by dividing RPKM values of RPF libraries by RPKM values of total RNA libraries] of 2D 4E-BP2-overexpressed neurons and TE of WT 4E-BP2-overexpressed neurons [Figure 5.7 (B)].

RPKM measurements of mRNA libraries demonstrate that there is no significant change in mRNA abundance between WT and 2D as evidenced by R^2=0.972 [Figure 5.7 (A)], suggesting that there are no differences in transcriptional responses following overexpression of either 4E-BP2 form. Conversely, RPKM reads of footprints normalised to mRNA abundance (translational efficiency; TE) show a pervasive change in the translational landscapes of WT versus 2D 4E-BP2 (R^2=0.681) [Figure 5.7 (B)]. Analysis of $\log_2$ of TE between 2D/WT replicates (0.667>ratio>1.5; $p < 0.05$) indicated that 212 genes are upregulated (repressed by WT overexpression), while 238 genes are downregulated (repressed by 2D overexpression), revealing two highly dissimilar translatomes (Differentially Translated Genes; DTGs) for WT and 2D [Figure 5.7(B)].

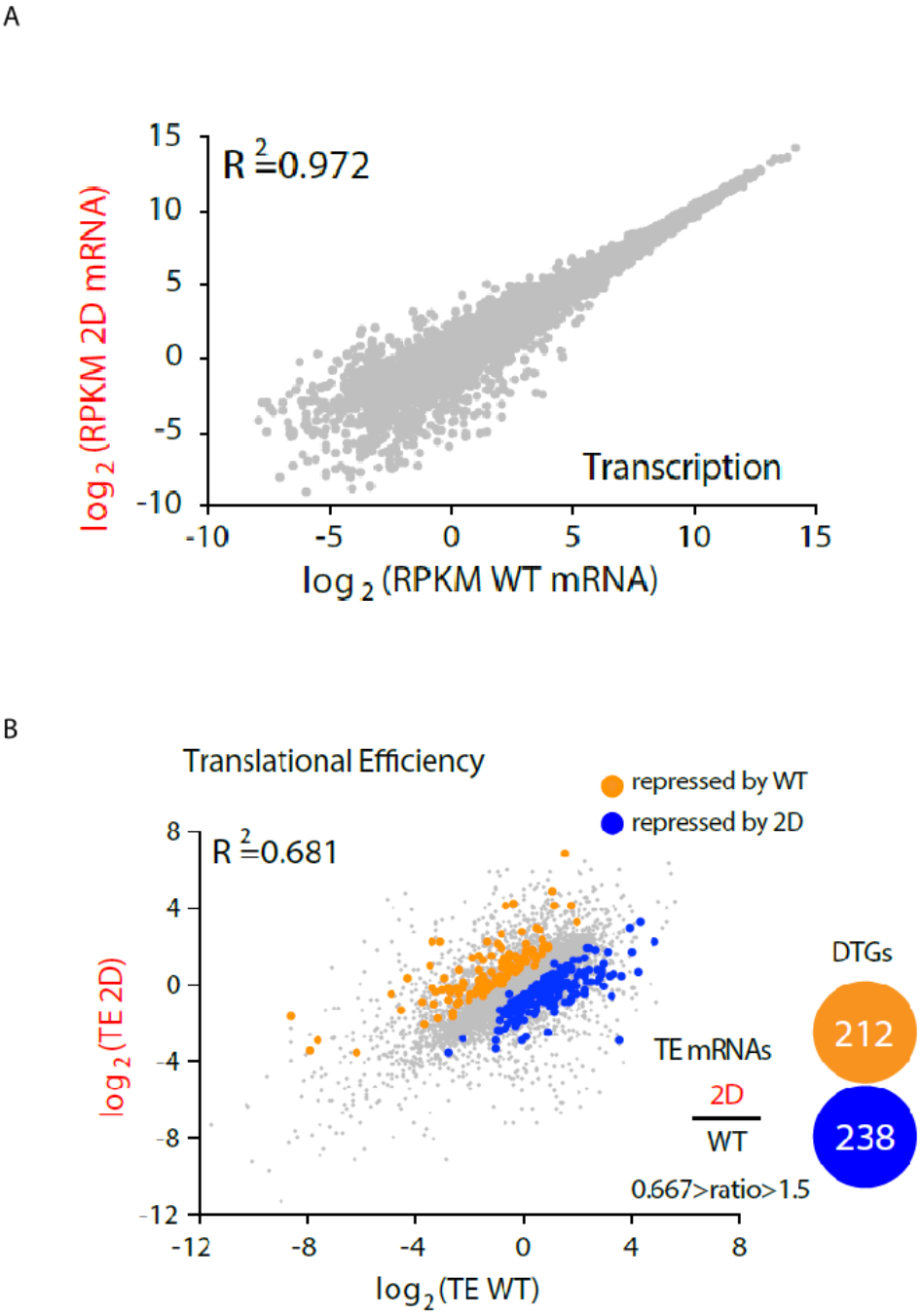

Figure 5.7 Scatter plots and correlations of RPKM measurements of transcriptional response and translational efficiency from DIV25 overexpressing WT or 2D 4E-BP2 neurons.

A. Scatter plot and correlation of RPKM measured from WT or 2D total mRNA from DIV25 neurons, as a proxy for transcription, from DIV25 overexpressing neurons. **B.** Scatter plot and correlation of translational efficiency (footprint RPKM normalised to mRNA RPKM) between WT and 2D overexpressing DIV25 neurons (log_2RPKM of 2D versus WT). Differentially translated Genes (DTGs), repressed by WT (orange) or 2D (blue) are shown for 0.667>ratio>1.5.

5.3.4 WT-sensitive mRNAs contain long 5' UTR, enriched in eIF4E/ mTOR-dependent regulatory sequence motifs

Since we discovered that overexpression of deamidated 4E-BP2 causes pervasive changes to the translatome, we proceeded to characterize the mRNAs which are regulated by either WT or 2D 4E-BP2. *Cis*-acting elements of mRNAs located either in the 5' or 3' UTR regulate the fate of newly synthesized mRNAs regarding their nucleo-cytoplasmic transport, stability, translational efficiency and subcellular localization (Grillo et al., 2010). Functional sequence elements and miRNAs found in UTRs can interact directly with key molecules of translational machinery or through RNA binding factors, modulating the expression of this gene (Grillo et al., 2010). These features can render the mRNAs sensitive to a certain regulatory mechanism of translation. Thus, elucidating these elements, we might understand the common elements that these mRNAs share and are regulated either by WT or 2D 4E-BP2. To characterise the mRNAs, we obtained 5´ UTR sequences for both lists of targets (WT or 2D) and carried out length, GC content and motif analysis using UTRdb (Grillo et al., 2010).

Figure 5.8 (A) illustrates the length and % GC content of 2D- and WT-sensitive mRNA 5´ UTRs. 2D-sensitive mRNA 5´ UTRs are shorter ($p < 0.001$) than WT-sensitive mRNA 5´ UTRs [Figure 5.8 (A)]. However, there is no significant change with respect to the % GC content between WT- and 2D-sensitive mRNA 5´ UTRs [Figure 5.8 (A)]. Figure 5.8 (B) indicates other features that are different between the two lists of mRNAs. Specifically, 2D-sensitive mRNAs 5´ UTRs harbour significantly fewer Terminal Oligopyrimidine Tract (TOP) ($p < 0.001$) and upstream Open Reading Frame (uORF) elements ($p < 0.001$) [Figure 5.8 (B)], as compared to WT-sensitive mRNA 5´UTRs. To conclude, mRNAs which are identified as targets of deamidated 4E-BP2, but not WT, have shorter 5´UTRs with markedly fewer TOPs and uORFs compared to mRNAs-targets of WT 4E-BP2.

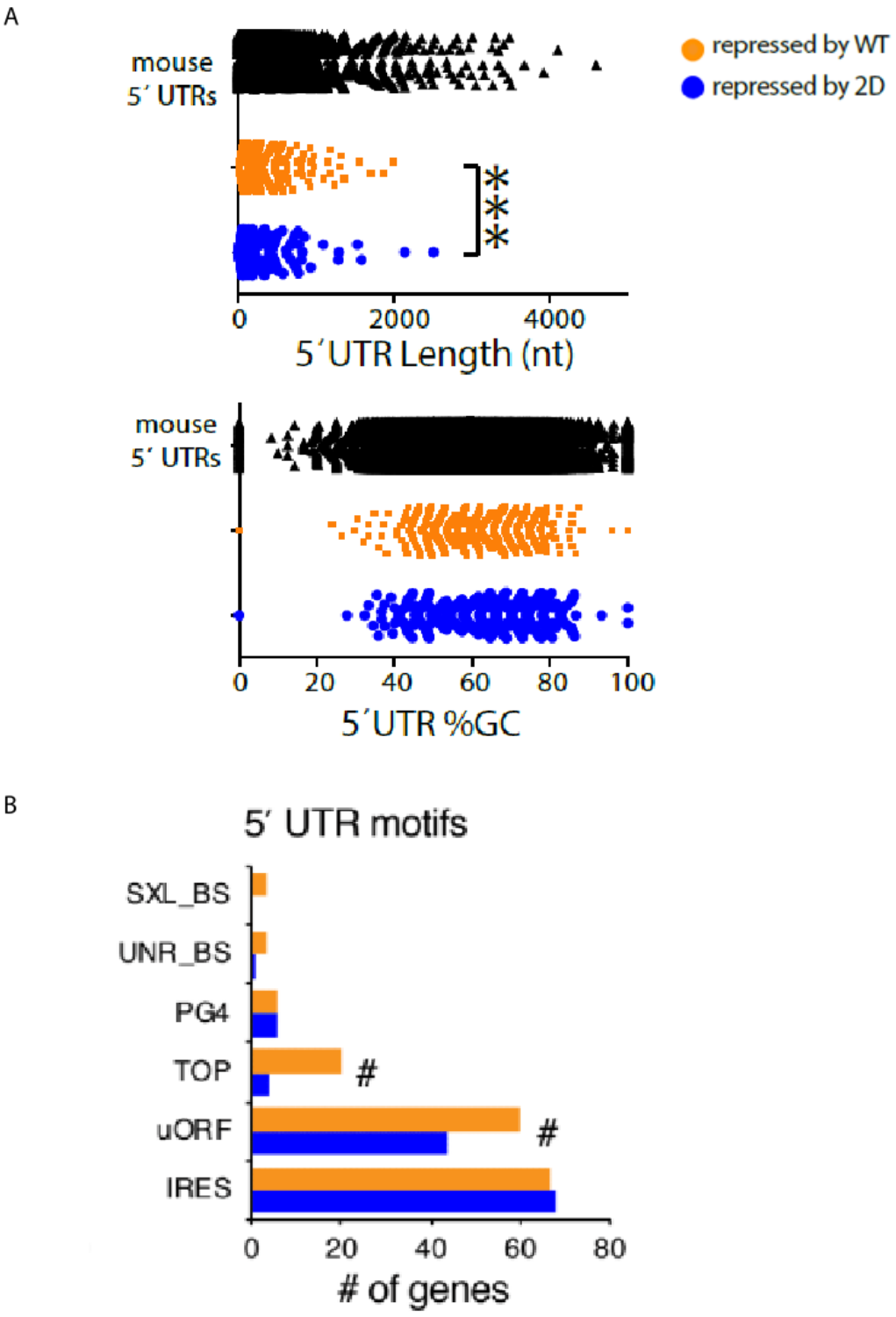

Figure 5.8 5′ UTR analysis of DTGs versus mouse 5′ UTR collection:

A. length (nt), %GC content and **B.** UTRdb motifs.

Data are shown as mean ±S.E.M. For length and %GC: One-way ANOVA; Bonferroni's post-hoc; ***p < 0.001. For motifs: Student's *t*-test; #p < 0.001.

5.3.5 Gene ontology analysis using DAVID identified distinct categories regulated by WT and 2D 4E-BP2

Gene ontology analysis was performed to identify enriched biological themes, depending on the genes we identified in each of the two groups, mRNAs that are regulated by WT, and mRNAs that are regulated by deamidated 4E-BP2. Figure 5.9 shows the number of genes in each category whereas the order of categories is by decreasing p-value. Multiple GO categories linked to transcription [$p < 0.05$; Biological Pathways (BP), Molecular Function (MF) and Cellular Compartment (CC)], are identified by DAVID analysis of the 212 WT-repressed genes (Figure 5.9), suggesting that overexpression of WT 4E-BP2 could elicit homeostatic modulation of transcription (left panel). In contrast, 2D-repressed genes display a DAVID GO profile ($p < 0.05$) which is distinct from WT including categories such as: MF: poly (A) RNA binding, NF-κB binding; BP: cerebral cortex development, NF-κB activity, glutathione metabolic process and oxidoreductase activity, CC: mitochondrion (Figure 5.9) (right panel). Targets (genes) that were identified to be repressed either by WT (yellow list) or 2D (blue list) and the actual p values are mentioned on the last page of the Appendix.

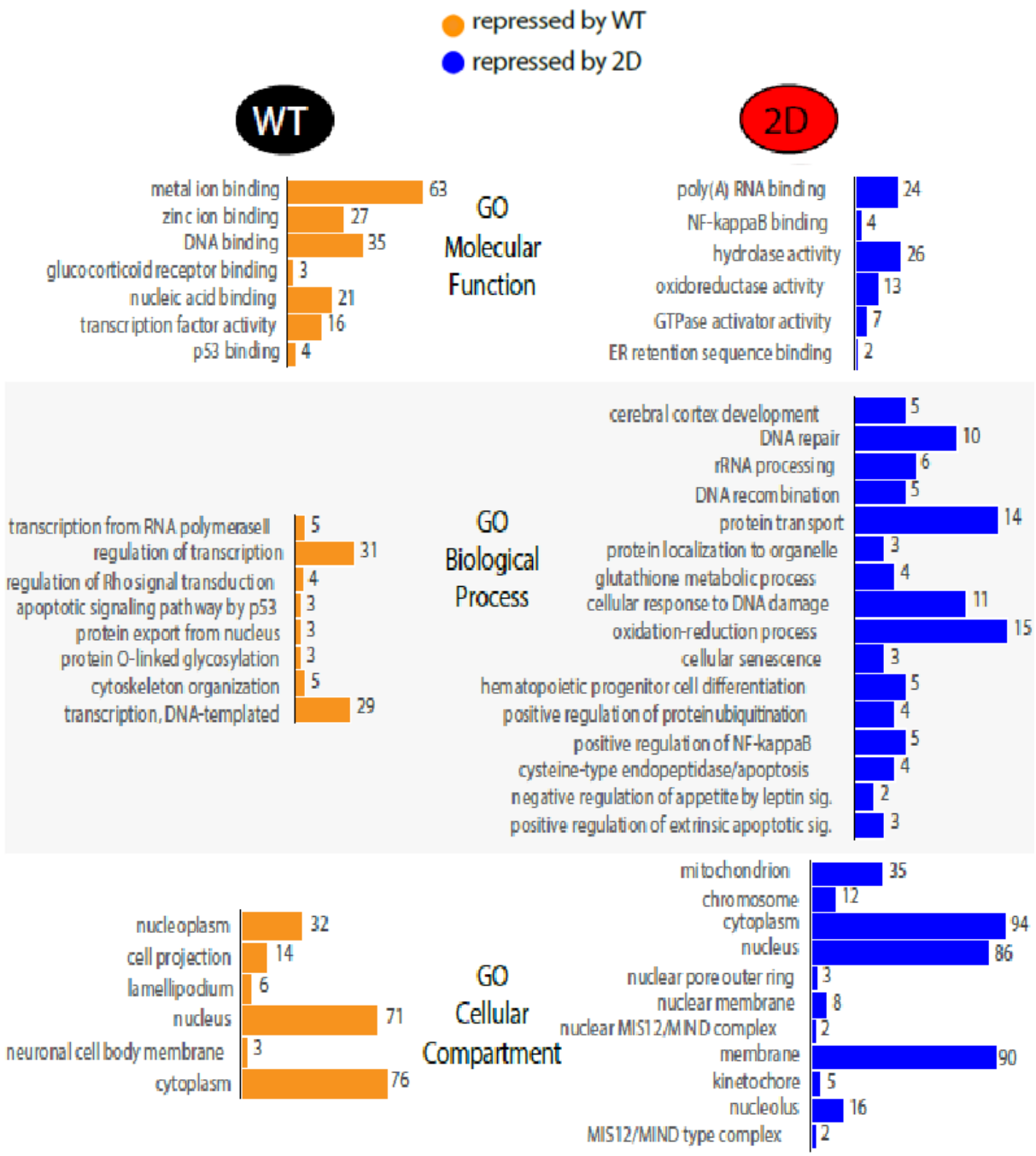

Figure 5.9 DAVID analysis of DTGs (WT left, orange; 2D right; blue) for Gene Ontology (GO) categories: Molecular Function, Biological Process and Cellular Compartment.

The number of genes in each category is shown and the order of categories is by increasing p-value (decreasing significance), All p-values shown here are < 0.05. The actual p-values are mentioned on the last page of the Appendix.

5.3.6 Ingenuity Pathway analysis identified NF-κB as the central node of top network predicted to be regulated by WT and 2D 4E-BP2

Moreover, we carried out Ingenuity Pathway Analysis of DTGs using the Molecular Activity Predictor (MAP) tool and we identified networks predicted to be regulated by WT and 2D 4E-BP2 (Figure 5.10). The top network is: Developmental Disorder, Hereditary Disorder and Neurological Disease (comprising 21 2D-sensitive, and 12 WT-sensitive genes) (Figure 5.10) with the central node being NF-κB (Figure 5.11). This predicted network suggests that the balance of WT-2D 4E-BP2 is important for regulating NF-κB activity (Figure 5.11). In summary, deamidated 4E-BP2 represses translation of a subset of mRNAs, which is distinct from WT 4E-BP2-regulated mRNAs, and seem to play a pivotal role in the regulation of NF-κB activity.

Top 5 networks

Network ID	Score	Focus Molecules	Top Diseases and Functions
1	58	33	Developmental Disorder, Hereditary Disorder, Neurological Disease
2	50	30	Cellular Assembly and Organization, Cellular Function and Maintenance, Cancer
3	45	28	Molecular Transport, Cell Cycle, Cellular Assembly and Organization
4	43	27	Cancer, Gastrointestinal Disease, Organismal Injury and Abnormalities
5	40	26	Cellular Function and Maintenance, Connective Tissue Development and Function, Tissue Morphology

Figure 5.10 Ingenuity Pathway Analysis of ribosome profiling DTGs with the Molecular Activity Predictor (MAP) analysis tool.

The top 5 scoring networks are shown.

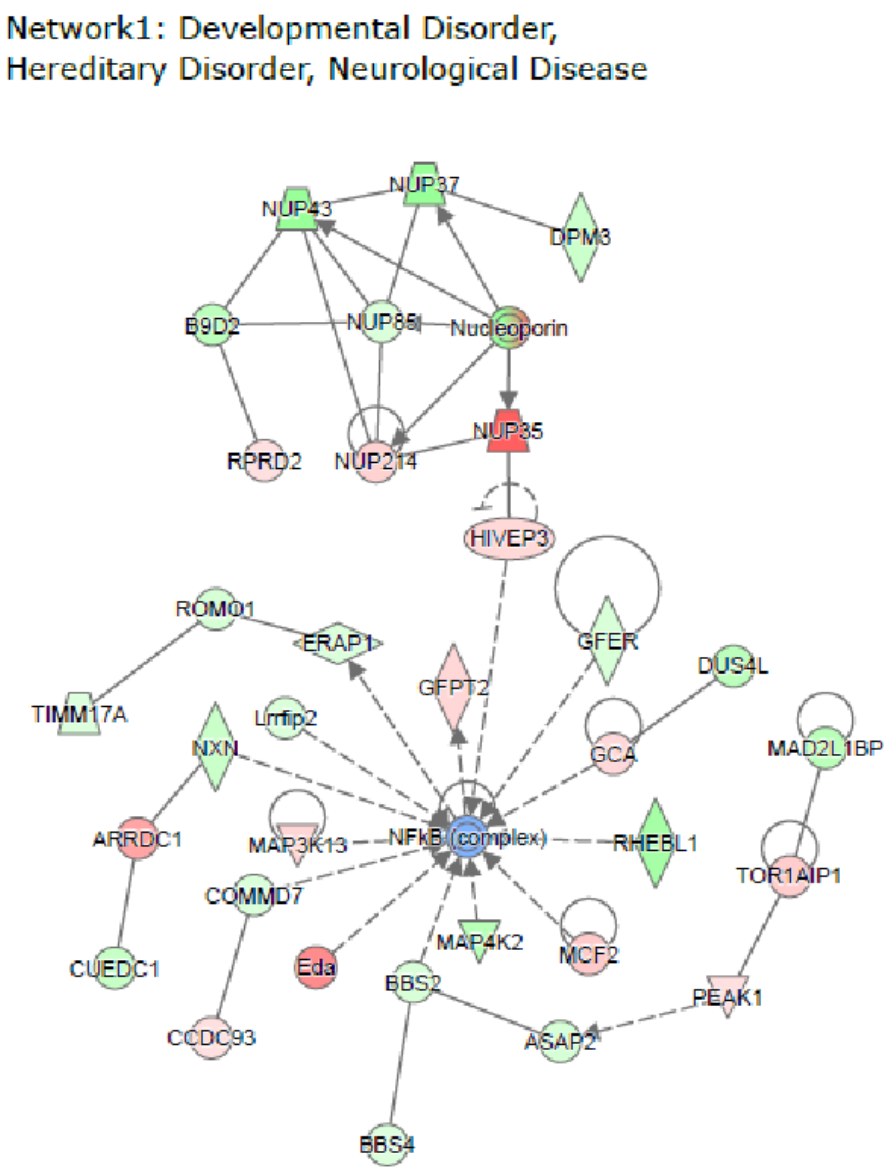

Figure 5.11 Detailed node graph of the top scoring network: Developmental Disorder, Hereditary Disorder, Neurological Disease, where NF-κB is the central node.

Direct and indirect relationships between nodes are shown for DTGs repressed by WT (red) or 2D (green) within the predicted network.

5.4 Discussion

4E-BP2 is a repressor of cap-dependent translation. During postnatal development, deamidation of 4E-BP2 arises and is concomitant with reduced mTOR activity. To mimic conditions of accumulation of deamidated 4E-BP2, we overexpressed each 4E-BP2 form (WT, deamidated) after infecting mouse cortical neurons with AAVs expressing 4E-BP2 under a neuron-specific hSyn promoter. Interestingly, we identified specific mRNAs that are regulated after overexpression of WT and deamidated 4E-BP2 and comparably the two translatomes indicate very low correlation. Thereby, we discovered that the identified neuronal translatomes after overexpression of WT and deamidated 4E-BP2 are dissimilar whereas transcriptomes do not exhibit any robust differences. Our finding highlights the importance of using approaches such as Ribosome profiling to study differentially the transcriptome and translatome and agrees with other studies that have distinguished transcriptome and translatome responses upon stress exposure of yeast cells. Severe stress had profound effects on both transcriptome and translatome whereas mild stress preferentially affected translatome (Halbeisen et al., 2009).

Cis-acting elements of mRNAs located either in the 5' or 3' UTR control the biological destiny of newly synthesized mRNAs by interacting with other translational or RNA binding factors and affecting the expression level, nucleo-cytoplasmic transport, stability, translational efficiency and subcellular localization of the mRNA (Grillo et al., 2010). Consequently, it was important to characterise these features on both distinct pools of mRNAs that we identified.

Interestingly, mRNAs regulated by deamidated 4E-BP2 harboured shorter 5' UTRs with significantly less TOPs and uORFs than mRNAs regulated by WT 4E-BP2. Our finding that WT DTGs are enriched in 5´ UTR features agrees with previous studies, characterising mTOR and eIF4E-sensitive mRNAs (Hsieh et al., 2012; Mamane et al., 2007; Thoreen et al., 2012; Truitt et al., 2015) and could result from the reduced binding of 2D to eIF4E (Bidinosti et al., 2010b), and/or from the increased sensitivity of 2D to mTOR inhibition. Differences regarding length of 5′ UTRs, number of TOP and uORFs in mRNA 5′ UTRs, indicate two different mechanisms of translation regulation of the WT – and 2D- regulated mRNAs. Long 5′ UTRs have been associated with low levels of translation across different cell types, indicating that length of 5′ UTRs affects translational efficiency (Blair et al., 2017). Regarding number of uORFs, ribosomes can initiate translation at uORFs, which affects

translation of the major open reading frame positively or negatively (Blair et al., 2017), underlining the important role of uORFs in protein synthesis. The importance of translation regulation through these *cis*-acting elements is also highlighted in identified changes of gene expression during neuronal differentiation. Ribosome occupancy in 5' UTR differs between human Embryonic Stem Cells (hESCs) and Neural Precursor Cells (NPCs), with specific genes having increased 5' UTR ribosomes during differentiation but decreased occupancy in the main ORF (Blair et al., 2017). Therefore, 5' UTR Ribosome occupancy downregulates protein synthesis in these genes. Long 5' UTRs have also been associated with low levels of protein synthesis in hESCs and NPCs whereas ORF length has been correlated with high ribosome occupancy in hESCs and NPCs (Blair et al., 2017).

Using UTRscan of DTGs, we highlighted novel aspects of a wider brain-specific mechanism involving 4E-BP2 deamidation. GO functional analysis displays a very small overlap between WT-2D translatomes, revealing that WT overexpression predominantly elicits widespread translational changes in genes involved in transcription, which could constitute a homeostatic response. Conversely, 2D-regulated genes are involved in cerebral cortex development and NF-κB activity. Moreover, 2D DTGs show a high correlation with mitochondria as a cellular compartment whereas WT DTGs are correlated with nucleoplasm. 4E-BPs are involved in regulation of cell survival responses through mitochondrial activity because MTFP1 (Mitochondrial Fission Process 1) is identified as target of mTORC1/4E-BP2 pathway (Morita et al., 2017). Upon inhibition of mTORC1, translation of MTFP1 decreases, altering phosphorylation and localization of DRP1 (GTPase Dynamin-Related Protein 1) and causing mitochondrial hyperfusion (Morita et al., 2017).

To conclude, we discovered that 2D overexpression engenders a widespread alteration of the neuronal translatome, thus demonstrating that 4E-BP2 deamidation is highly regulated by major neuronal signalling pathways and receptor activity, and that it plays a key functional role in translation. The lower stability of 2D, together with the non-overlapping puncta of WT and 2D detected in dendrites, support this hypothesis that the two forms of 4E-BP2 may regulate the function of different types of synapses, by selective translational de-repression of different mRNAs.

6. Elucidating the Structure of 4E-BP2

6.1 Introduction

4E-BPs are repressors of initiation of protein synthesis by impeding the formation of eIF4F complex which consists of initiation factors eIF4E, eIF4G and eIF4A. Specifically, 4E-BPs and eIF4G share a YXXXXLΦ eIF4E-binding motif (canonical) and an overlapping binding surface on eIF4E, thus competing for binding to eIF4E. Binding of 4E-BPs to eIF4E sterically inhibits binding of eIF4G, thus blocking the assembly of eIF4F complex (Mader et al., 1995; Marcotrigiano et al., 1999).

4E-BPs are intrinsically disordered proteins (IDPs), lacking stable secondary and tertiary structure. The N terminal region of eIF4E is also disordered compared to other regions of the protein and is named as intrinsically disordered region (IDR). IDPs/IDRs display a pivotal role in mediating protein – protein interactions by using dynamic instead of well-defined structures, especially IDRs that undergo posttranslational modifications such as phosphorylation (Dyson and Wright, 2005; Xie et al., 2007). Depending on the interaction with other proteins, IDPs/IDRs undergo a transition from a disordered to an ordered state, albeit some IDPs remain still disordered up to a certain degree even upon binding to other proteins (Fuxreiter and Tompa, 2012; Mittag et al., 2010). To elucidate the role of these proteins like 4E-BP2, either unmodified or upon posttranslational modifications such as deamidation, it is important to define their different structural states, hence understanding the significance of every region in mediating protein–protein interactions.

Studies of structure of IDPs/IDRs are quite challenging because most structural methods such as X-ray crystallography are inappropriate for these proteins. Recent advances in NMR spectroscopy and newly developed methods such as small – angle X-ray scattering (SAXS) allow the detailed analysis of structure of IDPs (Lukhele et al., 2013). Regarding the structure of 4E-BP2, NMR spectroscopy indicates that human 4E-BP2 owns a transient secondary structure with a helical propensity within the canonical binding site to eIF4E (Lukhele et al., 2013). In

agreement with this finding, SAXS on 4E-BP from *Strongylocentrotus purpuratus* suggests that the protein possesses a quite steady central region with a high helical propensity (Gosselin et al., 2011).

Recent studies of 4E-BP2 – eIF4E complex have identified that 4E-BP2 forms a bipartite interaction with eIF4E since a second motif, ^{78}IPGVT^{82}, on the 4E-BP2 sequence, apart from the canonical site, is very important and affects dynamics of the complex (Lukhele et al., 2013). Moreover, the C terminus of eIF4E is also crucial for stable 4E-BP2 binding to eIF4E (Mizuno et al., 2008). The rest of 4E-BP2 remains in a disordered state upon binding to eIF4E (Fuxreiter and Tompa, 2012). Similarly, apart from the N terminus, the rest of eIF4E does not fold upon interaction with 4E-BP2, implying that both proteins remain highly dynamic after formation of the complex (Lukhele et al., 2013). This dynamic structure facilitates the exposure of different sites of both proteins, allowing them to undergo posttranslational modifications by kinases and other partners (Dennis et al., 2011; Gingras et al., 1999b). Figure 6.1 illustrates a crystal structure of 4E-BP2 – eIF4E complex.

Structural studies have also identified differences on the binding surfaces of 4E-BP2 and eIF4G to eIF4E. Although 4E-BP2 and eIF4G share the canonical motif for binding to eIF4E, their binding surfaces differ significantly with 4E-BP2 displaying a more extensive surface than eIF4G which interacts mostly with the N terminus of eIF4E as NMR spectroscopy illustrates (Lukhele et al., 2013). Therefore, interaction of 4E-BP2 with eIF4E is not based only on the central region that involves the canonical motif, but it also includes regions outside of this motif as it was proved by the first SAXS study of the complex eIF4E-4E-BP2 (Gosselin et al., 2011). Apart from understanding the significance of protein regions in forming complexes with other partners, defining the structure of these proteins will allow us to design new or improve existing inhibitors/antagonists that could be used as therapeutic targets and dampen specific biological responses. For instance, the more extensive binding surface of 4E-BP2 to eIF4E, could explain why in the presence of 4EGi-1, a compound that has tumour suppressor activity, 4E-BP still binds to eIF4E compared to eIF4G that dissociates from eIF4E (Moerke et al., 2007).

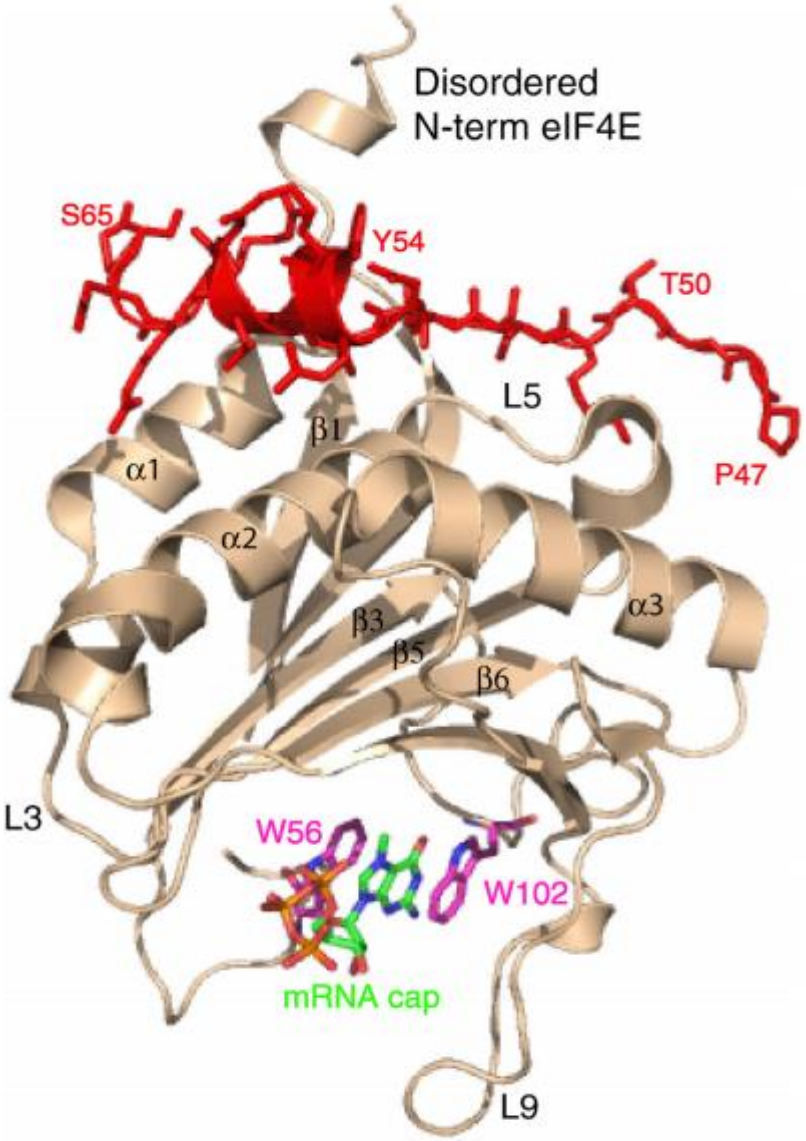

Figure 6.1 Crystal Structure of eIF4E in Complex with a Pro47-Thr70 4E-BP2 Peptide and m7 GTP cap.

Pro47-Thr70 4E-BP2 peptide (red) and m7 GTP cap (stick model; Protein Data Bank [PDB] code 3AM7; (Fukuyo et al., 2011). b strands (β), a helices (α), loops (L), and residues critical in cap binding are labeled.

Phosphorylation state of 4E-BPs determines their association with eIF4E. Hypo- or minimally phosphorylated 4E-BPs bind to eIF4E and inhibit protein synthesis whereas hyperphosphorylated 4E-BPs dissociate from eIF4E, allowing the initiation of protein synthesis (Hara et al., 2002). Posttranslational modifications such as phosphorylation can stabilise or destabilise specific regions of IDPs (Pufall et al., 2005; Tee and Proud, 2002; Theillet et al., 2012) or more rarely induce conformational changes to the whole structure of IDPs. Phosphorylation of 4E-BP2 at T37 and T46 induces folding of residues P18-R62 into a four-stranded β–domain which sequesters the canonical motif into a buried β – strand, blocking its access to eIF4E (Bah et al., 2015). Hypophosphorylated 4E-BP2 at T37 and T46 has decreased affinity for eIF4E and upon binding to eIF4E, 4E-BP2 is characterized by a more disordered state. On the contrary, fully phosphorylated 4E-BP2 is more stable, having a significant reduced affinity for eIF4E (Bah et al., 2015). Interestingly, stability of hypo- or hyper-phosphorylated 4E-BPs is dependent on whether the proteins are in a free or bound state. Free hyperphosphorylated 4E-BPs are very stable whereas upon binding to eIF4E, the complex is unstable (Yanagiya et al., 2012).

Figure 6.2 shows the structure of phosphorylated 4E-BP2, indicating that phosphorylation induces folding of 4E-BP2, leading the protein to a more stable secondary structure (Bah et al., 2015). On the other hand, free hypophosphorylated or non – phosphorylated 4E-BPs are unstable and are targeted for degradation. Hypophosphorylated 4E-BP1 is ubiquitinated at K57 by the KLHL25 – CUL3 E3 ligase (Yanagiya et al., 2012). Regarding 4E-BP2, we showed that hypophosphorylated 4E-BP2 is also very unstable (Figure 3.3). Furthermore, we also discovered that deamidated 4E-BP2 is unstable and gets degraded by CUL4B – DDBP1 E3 ligase complex (Figure 3.13).

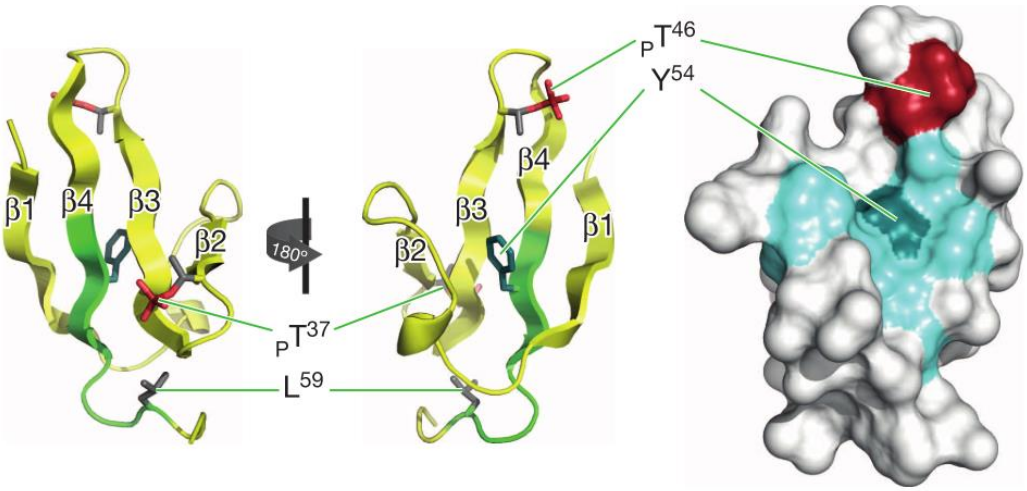

Figure 6.2 Phosphorylation-induced structure of R18–R62 of 4E-BP2.

Cartoon (left) and surface (right) representations of the solution NMR structure. Phosphorylated residues, pT37 and pT46 (red), the surface formed by residues of the hydrophobic cluster (right, cyan) and Y54 (cyan stick representation (left) or dark cyan surface (right)) are shown. The residues in the canonical eIF4E binding site (YXXXXLW) are shown in green (left), demonstrating the binding-incompatible extended structure (stick model; Protein Data Bank [PDB] code 2MX4); (Bah et al., 2015)

Nonenzymatic deamidation of asparaginyl or glutaminyl residues *in vitro* and *in vivo* changes protein structure. Deamidation at neutral pH introduces a negative charge on the residue and often leads to β – isomerization. Therefore, these changes in structure modify the properties of the proteins chemically and/or biologically by affecting the interactions with other proteins and/or their biological function, respectively (Robinson, 2002). Deamidated αA-crystallin has reduced chaperone activity and different secondary and tertiary structure than WT αA-crystallin (Gupta and Srivastava, 2004). Moreover, deamidated RNase U2 that contains isoAp32 unfolds the secondary structure of the protein, thus affecting its hydrolytic activity (Noguchi, 2010). However, whether deamidation can affect the disordered structure of 4E-BP2 remains unclear.

6.2 Experimental aim

The main aim of this thesis is to characterize the role of deamidated 4E-BP2 in the brain. Since posttranslational modifications display a pivotal role in determining the protein function and deamidation can change the properties of the protein, we asked whether deamidation of 4E-BP2 changes the protein structure. To answer this question, we expressed and purified recombinant 4E-BP2 WT and N99D/N102D and then, used SAXS, NMR and SRCD (Synchrotron Radiation Circular Dichroism) to be able to observe any differences between the secondary structures of both 4E-BP2 forms.

6.3 Results

6.3.1 Protein production and purification

Both 4E-BP2 WT and N99D/N102D (2D) were expressed and purified successfully. Expression of recombinant protein was induced with IPTG for 3 h at 28 ^{o}C. Figure 6.3 depicts results from the pilot tests after inducing expression of recombinant protein for 0, 1, 2, 4, 6, 8 h, o/n and resolving the soluble and insoluble fractions of lysed cells on an SDS-PAGE gel. After 3-4 h of induction of expression at 28 ^{o}C, we achieved the highest intensity of all protein bands corresponding to highest protein expression in the soluble fractions for 4E-BP2 N99D/N012D (bottom panel, Figure 6.3). For 4E-BP2 WT, high protein expression was achieved between 1 – 4 h, thus we decided to follow the same induction protocol of 3 h for both proteins (Figure 6.3).

Figure 6.4 (A) shows the efficiency of different steps during the expression and purification of recombinant 4E-BP2 WT. Lane 1 and 2 [Figure 6.4 (A)] correspond to samples of soluble and insoluble lysates respectively, after induction of expression for 3 h at 28 ^{o}C. These conditions allow for efficient induction of expression and solubility of proteins comparing the intensity of the bands between the soluble and insoluble fraction [Figure 6.4 (A)]. Lane 3 [Figure 6.4 (A)] shows the non-specific flow through fraction that did not bind the GST resin and lane 4 [Figure 6.4 (A)] indicates the efficient collection of tagless 4E-BP2 WT (~15kDa) after addition of 3C protease. Figure 6.3 (B) indicates samples on an SDS-PAGE gel from different fractions

collected after upconcentration of the eluted purified protein and before gel filtration (Lane 1), collected fractions during gel filtration [Lane 2 on top and bottom gel, fraction 4 (for WT) or 5 (for 2D),], (fraction 9, Lane 3 on both gels), (fraction 15, Lane 4 on both gels), [Lane 5 on both gels, (highest peak, upconcentrated eluted sample]. Collected fractions 4, 9, 15 (f4, f9, f15) from gel filtration corresponded to aggregated proteins and were separated successfully from the purified 4E-BP2 WT (Lane 5, top gel, Figure 6.4) and 2D (Lane 5, bottom gel, Figure 6.4). However, during the affinity purification step where the protein was bound to glutathione sepharose, we noticed that protein chaperone DnaK (~70kDa) from *Escherichia coli* was copurified [Figure 6.3 (B), Lane 2 – 4) but could be removed using size exclusion chromatography. The SEC elution position of the protein was the same for 4E-BP2 WT and 2D.

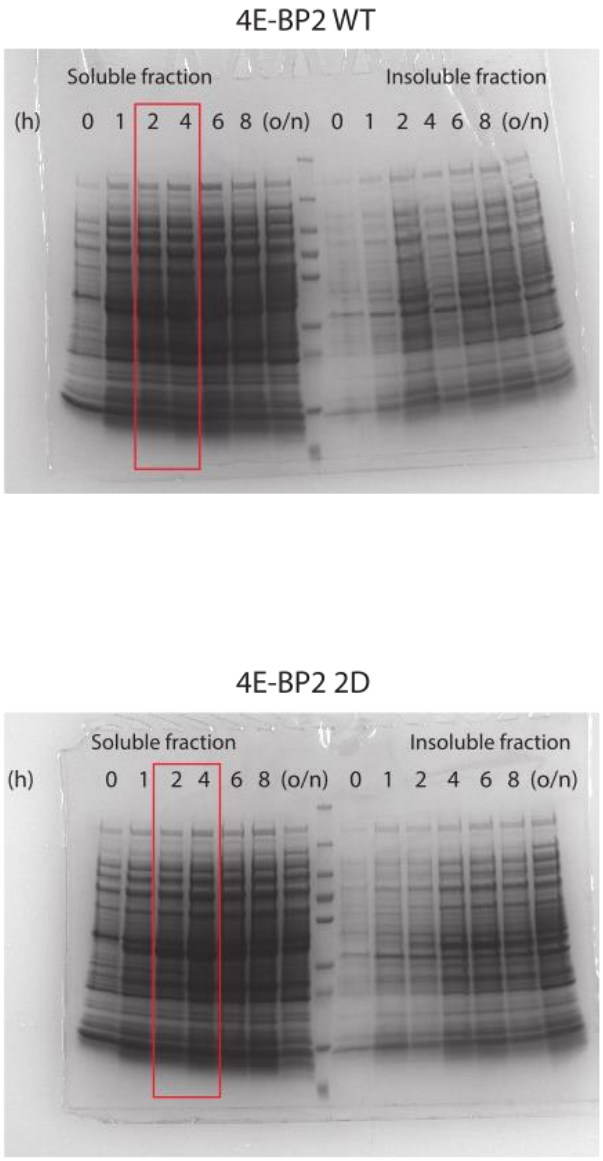

Figure 6.3 Results of SDS-PAGE analysis of directly expressed 4E-BP2 WT and 2D.

Expression was induced at 28 ^{o}C for 0, 1, 2, 4, 6, 8 h and o/n. Soluble and insoluble fractions of *Escherichia coli* cell lysates were analysed on an SDS-PAGE gel and Coomassie-stained protein bands were scanned.

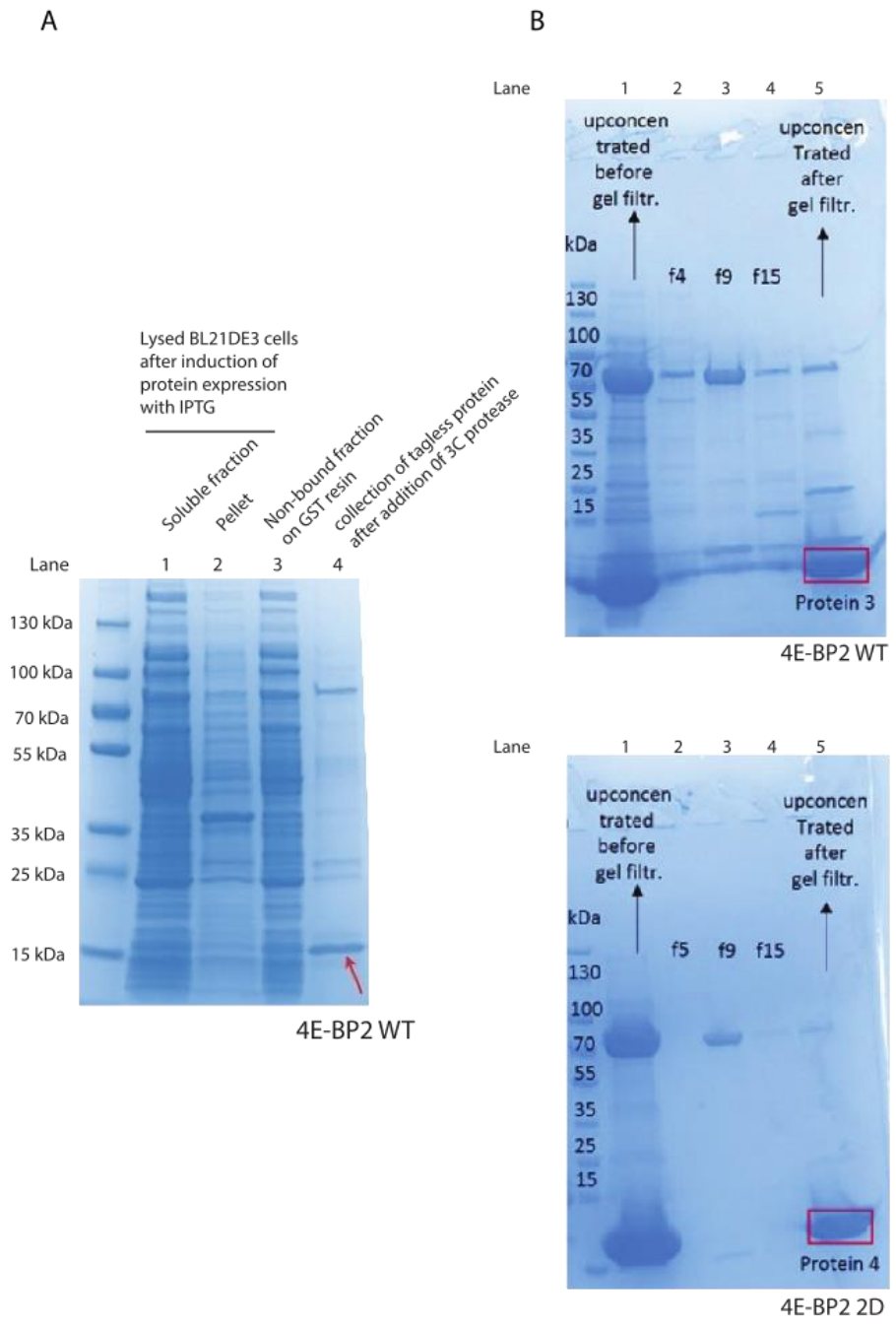

Figure 6.4 Results of SDS-PAGE analysis of expressed and purified recombinant 4E-BP2 WT and 2D.

A. Expression was induced at 28 ^{o}C for 3 h. Soluble (Lane 1) and insoluble (Lane 2) fractions of *Escherichia coli* cell lysates were analysed on an SDS-PAGE gel along with flow through fraction that did not bind GST resin (Lane 3) and eluted fraction corresponded to purified

tagless 4E-BP2 WT (Lane 4). Coomassie-stained protein bands were scanned. **B.** Samples collected before (Lane 1) and during gel filtration (Lane 2-5) were subjected to PAGE analysis and Coomassie-stained protein bands were scanned. Lane 5 corresponds to the upconcentrated 4E-BP2 protein that collected from the fraction showing the highest peak during gel filtration. Protein 3 = 4E-BP2 WT, Protein 4 = 4E-BP2 2D

6.3.2 Deamidation of 4E-BP2 does not change the intrinsic disordered structure of the protein

Purified recombinant 4E-BP2 WT and 2D were analysed by SAXS and SRCD to compare their structural characteristics. The SAXS scatter profiles of both proteins overlap quite well, presenting featureless profiles for the individual proteins as Figure 6.5 (A) shows. However, a small concentration dependence can be seen at low q values for both proteins, giving lower concentration-normalized intensities after dilution [Figure 6.5 (A)]. Therefore, the different datasets collected at different protein concentrations were analyzed separately to get an understanding of how much structural variation is possible in the different dilutions. The determination of molecular mass of the proteins using the forward scattering, calibrated with water, shows that the mass of the protein particle is somewhere between monomeric and dimeric in size (Table 6.1). The Kratky plots of the SAXS scatter profile for both proteins indicate that they appear unfolded as Figure 6.5 (B) displays. The ellipticity spectra given for both analyzed proteins indicates that the secondary structure of these proteins are random coils by the negative peak located near 199 nm [Figure 6.6 (A)], which is in line with the Kratky plots results [Figure 6.5 (B)], suggesting that both proteins appear unfolded. Moreover, Figure 6.6 (A) illustrates that the shape of the spectra overlaps well between the two proteins. Figure 6.6 (B) shows that the size of the proteins appears to reduce in size when diluted, which could be that there is a dimer/monomer mixture present depending on the protein concentration. The molecular mass determined for 4E-BP2 using SEC-MALS gave a value of 15.2 kDa which is closer to a monomeric state. However, this measurement was made with a more diluted protein sample compared to what the highest protein concentration were in the SAXS measurements. Figure 6.7 illustrates the SAXS models generated by DAMMIN and GASBOR which fit the experimental data well and show a similar elongated shape for both proteins. For the GASBOR models, a forced P2 symmetry or doubling the amount of dummy residues resulted in a better fit with the experimental data compared to a P1 symmetry with the amount of dummy residues present in a

monomer. This is also one indication that the proteins may form a dimeric state. The collected SEC-SAXS data gives only one peak, suggesting that the solution is at least dominated by one oligomeric state. The scatter profile obtained for the different SEC-SAXS runs overlap with the data obtained from batch measurements, which indicate that there were no present aggregates to distort the batch SAXS data.

Purified ^{15}N labelled 4E-BP2 WT and 2D proteins were also analysed by NMR. Figure 6.8 presents the collected NMR spectra with peaks located in a narrow region, indicative of intrinsically disordered proteins. Most of the peaks in the WT protein overlap with the peaks of 2D (Figure 6.8), suggesting that they share a similar structure but with some minor differences for a few residues.

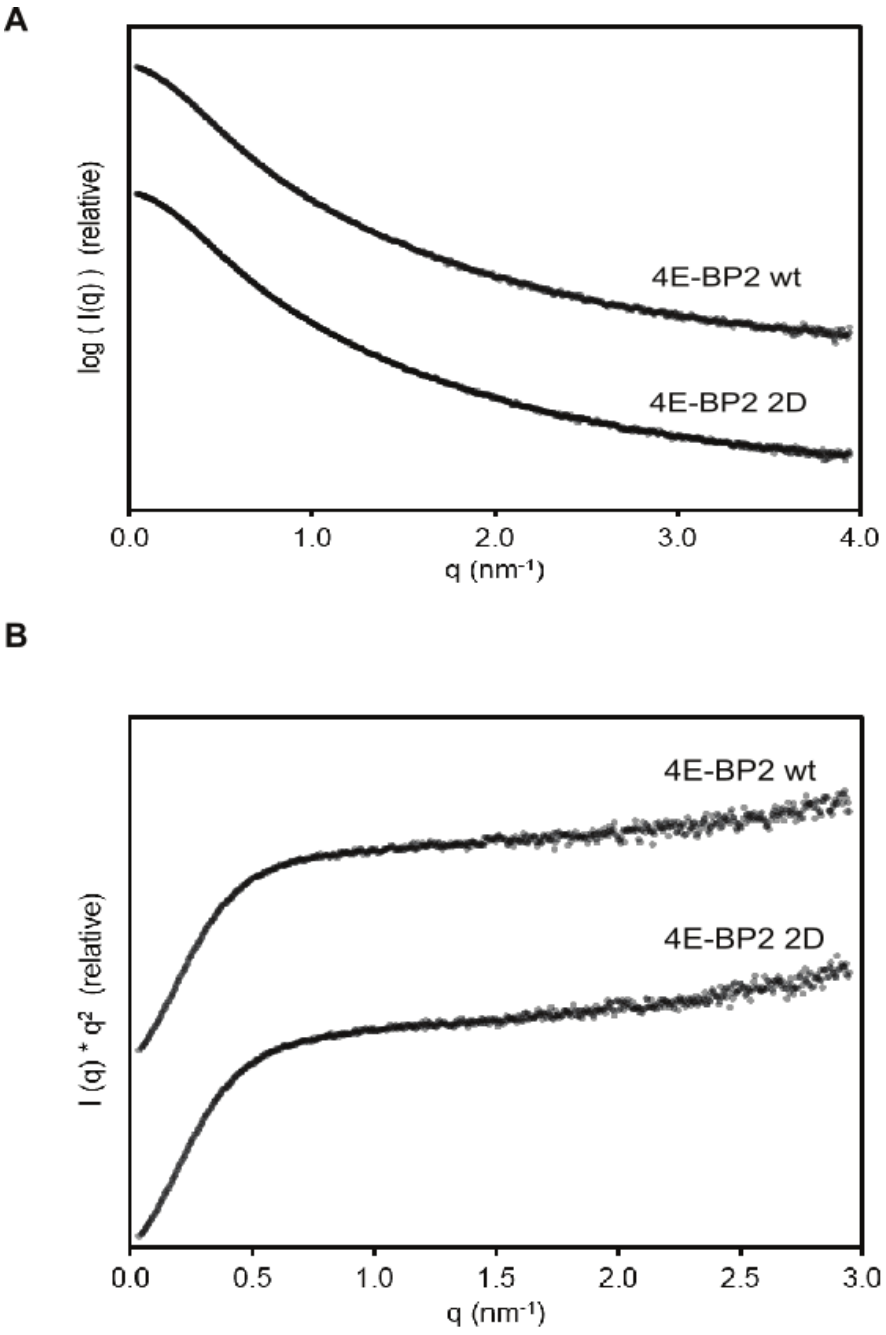

Figure 6.5 Biophysical data (A)SAXS scatter profiles, (B) Kratky plots on the 4E-BP WT and 2D**.**

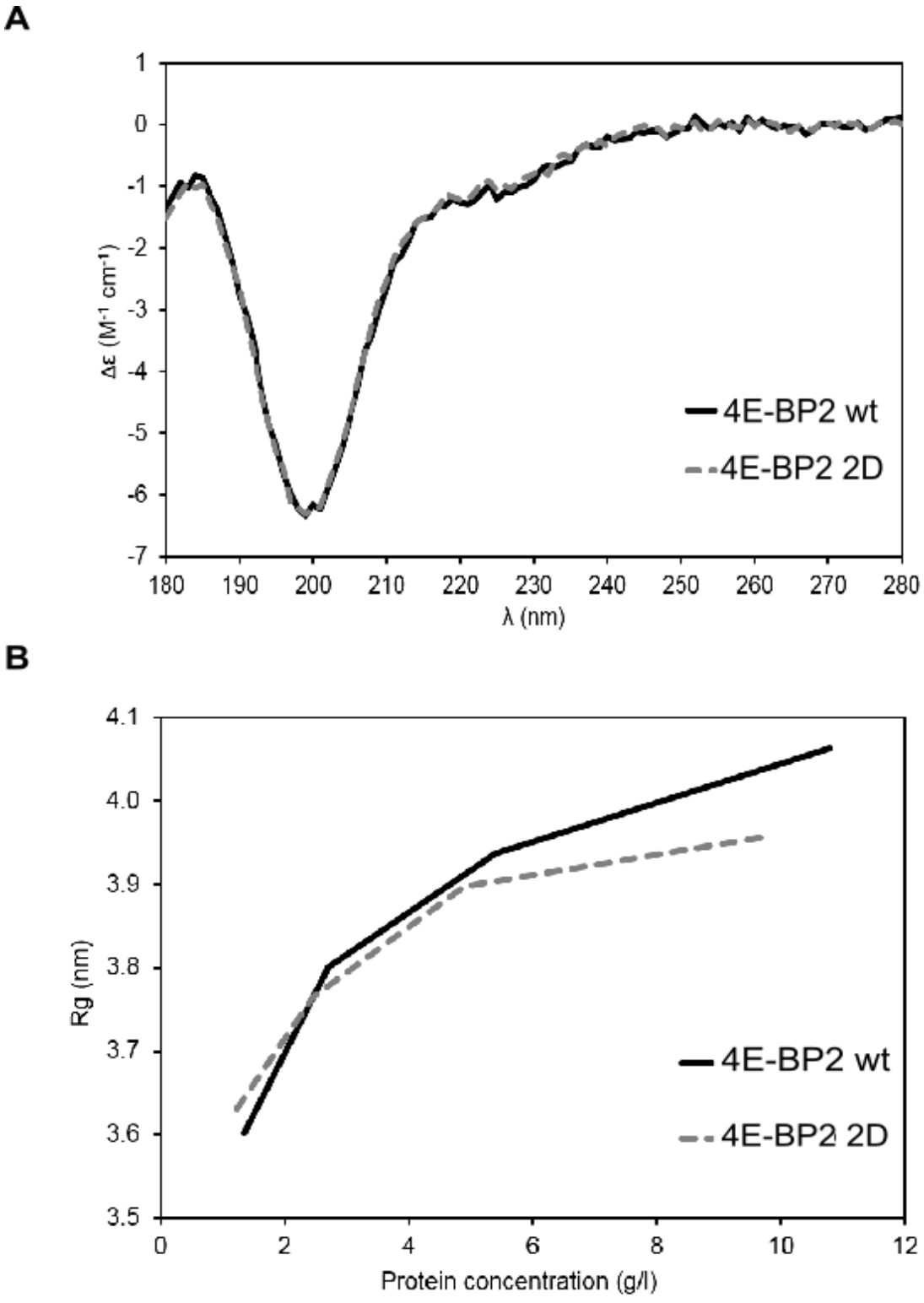

Figure 6.6 Biophysical data on the 4E-BP WT and 2D.

A. SRCD spectra, **B.** Rg calculated by the Debye function plotted versus the protein concentration during SAXS measurements.

Table 6.1 Extracted SAXS parameters for the different proteins measured at their highest concentration.

The calculated masses based on DAMMIN models were made as described previously (Petoukhov et al., 2012).

4E-BP2	Guinier Rg (nm)	Debye Rg (nm)	Dmax (nm)	MW_{calc} (kDa)	MW_{I0} (kDa)	MW_{DAMMIN} (kDa)	Protein conc. (mg/ml)
WT	3.8	4.1	15.1	13.1	20.7	32.2	10.8
N99D/N102D	3.5	4.0	14.5	13.0	19.8	28.5	9.8

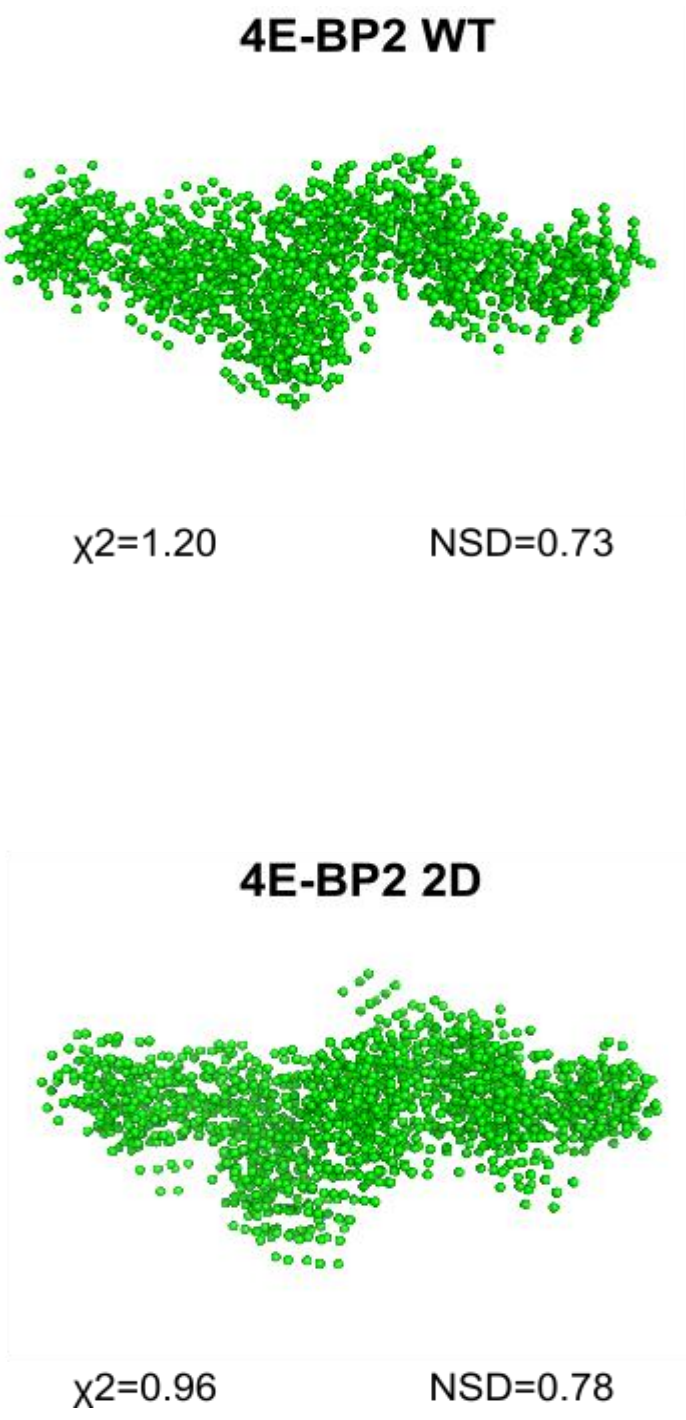

Figure 6.7 Ten superimposed DAMMIN models.

These models were generated using the SAXS data from the highest protein concentration with the average χ^2 score and normalized spatial discrepancy (NSD) for the different 4E-BP2 forms.

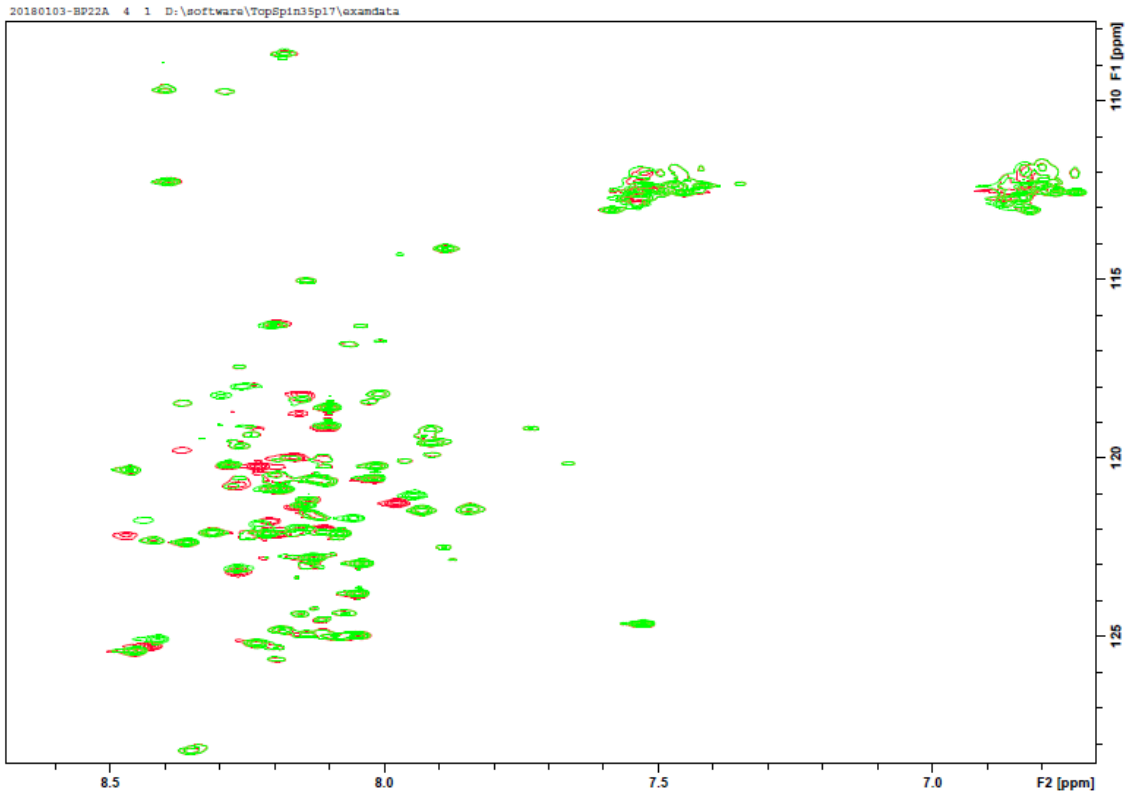

Figure 6.8 ^{1}H-^{15}N HSQC spectra for purified recombinant WT (green) and 2D (red) 4E-BP2 protein.

x-axis: ω_1-^{15}N (ppm); y-axis: ω_2-^{1}H (ppm)

6.4 Discussion

Taken together, the results of the structural characterization using SRCD and SAXS cannot detect any obvious differences between the proteins. The SRCD spectra depict clearly that the proteins consist of random coils and the Kratky plots obtained from SAXS show that the proteins behave as unfolded. The early elution position of the proteins in the SEC chromatogram is also an indication of an unfolded protein, appearing as a protein significantly larger than a folded globular protein of the same size. The unfolded state of these proteins may be one explanation why a protein chaperone was copurified in the earlier steps during the purification.

The size parameters that have been observed for other unfolded proteins using SAXS, giving a theoretical Rg of 3.8 nm and a Dmax of 10 nm for a protein of 122 residues (Fitzkee and Rose, 2004), are similar to values obtained from the 4E-BP experimental data. The even larger values of Dmax than expected from an unfolded protein suggests that 4E-BPs are more elongated than the average unfolded protein or alternatively may be the effect of dimerization. Interestingly, some of the experimental data strongly suggest that 4E-BP2 appears as dimeric unless their unfolded state makes them appear dimeric. The experimental data point the dimeric structure are the following : 1) the fact that the molecular mass determination give values between monomeric and dimeric masses using the forward scattering, 2) twice the number of dummy residues gave a better fit to the experimental data for GASBOR model generation, 3) the mass determination using the volume of DAMMIN models suggest a dimeric mass. When analyzed in a more dilute protein concentration with SEC-MALS, the oligomeric state appears monomeric. A mixture of dimeric and monomeric state present depending on the protein concentration would also explain the concentration dependence seen in the SAXS data at low q values.

In conclusion, any clear differences between 4E-BP2 WT and 2D could not be found using SRCD or SAXS. The differences seen between the generated SAXS models for WT and deamidated 4E-BP2are small compared to the variations between the generated models of one protein and therefore, SAXS is considered to have too low resolution to determine any potential differences. The largest difference between the different proteins was the position on SDS-PAGE gel, which could be a direct effect of their charge. Using NMR, small local variations could be observed for a few residues but the overall fold of these proteins is unlikely to be affected by these mutations.

7. Discussion and Future Directions

Proteins are synthesized and degraded simultaneously and continuously, responding to various stimuli that cells receive. Although protein synthesis is the last step of gene expression, the new assembled polypeptides can undergo different posttranslational modifications, allowing each cell to control and modify protein function in a rapid and energy-efficient way. Elucidating the role of these modifications is challenging if one considers that the human proteome is 10-100 times more complex than the actual genome (Cho, 2007). The present thesis examines the recently identified posttranslational asparagine deamidation of 4E-BP2, an inhibitor of cap-dependent translation, in the brain.

7.1 Overview of main findings

The goal of this thesis is to characterise the biological role of a novel posttranslational modification of 4E-BP2 in the mammalian brain. We describe a previously unidentified mechanism during early postnatal brain development, whereby the deamidated form of the cardinal brain translation initiation repressor 4E-BP2 is more susceptible to Ubiquitin proteasomal degradation (as compared to WT protein) because it binds with higher affinity to a complex comprising the mTORC1 protein Raptor and the Ubiquitin E3 ligase CUL4B. Deamidated 4E-BP2 stability is regulated by mTORC1 and AMPAR activity. Our data link this novel mTOR-dependent regulatory mechanism of deamidated 4E-BP2 to the regulation of translation of a distinct pool of mRNAs associated with cerebral development, mitochondria and primarily NF-κB activity.

7.2 Deamidated 4E-BP2 is susceptible to Ubiquitin proteasome degradation

For many proteins, deamidation is traditionally viewed as an “aging by-product”, which labels long-lived proteins for degradation (Robinson, 2002). In accordance with this, in Chapter 3, we do find that 2D is more ubiquitinated, less stable than WT 4E-BP2 and gets degraded by the proteasome. Only the deamidated form and not an alanine mutant (2A) exhibits reduced protein stability, suggesting that this phenotype is specifically induced by asparagine deamidation. Moreover, 2D stability is regulated by a major signalling pathway (mTOR) and the activity of AMPARs.

The susceptibility of deamidated 4E-BP2 to degradation by the Ubiquitin proteasome system agrees with other studies, linking deamidation with decreased protein stability since its presence at the N terminal of the sequence determines a destabilising residue (Varshavsky, 1997). Most of the proteins that undergo deamidation are aged proteins such as human crystallin (Gupta and Srivastava, 2004), albeit there are very few examples of proteins being regulated through deamidation during development. Bcl-xL, a pro-survival protein, undergoes asparagine deamidation and this mechanism is conserved from metazoans to mammals, providing increased cellular susceptibility to programmed cell death (Dho et al., 2013). Pattern recognition receptors, vital components of innate immunity and, specifically, RIG-I undergoes asparagine deamidation by viral homologues of phosphoribosylformylglycinamidine synthetase (PFAS) and, thereby herpes virus evades cytokine production (He et al., 2015). Our data revealed that deamidation provides a novel role to 4E-BP2 as only deamidated 4E-BP2 binds with higher affinity to the Raptor-CUL4B-DDB1 complex and is driven to the proteasome. We also showed that this mechanism of degradation is regulated by mTORC1 and AMPAR activity. Notably, 4E-BP1 is regulated by a different E3 Ubiquitin ligase, CUL3, which promotes hypo-phosphorylated 4E-BP1 ubiquitination and degradation, while hyper-phosphorylated 4E-BP1 is refractory to degradation (Yanagiya et al., 2012). Nevertheless, 4E-BP1 is highly expressed in glial cells, while 4E-BP2 (both WT and 2D) is predominantly expressed in neurons, suggesting a potential dichotomy between CUL4B-CUL3 mechanisms in neurons and glia.

Moreover, we identified that 4E-BP2 deamidation occurs in mouse neurons, but not in glial cells; therefore it is a neuron- and brain-specific posttranslational

modification since it is only detected in postnatal brain, and not in other peripheral tissues examined (Bidinosti et al., 2010b). Thus, our data support a neuron-centric role for 4E-BP2 deamidation during early postnatal development and into adulthood.

7.3 4E-BP2 undergoes asparagine deamidation in human brain; potential link with neurodevelopmental disorders

Interestingly, in Chapter 3, we identified that deamidated 4E-BP2 is also present in human brain. Potentially, this mechanism is evolutionary conserved from rodents to humans to preferentially regulate neuronal translation during a crucial developmental period for brain growth: synapse regulation, neuronal proliferation and migration and ultimately circuitry formation and behaviour (Pressler and Auvin, 2013; Semple et al., 2013). The period when 4E-BP2 undergoes deamidation (P10-P21) in mice (concomitant with a decrease in mTORC1 activity) (Beirowski et al., 2017; Bidinosti et al., 2010b; Wang et al., 2016) would correspond to 10 months-3 years of age in human infants (Semple et al., 2013). mTORC1 activity is dysregulated in several monogenic disorders co-diagnosed with high rates of autism, such as Fragile X Syndrome and Tuberous Sclerosis (Kelleher and Bear, 2008). Global knockout of *Eif4ebp2* engenders molecular, cellular and behavioural phenotypes, which are reminiscent of ASD (Gkogkas et al., 2013). Other studies have described a key role for 4E-BP2 in synaptic function, learning and memory (Banko et al., 2006; Banko et al., 2007; Banko et al., 2005; Ran et al., 2013). In this thesis, we studied the expression of deamidated and WT 4E-BP2 in different mouse models of ASD [*Fmr1* +/-, B6.129P2-*Fmr1*^{tm1Cgr}/J), *Shank3* +/- (B6.Cg-*Shank3*$^{tm2.1Bux}$/J), *Tsc2* +/- (B6;129S4-*Tsc2*^{tm1Djk}/J) and BTBR (BTBR *T*$^{+}$ *Itpr3*^{tf}/J) but we identified no differences comparing these mouse models and WT mice. Given these studies and our work, it is conceivable that dysregulated deamidated 4E-BP2 degradation, as a result of altered mTORC1 signalling during development, could be linked to a prodromal period of neurodevelopmental disorders such as ASD (via aberrant translational control of neuronal mRNAs) but further work needs to be carried out to address this link.

Deamidated 4E-BP2 is degraded by binding with higher affinity to the mTORC1 protein Raptor and the ubiquitin E3 ligase CUL4B, while pharmacological inhibition of mTORC1 promotes 2D accumulation and reduces Raptor-4E-BP2

binding (Schalm et al., 2003). Together, these data reveal that there is a causal relationship between Raptor-deamidated 4E-BP2 binding and protein stability, under the control of mTORC1 activity. Plausibly, accelerated 2D 4E-BP2 degradation (through formation of the Raptor-2D-CUL4B complex) could be part of a wider brain-specific mechanism involving CUL4B and the proteasome, mediating translational de-repression downstream of mTORC1 in certain synapses. Regulation of such synapses could be pivotal for the pathogenesis of ASD and other neurodevelopmental disorders, where there are known changes in mTORC1 activity (Costa-Mattioli and Monteggia, 2013; Huber et al., 2015; Kelleher and Bear, 2008).

Furthermore, CUL4B is also associated with ASD pathophysiology as it is an X-linked intellectual disability (XLID)-associated gene and its deletion in mice leads to embryonic lethality (Chen et al., 2012, Jiang et al., 2012). In addition, CUL4B overexpression increases ubiquitination and proteasomal degradation of Tuberous Sclerosis 2 protein [TSC2; an inhibitor of mTORC1 and syndromic ASD gene (Short et al., 1995)] and thus promotes mTORC1 signalling (Ghosh et al., 2008). Interestingly, XLID-linked truncating or missense mutations in CUL4B were shown to be defective in promoting degradation of TSC2 (Wang et al., 2013).

7.4 Mechanism of potential asparagine deamidation of 4E-BP2

Postnatal brain-specific asparagine deamidation of 4E-BP2 (N99D/N102D) is spontaneous and pH dependent, and there is no current evidence that it is catalysed by enzymes (Bidinosti et al., 2010b; Robinson, 2002). However unlikely it may be, a yet unidentified protein complex or enzyme could carry out 4E-BP2 deamidation, similarly to RIG-I (He et al., 2015), which regulates antiviral cytokine production or to the immune sensor c-GAS (cyclic GMP-AMP Synthase) (Zhang et al., 2018), where deamidation is catalysed by viral proteins.

A second potential mechanism is that changes in intracellular pH during postnatal development might lead 4E-BP2 to undergo deamidation since 4E-BP2 is sensitive to alkaline-induced deamidation (Robinson, 2002). Carbonic anhydrases (CAs) are key molecules for the regulation of pH in neurons and glia, in the blood-

brain barrier, in the interstitial fluid in the brain and at the level of the whole organism (Frost and McKenna, 2013). Interestingly, CA VII isoform expression in mouse CA1 pyramidal neurons is very low from birth until the 2nd postnatal week and rises during 3rd postnatal week, concomitantly with deamidation of 4E-BP2, reaching its peak after postnatal day 30 (Frost and McKenna, 2013). During the developmental window P10-18, CA VII is the only cytosolic isoform, accounting for CA activity in pyramidal neurons (Frost and McKenna, 2013). Furthermore, the second isoform, CAII, exhibits very low levels of expression until postnatal day 18 when neurons start expressing both CAVII and CAII isoforms. Interestingly, CA VII is chiefly found in the CNS and is neuron-specific whereas CA II is expressed in neurons and glia (Frost and McKenna, 2013). To test whether CA VII–mediated and/or CA II-mediated pH regulation contributes to the onset of 4E-BP2 deamidation in neurons, siRNAs will be used for both isoforms separately and together in mouse cortical neurons to downregulate their expression and check if expression of deamidated 4E-BP2 will be affected. To check whether changes of pH affect deamidation of 4E-BP2 in neurons, carbonylcyanide p-trifluoromethoxyphenylhydrazone (FCCP), will be used as a protonophore and uncoupler of mitochondrial oxidative phosphorylation in mitochondria, and Niclosamide, a weak lipophilic acid, on early DIV in mouse cortical neurons to acidify the cytosol and check whether 4E-BP2 will undergo deamidation under these conditions. To examine whether deamidation of 4E-BP2 is facilitated with alkaline pH shifts, fused fluorescent mCherry2–4E-BP2 proteins (WT, double deamidated) will be co-transfected with SypHER2, a genetically encoded fluorescent pH-indicator, appropriate for measuring fast intracellular pH shifts (Matlashov et al., 2015). Then, using live cell imaging, we will measure pH in the subcellular compartments that each 4E-BP2 form localizes.

7.5 Where does deamidated 4E-BP2 localize in neurons?

In Chapter 4, we explored the subcellular localization of different forms of 4E-BP2 in HEKs and mouse cortical neurons. Interestingly, expression of fluorescent 4E-BP2 fusion proteins is affected depending on the terminal where fluorescent protein was fused. mCherry2– and mCerulean3–*4E-BP2* constructs where fluorescent protein is fused on the N-terminal exhibit markedly higher expression compared to *4E-BP2*-mCherry2 and -mCerulean3 constructs where fluorescent protein is on the

C-terminal. One potential interpretation for this finding is that fusion of fluorescent protein on the C-terminal affects interaction of 4E-BP2 with Raptor since TOS motif, which is essential for this interaction, is composed by the last 5 amino acids (FEMDI) of the C-terminal. To check that hindered interaction of Raptor and 4E-BP2 affects expression of the protein, site – directed mutagenesis will be performed on these amino acids (substitutions, deletion) on the mCherry2– and mCerulean3–*4E-BP2* constructs and test their subcellular expression levels.

WT and 2D subcellular localization is similar, but there is little overlap between the fluorescent puncta corresponding to each form. Our main finding that deamidated 4E-BP2 exhibits a different subcellular localization than WT 4E-BP2 will be further explored to see whether the two 4E-BP2 forms localize in different neuronal compartments. Therefore, we will perform immunofluorescence of the same co–transfected neuronal cultures and we will stain neurons for Raptor, presynaptic and postsynaptic markers and check co-localization of WT and deamidated 4E-BP2 with each stained protein.

7.6 Does tertiary structure of deamidated 4E-BP2 change in monomeric state or in complex with other proteins?

Deamidation introduces a negative charge at the deamidation site and can also lead to β isomerization (Robinson, 2002). The pronounced slower migration of 2D-corresponding bands on SDS-PAGE suggests that deamidation may affect 4E-BP2. Moreover, mTORC1 phosphorylation induces folding of the intrinsically disordered 4E-BP2 protein (Bah et al., 2015). In Chapter 6, we investigated the secondary structures of WT and deamidated 4E-BP2. Surprisingly, we did not detect major changes in deamidated 4E-BP2 structure by SAXS, SCRD or NMR, as compared to WT. Both proteins are IDPs comprising random coils. Possibly, structural analysis of deamidated 4E-BP2 in complex with Raptor or eIF4E could reveal undetected conformational changes of its IDP state since the structure changes depending on the interaction with other protein partners.

7.7 A novel postnatal mechanism of translational control for regulation of NF-κB and cerebral cortex development

In Chapter 5, we discovered that 2D overexpression engenders a widespread alteration of the neuronal translatome, thus demonstrating that 4E-BP2 deamidation is highly regulated by major neuronal signalling pathways and receptor activity, and that it plays a key functional role. The lower stability of 2D, together with the non-overlapping puncta of WT and 2D detected in dendrites, support the hypothesis that the two forms of 4E-BP2 may regulate the function of different types of synapses, by selective translational de-repression of different mRNAs. In accordance with this premise, 2D was shown to preferentially regulate excitatory AMPA synaptic transmission (Bidinosti et al., 2010b). Moreover, our results, implying that AMPAR but not NMDAR inhibition promotes 2D degradation may hint that this is a calcium-independent mechanism present in excitatory cell, both upstream and downstream of 4E-BP2-dependent translation.

Our Ribosome profiling data in Chapter 5 highlighted novel aspects of a wider brain-specific mechanism involving 4E-BP2 deamidation. Overexpression of 4E-BP2 forms was carried out using AAV constructs driven by hSyn promoters in a culture which is predominantly neuronal (>90% of cells) (Davis and Temple, 1994), while we also demonstrated that deamidation arises in neurons, but not in glia. However, we cannot exclude the possibility that the translational changes detected may be due to a non-neuron autonomous effect on glial cells. Cell type-specific 'translatomics' [such as TRAP (Heiman et al., 2014)] would be required to answer this question. We detected a low correlation between the changes in the translatome, following overexpression of the two 4E-BP2 forms, and no significant changes in transcription. Moreover, differences that we identified in 5' UTR features between WT and 2D DTGs, support that each of the two 4E-BP2 forms characterizes a distinct mechanism of translational control with different mRNAs targets.

7.8 Link with mitochondria and Warburg effect

Remarkably, the highest scoring network predicted by IPA is 'Developmental Disorder, Hereditary Disorder, Neurological Disease', and NF-κB is the central node. A main avenue for NF-κB activity regulation perinatally in brain is through de-

repression, following phosphorylation of its inhibitor IκBα (nuclear factor of kappa light polypeptide gene enhancer in B-cells alpha). This mechanism is brain-derived neurotrophic factor (BDNF)-dependent prenatally and BDNF-independent postnatally (Gavalda et al., 2009; Gutierrez and Davies, 2011). Moreover, the top GO Cellular Compartment detected by DAVID in 2D regulated genes is the mitochondrion. Strikingly, 4E-BPs were shown to regulate mitochondrial dynamics and biogenesis by translational control of nucleus-encoded mitochondria-related mRNAs (Morita et al., 2013; Morita et al., 2017). We identified 35 mitochondrial mRNAs in 2D-regulated DTGs.

It is suggested that synaptic activity promotes a neuronal Warburg effect, shifting neuronal energy metabolism from oxidative phosphorylation towards aerobic glycolysis (Bas-Orth et al., 2017). In parallel, mitochondrial gene expression peaks during synaptogenesis (P0-P21) (Wirtz and Schuelke, 2011). Furthermore, the metabolic switch of the Warburg effect is underlined by the interplay between NF-κB and the tumour suppressor p53 through regulation of nuclear and mitochondrial gene-expression (Johnson and Perkins, 2012). 4E-BPs are linked with p53 as they regulate senescence by controlling synthesis of the p53-stabilizing protein Gas2 (Petroulakis et al., 2009). Finally, deamidation of the mitochondrial transmembrane protein B cell lymphoma-extra large (Bcl-xL) is a critical switch in the apoptotic response following DNA damage and GO analysis of 2D 4E-BP2-regulated DTGs showed that 11 DTGs are linked to the GO category: cellular response to DNA damage, while this category is not detected in WT DTGs GO analysis.

Taken together, our ribosome profiling data and the existing evidence regarding NF-κB activity and mitochondria underline the importance of our proposed brain-specific translational control mechanism of mTORC1- or AMPAR-mediated, Raptor-dependent accumulation of deamidated 4E-BP2 during a critical period of postnatal brain development (Figure 7.1), which could go awry in neurodevelopmental disorders, such as ASD.

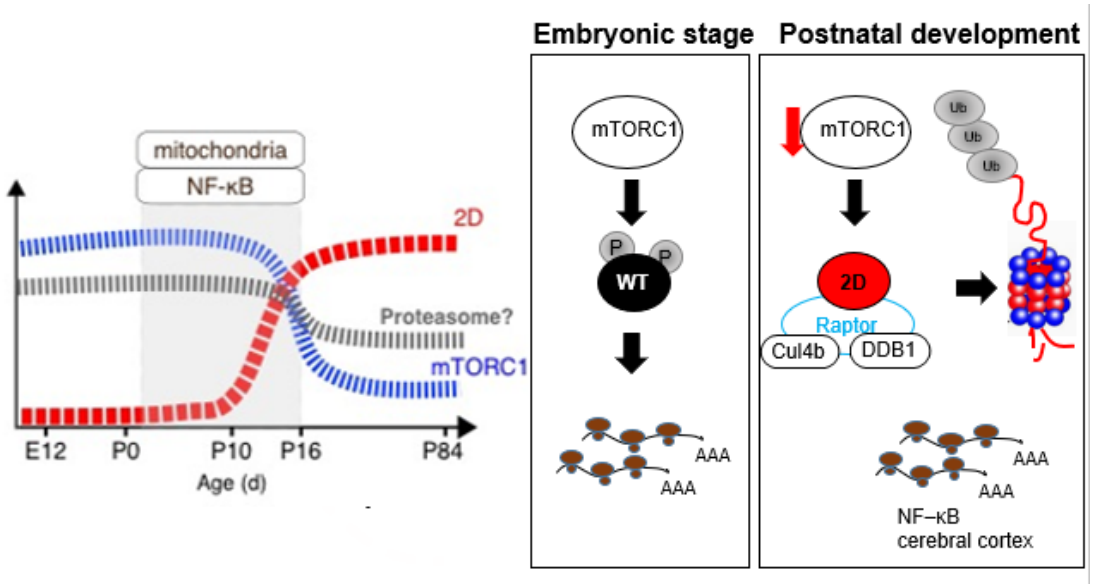

Figure 7.1 Diagrammatic summary of the mechanism described in this thesis.

Left: Diagram, illustrating that mTORC1 activity decreases whereas 4E-BP2 gets deamidated as we are moving from embryonic to postnatal development. After birth, there is a switch for NF-κB which is independent of BDNF-regulation and signalling through the canonical pathway in contrast to its embryonic regulation. Our model supports that mitochondria and proteasome activity possibly also depend on a regulatory switch before and after birth. **Right**: During embryonic stages, 4E-BP2 WT is a negative regulator of translation through phosphorylation by mTORC1 complex. During postnatal development, 4E-BP2 gets deamidated and is regulated through specific proteasomal degradation by the Raptor- CUL4B-DDB1 complex and concomitant with decreased mTORC1 activity. Our model connects this Raptor-dependent proteasomal degradation of deamidated 4E-BP2 with the regulation of translation of mRNAs, associated with NF-κB activity and cerebral cortex development.

References

Alvarez-Castelao, B., and Schuman, E.M. (2015). The Regulation of Synaptic Protein Turnover. J Biol Chem *290*, 28623-28630.

Andreassi, C., and Riccio, A. (2009). To localize or not to localize: mRNA fate is in 3'UTR ends. Trends Cell Biol *19*, 465-474.

Aritomi, M., Kunishima, N., Inohara, N., Ishibashi, Y., Ohta, S., and Morikawa, K. (1997). Crystal Structure of Rat Bcl-xL. The Journal of Biological Chemistry *272* 27886–27892.

Asaki, C., Usuda, N., Nakazawa, A., Kametani, K., and Suzuki, T. (2003). Localization of translational components at the ultramicroscopic level at postsynaptic sites of the rat brain. Brain Research *972*, 168-176.

Ayuso, M.I., Martinez-Alonso, E., Salvador, N., Bonova, P., Regidor, I., and Alcazar, A. (2015). Dissociation of eIF4E-binding protein 2 (4E-BP2) from eIF4E independent of Thr37/Thr46 phosphorylation in the ischemic stress response. PLoS One *10*, e0121958.

Bah, A., Vernon, R.M., Siddiqui, Z., Krzeminski, M., Muhandiram, R., Zhao, C., Sonenberg, N., Kay, L.E., and Forman-Kay, J.D. (2015). Folding of an intrinsically disordered protein by phosphorylation as a regulatory switch. Nature *519*, 106-109.

Banko, J.L., Hou, L., Poulin, F., Sonenberg, N., and Klann, E. (2006). Regulation of eukaryotic initiation factor 4E by converging signaling pathways during metabotropic glutamate receptor-dependent long-term depression. J Neurosci *26*, 2167-2173.

Banko, J.L., Merhav, M., Stern, E., Sonenberg, N., Rosenblum, K., and Klann, E. (2007). Behavioral alterations in mice lacking the translation repressor 4E-BP2. Neurobiol Learn Mem *87*, 248-256.

Banko, J.L., Poulin, F., Hou, L., DeMaria, C.T., Sonenberg, N., and Klann, E. (2005). The translation repressor 4E-BP2 is critical for eIF4F complex formation, synaptic plasticity, and memory in the hippocampus. J Neurosci *25*, 9581-9590.

Bas-Orth, C., Tan, Y.W., Lau, D., and Bading, H. (2017). Synaptic Activity Drives a Genomic Program That Promotes a Neuronal Warburg Effect. J Biol Chem *292*, 5183-5194.

Bauer, N.C., Doetsch, P.W., and Corbett, A.H. (2015). Mechanisms Regulating Protein Localization. Traffic *16*, 1039-1061.

Beirowski, B., Wong, K.M., Babetto, E., and Milbrandt, J. (2017). mTORC1 promotes proliferation of immature Schwann cells and myelin growth of differentiated Schwann cells. Proc Natl Acad Sci U S A *114*, E4261-E4270.

Benjamini, Y., and Hochberg, Y. (1995). Controlling the False Discovery Rate: A Practical and Powerful Approach to Multiple Testing. Journal of the Royal Statistical Society *57*, 289-300.

Berlanga, J.J., Baass, A., and Sonenberg, N. (2006). Regulation of poly(A) binding protein function in translation: Characterization of the Paip2 homolog, Paip2B. RNA *12*, 1556-1568.

Bidinosti, M., Martineau, Y., Frank, F., and Sonenberg, N. (2010a). Repair of isoaspartate formation modulates the interaction of deamidated 4E-BP2 with mTORC1 in brain. J Biol Chem *285*, 19402-19408.

Bidinosti, M., Ran, I., Sanchez-Carbente, M.R., Martineau, Y., Gingras, A.C., Gkogkas, C., Raught, B., Bramham, C.R., Sossin, W.S., Costa-Mattioli, M.*, et al.* (2010b). Postnatal

deamidation of 4E-BP2 in brain enhances its association with raptor and alters kinetics of excitatory synaptic transmission. Mol Cell *37*, 797-808.
Bingol, B., and Schuman, E.M. (2006). Activity-dependent dynamics and sequestration of proteasomes in dendritic spines. Nature *441*, 1144-1148.
Bingol, B., Wang, C.F., Arnott, D., Cheng, D., Peng, J., and Sheng, M. (2010). Autophosphorylated CaMKIIalpha acts as a scaffold to recruit proteasomes to dendritic spines. Cell *140*, 567-578.
Blackshear, P.J., Nemenoff, R.A., and Avruch, J. (1982). Preliminary characterization of a heat-stable protein from rat adipose tissue whose phosphorylation is stimulated by insulin. Biochem J *204*, 817-824.
Blair, J.D., Hockemeyer, D., Doudna, J.A., Bateup, H.S., and Floor, S.N. (2017). Widespread Translational Remodeling during Human Neuronal Differentiation. Cell Rep *21*, 2005-2016.
Bloodgood, B.K., and Sabatini, B.L. (2005). Neuronal Activity Regulates Diffusion Across the Neck of Dendritic Spines. Science.
Branco, T., and Hausser, M. (2010). The single dendritic branch as a fundamental functional unit in the nervous system. Curr Opin Neurobiol *20*, 494-502.
Brar, G.A., and Weissman, J.S. (2015). Ribosome profiling reveals the what, when, where and how of protein synthesis. Nat Rev Mol Cell Biol *16*, 651-664.
Buffington, S.A., Huang, W., and Costa-Mattioli, M. (2014). Translational control in synaptic plasticity and cognitive dysfunction. Annu Rev Neurosci *37*, 17-38.
Cajigas, I.J., Will, T., and Schuman, E.M. (2010). Protein homeostasis and synaptic plasticity. EMBO J *29*, 2746-2752.
Calmettes, P., Durand, D., Desmadril, M., Minard, P., Receveur, V., and Smith, J.G. (1994). How random is a highly denatured protein? . Biophysical Chemistry *53* 105-114
Cao, Q., and Richter, J.D. (2002). Dissolution of the maskin±eIF4E complexby cytoplasmic polyadenylation and poly(A)-binding protein controls cyclin B1 mRNA translation and oocyte maturation. The EMBO Journal *21*, 3852-3862.
Casadio, A., Martin, K.C., Giustetto, M., Zhu, H., Chen, M., Bartsch, D., Bailey, C.H., and Kandel, E.R. (1999). A Transient, Neuron-Wide Form of CREB-Mediated Long-Term Facilitation Can Be Stabilized at Specific Synapses by Local Protein Synthesis. Cell *99*, 221-237.
Cho, W.C.S. (2007). Proteomics Technologies and Challenges. Genomics, Proteomics & Bioinformatics *5*, 77-85.
Choi, K.M., McMahon, L.P., and Lawrence, J.C., Jr. (2003). Two motifs in the translational repressor PHAS-I required for efficient phosphorylation by mammalian target of rapamycin and for recognition by raptor. J Biol Chem *278*, 19667-19673.
Ciechanover;, A., and Brundin, P. (2003). The Ubiquitin Proteasome System in

Neurodegenerative Diseases:

Sometimes the Chicken, Sometimes the Egg. Neuron *40*, 427–446.
Clemens, M.J., Elia, A., and Morley, S.J. (2013). Requirement for the eIF4E binding proteins for the synergistic down-regulation of protein synthesis by hypertonic conditions and mTOR inhibition. PLoS One *8*, e71138.
Colina, R., Costa-Mattioli, M., Dowling, R.J., Jaramillo, M., Tai, L.H., Breitbach, C.J., Martineau, Y., Larsson, O., Rong, L., Svitkin, Y.V.*, et al.* (2008). Translational control of the innate immune response through IRF-7. Nature *452*, 323-328.
Coogan, A.N., O'Leary, D.M., and O'Connor, J. (1999). P42/44 MAP Kinase Inhibitor PD98059 Attenuates Multiple Forms of Synaptic Plasticity in Rat Dentate Gyrus In Vitro. The American Physiological Society, 103-110.

Costa-Mattioli, M., Gobert, D., Harding, H., Herdy, B., Azzi, M., Bruno, M., Bidinosti, M., Ben Mamou, C., Marcinkiewicz, E., Yoshida, M.*, et al.* (2005). Translational control of hippocampal synaptic plasticity and memory by the eIF2alpha kinase GCN2. Nature *436*, 1166-1173.
Costa-Mattioli, M., Gobert, D., Stern, E., Gamache, K., Colina, R., Cuello, C., Sossin, W., Kaufman, R., Pelletier, J., Rosenblum, K.*, et al.* (2007). eIF2alpha phosphorylation bidirectionally regulates the switch from short- to long-term synaptic plasticity and memory. Cell *129*, 195-206.
Costa-Mattioli, M., and Monteggia, L.M. (2013). mTOR complexes in neurodevelopmental and neuropsychiatric disorders. Nat Neurosci *16*, 1537-1543.
Costa-Mattioli, M., Sossin, W.S., Klann, E., and Sonenberg, N. (2009). Translational control of long-lasting synaptic plasticity and memory. Neuron *61*, 10-26.
Costache, V., Bilotto, S., Laguerre, L., Belle, R., Cosson, B., Cormier, P., and Morales, J. (2012). Dephosphorylation of eIF2alpha is essential for protein synthesis increase and cell cycle progression after sea urchin fertilization. Dev Biol *365*, 303-309.
Cullen, P.J., and Lockyer, P.J. (2002). Integration of calcium and Ras signalling. Nat Rev Mol Cell Biol *3*, 339-348.
Czaplinski, K. (2014). Understanding mRNA trafficking: are we there yet? Semin Cell Dev Biol *32*, 63-70.
Dai, C.L., Shi, J., Chen, Y., Iqbal, K., Liu, F., and Gong, C.X. (2013). Inhibition of protein synthesis alters protein degradation through activation of protein kinase B (AKT). J Biol Chem *288*, 23875-23883.
Davis, A., and Temple, S. (1994). A self-renewing multipotential stem cell in embryonic rat cerebral cortex>. Nature *372*, 263–266.
Dell'Acqua, M.L., Smith, K.E., Gorski, J.A., Horne, E.A., Gibson, E.S., and Gomez, L.L. (2006). Regulation of neuronal PKA signaling through AKAP targeting dynamics. Eur J Cell Biol *85*, 627-633.
Dennis, M.D., Schrufer, T.L., Bronson, S.K., Kimball, S.R., and Jefferson, L.S. (2011). Hyperglycemia-Induced O-GlcNAcylation and Truncation of 4E-BP1 Protein in Liver of a Mouse Model of Type 1 Diabetes. The Journal of Biological Chemistry *286*, 34286–34297.
Derkach, V.A., Oh, M.C., Guire, E.S., and Soderling, T.R. (2007). Regulatory mechanisms of AMPA receptors in synaptic plasticity. Nat Rev Neurosci *8*, 101-113.
Dever, T.E., and Green, R. (2012). The elongation, termination, and recycling phases of translation in eukaryotes. Cold Spring Harb Perspect Biol *4*, a013706.
Dho, S.H., Deverman, B.E., Lapid, C., Manson, S.R., Gan, L., Riehm, J.J., Aurora, R., Kwon, K.S., and Weintraub, S.J. (2013). Control of cellular Bcl-xL levels by deamidation-regulated degradation. PLoS Biol *11*, e1001588.
Ding, M., and Shen, K. (2008). The role of the ubiquitin proteasome system in synapse remodeling and neurodegenerative diseases. Bioessays *30*, 1075-1083.
Djakovic, S.N., Schwarz, L.A., Barylko, B., DeMartino, G.N., and Patrick, G.N. (2009). Regulation of the proteasome by neuronal activity and calcium/calmodulin-dependent protein kinase II. J Biol Chem *284*, 26655-26665.
Dobin, A., Davis, C.A., Schlesinger, F., Drenkow, J., Zaleski, C., Jha, S., Batut, P., Chaisson, M., and Gingeras, T.R. (2013). STAR: ultrafast universal RNA-seq aligner. Bioinformatics *29*, 15-21.
Dörrbaum, A.R., Kochen, L., Langer, J.D., and Schuman, E.M. (2018). Local and global influences on protein turnover in neurons and glia. Elife *7*.
Dowling, R.J., Topisirovic, I., Alain, T., Bidinosti, M., Fonseca, B.D., Petroulakis, E., Wang, X., Larsson, O., Selvaraj, A., Liu, Y.*, et al.* (2010). mTORC1-mediated cell proliferation, but not cell growth, controlled by the 4E-BPs. Science *328*, 1172-1176.

Dyson, H.J., and Wright, P.E. (2005). Intrinsically unstructured proteins and their functions. Nat Rev Mol Cell Biol *6*, 197-208.
Ehlers, M.D. (2003). Activity level controls postsynaptic composition and signaling via the ubiquitin-proteasome system. Nat Neurosci *6*, 231-242.
Fabian, M.R., Sonenberg, N., and Filipowicz, W. (2010). Regulation of mRNA translation and stability by microRNAs. Annu Rev Biochem *79*, 351-379.
Favata, M.F., Horiuchi, K., Manos, E.J., Daulerio, A.J., Stradley, D.A., Feeser, W.S., Van Dyk, D.E., Pitts, W.J., Earl, R.A., Hobbs, F.*, et al.* (1998). Identification of a Novel Inhibitor of Mitogen-activated Protein

Kinase Kinase. THE JOURNAL OF BIOLOGICAL CHEMISTRY *273* 18623–18632.
Fenteany, G., Standaert, R., Lane, W., Choi, S., Corey, E., and Schreiber, S. (1995). Inhibition of proteasome activities and subunit-specific amino-terminal threonine modification by lactacystin. Science *268*, 726-731.
Fitzkee, N.C., and Rose, G.D. (2004). Reassessing random-coil statistics in unfolded proteins. PNAS *101*, 12497-12502.
Fonseca, R., Vabulas, R.M., Hartl, F.U., Bonhoeffer, T., and Nagerl, U.V. (2006). A balance of protein synthesis and proteasome-dependent degradation determines the maintenance of LTP. Neuron *52*, 239-245.
Frank, J., Gao, H., Sengupta, J., Gao, N., and Taylor, D.J. (2007). The process of mRNA–tRNA translocation. PNAS *104* 19671–19678.
Frost, S.C., and McKenna, R. (2013). Carbonic Anhydrase: Mechanism, Regulation, Links to Disease, and Industrial Applications. Springer.
Fukuyo, A., In, Y., Ishida, T., and Tomoo, K. (2011). Structural scaffold for eIF4E binding selectivity of 4E-BP isoforms: crystal structure of eIF4E binding region of 4E-BP2 and its comparison with that of 4E-BP1. J Pept Sci *17*, 650-657.
Fuxreiter, M., and Tompa, P. (2012). Fuzzy Complexes: A More Stochastic View of Protein Function. In: Fuxreiter M., Tompa P. (eds) Fuzziness. Advances in Experimental Medicine and Biology *725*, Springer, New York, NY.
Gavalda, N., Gutierrez, H., and Davies, A.M. (2009). Developmental switch in NF-kappaB signalling required for neurite growth. Development *136*, 3405-3412.
Geda, P., Patury, S., Ma, J., Bharucha, N., Dobry, C.J., Lawson, S.K., Gestwicki, J.E., and Kumar, A. (2008). A small molecule-directed approach to control protein localization and function. Yeast *25*, 577-594.
Geiger, T., and Clarke, S. (1987). Deamidation, Isomerization, and Racemization at Asparaginyl and Aspartyl Residues in Peptides. The Journal of Biological Chemistry *262*, 758-794.
Ghosh, P., Wu, M., Zhang, H., and Sun, H. (2008). mTORC1 signaling requires proteasomal function and the involvement of CUL4-DDB1 ubiquitin E3 ligase. Cell Cycle *7*, 373-381.
Gilbert, J., and Heng-Ye, M. (2014). Translational Dysregulation in Autism. Cell & Developmental Biology *03*.
Gingras, A.C., Gygi, S.P., Raught, B., Polakiewicz, R.D., Abraham, R.T., Hoekstra, M.F., Aebersold, R., and Sonenberg, N. (1999b). Regulation of 4E-BP1 phosphorylation: a novel two-step mechanism. Genes and Development *13*, 1422-1437.
Gingras, A.C., Raught, B., Gygi, S.P., Niedzwiecka, A., Miron, M., Burley, S.K., Polakiewicz, R.D., Wyslouch-Cieszynska, A., Aebersold, R., and Sonenberg, N. (2001). Hierarchical phosphorylation of the translation inhibitor 4E-BP1 Genes & Development *15*, 2852–2864.
Gingras, A.C., Raught, B., and Sonenberg, N. (1999). eIF4 Initiation Factors : Effectors of mRNA recruitment to ribosomes and regulators of translation. Annu Rev Biochem 913–963.

Gkogkas, C., Sonenberg, N., and Costa-Mattioli, M. (2010). Translational control mechanisms in long-lasting synaptic plasticity and memory. J Biol Chem *285*, 31913-31917.
Gkogkas, C.G., Khoutorsky, A., Ran, I., Rampakakis, E., Nevarko, T., Weatherill, D.B., Vasuta, C., Yee, S., Truitt, M., Dallaire, P.*, et al.* (2013). Autism-related deficits via dysregulated eIF4E-dependent translational control. Nature *493*, 371-377.
Gordon, A., and J. Hannon, G. (2010). FASTX-Toolkit: FASTQ/A Short-Reads Preprocessing Tools. Available at: http://hannonlab.cshl.edu/fastx_toolkit.
Gosselin, P., Oulhen, N., Jam, M., Ronzca, J., Cormier, P., Czjzek, M., and Cosson, B. (2011). The translational repressor 4E-BP called to order by eIF4E: new structural insights by SAXS. Nucleic Acids Res *39*, 3496-3503.
Graber, T.E., McCamphill, P.K., and Sossin, W.S. (2013). A recollection of mTOR signaling in learning and memory. Learn Mem *20*, 518-530.
Grillo, G., Turi, A., Licciulli, F., Mignone, F., Liuni, S., Banfi, S., Gennarino, V.A., Horner, D.S., Pavesi, G., Picardi, E.*, et al.* (2010). UTRdb and UTRsite (RELEASE 2010): a collection of sequences and regulatory motifs of the untranslated regions of eukaryotic mRNAs. Nucleic Acids Res *38*, D75-80.
Grosshans, D.R., Clayton, D.A., Coultrap, S.J., and Browning, M.D. (2002). LTP leads to rapid surface expression of NMDA but not AMPA receptors in adult rat CA1. Nat Neurosci *5*, 27-33.
Gupta, R., and Srivastava, O.P. (2004). Deamidation affects structural and functional properties of human alphaA-crystallin and its oligomerization with alphaB-crystallin. J Biol Chem *279*, 44258-44269.
Gutierrez, H., and Davies, A.M. (2011). Regulation of neural process growth, elaboration and structural plasticity by NF-kappaB. Trends Neurosci *34*, 316-325.
Haghighat, A., Mader, S., Pause, A., and Sonenberg, N. (1995). Repression of cap-dependent translation by 4E-binding protein 1: competition with p220 for binding to eukaryotic initiation factor-4E. The EMBO Journal *14*, 5701-5709.
Halbeisen, R.E., Scherrer, T., and Gerber, A.P. (2009). Affinity purification of ribosomes to access the translatome. Methods *48*, 306-310.
Hamilton, A.M., Oh, W.C., Vega-Ramirez, H., Stein, I.S., Hell, J.W., Patrick, G.N., and Zito, K. (2012). Activity-dependent growth of new dendritic spines is regulated by the proteasome. Neuron *74*, 1023-1030.
Hamilton, A.M., and Zito, K. (2013). Breaking it down: the ubiquitin proteasome system in neuronal morphogenesis. Neural Plast *2013*, 196848.
Hara, K., Maruki, Y., Long, X., Yoshino, K., Oshiro, N., Hidayat, S., Tokunaga, C., Avruch, J., and Yonezawa, K. (2002). Raptor, a Binding Partner of Target of Rapamycin (TOR), Mediates TOR Action. Cell *110*.
Harper, J.W., and Bennett, E.J. (2016). Proteome complexity and the forces that drive proteome imbalance. Nature *537*, 328-338.
Hartmann-Petersen, R., Seeger, M., and Gordon, C. (2003). Transferring substrates to the 26S proteasome. TRENDS in Biochemical Sciences *Vol.28 No.1*.
Hay, N., and Sonenberg, N. (2004). Upstream and downstream of mTOR. Genes Dev *18*, 1926-1945.
Hayashi, M., Saito, Y., and Hawashima, S. (1992). Calpain activation is essential for membrane fusion of erythrocytes in the presence of exogenous Ca2+. BIOCHEMICAL AND BIOPHYSICAL RESEARCH COMMUNICATIONS *31*, 939-946.
He, S., Zhao, J., Song, S., He, X., Minassian, A., Zhou, Y., Zhang, J., Brulois, K., Wang, Y., Cabo, J.*, et al.* (2015). Viral pseudo-enzymes activate RIG-I via deamidation to evade cytokine production. Mol Cell *58*, 134-146.

Heiman, M., Kulicke, R., Fenster, R.J., Greengard, P., and Heintz, N. (2014). Cell type–specific mRNA purification by translating ribosome affinity purification (TRAP). Nature Protocols *9*, 1282.
Hershey, J.W., Sonenberg, N., and Mathews, M.B. (2012). Principles of translational control: an overview. Cold Spring Harb Perspect Biol *4*.
Hipkiss, A.R. (2006). Accumulation of altered proteins and ageing: causes and effects. Exp Gerontol *41*, 464-473.
Hock, A.K., Vigneron, A.M., Carter, S., Ludwig, R.L., and Vousden, K.H. (2011). Regulation of p53 stability and function by the deubiquitinating enzyme USP42. EMBO J *30*, 4921-4930.
Hsieh, A.C., Liu, Y., Edlind, M.P., Ingolia, N.T., Janes, M.R., Sher, A., Shi, E.Y., Stumpf, C.R., Christensen, C., Bonham, M.J*., et al.* (2012). The translational landscape of mTOR signalling steers cancer initiation and metastasis. Nature *485*, 55-61.
Hsu, W.L., Chung, H.W., Wu, C.Y., Wu, H.I., Lee, Y.T., Chen, E.C., Fang, W., and Chang, Y.C. (2015). Glutamate Stimulates Local Protein Synthesis in the Axons of Rat Cortical Neurons by Activating alpha-Amino-3-hydroxy-5-methyl-4-isoxazolepropionic Acid (AMPA) Receptors and Metabotropic Glutamate Receptors. J Biol Chem *290*, 20748-20760.
Huang da, W., Sherman, B.T., and Lempicki, R.A. (2009). Systematic and integrative analysis of large gene lists using DAVID bioinformatics resources. Nat Protoc *4*, 44-57.
Huber, K.M., Kayser, M.S., and Bear, M.F. (2000). Role for Rapid Dendritic Protein Synthesis in Hippocampal mGluR-Dependent Long-Term Depression. Science *288*, 1254-1256.
Huber, K.M., Klann, E., Costa-Mattioli, M., and Zukin, R.S. (2015). Dysregulation of Mammalian Target of Rapamycin Signaling in Mouse Models of Autism. J Neurosci *35*, 13836-13842.
Huber, T.B., Walz, G., and Kuehn, E.W. (2011). mTOR and rapamycin in the kidney: signaling and therapeutic implications beyond immunosuppression. Kidney Int *79*, 502-511.
Husi, H., Ward, A.M., Choudhary, J.S., Blackstock, W.P., and Gran, S.G.N. (2000). Proteomic analysis of NMDA receptor–adhesion protein signaling complexes. Nature Neuroscience.
Imig, J., Kanitz, A., and Gerber, A.P. (2012). RNA regulons and the RNA-protein interaction network. Biomol Concepts *3*, 403-414.
Ingolia, N.T. (2014). Ribosome profiling: new views of translation, from single codons to genome scale. Nat Rev Genet *15*, 205-213.
Ingolia, N.T., Brar, G.A., Rouskin, S., McGeachy, A.M., and Weissman, J.S. (2012). The ribosome profiling strategy for monitoring translation in vivo by deep sequencing of ribosome-protected mRNA fragments. Nat Protoc *7*, 1534-1550.
Ingolia, N.T., Ghaemmaghami, S., Newman, J.R., and Weissman, J.S. (2009). Genome-wide analysis in vivo of translation with nucleotide resolution using ribosome profiling. Science *324*, 218-223.
International Human Genome Sequencing, C. (2004). Finishing the euchromatic sequence of the human genome. Nature *431*, 931-945.
Jackson, R., and Standart, N. (2015). The awesome power of ribosome profiling. RNA *21*, 652-654.
Jackson, R.J., Hellen, C.U., and Pestova, T.V. (2010). The mechanism of eukaryotic translation initiation and principles of its regulation. Nat Rev Mol Cell Biol *11*, 113-127.
Johnson, R.F., and Perkins, N.D. (2012). Nuclear factor-kappaB, p53, and mitochondria: regulation of cellular metabolism and the Warburg effect. Trends Biochem Sci *37*, 317-324.
Kacharmina, J.E., Job, C., Crino, P., and Eberwine, J. (2000). Stimulation of glutamate receptor protein synthesis and membrane insertion within isolated neuronal dendrites. PNAS *97*, 11545–11550.

Kahvejian, A., Roy, G., and Sonenbergr, N. (2001). The mRNA Closed-loop Model: The Function of PABP and PABP-interacting Proteins in mRNA Translation. Cold Spring Harbor Symposia on Quantitative Biology *LXVI*, 293-300.
Kandel, E.R. (2001). The Molecular Biology of Memory Storage: A Dialogue Between Genes and Synapses. Science *294*, 1030-1038.
Kang, H., and Schuman, E.M. (1996). A Requirement for Local Protein Synthesis in Neurotrophin-Induced Hippocampal Synaptic Plasticity. Science *273*, 1402-1406.
Karve, T.M., and Cheema, A.K. (2011). Small changes huge impact: the role of protein posttranslational modifications in cellular homeostasis and disease. J Amino Acids *2011*, 207691.
Kelleher, R.J., 3rd, and Bear, M.F. (2008). The autistic neuron: troubled translation? Cell *135*, 401-406.
Kim, E., Lowenson, J.D., Maclaren, D.C., Clarke, S., and Young, S.G. (1997). Deficiency of a protein-repair enzyme results in the accumulation of altered proteins, retardation of growth, and fatal seizures in mice. Proc Natl Acad Sci USA Vol 94, pp 6132–6137, June 1997 *94*, 6132-7137.
King, H.A., and Gerber, A.P. (2016). Translatome profiling: methods for genome-scale analysis of mRNA translation. Brief Funct Genomics *15*, 22-31.
Kleign, M., Scheper, G.C., O. Voorma, H., and Thomas, A.M. (1998). Regulation of translation initiation factors by signal transduction. Eur J Biochem *253*, 531-544.
Kleijn, M., Scheper, G.C., Voorma, H.O., and Thomas, A.M. (1998). Regulation of translation initiation factors by signal transduction. Eur J Biochem *253*, 531-544.
Knowles, R.B., and Kosik, S.K. (1997). Neurotrophin-3 signals redistribute RNA in neurons. Proc Natl Acad Sci.
Konarev, P.V., Volkov, V.V., Sokolova, A.V., Koch, M.H.J., and Svergun, D.I. (2003). PRIMUS: a Windows PC-based system for small-angle scattering data analysis. Journal of Applied Crystallography *36*, 1277-1282.
Koromilas, A., Lazaris-Karatzas, A., and Sonenberg, N. (1992). mRNAs containing extensive secondary structure in their 5' non-coding region translate efficiently in cells overexpressing initiation factor eIF-4E. The EMBO Journal *11*, 4153-4158.
Krug, M., Lossner, B., and Ott, T. (1984). Anisomycin blocks the late phase of long-term potentiation in the dentate gyrus of freely moving rats. Brain Res Bul *(13): 39–42*
Kwon, H.B., and Castillo, P.E. (2008). Role of glutamate autoreceptors at hippocampal mossy fiber synapses. Neuron *60*, 1082-1094.
Langmead, B., Trapnell, C., Pop, M., and Salzberg, S.L. (2009). Ultrafast and memory-efficient alignment of short DNA sequences to the human genome.
Laplante, M., and Sabatini, D.M. (2012). mTOR signaling in growth control and disease. Cell *149*, 274-293.
Laplante, M., and Sabatini, D.M. (2013). Regulation of mTORC1 and its impact on gene expression at a glance. J Cell Sci *126*, 1713-1719.
Li, K.W., Hornshaw, M.P., Van Der Schors, R.C., Watson, R., Tate, S., Casetta, B., Jimenez, C.R., Gouwenberg, Y., Gundelfinger, E.D., Smalla, K.H.*, et al.* (2004). Proteomics analysis of rat brain postsynaptic density. Implications of the diverse protein functional groups for the integration of synaptic physiology. J Biol Chem *279*, 987-1002.
Livingstone, M., Larsson, O., Sukarieh, R., Pelletier, J., and Sonenberg, N. (2009). A chemical genetic screen for mTOR pathway inhibitors based on 4E-BP-dependent nuclear accumulation of eIF4E. Chem Biol *16*, 1240-1249.

Lukhele, S., Bah, A., Lin, H., Sonenberg, N., and Forman-Kay, J.D. (2013). Interaction of the eukaryotic initiation factor 4E with 4E-BP2 at a dynamic bipartite interface. Structure *21*, 2186-2196.
Lynch, M., Fitzgerald, C., Johnston, K.A., Wang, S., and Schmidt, E.V. (2004). Activated eIF4E-binding protein slows G1 progression and blocks transformation by c-myc without inhibiting cell growth. J Biol Chem *279*, 3327-3339.
Ma, X.M., and Blenis, J. (2009). Molecular mechanisms of mTOR-mediated translational control. Nat Rev Mol Cell Biol *10*, 307-318.
Mader, S., Lee, H., Pause, A., and Sonenberg, N. (1995). The Translation Initiation Factor eIF-4E Binds to a Common Motif Shared by the Translation Factor eIF-4γ and the Translational Repressors 4E-Binding Proteins

Molecular and Cellular Biology *15*, 4990–4997.
Malenka, R.C., and Bear, M.F. (2004). LTP and LTD: an embarrassment of riches. Neuron *44*, 5-21.
Mamane, Y., Petroulakis, E., Martineau, Y., Sato, T.A., Larsson, O., Rajasekhar, V.K., and Sonenberg, N. (2007). Epigenetic activation of a subset of mRNAs by eIF4E explains its effects on cell proliferation. PLoS One *2*, e242.
Marcotrigiano, J., Gingras, A.-C., Sonenberg, N., and Burley, S.K. (1997). Cocrystal Structure of the Messenger RNA 5' Cap-Binding Protein (eIF4E) Boundto7-methyl-GDP. Cell *89*, 951–961.
Marcotrigiano, J., Gingras, A.C., Sonenberg, N., and Burley, S.K. (1999). Cap-Dependent Translation Initiation in Eukaryotes Is Regulated by a Molecular Mimic of eIF4G. Molecular Cell *3*, 707-716.
Martin, K.C., Casadio, A., Zhu, H., Yaping, E., Rose, J.C., Chen, M., Bailey, C.H., and Kandel, E.R. (1997). Synapse-Specific, Long-Term Facilitation of Aplysia Sensory to Motor Synapses: A Function for Local Protein Synthesis in Memory Storage. Cell *91*, 927-938.
Martineau, Y., Azar, R., Bousquet, C., and Pyronnet, S. (2013). Anti-oncogenic potential of the eIF4E-binding proteins. Oncogene *32*, 671-677.
Matlashov, M.E., Bogdanova, Y.A., Ermakova, G.V., Mishina, N.M., Ermakova, Y.G., Nikitin, E.S., Balaban, P.M., Okabe, S., Lukyanov, S., Enikolopov, G.*, et al.* (2015). Fluorescent ratiometric pH indicator SypHer2: Applications in neuroscience and regenerative biology. Biochim Biophys Acta *1850*, 2318-2328.
McGlincy, N.J., and Ingolia, N.T. (2017). Transcriptome-wide measurement of translation by ribosome profiling. Methods *126*, 112-129.
Michel, A.M., and Baranov, P.V. (2013). Ribosome profiling: a Hi-Def monitor for protein synthesis at the genome-wide scale. Wiley Interdiscip Rev RNA *4*, 473-490.
Mikkat, S., Kischstein, T., Kreutzer, M., and Glocker, M.O. (2013). Mass spectrometric peptide analysis of 2DE-separated mouse spinal cord and rat hippocampus proteins suggests an NGxG motif of importance for in vivo deamidation. Electrophoresis *34*, 1610-1618.
Miniaci, M.C., Kim, J.H., Puthenveettil, S., K., S., Zhu, H., Kandel, E.R., and Bailey, C.H. (2008). Several Days of CPEB-Dependent Local Protein Synthesis Are Required to Stabilize Synaptic Growth for Persistence of LongTerm Facilitation in Aplysia. Neuron *59*, 1024-1036.
Mittag, T., Kay, L.E., and Forman-Kay, J.D. (2010). Protein dynamics and conformational disorder in molecular recognition. J Mol Recognit *23*, 105-116.
Mizuno, A., In, Y., Fujita, Y., Abiko, F., Miyagawa, H., Kitamura, K., Tomoo, K., and Ishida, T. (2008). Importance of C-terminal flexible region of 4E-binding protein in binding with eukaryotic initiation factor 4E. FEBS Lett *582*, 3439-3444.

Moerke, N.J., Aktas, H., Chen, H., Cantel, S., Reibarkh, M.Y., Fahmy, A., Gross, J.D., Degterev, A., Yuan, J., Chorev, M.*, et al.* (2007). Small-molecule inhibition of the interaction between the translation initiation factors eIF4E and eIF4G. Cell *128*, 257-267.
Morita, M., Gravel, S.P., Chenard, V., Sikstrom, K., Zheng, L., Alain, T., Gandin, V., Avizonis, D., Arguello, M., Zakaria, C.*, et al.* (2013). mTORC1 controls mitochondrial activity and biogenesis through 4E-BP-dependent translational regulation. Cell Metab *18*, 698-711.
Morita, M., Prudent, J., Basu, K., Goyon, V., Katsumura, S., Hulea, L., Pearl, D., Siddiqui, N., Strack, S., McGuirk, S.*, et al.* (2017). mTOR Controls Mitochondrial Dynamics and Cell Survival via MTFP1. Mol Cell *67*, 922-935 e925.
Nandi, D., Tahiliani, P., Kumar, A., and Chandu, D. (2006). The ubiquitin-proteasome system. J Biosci 31 *31*, 137–155.
Noguchi, S. (2010). Structural changes induced by the deamidation and isomerization of asparagine revealed by the crystal structure of Ustilago sphaerogena ribonuclease U2B. Biopolymers *93*, 1003-1010.
Nojima, H., Tokunaga, C., Eguchi, S., Oshiro, N., Hidayat, S., Yoshino, K., Hara, K., Tanaka, N., Avruch, J., and Yonezawa, K. (2003). The mammalian target of rapamycin (mTOR) partner, raptor, binds the mTOR substrates p70 S6 kinase and 4E-BP1 through their TOR signaling (TOS) motif. J Biol Chem *278*, 15461-15464.
Ostroff, E.L., Fiala, C.J., Allwardt, B., and Harris, K.M. (2002). Polyribosomes Redistribute from Dendritic Shafts into Spines with Enlarged Synapses during LTP in Developing Rat Hippocampal Slices. Neuron *35: 535–545*.
Pang, Y.L., Poruri, K., and Martinis, S.A. (2014). tRNA synthetase: tRNA aminoacylation and beyond. Wiley Interdiscip Rev RNA *5*, 461-480.
Pause, A., Belsham, G.J., Gingras, A.C., Donzé, O., Lin, T.A., Lawrence, J.C., and Sonenberg, N. (1994). Insulin-dependent stimulation of protein synthesis by phosphorylation of a regulator of 5'-cap function. Nature *371*, 762–767.
Pepperkok, R., Hotz-Wagenblatt, A., König, N., Girod, A., Bossemeyer, D., and Kinzel, V. (2000). Intracellular Distribution of Mammalian Protein Kinase A Catalytic Subunit Altered by Conserved Asn2 Deamidation. The Journal of Cell Biology *148*, 715-726.
Pernot, P., Round, A., Barrett, R., De Maria Antolinos, A., Gobbo, A., Gordon, E., Huet, J., Kieffer, J., Lentini, M., Mattenet, M.*, et al.* (2013). Upgraded ESRF BM29 beamline for SAXS on macromolecules in solution. J Synchrotron Radiat *20*, 660-664.
Petoukhov, M.V., Franke, D., Shkumatov, A.V., Tria, G., Kikhney, A.G., Gajda, M., Gorba, C., Mertens, H.D., Konarev, P.V., and Svergun, D.I. (2012). New developments in the ATSAS program package for small-angle scattering data analysis. J Appl Crystallogr *45*, 342-350.
Petroulakis, E., Parsyan, A., Dowling, R.J., LeBacquer, O., Martineau, Y., Bidinosti, M., Larsson, O., Alain, T., Rong, L., Mamane, Y.*, et al.* (2009). p53-dependent translational control of senescence and transformation via 4E-BPs. Cancer Cell *16*, 439-446.
Pickart (2001). Mechanisms underlying ubiquitination. Annu Rev Biochem *70*, 503-533.
Poulin, F., Gingras, A.C., Olsen, H., Chevalier, S., and Sonenberg, N. (1998). 4E-BP3, a New Member of the Eukaryotic Initiation Factor 4E-binding Protein Family. *273, No. 22, Issue of May 29, pp.* , 14002–14007.
Pressler, R., and Auvin, S. (2013). Comparison of Brain Maturation among Species: An Example in Translational Research Suggesting the Possible Use of Bumetanide in Newborn. Front Neurol *4*, 36.
Price, J.C., Guan, S., Burlingame, A., Prusiner, S.B., and Ghaemmaghami, S. (2010). Analysis of proteome dynamics in the mouse brain. Proceedings of the National Academy of Sciences *(107): 14508–14513*.

Pufall, M.A., ., Lee, G.M., Nelson, M.L., Kang, H.S., Velyvis, A., Kay, L.E., McIntosh, L.P., and Graves, B.J. (2005). Variable Control of Ets-1 DNA Binding by Multiple Phosphates in an Unstructured Region. Science *309*, 142-145.
Qin, Z., Kaufman, R.S., Khoury, R.N., Khoury, M.K., and Aswad, D.W. (2013). Isoaspartate accumulation in mouse brain is associated with altered patterns of protein phosphorylation and acetylation, some of which are highly sex-dependent. PLoS One *8*, e80758.
Quackenbush, J. (2002). Microarray data normalization and transformation. Nat Genet *32 Suppl*, 496-501.
Raasakka, A., Myllykoski, M., Laulumaa, S., Lehtimaki, M., Hartlein, M., Moulin, M., Kursula, I., and Kursula, P. (2015). Determinants of ligand binding and catalytic activity in the myelin enzyme 2',3'-cyclic nucleotide 3'-phosphodiesterase. Sci Rep *5*, 16520.
Ran, I., Gkogkas, C.G., Vasuta, C., Tartas, M., Khoutorsky, A., Laplante, I., Parsyan, A., Nevarko, T., Sonenberg, N., and Lacaille, J.C. (2013). Selective regulation of GluA subunit synthesis and AMPA receptor-mediated synaptic function and plasticity by the translation repressor 4E-BP2 in hippocampal pyramidal cells. J Neurosci *33*, 1872-1886.
Rangaraju, V., Tom Dieck, S., and Schuman, E.M. (2017). Local translation in neuronal compartments: how local is local? EMBO Rep *18*, 693-711.
Raught, B., and Gingras, A.C. (1999). eIF4E activity is regulated at multiple levels. The International Journal of Biochemistry & Cell Biology *31*, 43-57.
Rebola, N., Lujan, R., Cunha, R.A., and Mulle, C. (2008). Adenosine A2A receptors are essential for long-term potentiation of NMDA-EPSCs at hippocampal mossy fiber synapses. Neuron *57*, 121-134.
Reissner, K.J., and Aswad, D.W. (2003). Deamidation and isoaspartate formation in proteins: unwanted alterations or surreptitious signals? Cell Mol Life Sci *60*, 1281-1295.
Robinson, and Robinson (2004). Molecualr Clocks: Deamidation of Asparaginyl and Glutaminyl Residues in Peptides and Proteins. Althouse Press, Cave Junction, OR.
Robinson, N.E. (2002). Protein deamidation. PNAS *99*, 5283–5288.
Robinson, N.E., and Robinson, A.B. (2001). Deamidation of human proteins. PNAS *98*, 12409–12413.
Rong, L., Livingstone, M., Sukarieh, R., Petroulakis, E., Gingras, A.C., Crosby, K., Smith, B., Polakiewicz, R.D., Pelletier, J., Ferraiuolo, M.A*., et al.* (2008). Control of eIF4E cellular localization by eIF4E-binding proteins, 4E-BPs. RNA *14*, 1318-1327.
Ruvinsky, I., and Meyuhas, O. (2006). Ribosomal protein S6 phosphorylation: from protein synthesis to cell size. Trends Biochem Sci *31*, 342-348.
Sabatini, B., Oertner, T.G., and Svoboda, K. (2002). The Life Cycle of Ca2+ Ions in Dendritic Spines Neuron *33*, 439-452.
Santos, S.D., Carvalho, A.L., Caldeira, M.V., and Duarte, C.B. (2009). Regulation of AMPA receptors and synaptic plasticity. Neuroscience *158*, 105-125.
Schalm, S.S., and Blenis, J. (2002). Identification of a Conserved Motif Required for mTOR Signaling.
Schalm, S.S., Fingar, D.C., Sabatini, D.M., and Blenis, J. (2003). TOS Motif-Mediated Raptor Binding Regulates 4E-BP1 Multisite Phosphorylation and Function. Current Biology *13*, 797-806.
Scheetz, A.J., Nairn, A.C., and Constantine-Paton, M. (2000). NMDA receptor-mediated control of protein synthesis at developing synapses. Nature Neuroscience *(3): 211-216*.
Scheper, G.C., and Proud, C.G. (2002). Does phosphorylation of the cap-binding protein eIF4E play a role in translation initiation? Eur J Biochem 2 *269*, 5350-5359.
Schmitz, Y., Luccarelli, J., Kim, M., Wang, M., and Sulzer, D. (2009). Glutamate controls growth rate and branching of dopaminergic axons. J Neurosci *29*, 11973-11981.

Schwanhausser, B., Busse, D., Li, N., Dittmar, G., Schuchhardt, J., Wolf, J., Chen, W., and Selbach, M. (2011). Global quantification of mammalian gene expression control. Nature *473*, 337-342.
Scott, M.S., Calafell, S.J., Thomas, D.Y., and Hallett, M.T. (2005). Refining protein subcellular localization. PLoS Comput Biol *1*, e66.
Semple, B.D., Blomgren, K., Gimlin, K., Ferriero, D.M., and Noble-Haeusslein, L.J. (2013). Brain development in rodents and humans: Identifying benchmarks of maturation and vulnerability to injury across species. Prog Neurobiol *106-107*, 1-16.
Shen, H., Korutla, L., Champtiaux, N., Toda, S., LaLumiere, R., Vallone, J., Klugmann, M., Blendy, J.A., Mackler, S.A., and Kalivas, P.W. (2007). NAC1 regulates the recruitment of the proteasome complex into dendritic spines. J Neurosci *27*, 8903-8913.
Short, M.P., Richardson Jr., E.P., Haines, J.L., and Kwiatkowski, D.J. (1995). Clinical, Neuropathological and Genetic Aspects of the Tuberous Sclerosis Complex. Brain Pathology *5*, 173-179.
Smith, W.B., Starck, S.R., Roberts, R.W., and Schuman, E.M. (2005). Dopaminergic stimulation of local protein synthesis enhances surface expression of GluR1 and synaptic transmission in hippocampal neurons. Neuron *45*, 765-779.
Somers, J., Poyry, T., and Willis, A.E. (2013). A perspective on mammalian upstream open reading frame function. Int J Biochem Cell Biol *45*, 1690-1700.
Sonenberg, N., Rupprecht, K.M., Hecht, S.M., and Shatkin, A.J. (1979). Eukaryotic mRNA cap binding protein: purification by affinity chromatography on sepharose-coupled m7GDP. Proceedings of the National Academy of Sciences *76*, 4345-4349.
Spiegel, P.C., Ermolenko, D.N., and Noller, H.F. (2007). Elongation factor G stabilizes the hybrid-state conformation of the 70S ribosome. Rna *13*, 1473-1482.
Stephenson, R.C., and Clarke, S. (1989). Succinimide Formation from Aspartyl and Asparaginyl Peptides as a Model for the Spontaneous Degradation of Proteins. The Journal of Biological Chemistry *264*, 6164-6170.
Steward, O., Falk, M.P.A., and E.R., T. (1996). Ultrastructural basis for gene expression at the synapse:

synapse-associated polyribosome complexes Journal of Neurocytology *25: 717-734*
Steward, O., and Falk, P.M. (1986). Protein-synthetic machinery at postsynaptic sites during synaptogenesis: a quantitative study of the association between polyribosomes and developing synapses. Journal of Neuroscience *(2) 412-423*.
Steward, O., and Schuman, E.M. (2001). Protein synthesis at synaptic sites on dendrites Annu Rev Neurosci *24*, 299-325.
Steward, O., and Schuman, E.M. (2003). Compartmentalized Synthesis and Degradation of Proteins in Neurons. Neuron *Vol. 40, 347–359*.
Sutton, M.A., and Schuman, E.M. (2006). Dendritic protein synthesis, synaptic plasticity, and memory. Cell *127*, 49-58.
Sutton, M.A., Taylor, A.M., Ito, H.T., Pham, A., and Schuman, E.M. (2007). Postsynaptic decoding of neural activity: eEF2 as a biochemical sensor coupling miniature synaptic transmission to local protein synthesis. Neuron *55*, 648-661.
Svergun, D.I. (1999). Restoring Low Resolution Structure of Biological Macromolecules from Solution Scattering Using Simulated Annealing. Biophysical Journal *76*, 2879–2886.
Svergun, D.I., Petoukhov, M.V., and Koch, M.H.J. (2001). Determination of Domain Structure of Proteins from X-Ray Solution Scattering. Biophysical Journal *80*, 2946–2953.

Svitkin, Y.V., P., A., Haghighat, A., Pyronnet, S., Witherell, G., Belsham, G.J., and Sonenberg, N. (2001). The requirement for eukaryotic initiation factor 4A (eIF4A) in translation is in direct proportion to the degree of mRNA 5' secondary structure. RNA *7*, 382–394.
Swanger, S.A., He, Y.A., Richter, J.D., and Bassell, G.J. (2013). Dendritic GluN2A synthesis mediates activity-induced NMDA receptor insertion. J Neurosci *33*, 8898-8908.
Tai, H.C., Besche, H., Goldberg, A.L., and Schuman, E.M. (2010). Characterization of the Brain 26S Proteasome and its Interacting Proteins. Front Mol Neurosci *3*.
Tai, H.C., and Schuman, E.M. (2008). Ubiquitin, the proteasome and protein degradation in neuronal function and dysfunction. Nat Rev Neurosci *9*, 826-838.
Tashiro, A., Dunaevsky, A., Blazeski, R., Mason, C.A., and Yuste, R. (2003). Bidirectional Regulation of Hippocampal Mossy Fiber Filopodial Motility by Kainate Receptors: A Two-Step Model of Synaptogenesis. Neuron *38*, 773-784.
Tee, A.R., and Proud, C.G. (2002). Caspase Cleavage of Initiation Factor 4E-Binding Protein 1 Yields a Dominant Inhibitor of Cap-Dependent Translation and Reveals a Novel Regulatory Motif. Molecular and Cellular Biology *22*, 1674-1683.
Theillet, F.X., Smet-Nocca, C., Liokatis, S., Thongwichian, R., Kosten, J., Yoon, M.K., Kriwacki, R.W., Landrieu, I., Lippens, G., and Selenko, P. (2012). Cell signaling, post-translational protein modifications and NMR spectroscopy. J Biomol NMR *54*, 217-236.
Thoreen, C.C., Chantranupong, L., Keys, H.R., Wang, T., Gray, N.S., and Sabatini, D.M. (2012). A unifying model for mTORC1-mediated regulation of mRNA translation. Nature *485*, 109-113.
Thoreen, C.C., Kang, S.A., Chang, J.W., Liu, Q., Zhang, J., Gao, Y., Reichling, L.J., Sim, T., Sabatini, D.M., and Gray, N.S. (2009). An ATP-competitive mammalian target of rapamycin inhibitor reveals rapamycin-resistant functions of mTORC1. J Biol Chem *284*, 8023-8032.
Thrower, J., Laura Hoffman, Rechsteiner, M., and M.Pickart, C. (2000). Recognition of the polyubiquitin proteolytic signal. The EMBO Journal.
Tian, B., and Manley, J.L. (2017). Alternative polyadenylation of mRNA precursors. Nat Rev Mol Cell Biol *18*, 18-30.
Tiedge, H., and Brosius, J. (1996). Translational Machinery in Dendrites of Hippocampal

Neurons in Culture. The Journal of Neuroscience *16(22):7171–7181*.
Tiruchinapalli, D.M., Oleynikov, Y., Kelic, S., Shenoy, S.M., Hartley, A., Stanton, P.K., Singer, H.R., and G.J., B. (2003). Activity-Dependent Trafficking and Dynamic Localization of

Zipcode Binding Protein 1 and β - Actin mRNA in Dendrites

and Spines of Hippocampal Neurons. The Journal of Neuroscience.
Tomoo, K., Matsushita, Y., Fujisaki, H., Abiko, F., Shen, X., Taniguchi, T., Miyagawa, H., Kitamura, K., Miura, K., and Ishida, T. (2005). Structural basis for mRNA Cap-Binding regulation of eukaryotic initiation factor 4E by 4E-binding protein, studied by spectroscopic, X-ray crystal structural, and molecular dynamics simulation methods. Biochim Biophys Acta *1753*, 191-208.
Topisirovic, I., and Sonenberg, N. (2011). mRNA translation and energy metabolism in cancer: the role of the MAPK and mTORC1 pathways. Cold Spring Harb Symp Quant Biol *76*, 355-367.
Traynelis, S.F., Wollmuth, L.P., McBain, C.J., Menniti, F.S., Vance, K.M., Ogden, K.K., Hansen, K.B., Yuan, H., Myers, S.J., and Dingledine, R. (2010). Glutamate receptor ion channels: structure, regulation, and function. Pharmacol Rev *62*, 405-496.
Truitt, M.L., Conn, C.S., Shi, Z., Pang, X., Tokuyasu, T., Coady, A.M., Seo, Y., Barna, M., and Ruggero, D. (2015). Differential Requirements for eIF4E Dose in Normal Development and Cancer. Cell *162*, 59-71.

Tsai, N.P. (2014). Ubiquitin proteasome system-mediated degradation of synaptic proteins: An update from the postsynaptic side. Biochim Biophys Acta *1843*, 2838-2842.
Tsukiyama-Kohara (2001). Adipose tissue reduction in mice lacking the translational inhibitor 4E-BP1. Nature Medicine.
Udagawa, T., Swanger, S.A., Takeuchi, K., Kim, J.H., Nalavadi, V., Shin, J., Lorenz, L.J., Zukin, R.S., Bassell, G.J., and Richter, J.D. (2012). Bidirectional control of mRNA translation and synaptic plasticity by the cytoplasmic polyadenylation complex. Mol Cell *47*, 253-266.
van Tijn, P., Hol, E.M., van Leeuwen, F.W., and Fischer, D.F. (2008). The neuronal ubiquitin-proteasome system: murine models and their neurological phenotype. Prog Neurobiol *85*, 176-193.
Vanhouttey, P., and Bading, H. (2003). Opposing roles of synaptic and extrasynaptic NMDA receptors in neuronal calcium signalling and BDNF gene regulation. Current Opinion in Neurobiology *13*, 366–371.
Varshavsky, A. (1997). The N-end rule pathway of protein degradation. Genes to cells

Venne, A.S., Solari, F.A., Faden, F., Paretti, T., Dissmeyer, N., and Zahedi, R.P. (2015). An improved workflow for quantitative N-terminal charge-based fractional diagonal chromatography (ChaFRADIC) to study proteolytic events in Arabidopsis thaliana. Proteomics *15*, 2458-2469.
Wahlsten, D., Metten, P., Phillips, T.J., Boehm, S.L., 2nd, Burkhart-Kasch, S., Dorow, J., Doerksen, S., Downing, C., Fogarty, J., Rodd-Henricks, K*., et al.* (2003). Different data from different labs: lessons from studies of gene-environment interaction. J Neurobiol *54*, 283-311.
Walsh, C.T., Garneau-Tsodikova, S., and Gatto, G.J., Jr. (2005). Protein posttranslational modifications: the chemistry of proteome diversifications. Angew Chem Int Ed Engl *44*, 7342-7372.
Wang, C., Wang, Z., Xiong, Z., Dai, H., Zou, Z., Jia, C., Bai, X., and Chen, Z. (2016). mTORC1 Activation Promotes Spermatogonial Differentiation and Causes Subfertility in Mice. Biol Reprod *95*, 97.
Wang, H.L., Chang, N.C., Weng, Y.H., and Yeh, T.H. (2013). XLID CUL4B mutants are defective in promoting TSC2 degradation and positively regulating mTOR signaling in neocortical neurons. Biochim Biophys Acta *1832*, 585-593.
Wang, L., Harris, T.E., Roth, R.A., and Lawrence, J.C., Jr. (2007). PRAS40 regulates mTORC1 kinase activity by functioning as a direct inhibitor of substrate binding. J Biol Chem *282*, 20036-20044.
Washington, E.J., Banfield, M.J., and Dangl, J.L. (2013). What a difference a Dalton makes: bacterial virulence factors modulate eukaryotic host cell signaling systems via deamidation. Microbiol Mol Biol Rev *77*, 527-539.
Wells, D.G., Dong, X., Quinlan, E.M., Huang, Y., Bear, M.F., Richter, J.D., and J.R., F. (2001). A Role for the Cytoplasmic Polyadenylation Element in NMDA

Receptor-Regulated mRNA Translation in Neurons. The Journal of Neuroscience *21(24) : 9541–9548*.
Wirtz, S., and Schuelke, M. (2011). Region-specific expression of mitochondrial complex I genes during murine brain development. PLoS One *6*, e18897.
Woelk, T., Sigismund, S., Penengo, L., and Polo, S. (2007). The ubiquitination code: a signalling problem. Cell Div *2*, 11.
Xiao, Z., Zou, Q., Liu, Y., and Yang, X. (2016). Genome-wide assessment of differential translations with ribosome profiling data. Nat Commun *7*, 11194.

Xie, H., Vucetic, S., Iakoucheva, L.M., Oldfield, C.J., Dunker, A.K., Obradovic, Z., and Uversky, V.N. (2007). Functional Anthology of Intrinsic Disorder. 3. Ligands, Post-Translational Modifications, and Diseases Associated with Intrinsically Disordered Proteins. Journal of Proteome Research *6*, 1917-1932.
Yanagiya, A., Suyama, E., Adachi, H., Svitkin, Y.V., Aza-Blanc, P., Imataka, H., Mikami, S., Martineau, Y., Ronai, Z.A., and Sonenberg, N. (2012). Translational homeostasis via the mRNA cap-binding protein, eIF4E. Mol Cell *46*, 847-858.
Yao, I., Takagi, H., Ageta, H., Kahyo, T., Sato, S., Hatanaka, K., Fukuda, Y., Chiba, T., Morone, N., Yuasa, S.*, et al.* (2007). SCRAPPER-dependent ubiquitination of active zone protein RIM1 regulates synaptic vesicle release. Cell *130*, 943-957.
Yates, A., Akanni, W., Amode, M.R., Barrell, D., Billis, K., Carvalho-Silva, D., Cummins, C., Clapham, P., Fitzgerald, S., Gil, L.*, et al.* (2016). Ensembl 2016. Nucleic acids research *44*, D710-716.
Young D., S.K., Yang S., Jan Y., Jan Y. (2010). Altered ultrasonic vocalizations in a tuberous sclerosis mouse model of autism.
Zhang, J., Zhao, J., Xu, S., Li, J., He, S., Zeng, Y., Xie, L., Xie, N., Liu, T., Lee, K.*, et al.* (2018). Species-Specific Deamidation of cGAS by Herpes Simplex Virus UL37 Protein Facilitates Viral Replication. Cell Host Microbe *24*, 234-248 e235.
Zheng, J.Q., Wan, J., and Poo, M. (1996). Essential Role of Filopodia in Chemotropic Growth Cone Induced by a Glutamate Turning of Nerve Gradient. The Journal of Neuroscience *76*, 1140-l 1149.

Appendix

Geneblock sequences

(For cloning at the C-terminal of fused 4E-BP2 fluorecent protein)

4E-BP2 WT

CGCCCTCGAGATGTCCTCGTCAGCCGGCAGCGGCCACCAGCCCAGCCAGAGC
CGCGCCATCCCCACCCGCACCGTGGCCATCAGCGACGCCGCGCAGCTACCTC
ATGACTATTGCACCACGCCCGGGGGGGACGCTCTTCTCCACCACACCGGGAGG
AACTCGAATCATTTATGACAGAAAGTTTCTGTTGGATCGTCGCAATTCTCCCAT
GGCTCAGACCCCACCCTGCCATCTGCCCAATATCCCAGGAGTCACTAGCCCTG
GCACCTTAATTGAAGACTCCAAAGTAGAAGTAAACAATTTGAACAACTTGAACA
ATCACGACAGGAAACATGCAGTTGGGGATGATGCTCAGTTCGAGATGGACATC
TGAGAATTCCGGCG

4E-BP2 N99D/N102D

CGCCCTCGACATGTCCTCGTCAGCCGGCAGCGGCCACCAGCCCAGCCAGAGC
CGCGCCATCCCCACCCGCACCGTGGCCATCAGCGACGCCGCGCAGCTACCTC
ATGACTATTGCACCACGCCCGGGGGGGACGCTCTTCTCCACCACACCGGGAGG
AACTCGAATCATTTATGACAGAAAGTTTCTGTTGGATCGTCGCAATTCTCCCAT
GGCTCAGACCCCACCCTGCCATCTGCCCAATATCCCAGGAGTCACTAGCCCTG
GCACCTTAATTGAAGACTCCAAAGTAGAAGTAAACAATTTGGACAATCTAGACA
ATCACGACAGGAAACATGCAGTTGGGGATGATGCTCAGTTCGAGATGGACATC
TGAGAATTCCGGCG

4E-BP2 N99A/N102A

CGCCCTCGACATGTCCTCGTCAGCCGGCAGCGGCCACCAGCCCAGCCAGAGT
CGCGCCATCCCCACCCGCACCGTGGCCATCAGCGACGCCGCGCAGCTACCTC
ATGACTATTGCACCACGCCCGGGGGGGACGCTCTTCTCCACCACACCGGGAGG

AACTCGAATCATTTATGACAGAAAGTTTCTGTTGGATCGTCGCAATTCTCCCAT
GGCTCAGACCCCACCCTGCCATCTGCCCAATATCCCAGGAGTCACTAGCCCTG
GCACCTTAATTGAAGACTCCAAAGTAGAAGTAAACAATTTGGCCAACTTGGCCA
ATCACGACAGGAAACATGCAGTTGGGGATGATGCTCAGTTCGAGATGGACATC
TGA GAATTCCGGCG

(For cloning at the N-terminal of fused 4E-BP2 fluorescent protein)

4E-BP2 WT

CGCCCTCGAGATGTCCTCGTCAGCCGGCAGCGGCCACCAGCCCAGCCAGAGC
CGCGCCATCCCCACCCGCACCGTGGCCATCAGCGACGCCGCGCAGCTACCTC
ATGACTATTGCACCACGCCCGGGGGGACGCTCTTCTCCACCACACCGGGAGG
AACTCGAATCATTTATGACAGAAAGTTTCTGTTGGATCGTCGCAATTCTCCCAT
GGCTCAGACCCCACCCTGCCATCTGCCCAATATCCCAGGAGTCACTAGCCCTG
GCACCTTAATTGAAGACTCCAAAGTAGAAGTAAACAATTTGAACAACTTGAACA
ATCACGACAGGAAACATGCAGTTGGGGATGATGCTCAGTTCGAGATGGACATC
GAATTCCGGCG

4E-BP2 N99D/N102D

CGCCCTCGACATGTCCTCGTCAGCCGGCAGCGGCCACCAGCCCAGCCAGAGC
CGCGCCATCCCCACCCGCACCGTGGCCATCAGCGACGCCGCGCAGCTACCTC
ATGACTATTGCACCACGCCCGGGGGGACGCTCTTCTCCACCACACCGGGAGG
AACTCGAATCATTTATGACAGAAAGTTTCTGTTGGATCGTCGCAATTCTCCCAT
GGCTCAGACCCCACCCTGCCATCTGCCCAATATCCCAGGAGTCACTAGCCCTG
GCACCTTAATTGAAGACTCCAAAGTAGAAGTAAACAATTTGGACAATCTAGACA
ATCACGACAGGAAACATGCAGTTGGGGATGATGCTCAGTTCGAGATGGACATC
GAATTCCGGCG

4E-BP2 N99A/N102A

CGCCCTCGACATGTCCTCGTCAGCCGGCAGCGGCCACCAGCCCAGCCAGAGT
CGCGCCATCCCCACCCGCACCGTGGCCATCAGCGACGCCGCGCAGCTACCTC
ATGACTATTGCACCACGCCCGGGGGGACGCTCTTCTCCACCACACCGGGAGG
AACTCGAATCATTTATGACAGAAAGTTTCTGTTGGATCGTCGCAATTCTCCCAT
GGCTCAGACCCCACCCTGCCATCTGCCCAATATCCCAGGAGTCACTAGCCCTG
GCACCTTAATTGAAGACTCCAAAGTAGAAGTAAACAATTTGGCCAACTTGGCCA

ATCACGACAGGAAACATGCAGTTGGGGATGATGCTCAGTTCGAGATGGACATC
GAATTCCGGCG

Recombinant Protein sequences

4E-BP2 WT

ATGTCCTCGTCAGCCGGCAGCGGCCACCAGCCCAGCCAGAGCCGCGCCATCC
CCACCCGCACCGTGGCCATCAGCGACGCCGCGCAGCTACCTCATGACTATTG
CACCACGCCCGGGGGGGACGCTCTTCTCCACCACACCGGGAGGAACTCGAATC
ATTTATGACAGAAAGTTTCTGTTGGATCGTCGCAATTCTCCCATGGCTCAGACC
CCACCCTGCCATCTGCCCAATATCCCAGGAGTCACTAGCCCTGGCACCTTAAT
TGAAGACTCCAAAGTAGAAGTAAACAATTTGAACAACTTGAACAATCACGACAG
GAAACATGCAGTTGGGGATGATGCTCAGTTCGAGATGGACATCTGA

4E-BP2 N99D/N102D

ATGTCCTCGTCAGCCGGCAGCGGCCACCAGCCCAGCCAGAGCCGCGCCATCC
CCACCCGCACCGTGGCCATCAGCGACGCCGCGCAGCTACCTCATGACTATTG
CACCACGCCCGGGGGGGACGCTCTTCTCCACCACACCGGGAGGAACTCGAATC
ATTTATGACAGAAAGTTTCTGTTGGATCGTCGCAATTCTCCCATGGCTCAGACC
CCACCCTGCCATCTGCCCAATATCCCAGGAGTCACTAGCCCTGGCACCTTAAT
TGAAGACTCCAAAGTAGAAGTAAACAATTTGGACAATCTAGACAATCACGACAG
GAAACATGCAGTTGGGGATGATGCTCAGTTCGAGATGGACATCTGA

Software and Algorithms

Adobe Illustrator	https://www.adobe.com/creativecloud.html
GraphPad PRISM	https://www.graphpad.com/scientific-software/prism/
Fiji ImageJ software	https://fiji.sc/
Imaris software	http://www.bitplane.com/
NIS-Elements-v4.13 software	https://www.nikoninstruments.com/en_GB
Huygens Software 4.5.1p3	https://svi.nl/HuygensSoftware
ImageStudio Software	https://www.licor.com
ATSAS software suite	https://www.embl-hamburg.de/biosaxs/software.html
DAMMIN	https://www.embl-hamburg.de/biosaxs/dammin.html
GASBOR	https://www.embl-hamburg.de/biosaxs/gasbor.html
Multifastats	https://github.com/davidrequena/multifastats
Ingenuity Pathway Analysis (IPA)	https://www.qiagenbioinformatics.com/products/ingenuity-pathway-analysis/
Database for Annotation, Visualization and Integrated Discovery (DAVID)	https://david.ncifcrf.gov/

Category	Term	Count	%	PValue	Genes	Gene names	List Total	Pop Hits	Pop Total	Fold Enrichment	Bonferroni	Benjamini	FDR
MF	GO:0002039~p53 binding	4	1.8957346	0.032810469	ENSMUSG00000021481, ENSMUSG00000027663, ENSMUSG00000055024, ENSMUSG00000052676	Zfp346, Zmat3, Zmat1, Ep300	175	70	17446	5.696653061	0.999920608	0.740430198	35.71434319
MF	GO:0003700~transcription factor activity, sequence-specific DNA binding	16	7.5829384	0.031009081	ENSMUSG00000037674, ENSMUSG00000054939, ENSMUSG00000044296, ENSMUSG00000059436, ENSMUSG00000055024, ENSMUSG00000028341, ENSMU	Mef2d, Nfat5, Tsc22d2, Nr4a3, Hivep3, Gmeb1, Rfx7, Cbfa2t2, Rere, Zfp879,	175	883	17446	1.806413202	0.999865576	0.773667887	34.11039548
MF	GO:0003676~nucleic acid binding	21	9.9526066	0.02212877	ENSMUSG00000021481, ENSMUSG00000022635, ENSMUSG00000024831, ENSMUSG00000027663, ENSMUSG00000055480, ENSMUSG00000052488, ENSMU	Zfp592, Zfp346, Zcrb1, Zbtb20, Rbm27, Ighmbp2, Zmat3, Hivep3, Thap3, Zfp8	175	1237	17446	1.692417138	0.998222898	0.718199039	25.64853962
MF	GO:0035259~glucocorticoid receptor binding	3	1.4218009	0.013625888	ENSMUSG00000029478, ENSMUSG00000028341, ENSMUSG00000055024	Nr4a3, Ncor2, Ep300	175	18	17446	16.6152381	0.979403602	0.621166985	16.61513115
MF	GO:0003677~DNA binding	35	16.587678	3.04E-04	ENSMUSG00000002028, ENSMUSG00000029478, ENSMUSG00000024384, ENSMUSG00000044296, ENSMUSG00000031783, ENSMUSG00000059436, ENSMU	Mef2d, Kmt2a, Nfat5, Polr2a, Zfp592, Cers2, Tshz3, Zbtb20, Rfc4, Iws1, Ighmt	175	1847	17446	1.889117488	0.082489832	0.028289352	0.402088933
MF	GO:0008270~zinc ion binding	27	12.796209	2.39E-05	ENSMUSG00000021481, ENSMUSG00000021982, ENSMUSG00000055128, ENSMUSG00000055024, ENSMUSG00000028341, ENSMU	Kmt2a, Zfp346, Cdadc1, March11, Zcrb1, Adamts5, Ighmbp2, Ablim1, Zmat3,	175	1075	17446	2.503877741	0.006741118	0.003376259	0.031649511
MF	GO:0046872~metal ion binding	63	29.85782	2.52E-07	ENSMUSG00000025241, ENSMUSG00000097333, ENSMUSG00000028341, ENSMUSG00000051586, ENSMUSG00000022708, ENSMUSG00000091722, ENSMU	Kmt2a, Polr2a, Zfp592, Helz, Tshz3, Zfp346, Cdadc1, March11, Zcrb1, Zbtb20,	175	3355	17446	1.872	7.14E-05	7.14E-05	3.34E-04

Category	Term	Count	%	PValue	Genes	Gene names	List Total	Pop Hits	Pop Total	Fold Enrichment	Bonferroni	Benjamini	FDR
BP	GO:0006351~transcription, DNA-templated	29	13.744076	0.010594652	ENSMUSG00000029478, ENSMUSG00000002028, ENSMUSG00000024384, ENSMUSG00000044296, ENSMUSG00000059436, ENSMUSG00000031783, ENSMU	Mef2d, Kmt2a, Nfat5, Polr2a, Zfp592, Tshz3, Zbtb20, Iws1, Ighmbp2, Nr4a3, H	172	1885	18082	1.617352415	0.999889086	0.999889086	15.20416718
BP	GO:0007010~cytoskeleton organization	5	2.3696682	0.01709099	ENSMUSG00000036053, ENSMUSG00000051586, ENSMUSG00000060090, ENSMUSG00000025085, ENSMUSG00000025265	Ablim1, Fgd1, Fmnl2, Mical3, Rp2	172	104	18082	5.054226297	0.999999603	0.999369852	23.42703016
BP	GO:0006493~protein O-linked glycosylation	3	1.4218009	0.026731712	ENSMUSG00000035245, ENSMUSG00000060988, ENSMUSG00000047146	Eogt, Tet1, Galnt13	172	27	18082	11.68087855	1	0.999557123	34.26569615
BP	GO:0006611~protein export from nucleus	3	1.4218009	0.030543661	ENSMUSG00000040594, ENSMUSG00000040312, ENSMUSG00000001855	Nup214, Cchcr1, Ranbp17	172	29	18082	10.87530072	1	0.998680485	38.14109269
BP	GO:0072332~intrinsic apoptotic signaling pathway by p53 class mediator	3	1.4218009	0.034556664	ENSMUSG00000021481, ENSMUSG00000027663, ENSMUSG00000052676	Zfp346, Zmat3, Zmat1	172	31	18082	10.17366842	1	0.997554988	41.98928967
BP	GO:0035023~regulation of Rho protein signal transduction	4	1.8957346	0.036539753	ENSMUSG00000030220, ENSMUSG00000034801, ENSMUSG00000031139, ENSMUSG00000025265	Fgd1, Arhgdib, Mcf2, Sos2	172	77	18082	5.461189973	1	0.995030457	43.80715042
BP	GO:0006355~regulation of transcription, DNA-templated	31	14.691943	0.037255181	ENSMUSG00000002028, ENSMUSG00000029478, ENSMUSG00000024384, ENSMUSG00000044296, ENSMUSG00000097333, ENSMUSG00000059436, ENSMU	Mef2d, Kmt2a, Nfat5, Zfp592, Tshz3, Zbtb20, Iws1, Ighmbp2, Nup35, Nr4a3, H	172	2279	18082	1.429997857	1	0.990317006	44.44978616
BP	GO:0006366~transcription from RNA polymerase II promoter	5	2.3696682	0.042144372	ENSMUSG00000028634, ENSMUSG00000031783, ENSMUSG00000005198, ENSMUSG00000056854, ENSMUSG00000003847	Nfat5, Polr2a, Hivep3, Polr2c, Pou3f4	172	138	18082	3.808982137	1	0.989966709	48.66089212

Category	Term	Count	%	PValue	Genes	Gene names	List Total	Pop Hits	Pop Total	Fold Enrichment	Bonferroni	Benjamini	FDR
CC	GO:0005737~cytoplasm	76	36.018957	0.039068956	ENSMUSG00000046139, ENSMUSG00000031783, ENSMUSG00000059436, ENSMUSG00000020848, ENSMUSG00000051586, ENSMUSG00000091722, ENSMU	Ramp2, Mef2d, Gstt1, Rin2, Kmt2a, Btbd6, Nfat5, Dnajb9, Nipsnap3b, Btbd11	188	6631	19662	1.198683168	0.999693436	0.740330914	39.3911363
CC	GO:0032809~neuronal cell body membrane	3	1.4218009	0.030873562	ENSMUSG00000058975, ENSMUSG00000047787, ENSMUSG00000042671	Rgs8, Flrt1, Kcnc1	188	29	19662	10.81914894	0.998281183	0.720072268	32.5663271
CC	GO:0005634~nucleus	71	33.649289	0.026862721	ENSMUSG00000046139, ENSMUSG00000029478, ENSMUSG00000059436, ENSMUSG00000031783, ENSMUSG00000028809, ENSMUSG00000028341, ENSMU	Mef2d, Gstt1, Nup214, Kmt2a, Nfat5, Polr2a, Zfp592, Mettl16, Nipsnap3b, Ce	188	6019	19662	1.23368376	0.996024934	0.748906146	28.97464801
CC	GO:0030027~lamellipodium	6	2.8436019	0.020490302	ENSMUSG00000040852, ENSMUSG00000029359, ENSMUSG00000033763, ENSMUSG00000025608, ENSMUSG00000025085, ENSMUSG00000025265	Ablim1, Fgd1, Podxl, Tesc, Mtss1l, Plekhh2	188	164	19662	3.82628438	0.985045417	0.753627952	22.90447699
CC	GO:0042995~cell projection	14	6.6350711	0.018849414	ENSMUSG00000040852, ENSMUSG00000024831, ENSMUSG00000059436, ENSMUSG00000029359, ENSMUSG00000025608, ENSMUSG00000025265, ENSMU	Tshz3, Atat1, Ighmbp2, Fgd1, Podxl, Tesc, Mtss1l, Nphp4, Plekhh2, Rgs8, Flrt1	188	712	19662	2.056448721	0.978994138	0.855066008	21.26593982
CC	GO:0005654~nucleoplasm	32	15.165877	0.002673719	ENSMUSG00000002028, ENSMUSG00000029478, ENSMUSG00000024384, ENSMUSG00000028607, ENSMUSG00000031783, ENSMUSG00000059436, ENSMU	Mef2d, Kmt2a, Nfat5, Polr2a, Tshz3, Mlh3, Zcrb1, Zbtb20, Iws1, Nup35, Cpt2,	188	1935	19662	1.729572819	0.419283077	0.419283077	3.307948191

Category	Term	Count	%	PValue	Genes	Gene names	List Total	Pop Hits	Pop Total	Fold Enrichment	Bonferroni	Benjamini	FDR
MF	GO:0046923~ER retention sequence binding	2	0.8438819	0.042416269	ENSMUSG00000079111, ENSMUSG00000010830	Kdelr3, Kdelr2	189	4	17446	46.15343915	0.999999742	0.920204648	44.72121526
MF	GO:0005096~GTPase activator activity	7	2.9535865	0.042246836	ENSMUSG00000022488, ENSMUSG00000035151, ENSMUSG00000052632, ENSMUSG00000024883, ENSMUSG00000002458, ENSMUSG00000036533, ENSMU	Rgs19, Nckap1l, Rin1, Agfg2, Elmod2, Cdc42ep3, Asap2	189	235	17446	2.749566588	0.999999725	0.951275019	44.58729307
MF	GO:0016491~oxidoreductase activity	13	5.4852321	0.030815214	ENSMUSG00000024579, ENSMUSG00000020844, ENSMUSG00000028690, ENSMUSG00000029348, ENSMUSG00000040888, ENSMUSG00000025068, ENSMU	Dus4l, Rrm2, Nxn, Pcyox1l, Tm7sf2, Gsto1, Pecr, Sord, Mmachc, Asphd2, Gfer	189	604	17446	1.986737447	0.999982529	0.935348817	34.82429076
MF	GO:0016787~hydrolase activity	26	10.970464	0.024141547	ENSMUSG00000020380, ENSMUSG00000042210, ENSMUSG00000041429, ENSMUSG00000025232, ENSMUSG00000010461, ENSMUSG00000021900, ENSMU	Nudt14, Ddx39, Hyal2, Eya4, Endog, Adat2, Rad50, Erap1, Btd, Nudt12, Hexa,	189	1533	17446	1.565543924	0.999807074	0.942217455	28.41106772
MF	GO:0051059~NF-kappaB binding	4	1.6877637	0.004433733	ENSMUSG00000028191, ENSMUSG00000056941, ENSMUSG00000044303, ENSMUSG00000075486	Bcl10, Cdkn2a, Commd7, Commd6	189	31	17446	11.91056494	0.788864895	0.540505598	5.896417353
MF	GO:0044822~poly(A) RNA binding	24	10.126582	0.002027228	ENSMUSG00000021392, ENSMUSG00000027201, ENSMUSG00000021731, ENSMUSG00000037740, ENSMUSG00000054889, ENSMUSG00000038279, ENSMU	Farsa, Ddx39, Ccdc59, Pes1, Nol8, Mrps30, Yars2, Srfbp1, Rps14, Myef2, Ebn	189	1113	17446	1.990444815	0.508478641	0.508478641	2.737250277
MF	GO:0019855~calcium channel inhibitor activity	2	0.8438819	0.083042564	ENSMUSG00000037434, ENSMUSG00000027257		189	8	17446	23.07671958	1	0.986894342	69.44673632

Category	Term	Count	%	PValue	Genes	Gene names	List Total	Pop Hits	Pop Total	Fold Enrichment	Bonferroni	Benjamini	FDR
BP	GO:2001238~positive regulation of extrinsic apoptotic signaling pathway	3	1.2658228	0.04991324	ENSMUSG00000028191, ENSMUSG00000010047, ENSMUSG00000036986	Hyal2, Bcl10, Pml	204	32	18082	8.309742647	1	0.948682034	55.12412791
BP	GO:0038108~negative regulation of appetite by leptin-mediated signaling	2	0.8438819	0.044159559	ENSMUSG00000031755, ENSMUSG00000025235	Bbs4, Bbs2	204	4	18082	44.31862745	1	0.938833987	50.67725685
BP	GO:0006919~activation of cysteine-type endopeptidase activity involved i	4	1.6877637	0.039547641	ENSMUSG00000028191, ENSMUSG00000044303, ENSMUSG00000014771, ENSMUSG00000036986	Pdcd2, Bcl10, Pml, Cdkn2a	204	67	18082	5.291776412	1	0.931071677	46.81848323
BP	GO:0051092~positive regulation of NF-kappaB transcription factor activity	5	2.1097046	0.034484501	ENSMUSG00000028191, ENSMUSG00000023755, ENSMUSG00000036526, ENSMUSG00000028179, ENSMUSG00000032497	Rhebl1, Cth, Bcl10, Lrrfip2, Card11	204	109	18082	4.065929124	1	0.918333121	42.25765094
BP	GO:0031398~positive regulation of protein ubiquitination	4	1.6877637	0.029889055	ENSMUSG00000028191, ENSMUSG00000070520, ENSMUSG00000032966, ENSMUSG00000022184	Fbxo4, Bcl10, Fkbp1a, Nsmce3	204	60	18082	5.909150327	1	0.904312484	37.80356082
BP	GO:0002244~hematopoietic progenitor cell differentiation	5	2.1097046	0.024592458	ENSMUSG00000002781, ENSMUSG00000029798, ENSMUSG00000002343, ENSMUSG00000010047, ENSMUSG00000033106	Armc6, Tmem143, Hyal2, Herc6, Slc7a6os	204	98	18082	4.522308924	1	0.877627101	32.27153053
BP	GO:0090398~cellular senescence	3	1.2658228	0.020865319	ENSMUSG00000044303, ENSMUSG00000049932, ENSMUSG00000036986	Pml, Cdkn2a, H2afx	204	20	18082	13.29558824	0.999999997	0.858688393	28.10620477
BP	GO:0055114~oxidation-reduction process	15	6.3291139	0.020603004	ENSMUSG00000024579, ENSMUSG00000020844, ENSMUSG00000028690, ENSMUSG00000029348, ENSMUSG00000040888, ENSMUSG00000021606, ENSMU	Ndufa11, Dus4l, Rrm2, Nxn, Ndufs6, Pcyox1l, Tm7sf2, Gsto1, Pecr, Sord, Mma	204	676	18082	1.966802993	0.999999996	0.883117775	27.8041983
BP	GO:0006974~cellular response to DNA damage stimulus	11	4.6413502	0.020503317	ENSMUSG00000020380, ENSMUSG00000014243, ENSMUSG00000032555, ENSMUSG00000070520, ENSMUSG00000041429, ENSMUSG00000010461, ENSMU	Ddx39, Eya4, Zswim7, Mapkapk2, Rad50, Mbd4, Topbp1, Kin, Nthl1, H2afx, N	204	420	18082	2.321451914	0.999999996	0.909563345	27.68911564
BP	GO:0006749~glutathione metabolic process	4	1.6877637	0.017591859	ENSMUSG00000027603, ENSMUSG00000028690, ENSMUSG00000028179, ENSMUSG00000025068	Gsto1, Ggt7, Cth, Mmachc	204	49	18082	7.235694278	0.999999993	0.904910369	24.25129266
BP	GO:0033365~protein localization to organelle	3	1.2658228	0.017050128	ENSMUSG00000031755, ENSMUSG00000025235, ENSMUSG00000020430	Pes1, Bbs4, Bbs2	204	18	18082	14.77287582	0.999999883	0.930039654	23.59497532
BP	GO:0015031~protein transport	14	5.907173	0.016483462	ENSMUSG00000031755, ENSMUSG00000040034, ENSMUSG00000079657, ENSMUSG00000079111, ENSMUSG00000025235, ENSMUSG00000020739, ENSMU	Kdelr3, Ift27, Copz2, Nup85, Timm9, Bbs4, Bbs2, Slc7a6os, Nup37, Nup43, Se	204	592	18082	2.096151298	0.9999998	0.954261973	22.90275388
BP	GO:0006310~DNA recombination	5	2.1097046	0.015408861	ENSMUSG00000020380, ENSMUSG00000014243, ENSMUSG00000070520, ENSMUSG00000037262, ENSMUSG00000049932	Zswim7, Rad50, Kin, H2afx, Nsmce3	204	85	18082	5.213956171	0.999999449	0.972749524	21.57390576
BP	GO:0006364~rRNA processing	6	2.5316456	0.013892944	ENSMUSG00000021392, ENSMUSG00000038279, ENSMUSG00000044303, ENSMUSG00000033126, ENSMUSG00000020430, ENSMUSG00000028729	Pes1, Nol8, Ebna1bp2, Ybey, Nop2, Cdkn2a	204	126	18082	4.220821662	0.999997701	0.986801905	19.66283516
BP	GO:0006281~DNA repair	10	4.2194093	0.009964714	ENSMUSG00000020380, ENSMUSG00000014243, ENSMUSG00000032555, ENSMUSG00000070520, ENSMUSG00000041429, ENSMUSG00000010461, ENSMU	Eya4, Zswim7, Rad50, Mbd4, Topbp1, Eepd1, Kin, Nthl1, H2afx, Nsmce3	204	318	18082	2.78733506	0.999907992	0.990407927	14.50582647
BP	GO:0021987~cerebral cortex development	5	2.1097046	0.007175608	ENSMUSG00000031755, ENSMUSG00000038119, ENSMUSG00000025235, ENSMUSG00000028640, ENSMUSG00000049932	Bbs4, Tfap2c, Bbs2, Cdon, H2afx	204	68	18082	6.517445213	0.998747946	0.998747946	10.6578984

Category	Term	Count	%	PValue	Genes	Gene names	List Total	Pop Hits	Pop Total	Fold Enrichment	Bonferroni	Benjamini	FDR
CC	GO:0000444~MIS12/MIND type complex	2	0.8438819	0.042833351	ENSMUSG00000027635, ENSMUSG00000040599	Dsn1, Mis12	215	4	19662	45.7255814	0.999961175	0.602799021	42.99464633
CC	GO:0005730~nucleolus	16	6.7510549	0.04243811	ENSMUSG00000021392, ENSMUSG00000032398, ENSMUSG00000038279, ENSMUSG00000044303, ENSMUSG00000021900, ENSMUSG00000060036, ENSMU	Pes1, Nol8, Btd, Maf1, Rps14, Ebna1bp2, Snapc5, Nek11, Pml, Bend3, Nop2,	215	842	19662	1.737789317	0.999957272	0.634345434	42.69170774
CC	GO:0000776~kinetochore	5	2.1097046	0.04225356	ENSMUSG00000040034, ENSMUSG00000020739, ENSMUSG00000035351, ENSMUSG00000040599	Nup85, Dsn1, Nup37, Nup43, Mis12	215	120	19662	3.810465116	0.999955319	0.671390018	42.54974929
CC	GO:0016020~membrane	90	37.974684	0.039362758	ENSMUSG00000023266, ENSMUSG00000036533, ENSMUSG00000017188, ENSMUSG00000031168, ENSMUSG00000010047, ENSMUSG00000021079, ENSMU	Fndc5, Ndufa11, Rgs19, Tmem143, Bcam, Cyth2, Coq8b, Farsa, Ddx39, Tmco6	215	6998	19662	1.176136704	0.999910095	0.68795074	40.28335253
CC	GO:0000818~nuclear MIS12/MIND complex	2	0.8438819	0.021649965	ENSMUSG00000027635, ENSMUSG00000040599	Dsn1, Mis12	215	2	19662	91.45116279	0.993767397	0.515880267	24.49702507
CC	GO:0031965~nuclear membrane	8	3.3755274	0.012075324	ENSMUSG00000037434, ENSMUSG00000044857, ENSMUSG00000020739, ENSMUSG00000037580, ENSMUSG00000029810, ENSMUSG00000032590, ENSMU	Nup85, Gsto1, Tmem176b, Apeh, Pml, Slc30a1, Gch1, Lemd2	215	226	19662	3.237209302	0.940306187	0.374844263	14.44136563
CC	GO:0031080~nuclear pore outer ring	3	1.2658228	0.00500936	ENSMUSG00000040034, ENSMUSG00000020739, ENSMUSG00000035351	Nup85, Nup37, Nup43	215	10	19662	27.43534884	0.688106103	0.207861037	6.243808157
CC	GO:0005634~nucleus	86	36.28692	0.002745092	ENSMUSG00000030880, ENSMUSG00000027201, ENSMUSG00000032398, ENSMUSG00000041429, ENSMUSG00000020844, ENSMUSG00000031168, ENSMU	Smg5, Pnck, Ddx39, Vax1, Tmco6, Eya4, Fsd1, Zswim7, Pdcd2, Fhod1, Lage3,	215	6019	19662	1.306662236	0.471513002	0.14737399	3.467488719
CC	GO:0005737~cytoplasm	94	39.662447	0.001825217	ENSMUSG00000032489, ENSMUSG00000039676, ENSMUSG00000027201, ENSMUSG00000036533, ENSMUSG00000020844, ENSMUSG00000024228, ENSMU	Smg5, Coasy, Vwf, Pnck, Rgs19, Nudt14, Cyth2, Coq8b, Farsa, Ddx39, Tmco6,	215	6631	19662	1.29639712	0.345469604	0.131753036	2.318089528
CC	GO:0005694~chromosome	12	5.0632911	0.001424244	ENSMUSG00000020380, ENSMUSG00000032555, ENSMUSG00000070520, ENSMUSG00000040034, ENSMUSG00000020739, ENSMUSG00000036181, ENSMU	Rad50, Pes1, Nup85, Dsn1, Topbp1, Nup37, Hist1h1c, Nup43, Mis12, Pum3, H	215	344	19662	3.190156842	0.281550753	0.152386145	1.813129244
CC	GO:0005739~mitochondrion	35	14.767932	4.84E-04	ENSMUSG00000035142, ENSMUSG00000037740, ENSMUSG00000026096, ENSMUSG00000044303, ENSMUSG00000041429, ENSMUSG00000017188, ENSMU	Hddc2, Coasy, Ndufa11, Tmem143, Coq8b, Cox6c, Lrrk1, Endog, Coa3, Adck1,	215	1721	19662	1.85984352	0.106186124	0.106186124	0.619272854